# POLITECNICO DI MILANO

## School of Civil, Environmental and Territorial Engineering

### Master of Science in Environmental and Geomatic Engineering



# NEW GNSS PRECISE POSITIONING BY MOBILEPHONES

Supervisor: Prof. Ludovico Biagi

Master Graduation Thesis by:
Can Delice
Matr. 833666

Academic Year 2018/2019

## Abstract

In Android Release N ("Nougat"), Google introduced APIs giving access to GNSS raw measurements from android smartphones. After this announcement, users will be able to log GNSS raw measurements such as GPS satellite information (C/No, azimuth, elevation if a particular satellite has been used in the PVT), NMEA sentences and PVT solution with the proper time stamp. This can open many possibilities for the single-frequency GNSS receivers, also called low-cost GNSS receiver, integrated in smartphones.

An opportunity to do better and complete research with GNSS raw measurements from the single-frequency GNSS receivers can improve the accuracies for smart mobile devices. Tens meters accuracy could be enough for most of daily navigation purposes; however, it could be better to increase it for some particular cases: usages needs higher accuracy (decimeter of accuracy) like navigation for impaired people.

In this aspect, mainly, the research investigates assessment of kinematic and short session static accuracies with single frequency low-cost receivers. Additionally, shares what kind of difficulties are faced, how good the results are evaluated, when the single-frequency GNSS receiver raw measurements are processed and analyzed with well know software packages for geodetic post-processing.

To explain in detail, in the research, accuracy assessment of relative static point positioning is practiced for U-blox LEA-4T. U-blox is a single-frequency GNSS receiver that measures the pseudoranges with the C/A code only. For the research, U-blox data quality is investigated for short sessions. In this aspect, the research contains the processing and analysis of static positioning for short time periods with U-blox. Besides, RTKLIB has been tested for processing the U-blox data in short static sessions. Then, Samsung Galaxy S8 is studied as low-cost single frequency receiver with kinematic, single point positioning, DGPS and static point positioning approach. In order to log desired data in android smartphone, OruxMap, GNSS Logger, Geo++ RINEX Logger and RinexOn applications are tested. Estimated point positions in real-time by Samsung Galaxy S8 chipset from API Level 23 and estimated point positions by RTKLIB post-processing from API Level 24 are analyzed in detail.

One of the major challenges to reach better accuracies in the research comes from short period of time (5 – 10 minutes) surveys; therefore, experiments are performed with short static sessions with mobile devices.

For accuracy assessment, one reference network with stop-and-go surveying technique, one reference trajectory with kinematic surveying technique were established surveying them with geodetic receiver Leica GRX1200.

The outline of the thesis is as follows:

- Chapter 1 introduces the research motivation and objectives.
- Chapter 2 presents an overview about GNSS systems and explains the fundamentals of satellite positioning, code and phase observations, including error sources, and differencing positioning techniques.
- Chapter 3 introduces GNSS receivers and software packages used in the thesis
- Chapter 4 first describes the research approach. Then, continues with defining the reference network and trajectory set-up. Also, it explains applied clustering methods to smooth the point cloud in detail.
- Chapter 5 is a presentation of the experiments performed to test the single frequency GNSS receivers. The chapter includes the processing and analyze of results with the discussion of the results.
- Chapter 6 is the conclusion part with recommendation for the future work.

# Acknowledgements

# Contents

# List of Figures

xii

# List of Tables

# Table of Acronyms

API    Application Programming Interface

ARP    Antenna Reference Point

ASCII    American Standard Code for Information Interchange

BDCS    BeiDou Coordinate System

BDS    BeiDou Navigation Satellite System

BDT    BeiDou Navigation Satellite System Time

BIH    Bureau International de l'Heure

CDMA    Code Division Multiple Access

CGCS2000    China Geodetic Coordinate System 2000

CS    Commercial Service

CTP    Conventional Terrestrial Pole

DOD    US Department of Defense

ECEF    Earth-Centered Earth-Fixed

EGNOS    European Geostationary Navigation Overlay Service

ETRF    European Terrestrial Reference Frame

FDMA    Frequency Division Multiple Access

FOC    Full Operational Capability

FTP    File Transfer Protocol

GEO    Geostationary Earth Orbit

GGSP    Galileo Geodetic Service Provider

GIS    Geographic Information System

GLONASS    GLObalnaya NAvigazionnaya Sputnikovaya Sistema

GNSS    Global Navigation Satellite System

GPS    Global Positioning System

GSA    European Global Navigation Satellite System Agency

GST    Galileo System Time

GTRF    Galileo Terrestrial Reference Frame

JD    Julian Date

IERS    International Earth Rotation Service

INT    Integer Operator

IoT    Internet of Things

IRM    International Earth Rotation Service Reference Meridian

IRNSS    Indian Regional Navigation Satellite System

IRP    International Earth Rotation Service Reference Pole

ITRF    International Terrestrial Reference Frame

ITRS    International Terrestrial Reference System

LGO    Leica Geo Office

LSE    Least Square Estimation

MBOC    Multiplexed Binary Offset Carrier

MEO    Medium Earth Orbit

MIL-STD-810    United States Military Standard

MSAS    Multi-functional Satellite Augmentation System

NAP    N0uclear detection system Analysis Package

NavIC    Navigation Indian Constellation

NAVSTAR    NAVigation Satellite Timing And Ranging

NDS    nuclear detection system

NGA    National Geospatial-Intelligence Agency

NMEA    National Marine Electronics Association

OS    Open Service

PCO    Phase Center Offset

PCV    Phase Center Variations

PPP    Precise Point Positioning

PRN    Pseudo-Random Noise

PRS    Public Regulated Service

QZSS    Quasi-Zenith Satellite System

RINEX    Receiver Independent Exchange Format

RMS    Root Mean Square

RTK    Real Time Kinematic

SAR    Search and Rescue Service

SBAS    Satellite Based Augmentation Systems

SNR    Signal to Noise Ratio

SPS     Standard Positioning Service

TAI     Temps Atomique International

TEC     Total Electron Content

TECU     Total Electron Content Unit

USNO     US Naval Observatory

USSR     Union of Soviet Socialist Republics

UTC     Coordinated Universal Time

WAAS     Wide Area Augmentation System

WGS 84     World Geodetic System 1984

# 1  INTRODUCTION

## 1.1  Motivation

Almost three decades have passed since the first Global Navigation Satellite System (GNSS), commonly known as Global Positioning System (GPS), became available to the public. Since then the number of devices which are equipped with a GPS receiver has been continuously increasing. The growing interest on the position information has initiated the creation of new GNSSs with improved performance characteristics: such as Galileo represents Europe's initiative to build it's "own" GNSS (Skournetou & Lohan, 2011).

Standard geodetic GNSS surveys are based on the high-quality GNSS receivers and antennas. Generally, they are dual-frequency receivers to solve the ambiguities faster and more reliably. On the other hand, single-frequency receivers are used widely for navigation purposes in smart mobile devices such as smartphones, in car navigation system, smartwatch, tablet with navigation applications. In the last years, single-frequency receivers are improved their reliability to use in various fields (U-blox can reach to the couple of cm accuracy level).

While all these are continuous, Google's announcement that GNSS raw measurements would be made available from Android 7.0 devices (i.e., Nougat) marked the first-time developers had access to carrier and code measurements and decoded navigation messages from a mass-market device. In other words, users will be able to log GNSS raw measurements such as GPS satellite information (C/No, azimuth, elevation if a particular satellite has been used in the PVT), NMEA sentences and PVT solution with the proper time stamp. Lukasz Bonenberg from the University of Nottingham and a member of the European Global Navigation Satellite System Agency's (GSA) GNSS Raw Measurements Task Force says "*We believe these raw measurements are a real game changer, re-defining the GNSS on our smartphones, not only does it allow us to work directly with GNSS data – for post-processing, testing and teaching – but also to find new ways of using GNSS on smartphones, which will lead to new applications that add value to smartphone-based services.*"

The advantages of using these measurements are many. For instance, developers can use this information to implement advanced GNSS techniques in mass-market devices and to compute a position using selected satellites/constellations, when combined with external sensors, raw

measurements increase the time when position, velocity and time (PVT) can be computed. More so, Receiver Autonomous Integrity Monitoring provides another layer of integrity in mass-market devices using raw measurements (European Global Navigation Satellite System Agency, 2017).

The technique used to get up the position in single-frequency GNSS receivers is the absolute point positioning that reach an accuracy of tens meters. 10-meter accuracy positioning might be quite acceptable for certain applications including basic navigation to get from point A to point B. But there are many situations that people encounter in daily lives where a predictable accuracy of 1 meter or better could be hugely useful such as identifying the correct lane in which a vehicle is traveling or identifying a particular parking space (not to mention various vehicle-to-vehicle positioning and situational awareness needs).

No doubt, the opportunity to access GNSS raw measurements from Android devices will cause improvement of single-frequency GNSS receivers in time. In this aspect, the main motivation of this research is developed on the study with single-frequency GNSS receivers. In comparison to single-frequency GNSS receivers integrated in android devices, u-blox modules are single-frequency GNSS receiver measure the pseudoranges with the C/A code only. Therefore, u-blox modules are included in the research.

## 1.2   Research Objectives

The main objective of the research is testing the single frequency GNSS receivers in order to observe their reliability to use for navigation and scientific purposes.

1.  With this aspect, the first objective is the accuracy assessment of relative static point positioning for U-blox LEA-4T. It is a single-frequency GNSS receiver accesses only L1 frequency.
2.  Then, creating the reference with geodetic receiver Leica GRX1200. In this purpose, by using stop-and-go and kinematic surveying methods, two references must be created to make comparisons.
3.  The assessment of accuracy of position information obtained in real-time from android chipset. For this, Samsung Galaxy S8 device is used which has single frequency GNSS receiver.

4. The accuracy assessment by the collecting the raw GNSS measurement in motion. For this, using Samsung Galaxy S8 and processing the raw measurements with different ways.

5. The accuracy assessment by the collecting the raw GNSS measurement in static approach. For this, using Samsung Galaxy S8 and store raw measurements in RINEX format to be able to use well know post processing software packages.

## 1.3 Thesis Outline

The outline of the thesis is as follows:

- Chapter 1 introduces the research motivation and objectives.

- Chapter 2 presents an overview about GNSS systems and explains the fundamentals of satellite positioning, code and phase observations, including error sources, and differencing positioning techniques.

- Chapter 3 introduces GNSS receivers and software packages used in the thesis

- Chapter 4 first describes the research approach. Then, continues with defining the reference network and trajectory set-up. Also, it explains applied clustering methods to smooth the point cloud in detail.

- Chapter 5 is a presentation of the experiments performed to test the single frequency GNSS receivers. The chapter includes the processing and analyze of results with the discussion of the results.

- Chapter 6 is the conclusion part with recommendation for the future work.

# 2 GLOBAL NAVIGATION SATELLITE SYSTEM (GNSS)

Global Navigation Satellite System (GNSS) is a global satellites coverage that provides positioning and timing data for GNSS receivers. Satellites transmit coded signal to receivers that calculate geographic location "longitude, latitude, altitude/elevation, speed, direction and time" to high precision by obtained data from received signal (G S, 2010).

Accuracy, integrity, continuity and availability are the main standards how the performance of GNSS are evaluated. In these standards, accuracy is the difference between real and measured position, speed and time. Integrity is the capacity that the system provides a warning under an anomaly in the position data. Continuity is the ability that system works without interruptions. Availability is the time percentage of system provides accuracy, integrity and continuity standards above the thresholds (European Global Navigation Satellite System Agency, 2017).

GNSS technologies are utilized in almost every sector with different specific applications and solutions. These sub-sections could be classified under three group:

- **Mass market** – presenting high-volume receivers for consumer devices. Automotive (not safety critical), consumer drones, smartphones, and specialized Internet of Things (IoT) devices from mHealth to robotics are all covered.
- **Transport safety and liability critical solutions** – presenting receivers built in accordance with standards to deliver such solutions. Automotive, aviation, professional drones, maritime, search and rescue and, new to this issue of the transportation, space borne GNSS applications are all covered.
- **High precision and timing solutions** – presenting receivers designed to deliver the highest accuracy (position or time) possible. Agriculture, GIS, Surveying and Timing and Synchronization applications are all covered (European GNSS Agency, 2016).

At the moment, there are six existing operational or under development GNSS:

- The Global Positioning System (GPS);
- BeiDou Navigation Satellite System (BDS);
- Galileo;

- GLONASS (Globalnaya Navigazionnaya Sputnikovaya Sistema, or Global Navigation Satellite System);

- Indian Regional Navigation Satellite System (IRNSS) / Navigation Indian Constellation (NavIC) and

- Quasi-Zenith Satellite System (QZSS) (Global Positioning System, 2017).

The four GNSS – GPS, GLONASS, BeiDou and Galileo – are currently in either full operational capability (FOC) or nearing FOC status, with the two most recent constellations due to complete deployment by 2020. As a result, there were already over 100 GNSS satellites in orbit as of December 2017.

Three Regional Navigation Satellite Systems, namely the Indian NavIC, the Chinese BeiDou (phase 2) and Japanese QZSS complete the picture and further increase the number of navigation satellites in their respective coverage areas.

GNSS has three major segments or "components": space segment, control segment and user segment. These are represented in Figure 2.1.
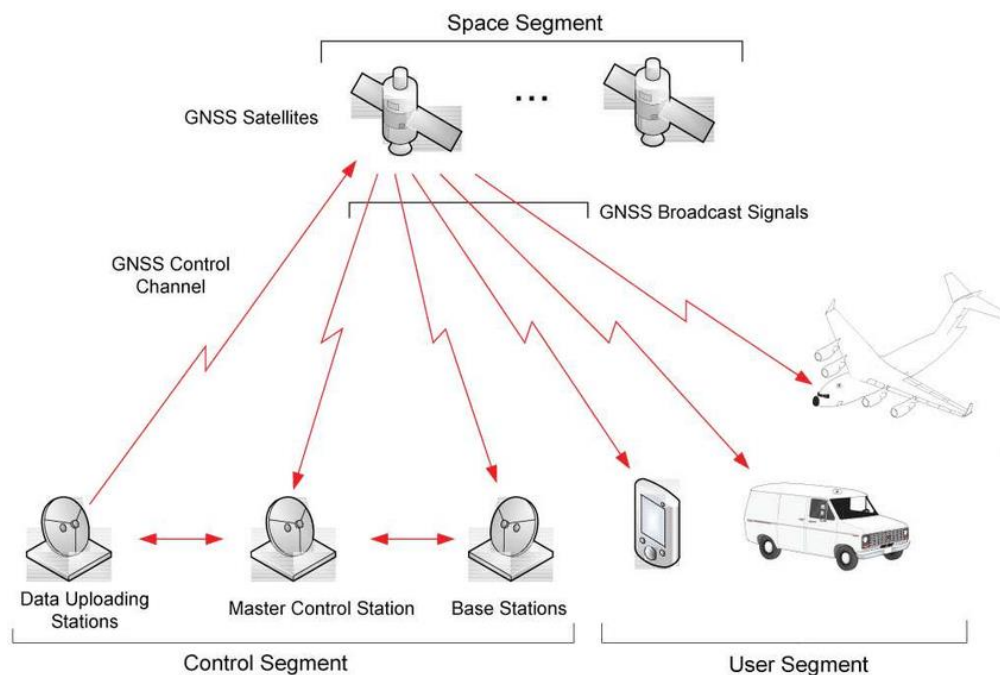


*Figure 2.1: GNSS segments (Jeffrey, 2010)*

**Space Segment**

The space segment consists of GNSS satellites which have different constellations and orbits for each GNSS. GNSS satellites are orbited about 20,000 km above the earth in order to contribute global coverage (Jeffrey, 2010).

**Control Segment**

The control segment includes master control stations, data uploading stations and monitoring stations on the world. Satellites' orbit parameters and high precision clocks are obtained from master stations for every GNSS system. Also master control stations provide analysis of the signals and transmission of orbit and time corrections to the satellites by using data uploading stations. Monitor stations, as comes from its name, monitor the satellites' signals and status and report this to master control station. The ground antennas periodically upload the satellite ephemerides and clock information from the master control station to each GNSS satellite (Hofman-Wellenhof, Lichtenegger, & Wasle, 2008).

**User Segment**

The user segment comprises equipment that are utilized to process the signals from GNSS satellites and determine the location and time. Mainly, the primary components are mapping applications, receivers and antennas (Jeffrey, 2010).

## 2.1 Global Positioning System (GPS)

GPS is the first global satellite-based system utilized to satisfy the requirements for the military forces. Official name, NAVSTAR (NAVigation Satellite Timing and Ranging) GPS derives and applies 3-dimensiona (3-D) positioning, time and velocity in a common reference system anywhere on Earth on a continuous basis.

The first satellite was launched in 1978 for US Department of Defense (DOD). GPS was available only for military use until the incident of the Korean Airlines Flight 007 in 1983. After the incident, the President of USA, Ronald Reagan, offered a free civilian access to GPS (Hofman-Wellenhof, Lichtenegger, & Wasle, 2008).

### 2.1.1  Reference Systems

#### *2.1.1.1  Coordinate System*

"World Geodetic System 1984 (WGS 84), the standard U.S Department of Defense, is the definition of the global reference system for the geospatial information and reference system for GPS. It is compatible with the International Terrestrial Reference System (ITRS). WGS 84 is an Earth-centered, Earth-fixed reference system and geodetic datum. WGS 84 is based on a consistent set of constants and model parameters that describe the Earth's size, shape and gravity and geomagnetic fields." (UNOOSA). The definition of the frame is presented as follows:

- The origin is located the center of Earth mass.
- The scale is that of the local Earth frame, in the meaning of a relativistic theory of gravitation. It aligns with ITRS.
- The Z-Axis is the direction of the IERS Reference Pole (IRP). This direction corresponds to the direction of BIH Conventional Terrestrial Pole (CTP) (epoch 0984.0) with an uncertainty of 0.005''.
- The X-Axis is intersection of the IERS Reference Meridian (IRM) and the plane passing through the origin and normal to the Z-axis. The IRM is coincident with the BIH Zero Meridian (epoch 1984.0) with an uncertainty of 0.005''.
- The Y-Axis completes a right-handed, Earth-Centered Earth-Fixed (ECEF) orthogonal coordinate system.
- The time evolution in orientation will create no residual global rotation with regards to the crust (National Imagery and Mapping Agency, 2000).

The parameters of WGS 84 have shown in Table 2.1.

*Table 2.1: WGS 84 parameters (National Imagery and Mapping Agency, 2000)*

| Parameter | Notation | Value |
|---|---|---|
| Semi-major Axis | a | 6378137.0 meters |
| Flattening Factor of the Earth | 1/f | 298.257223563 |
| Nominal Mean Angular Velocity of the Earth | ω | 7292115 x 10-11 radians/second |
| Nominal Mean Angular Velocity of the Earth | GM** | 3.986004418 x 1014 meter3 /second2 |

**The value of GM for GPS users is $3.9860050 \times 1014 \ m^3 / sec^2$ as specified in the references below

## 2.1.1.2 Time System

GPS time system defined that is related to the atomic time system or "Temps Atomique International (TAI)" and referenced to coordinated universal time (UTC) by the US Naval Observatory (USNO). GPS time constantly backwards 19 seconds with TAI.

$$TAI = GPS \ time + 19.000^S \qquad (2.1)$$

GPS time is defined coincident to UTC at 00 hours:00 minutes:00 seconds of January 6th, 1980. GPS time may differ from UTC, because GPS time is a continuous time scale, whereas UTC is corrected periodically with an integer number of leap seconds. Therefore, GPS time system is different from UTC, which will always be ahead of it by a defined number of leap seconds. This offset is also given in the navigation (NAV) message and automatically corrected by the receiver. According to USNO, July 1st, 2015, GPS time is ahead of UTC by seventeen (17) seconds. After December 31st, 2016 at 23:59:60, GPS time is ahead of UTC by eighteen (18) seconds. For more information about GPS timing data be consult with official USNO page (USNO).

GPS time is counted in terms of GPS weeks and seconds as starting from GPS standard epoch. Following formula show GPS week's relation with Julian Date (JD) and integer operator (INT):

$$WEEK = INT [(JD - 2444244.5)/7] \qquad (2.2)$$

The date and time format for GPS time is usually GPS week/seconds of week. The largest unit used in starting GPS time is one week, defined as 604800 seconds.

## 2.1.2  The GPS Segments

**Space Segment**

The GPS space segment can be defined as a constellation of satellites transmitting signals to user receivers. Since the first satellite was launched to the orbit in 1978, the United States Air Forces has had 31 operational GPS satellites at orbit until April 4th, 2019. These satellites are on the orbit in order to ensure the commitment to maintain at least 24 operational GPS satellites, 95% of the time. After June 2011, GPS efficiently works as a 27-slot constellation with improved coverage (Global Positioning System, 2017).

GPS satellites orbiting in six orbital planes (A to F) at an altitude about 20,200 km. Each orbital plane has four satellites with an inclination of 55° with respect to equatorial plane in a Medium Earth Orbit (MEO). Orbital period is 11 hours 58 minutes, which mean each satellite circles the Earth twice a day, as shown on Figure 2.2.
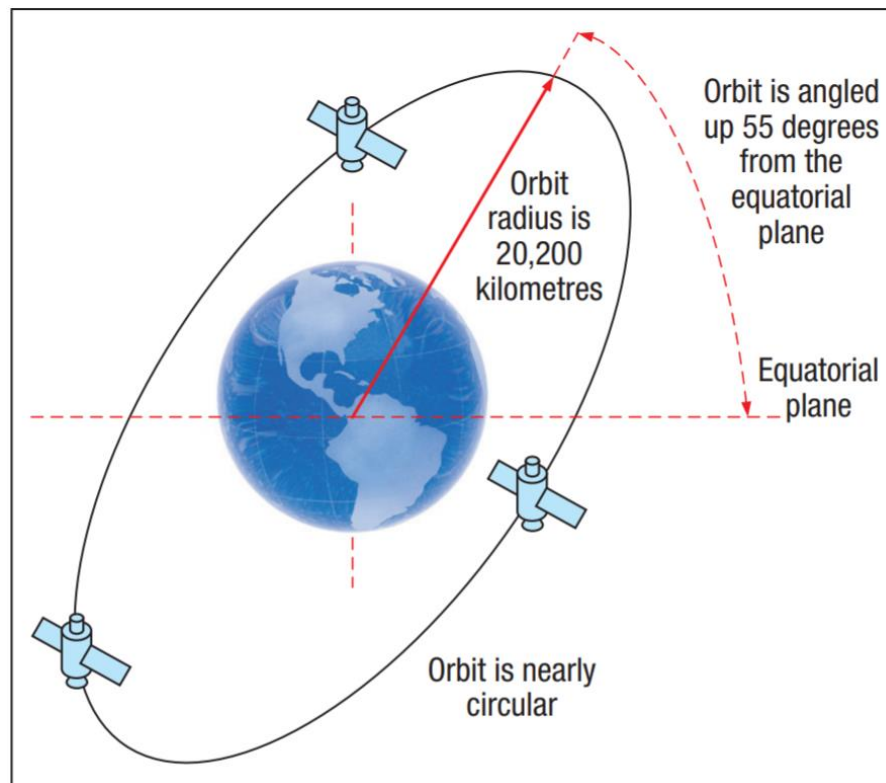
*Figure 2.2: GPS satellite orbit (NASA, 2017)*

**Control Segment**

Control segment tracks the GPS satellites, monitors their transmissions, performs analyses and uploads the prediction of ephemerides, clock corrections and navigational data parameters to the satellites. As mentioned before under GNSS control segment, the control segment consists of a master control station, monitor stations and data uploading stations (which are called ground antennas for GPS).

GPS control segment has a master control station at Falcon Air Force Base in Colorado, CO and an alternate master control station at Vandenberg AFB, California. There are 16 monitor station, 6 of 16 are maintained by Air Forces, 10 of 16 are maintained by National Geospatial-Intelligence Agency (NGA). Also, there are 11 command and control antennas. The locations of these facilities are shown on Figure 2.3.
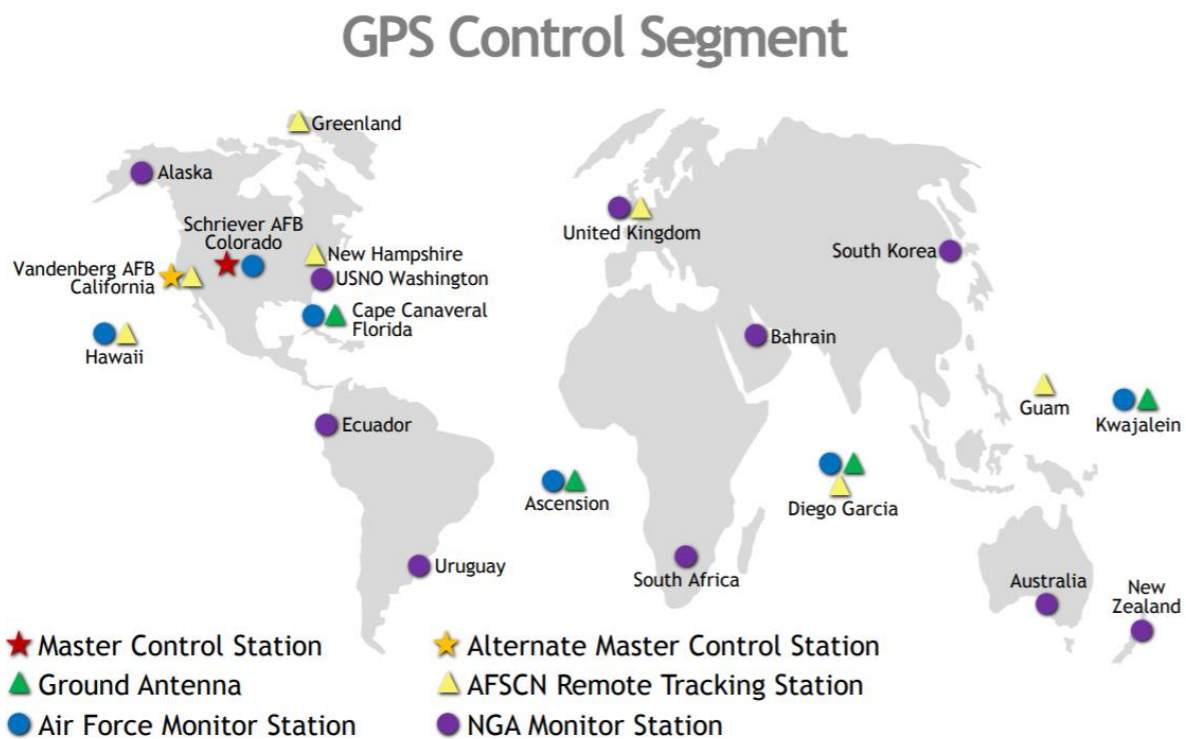


*Figure 2.3: GPS control segment (NASA, 2017)*

The master control station controls the GPS satellites and operates them. Also, collecting the data from monitor stations and calculating the satellite orbit and clock parameters by using a Kalman estimator is the assignment of master control station.

The monitor stations continuously measure pseudoranges to satellites. Every 1.5 seconds, measured pseudoranges are used to produce 15 minutes interval data by using ionospheric and meteorological data. The produced data is transmitted to the master control station.

The ground antennas periodically upload the satellite ephemerides and clock information from the master control station to each GPS satellite as S-band radio links (G S, 2010).

**User Segment**

The user segment consists of GPS receivers for both military and civilian users. GPS receivers track signals of each satellite in view and calculate 3-D position and time by using transit time of signal at least from 4 satellites. GPS technology is used for navigation, reconnaissance, target tracking and missile guidance systems, search and rescue purposes by military uses. For civilian applications, GPS technology is widely spread almost every field from surveying to tracking to agriculture to any field can be imagined. However, GPS application generally falls into 5 main categories for both civilian and military usage: Positioning, navigation, tracking, mapping and timing (NovAtel, 2010).

## 2.1.3  The GPS Signals

In this section, the characteristics of the GPS signals and the types of information encoded digitally on the signal are summarized. The GPS signals are fundamentally driven with the fundamental frequency that is 10.23 MHZ by an atomic clock. GPS satellites continuously transmit signals on two frequencies, L1 and L2 which are called as "Legacy Signals". There are also L2C, L5 and L1C that are a new project to modernize the GPS space and ground segments, in order to use advantages of new technologies and satisfy user requirements.

The carrier signals (L1, L2 and L5) are as sine waves:

- L1 is created by multiplying the frequency by 154. It is at frequency = 1575.42 MHZ; wavelength = 19.05 cm,
- L2 is created by multiplying the frequency by 120. It is at frequency = 1227.60 MHZ; wavelength = 24.45 cm, and
- L5 is created by multiplying the frequency by 115. It is at frequency = 1176.45 MHZ; wavelength = 25.48 cm

The reason for the second signal is for calibration of the delay of the signal in the Earth's ionosphere (Blewitt, 1997). On the other hand;

- L2C is a civilian-use signal, to be broadcast on the L2 frequency (1227.60 MHZ), which to be transmitted on a frequency other than the L1 frequency used for the coarse/acquisition (C/A) signal.
- L1C is a civilian-use signal, to be broadcast on the L1 frequency (1575.42 MHZ), which contains the C/A signal used by all current GPS users.

Spectra of the GPS signals (L1, L2 and L5) with GPS modernization project is presented in Figure 2.4. The new signals which are added with GPS modernization program could be of limited use until they are broadcasted from 18 to 24 satellites:

- L2C = The first GPS satellite featuring L2C launched in 2005. Every GPS satellite fielded since then has included an L2C transmitter.
- L5 = The first GPS satellite featuring L5 launched in 2010. It is planned to give service with 24 satellite until 2021.
- L1C = The first GPS satellite featuring L1C launched in 2016. It is planned to give service with 24 satellites until 2026 (Global Positioning System, 2017).
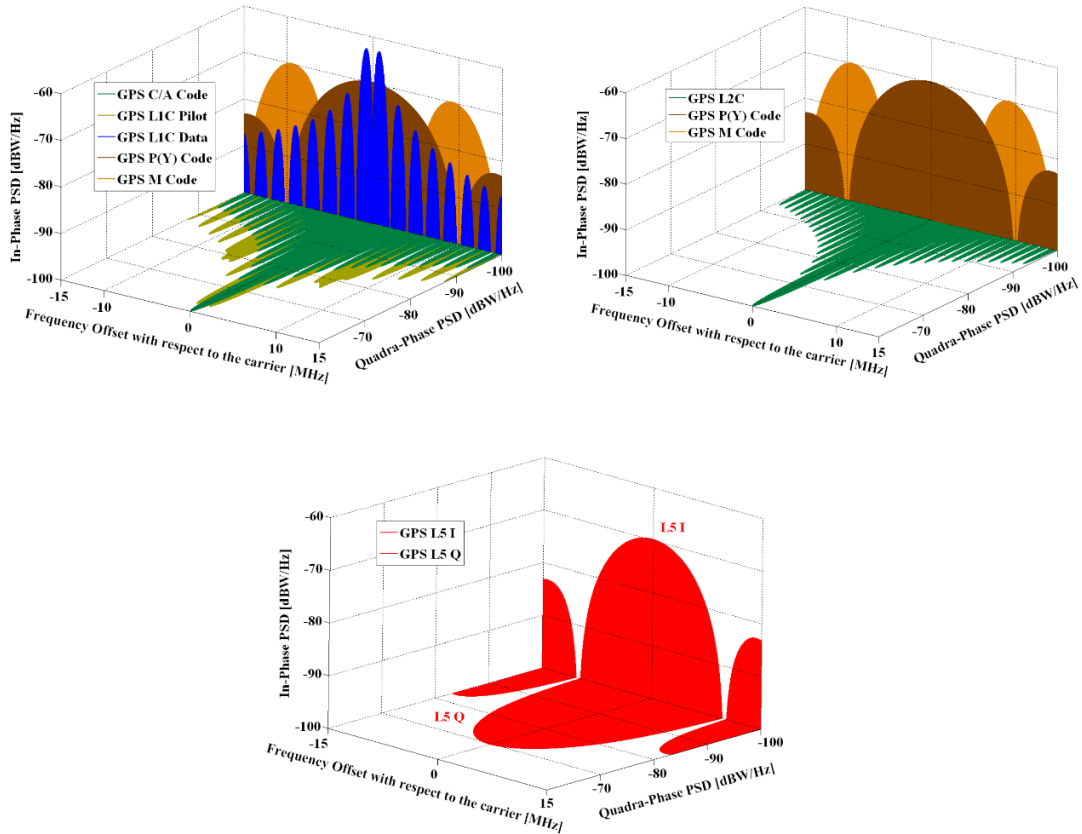
*Figure 2.4: GPS signal modernization project.*

**L2C**

L2C is a new civil signal on carrier L2 that designed to meet commercial needs. It is composed of the L2CM-code (moderate-length code) and the 75 times longer L2CL-code (long-length code). The L2CM-code has a length of 20 milliseconds and counts 10 230 chips. The L2CL-code has a length of 1.5-second and counts 767 250 chips (Hegarty, 2014).

When L2C combined with L1 C/A in a dual-frequency receiver enables ionospheric correction, a technique that boosts accuracy. Civilians with dual-frequency GPS receivers can perform the same accuracy as the military. Also, L2C enables faster signal acquisition, enhanced reliability, and greater operating range by existing dual-frequency operations for professional users. L2C broadcasts has a higher effective poser than L1 C/A signal. It makes easier to receive signal under trees and even indoors (Global Positioning System, 2017).

14

**L5**

L5 is a new civilian signal that designed to meet demanding requirements for safety-of-life transportation and other high-performance applications. L5 broadcast is exclusively reserved for aviation safety services. It has higher power, greater bandwidth, and an advanced signal design. The future planes will use L5 in combination with L1 C/A to improve accuracy (via ionospheric correction) and robustness (via signal redundancy) (Global Positioning System, 2017).

**L1C**

L1C is a new civilian signal that is designed to enable interoperability between GPS and international satellite navigation systems. L1C is different from L1 C/A. L1C features a multiplexed binary offset carrier (MBOC) modulation scheme that enables international cooperation.  The design will improve mobile GPS reception in cities and other challenging environments. The United States and Europe agreed to develop L1C as a common civil signal for GPS and Galileo. In this way the combined use of both systems will be facilitated. Japan's Quasi-Zenith Satellite system (QZSS) and China's BeiDou system that are also adopting L1C similar signals (Hegarty, 2014).

### *2.1.3.1 Codes*

Information is encoded in the form of binary bits on the carrier signals by a process known as phase modulation. The GPS signals are composed of three components:

- C/A (Coarse/Acquisition) code;
- P-code (precise);
- Navigation data and
- M-code.

## C/A code

The C/A code is modulated on the L1 channel. This is a code sequence repeats every 1 ms. It is a pseudo-random noise (PRN) code, which is a randomly generated binary sequence, but is in fact generated by a known algorithm. Each satellite has a unique PRN sequence for satellite identification (GPS receivers can identify which satellite is transmitting a particular code). The carrier can transmit the C/A code at 1.023 Mbps (million bits per second). The "chip length", or physical distance between binary transitions (between digits +1 and −1), is 293 meters. The C/A code contains the time according to the satellite clock when the signal is transmitted. The C/A code is available for military and civilian users and provides Standard Positioning Service (SPS). Users can reach 15 meters horizontal accuracy 95% of the time by using the Standard Positioning Service (Blewitt, 1997).

## P code

The P (precise) code is modulated on both, L1 and L2 channel. the P code is better for more precise positioning than the C/A code. The carrier can transmit the P code at 10.23 Mbps, with a chip length of 29.3 meters. The P code repeats every 267 days. The code is reset every 7 days. Each satellite transmits a unique "PRN" for weekly segments of the P code. The P code provides the satellite clock time or transmission like the C/A code. Unlike the C/A code, the P code has ten times more resolution for military. Because it is used for military purposes, P code is encrypted by a process known as "Anti-Spoofing", or "A/S" (Blewitt, 1997).

Anti-Spoofing (A/S) is encryption for the P code. It is necessary for the military in order to prevent the enemies from imitating a GPS signal. Because of A/S, inaccessible P code is not a significant problem for the civilian users, since precise GPS techniques can measure the phase of the carrier signal itself, rather than to deliver the pseudoranges from the P code. Modern geodetic receivers can form 2 precise pseudorange observables on the L1 and L2 channels, even not having full access to the P code. However, the phase noise of the L2 carrier phase can increase from 1 mm to 1 cm for some types of receivers. This can be negligible on long sessions for static positioning. However, it can have noticeable effect on short sessions, or on kinematic positioning. Also, the signal could

have larger disruption at low elevations (up to 2 cm) where signal strength is at a minimum as expected (Blewitt, 1997).

**Navigation Message**

The Navigation Message is modulated on the L1 channel. It is transmitted at 50 bps. The Navigation Message is transmitted with very slow rate comparing to others. It is a 1500 bits sequence. Therefore, it takes 30 second to transmit. The Navigation Message includes information on the Broadcast Ephemeris (satellite orbital parameters), satellite clock corrections, almanac data (a crude ephemeris for all satellites), ionosphere information, and satellite health status (Blewitt, 1997). This information is necessary in order to perform the position service.

**M-Code**

A major component of the modernization process is a new military signal. Called the Military code, or M-code, it was designed to further improve the anti-jamming and secure access of the military GPS signals. M-code is transmitted in the same L1 and L2 frequencies already in use by the previous military code, the P(Y)-code. The new signal is shaped to place most of its energy at the edges (away from the existing P(Y) and C/A carriers). Very little has been published about this new, restricted code. It contains a PRN code of unknown length transmitted at 5.115 MHz. Unlike the P(Y)-code, the M-code is designed to be autonomous, meaning that a user can calculate their position using only the M-code signal. From the P(Y)-code's original design, users had to first lock onto the C/A code and then transfer the lock to the P(Y)-code.

## 2.2   Other Global Navigation Systems

In addition to the very well-known and widely used NAVSTAR GPS, there are other GNSSs. The Russian GLONASS system modernized and fully operated as GPS. The European satellite navigation system Galileo and Chinese BeiDou Navigation System are still under development. Galileo and BeiDou will be planned to be fully operational by 2020. India is working on Indian Regional Navigation Satellite system (IRNSS), and Japanese are processing on Quasi-zenith

satellite system. IRNSS and Quasi-zenith are planned to be regional navigation and augmentation systems.

This section provides brief description of GLONASS, Galileo, BeiDou, IRNSS and Quasi-zenith satellite systems in order to understand their constellation and services.

## 2.2.1 GLONASS

The development of GLONASS has been started by the former Union of Soviet Socialist Republics (USSR) in 1976, three years after the start of the GPS program. Nowadays, the program working under the Russian Federal Space Agency. GLONASS is an acronym of "Global'naya Navigatsionnaya Sputnikovaya Sistema" which translated to its English equivalent, "Global Navigation Satellite System". The purpose of GLONASS is well defined in the GLONASS interface control document released by the Coordination Scientific Information Center (2008): *"to provide unlimited number of air, marine, and any other type of users with all-weather three-dimensional positioning, velocity measuring and timing anywhere in the world or near-earth space."*. Surely, "on a continuous basis" has to be added to this definition.

GLONASS is operated by Russian military forces. When the nominal satellite constellation is completed at 1996, GLONASS was available for civil users but restricted to one signal. Since that time, the Russian government declared open access and free use of the standard positioning service for civil users (United Nations, 2004).

### 2.2.1.1 Reference Systems

**Coordinate System**

PZ-90.02 is the standard Ministry of Defense of the Russian Federation definition of global reference system for geospatial information and a reference system for GLONASS. It is compatible with ITRS as WGS 84. PZ-90.02 is an Earth-centered, Earth-fixed reference system and geodetic datum. Definition of frame is presented as follows:

- The origin is located in the center of Earth mass.
- The Z-axis is directed towards the Earth's poles as defined by the International Earth Rotation Service (IERS) and the International Bureau of time (BIH).
- The X axis is directed to the point of intersection of the equator and the prime meridian established by the International Bureau of the time (BIH).
- The Y-axis completes the system to the right-handed one.
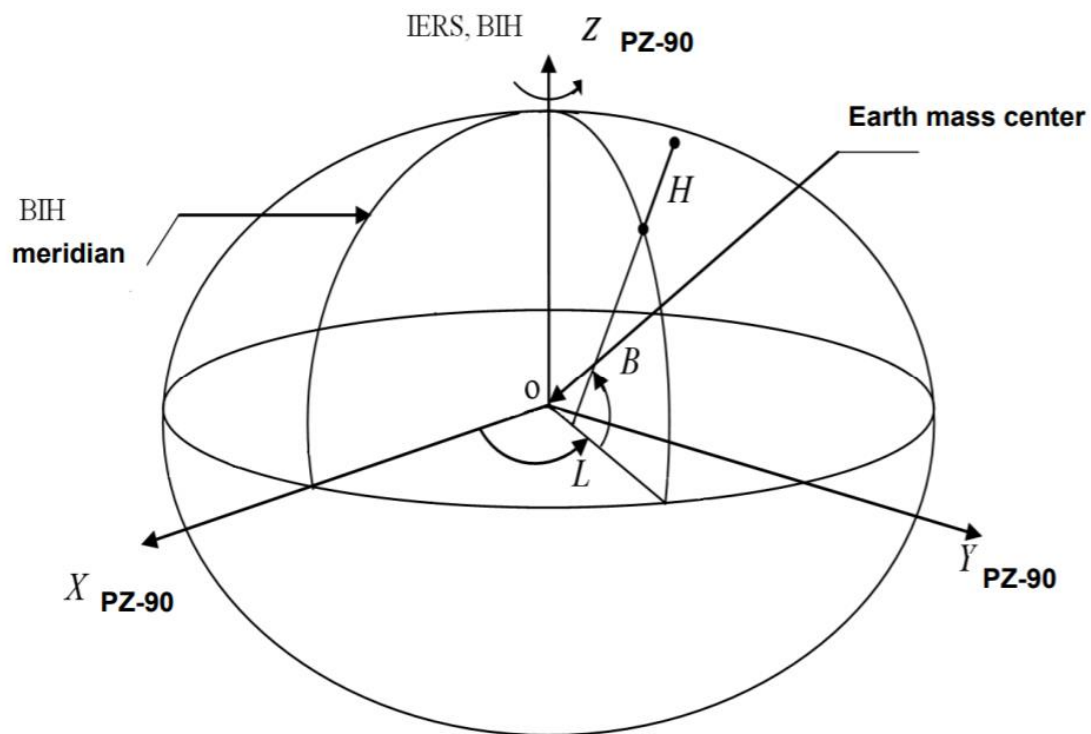


*Figure 2.5: PZ-90 Global reference system (Vdovin & Dorofeeva, 2012)*

Geodetic constants and significant parameters of the terrestrial ellipsoid PZ-90.02 are given in Table 2.2.

*Table 2.2: Geodesic constants and parameters of ellipsoid PZ 90*

| | |
|---|---|
| Angular velocity of the earth ($\omega_e$) wrt vernal equinox | 7,292115x$10^{-5}$ rad/s |
| Earth gravitational constant ($\mu$) | 398 600,4418$\times 10^9$ m$^3$ /s$^2$ |
| Gravitational constant of atmosphere (fMa) | 0.35$\times$109 m$^3$ /s$^2$ |
| Speed of light (c) | 299 792 458 m/s |
| Semi-major axis (a) | 6 378 136 m |
| Flattening (f) | 1/298,257 84 |
| Equatorial acceleration of gravity | 978 032,84 mGal |
| Correction to acceleration of gravity at sea-level due to Atmosphere | 0,87 mGal |
| Normal potential at surface of common terrestrial ellipsoid (U0) | 62 636 861,4 m$^2$ /s$^2$ |

**Time System**

The GLONASS time is generated on a base of GLONASS Central Synchronizer time which has a daily instability is better than $2 \times 10^{-15}$. The time scales of the GLONASS satellites are periodically compared with the GLONASS Central Synchronizer hydrogen clocks time scale. Corrections to each onboard time scale relative to GLONASS time and UTC is recomputed and uploaded to the satellites twice a day by a control segment (Coordination Scientific Information Center, 2016).

The GLONASS time has a constant offset of three hours with respect to UTC which is implementing the difference between Moscow time (UTC) and Greenwich time (UTC). Apart from the constant offset, there is leap seconds for the GLONASS time. This difference between GLONASS time and UTC should be within 1 millisecond. The navigation message contains the information on this difference by the parameter $\tau_c$. Thus, UTC can be computed from GLONASS time by

$$UTC = GLONASS\ time\ +\ \tau_c - 3^h \tag{2.3}$$

The correction of the GLONASS time because of leap seconds is carried out in agreement with the UTC corrections as performed by the Bureau International de l'Heure in Paris. Users may get the information on the intended correction in advance (at least three months ahead of the occurrence) via bulletins and notifications. These corrections are performed once a year

(Coordination Scientific Information Center, 2016). Due to the leap second correction there is no integer-second difference between GLONASS time and UTC except constant three hours difference.

## 2.2.1.2 GLONASS Segments

GLONASS system contains three segments as GPS:

- The space segment: Constellation satellites around the earth
- The control segment: Ground-based control facilities
- The user segment: User equipment

The GLONASS constellation consists of 21 active satellites plus 3 active on orbit spares. The 24 satellites are located in three orbital planes 120° apart in right ascension. 8 satellites are equally spaced in each plane with argument of latitude displacement 45°. The performance of all 24 satellites is monitored by GLONASS control segment and the best 21 are activated. The remaining three is held for back up or in reserve. Each GLONASS satellite is in a 19,100 km altitude circular orbit with an inclination of 64.8°. The orbital period is 11 hours and 15 minutes (Feairheller & Clark, 2006). This constellation assures that at least five satellites are simultaneously visible on 99% of the sites on the earth (Habrich, 1999).

The main tasks of the control segment are: tracking of the satellites for the orbit and clock determination and prediction, upload of the navigation message to the satellites, time synchronization of the satellites, and controlling the offset between GLONASS system time and UTC. The control segment also performs non-operational activities, such as procurement and launch activities.

The control segment contains the System Control Center, and the network of the Command and Tracking Stations that are located in Russia (Coordination Scientific Information Center, 2016).

User equipment consists of receives and processors receiving and processing the GLONASS navigation signals, and allows user to calculate the coordinates, velocity and time.

## 2.2.1.3 GLONASS Signal Structure

L-frequency range radio links are used as an interface between space segment and user equipment. According to GLONASS interface control document (Coordination Scientific Information Center, 2016), GLONASS space segment satellites, "Glonass" and "Glonass-M" transmits navigational radio signals in two frequency sub-bands: L1 ~ 1,6 GHz, and L2 ~ 1,25 GHz. Additionally, the third carrier frequency is announced in various publications.

GLONASS satellites continuously transmit the standard accuracy signal (C/A-code) and the high-accuracy signal (P-code) on two carrier frequencies, L1 and L2. Similar to GPS, the C/A-code is only modulated onto L1, whereas the P-code is modulated onto L1 and L2. Additional information has been placed in the navigation message (Hofman-Wellenhof, Lichtenegger, & Wasle, 2008). Ranging code is a sequence of maximum length of shift register with a period 1 millisecond and bit rate 511 kbps. Navigation message transmitted at 50 bps, and 100 Hz auxiliary meander sequence (GNSS science support centre - eESA, 2014).

GLONASS implements the frequency division multiple access (FDMA) technique to differentiate between the signals of different satellites. According to GLONASS interface control document (Coordination Scientific Information Center, 2016), the GLONASS signals are more resistant against narrowband interference, also the cross-correlation between different GLONASS signals is low, despite short ranging codes with FDMA. On the other hand, FDMA requires radio frequency front-end components with extra-wide bandwidths. FDMA is a different technique from Code Division Multiple Access (CDMA), used by GPS.

The carrier frequencies and all timing processes are derived from the atomic frequency standards. The FDMA design requires unique carrier frequencies for all satellites defined by

$$f_{1k} = f_1 + \Delta f_1 k = 1602.0000 + 0.5625\ k \quad [MHz] \qquad (2.4)$$

$$f_{2k} = f_2 + \Delta f_2 k = 1246.0000 + 0.4375\ k \quad [MHz] \qquad (2.5)$$

where k differentiates the frequency channels. The factors Δf1, and Δf2 denote the frequency increments of satellite signals in two channels.

## 2.2.2  Galileo

Galileo is Europe's Global satellite Navigation System, designed to be compatible with all existing and planned GNSS. It is planned to be interoperable with GPS and GLONASS, while providing autonomous navigation, positioning and timing information.  While GPS (U.S. Air Force), GLONASS (Russian Minister of Defense), BeiDou (China Satellite Navigation Office – view section 2.2.3.) and the regional satellite navigation system developed by Japan, "QZSS", are military system under military control; Galileo is a civil-controlled system. As mention in Galileo signal in space interface control document (European Union, 2018), *"Galileo is a joint initiative of the European Commission (EC), European Global Navigation Satellite System Agency (GSA) and the European Space Agency (ESA).".*

Galileo started to provide initial services to the public, "Early Operational Capability", on December 15th, 2016. It is expected to reach Full Operational Capability in 2019. When Galileo reach fully operational phase, it will provide four services worldwide:

- Open Service (OS): It is open and free-charge service to the users. Service provides positioning and synchronization information for the satellite radio navigation applications with 1 meter positioning accuracy.
- Commercial Service (CS): It is encrypted and more accurate than OS, to the nearest centimeter positioning accuracy. It will be provided by an additional navigation signal and added-value services in a different frequency band.
- Public Regulated Service (PRS): It is restricted to government-authorized users, for sensitive applications which require a high level of service continuity (security and strategic infrastructure such as energy, telecommunications and finance).
- Search and Rescue Service (SAR): It is Galileo's worldwide search and rescue service for international satellite-based search and rescue distress alert detection.

(GNSS science support centre - eESA, 2018).


The fully operational Galileo system will consist 30 satellites (24 in full service and 6 spares) in Medium Earth Orbit (MEO) at an altitude of 23,222 km. The satellites will occupy each of three orbital planes inclined at an angle of 56° to the equator. The satellites will be spread evenly around

each plane and will take about 14 hours to orbit the Earth. Two satellites in each plane will be a spare; on stand-by should any operational satellite fail (GNSS science support centre - eESA, 2018).

The Galileo ground segment consists of two Galileo Control Centers situated in Oberpfaffenhofen (Germany) and Fucino (Italy), a network of Telemetry, Tracking and Control stations, a network of Mission Uplink Stations, and a network of Galileo Sensor Stations.

## Reference system of Galileo

The Galileo terrestrial reference frame (GTRF) will be global reference system for geospatial information and reference system for Galileo. GTRF will be closely related to the international terrestrial reference frame (ITRF), which has been established by the International Earth Rotation Service (IERS) (Hein & Pany, 2002). The GTRF is specified to difference from the latest version of ITRF by less than 3 centimeters (2$\sigma$). This will be ensured by the Galileo Geodetic Service Provider (GGSP). Also, the GGSP is responsible for the involvement of the geodetic community during the definition, implementation, and maintenance of GTRF (Swann, 2006).

The Galileo system time (GST) is a continuous atomic time scale with a nominal constant offset (i.e., integer number of seconds) with respect to the international atomic time (TAI). With respect to the coordinated universal time (UTC), the modulo 1 second offset is variable due to the insertion of leap seconds (Hofman-Wellenhof, Lichtenegger, & Wasle, 2008).

## Signals of Galileo

As it is mentioned in Galileo signal in space interface control document (European Union, 2018), the Galileo navigation Signals are transmitted in the four frequency bands (indicated in Table 2.3): E1, E6, E5a and E5b bands. The E5a and E5b signals are part of the E5 signal in its full bandwidth. While the Galileo's carrier frequency E5a coincides with the GPS carrier frequency L5, the Galileo's frequency band E1 includes the carrier frequency L1 of the GPS system as shown in Table 2.3.

| E1 | Carrier frequency 1575.420 MHz; also denoted as L1 (US denomination) |
|---|---|
| E6 | Carrier frequency 1278.750 MHz |
| E5 | Carrier frequency 1191.795 MHz; also denoted as E5a+E5b |
| E5a | Carrier frequency 1191.795 MHz; also denoted as E5a+E5b |
| E5b | Carrier frequency 1207.140 MHz |
| SAR downlink | Frequency band 1 544.050–1 545.150 MHz |
| SAR uplink | Frequency band 406.0–406.1 MHz |

### 2.2.3  BeiDou Navigation System (BDS)

The BeiDou Navigation Satellite Demonstration System is a Chinese satellite navigation system managed by China Satellite Navigation Office. China Satellite Navigation Office presents the preparation, revision, distribution, and retention of BeiDou Navigation Satellite System Signal In Space Interface Control Document. Information in this section is organized according to Space Interface Control Document (China Satellite Navigation Office, 2017) and China's BeiDou Navigation Satellite System (The State Council Information Office of the People's Republic of China, 2016).

The construction and development of BeiDou Navigation Satellite System (BDS) is divided into three phases: BDS-1, BDS-2, and BDS-3 in sequence:

- The first step, the constructing the BDS-1 includes the launching of two Geostationary Earth Orbit (GEO) satellites which were completed and put into operation in 2000. The system provides the positioning, timing, wide-area differential and short message communication services. The third GEO satellite was launched in 2003, in order to enhance the system's performance.
- The second step, the constructing the BDS-2 includes the launching of 14 satellites (5 GEO satellites, 5 Inclined Geosynchronous Satellite Orbit (IGSO) satellites and 4 Medium Earth Orbit (MEO) satellites) in order to finish the space constellation deployment. BDS-2 step

of project is completed in 2012. The BDS-2 which is compatible with BDS-1, adds the passive-positioning scheme, and provides the positioning, velocity measurement, timing, wide-area differential and short message communication services in the Asia-Pacific region.

- The third step, the constructing the BDS-3 is planned the launch of 35 satellites in order to provide basic services to global users.

**Coordinate System**

BDS adopts the BeiDou Coordinate System (BDCS) which has the same ellipsoid parameters of the China Geodetic Coordinate System 2000 (CGCS2000), which is defined as follows:

- The origin is located at the Earth's center of mass.
- The Z-Axis is the direction of the IERS Reference Pole (IRP).
- The X-Axis is the intersection of the IERS Reference Meridian (IRM) and the plane passing through the origin and normal to the Z-Axis.
- The Y-Axis, together with Z-Axis and X-Axis, constitutes a right-handed orthogonal coordinate system.
- The length unit is the international system of units (SI) meter.

The BDCS is compatible with the international terrestrial reference frame (ITRF). The parameters of the BDCS Ellipsoid are shown in Table 2.4.

*Table 2.4: Parameters of the BDCS ellipsoid*

| Parameter | Definition |
|---|---|
| Semi-major axis | $a = 6378137.0$ m |
| Geocentric gravitational constant | $\mu = 3.986004418\ 10 \times m^3 /s^2$ |
| Flattening | $f = 1/298.257222101$ |
| Earth's rotation rate | $\Omega_e = 7.2921150 \times 10^{-5}$ rad/s |

**Time System**

The time reference of BDS is named as the BeiDou Navigation Satellite System Time (BDT). BDT uses the international system of units second as the base unit and accumulates continuously without leap seconds. The start epoch of BDT is 00:00:00 on January 1, 2006 of Coordinated Universal Time (UTC). BDT connects with UTC and the deviation of BDT to UTC is maintained within 50 nanoseconds. The leap second information is broadcast in the navigation message.

## 2.3   Fundamentals of Satellite Positioning

GNSS receivers are designed to locate the three-dimensional space position by calculating a mathematical process called trilateration. Trilateration method determines the object's position by measuring distances from other objects with known locations. In this case, the GNSS receiver has to know "the satellites locations in space" and "the distance between each satellite and the receiver" in order to calculate the receiver location (G S, 2010).

### 2.3.1   Determination of Satellites Locations in Space

The satellites broadcast two types of data, almanac and ephemeris. Each satellite broadcasts almanac data for all satellites. This almanac data contains the approximate orbit of the satellite and is considered valid for up to several months. Ephemeris data contains the more precise orbital and clock correction for each satellite and is necessary for precise positioning. Each satellite broadcasts only its own ephemeris data. This data is only considered valid for about 30 minutes. The ephemeris data is broadcast by each satellite every 30 seconds.

Additionally, International GNSS Service (IGS) analysis center provides satellite orbit solutions sub-daily, daily, or weekly, depending upon the data product. The IGS analysis center retrieves these solutions and produces combined products, which are ultra-rapid, rapid, and final. The ultra-rapid product, useful for real-time and near real-time applications, at regular intervals four times per day; the ultra-rapid solution includes both observed and predicted satellite orbits. The rapid orbit combination is a daily solution available approximately 17 hours after the end of the previous UTC day. The final, and most consistent and highest quality IGS solutions, consists of daily orbit files, generated on a weekly basis approximately 13 days after the end of the solution week.

## 2.3.2 Determination Distance Between Each Satellite and The Receiver

GPS receivers determine the distance between each satellite and the receiver by using signal travel time or "transit time". By using basic physics formula: *"The distance from a given satellite to the object equals the velocity of the transmitted signal multiplied by travel time of radio waves transmitted from satellites to reach the object (transit time)"* as shown below;

$$P_R^S(t) = \Delta t_R^S \times c \qquad\qquad (2.6)$$

$PR_S(t)$ : pseudorange between satellite and receiver

$\Delta t_S^R$  : travel time between receiver and satellite

c     : speed of the radio wave, $3 \times 10^8$ m/s

Equation above (2.6) is practically impossible, because the satellites clocks and GPS time cannot be perfectly synchronized, or it is impossible to know the offset of each clock with respect to GPS time. The offset between satellites clocks ($t^S$) and GPS time ($t^{GPS}$) can be defined as follows, Equation (2.7):

$$dt^S = t^S - t^{GPS} \qquad\qquad (2.7)$$

The offset of satellites clocks can be accurately enough described by a polynomial of second order in time, Equation (2.8):

$$dt^S(t^{GPS}) = dt_0^S + a^S t^{GPS} + b^S t_{GPS}^2 \qquad\qquad (2.8)$$

Because the receiver clock experiences an offset, $dt_R$, as shown on Equation (2.9):

$$P_R^S(t) = c\Delta t = c\tau + c(dt_R - dt^S) \qquad\qquad (2.9)$$

$\tau$: is the travel time

$\Delta t$: is the measured time

The GPS receiver knows the velocity of signal; however, the GPS receiver has to estimate signal's travel time from the satellite to the receiver. The GPS receiver can determine the time signal reached to the receiver by checking its internal time. However, it is more complicated to define travel time. The satellite generates and transmits Pseudo Random Noise (PRN) code. When a satellite generates the PRN code, the GPS receiver memories and generates the same code and tries to synchronize it to satellite's code. The receiver compares the both codes to identify how much delay (shift) needed in order to synchronize them. This delay time (shift) is defined as travel time ($\Delta t$). Therefore, the distance equal to the delay time (shift) ($\Delta t$) multiplied by the velocity of signal (c) (G S, 2010).
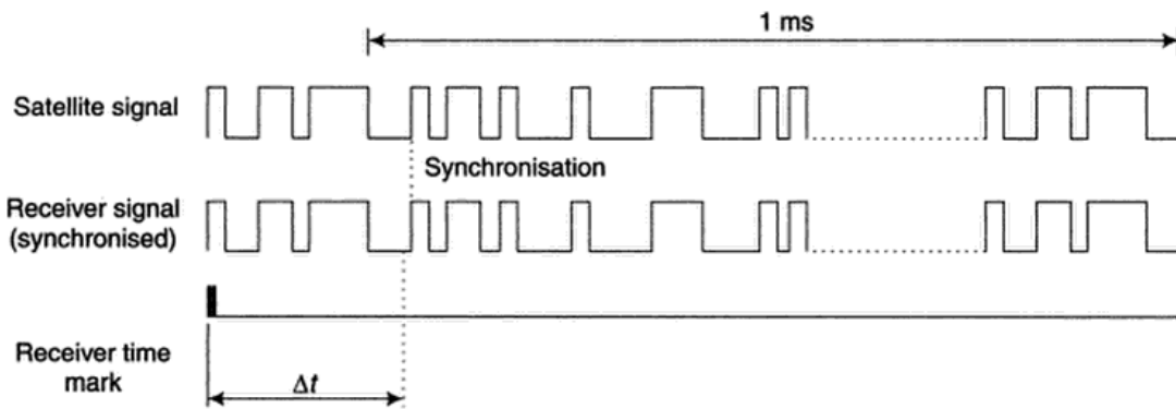


*Figure 2.6: Measuring signal travel time (G S, 2010)*

## 2.3.3  Determination Receiver Position in 3-D

After receiver calculate the distance measurements, it is time to define receiver location. It is a mathematical process called trilateration. At least four satellites are required to define the position in 3-D space.

If the GPS receiver knows only one satellite's position and the distance between the receiver and the satellite, user position can be anywhere on the surface of the sphere, as shown on Figure 2.7 at the left side.  From Figure 2.7, GPS receiver is somewhere on a sphere which centered by satellite A and with the diameter 20.000 km.
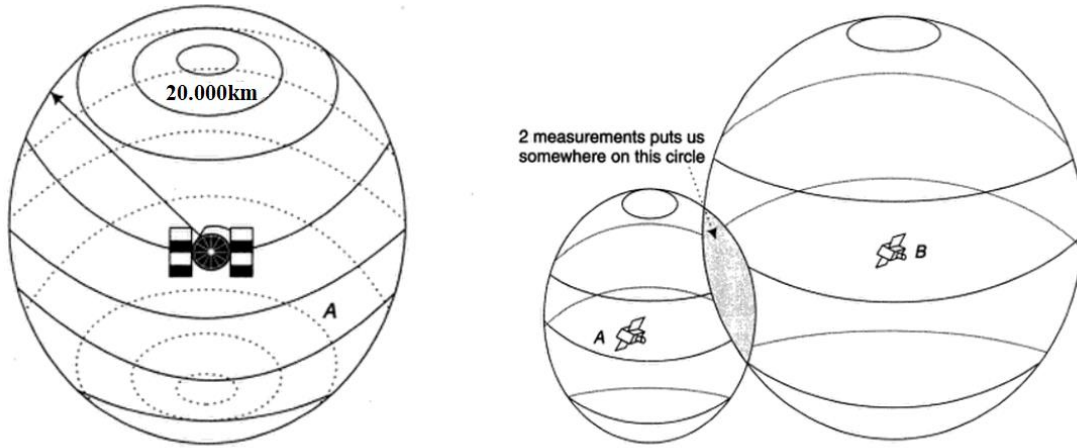
*Figure 2.7: 3D position determination using a single satellite (left side) and 2 satellites (right side)*

If the GPS receiver knows two satellites' position and their distance to GPS receiver, location of the receiver will be somewhere on the circle of intersection of two spheres with radiuses $\rho_A$ and $\rho_B$, shown as Figure 2.7 at the right side.

If the GPS receiver knows three satellites' position and their distance to GPS receiver, location of the receiver will be one of the two points where the three spheres intersect, as shown at Figure 2.8.
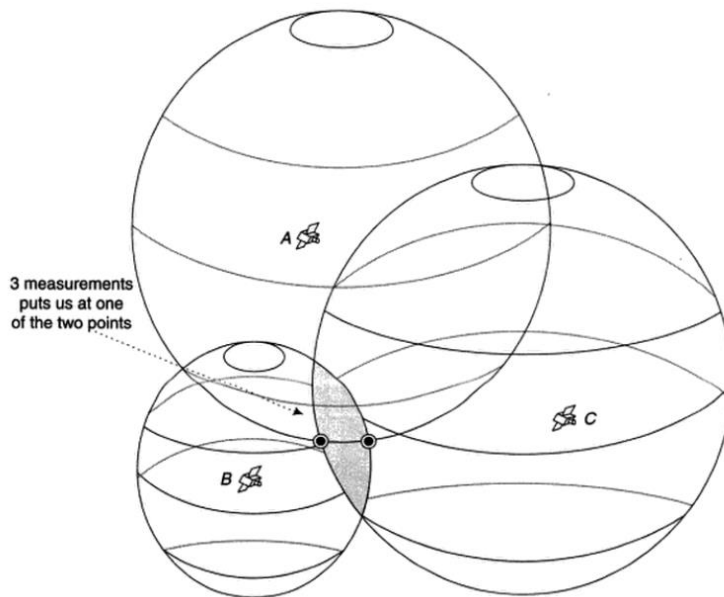


*Figure 2.8: 3D position determination by using 3 satellites*

30

Mostly, for 3-D position determination by using 3 satellites, only one solution will be visible in practice. Other one may be outside of the operational area (i.e. in space or inside the earth). Adding fourth satellite to calculations is needed to correct for clock error, $dt_R$.

## 2.3.4 Carrier Phase Observation Model

All current GNSS satellites transmit signals in the L-band. These signals consist of a carrier modulated by a PRN code. The phase of a signal is fundamentally a property of sinusoids. Every sinusoid has an amplitude and a phase and can be written in complex notation as $A_{\exp} j(\omega t + \theta)$, where $A$ is the amplitude, $\omega$ is the radial frequency, and $\theta$ is the phase in radians at $t = 0$.

When the carrier is modulated by a PRN code, the resulting signal is no longer a pure sinusoid; however, can be expressed as a linear combination of sinusoids by Fourier's Theorem. If the receiver can estimate the received RF phase, then three unknowns remain that must be estimated in order to determine the range. These are:

1. The receiver time $t_R$;
2. The initial satellite phase offset $\phi^S$ and
3. The integer number of cycles between satellite and receive.

In most carrier phase processing applications, the effects of the first two are removed by differencing of observations; differencing between satellites removes errors in the receiver time component, while differencing between receivers removes errors in the satellite phase offset.

In the following sections, carrier phase will be described, modelled and analyzed in terms of performing relative positioning. "Basic of the GPS technique: Observation equation" document used as reference for section (Blewitt, 1997).

**The carrier phase measurement**

As mention in Carrier phase and its measurement for GNSS document; the carrier phase measurement is a measure of the range between satellite and receiver expressed in units of cycles (the number of wavelengths of the signal) of the carrier frequency. The carrier phase measurement

is used for high precision applications (order of millimeters). However, the whole number of cycles between satellite and receiver is not measurable (O'D Riscoll, 2010).
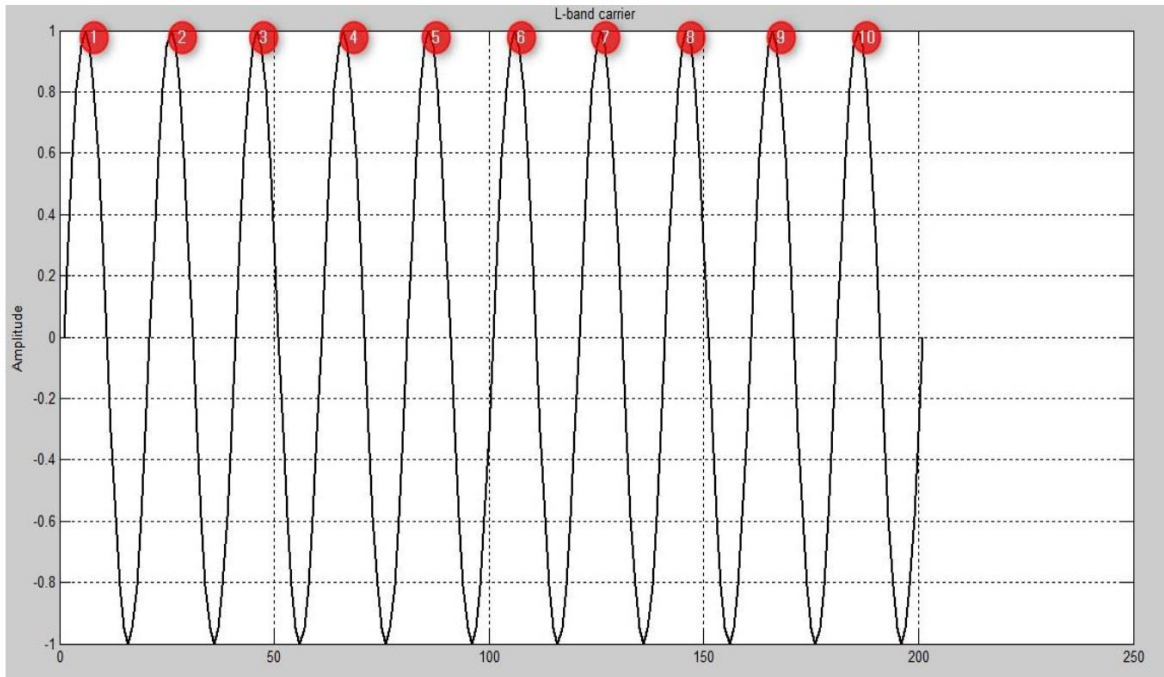


*Figure 2.9: Received L-band carrier signal (in red, number of cycles)*

"Phase" is simply "angle of rotation," which is in units of "cycles" for GPS analysis. As shown in Figure 2.10, consider a point moving anti-clockwise on a circle, and draw a line from the center of the circle to the point. The phase $\phi(t)$ at any given time $t$ can be defined as the angle through which this line has rotated.

Phase is related with the concept of time, which is always based on some form of periodic motion, such as the rotation of the Earth, the orbit of the Earth around the Sun (dynamic time), or the oscillation of a quartz crystal in a wristwatch (atomic time). Angles of rotation give the measure of time. In this way, phase can be thought of as a measure of time (after conversion into appropriate units). We can write this formally as:

$$T(t) = k(\varphi(t) - \varphi_0) \qquad (2.10)$$

Where $T(t)$ is the time according to the clock at time $t$, $\phi_0 = \phi(0)$ is so that the clock reads zero when $t = 0$, and $k$ is a calibration constant, converting the units of cycles into units of seconds. Indeed, we can take the above equation as the definition of clock time.

The "frequency," expressed in units of cycles per second, is the number of times the line completes a full 360° rotation in one second (which is generally a fractional number). One can better define frequency instantaneously as the first derivative of phase with respect to time; that is, the angular speed.

$$f \equiv \frac{d\varphi(t)}{dt} \qquad (2.11)$$

Constant frequency is the basis of an ideal clock. If the frequency can be written as a constant, $f_0$, then we can write the phase of an ideal clock as:

$$\varphi_{ideal} = f_0 t + \varphi_0 \qquad (2.12)$$

Therefore,

$$T_{ideal} = k f_0 t \qquad (2.13)$$

An appropriate choice for the calibration constant is $k = 1/f_0$, where $f_0$ is the nominal frequency of the oscillator. Going back to original equation for clock time, we can now define clock time as:

$$T(t) = \frac{\varphi(t) - \varphi_0}{f_0} \qquad (2.14)$$
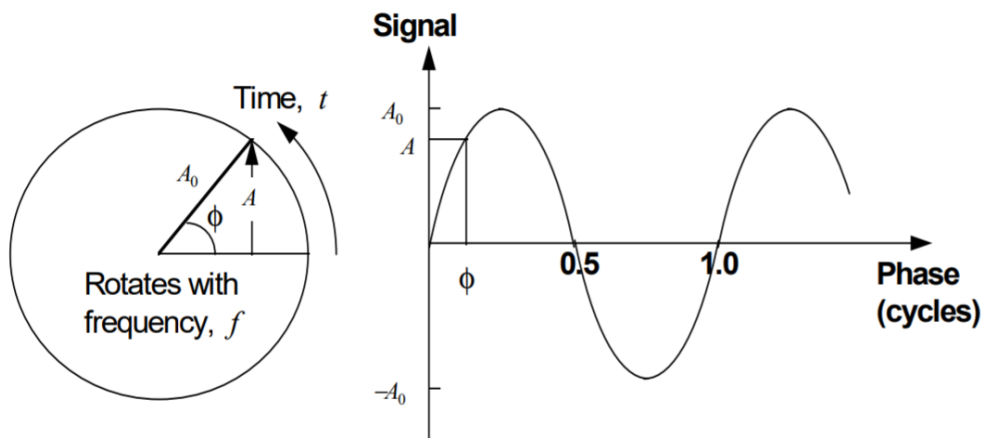


Figure 2.10: The meaning of the phase (Blewitt, 1997)

At time t, the height of point A(t) above the center of the circle in Figure 2.10 is given by:

$$A(t) = A_0 \sin[2\pi\varphi(t)] \tag{2.15}$$

Where $A_0$ is the radius of the circle. Since the concept of phase is applied to periodic signals, $A(t)$ can be called "the signal" and $A_0$ can be called "the amplitude of the signal". For example, in the case of radio waves, $A(t)$ would be the strength of the electric field, which oscillates in time as the wave passes by. Inverting the above formula, we can therefore determine the phase $\phi(t)$ if we measure the signal $A(t)$ (and similarly, we could infer the clock time). For an ideal clock, the signal would be a pure sinusoidal function of time:

$$A_{ideal} = A_0 \sin 2\pi\varphi_{ideal} \tag{2.16}$$

$$A_{ideal} = A_0 \sin(2\pi f_0 t + 2\pi\varphi_0) \tag{2.17}$$

The range between satellite and user receiver is in units of cycles of the carrier frequency but in the model an integer number of cycles $N$ is missing. To deal with this, the following assumption holds true. There is no way of knowing which integer N to add to this recorded phase. So, it really did equal the difference in phase between the replica signal ($\varphi_R$) and the GPS signal ($\varphi_G$). This is fundamentally because we have no direct measure of the total phase of the incoming GPS signal. We can express this as follows:

$$\Phi + N = \varphi_R - \varphi_G \tag{2.18}$$

Capital $\Phi$ emphasize the phase value actually recorded by the receiver. Provided the receiver does keep track of how many complete signal oscillations there have been since the first measurement, it can attach this number of cycles to the integer portion of the recorded beat phase. However, there will still be an overall ambiguity N that applies to all measurements.

If there are some kind of geometrical interpretation for $N$, the unknown value of N can be written as:

$$N = (integer\ portion\ of\ \varphi_R - \varphi_G) - (integer\ portion\ of\ \Phi) \tag{2.19}$$

The second term is completely arbitrary and depends on the receiver firmware. For example, some receivers set this value to zero for the first measurement and drop this term. By assuming the receiver and satellite clocks keep perfect time for interpretation of $N$ as equal to the number of carrier wavelengths between the receiver (at the time it makes the first observation), and the satellite (at the time it transmitted the signal). All these made under assumptions about perfect clocks and the particular nature of the firmware.

**Carrier phase observation model**

The satellite carrier signal is mixed with reference signal generated by receiver's clock. The result, after high pass filtering, is a "beating" signal. The phase of this beating signal equals the reference phase minus the incoming GPS carrier phase from a satellite; however, it is ambiguous by an integer number of cycles. "Carrier beat phase" is not the phase of the incoming signal.

Observation of satellite S produces the carrier beat phase observable $\Phi^S$ :

$$\Phi^S(t) = \varphi(t) - \varphi^S(t) - N^S \qquad (2.20)$$

Where $\phi$ is the replica phase generated by the receiver clock, and $\phi^S$ is the incoming signal phase received from GPS satellite $S$. The measurement is made when the receiver clock time is $t$.

The phase of the incoming signal received at receiver clock time $t$ is identical to the phase that was transmitted from the satellite at satellite clock time $t^S$.

$$\varphi^S(x, y, z, t) = \varphi_{transmit}^S\left(x^S, y^S, z^S, t_{transmit}^S\right) \qquad (2.21)$$

Then the model of how long it takes a wave front of constant phase to propagate from the satellite to the receiver must be considered. Therefore, the appropriate satellite clock time at the time of signal transmission, $t^S$ must be modelled. Before that, the clock time as a function of phase and nominal frequency could be calculated:

$$T(t) = \frac{\varphi(t) - \varphi_0}{f_0} \qquad (2.22)$$

The phase terms with clock times:

$$\varphi(t) = f_0 t + \varphi_0 \qquad (2.23)$$

$$\varphi_{transmit}^S(t^S) = f_0 t_{transmit}^S + \varphi_0^S \qquad (2.24)$$

Therefore, the carrier phase observable becomes:

$$\Phi^S(t) = f_0 t + \varphi_0 - f_0 t^S - \varphi_0^S - N^S \qquad (2.25)$$

$$\Phi^S(t) = f_0(t_R - t^S) + \varphi_0 - \varphi_0^S - N^S \qquad (2.26)$$

It is convenient to convert the carrier phase model into units of range. This simplifies concepts, models, and software. In the range formulation, we multiply the carrier phase equation by the nominal wavelength.

$$L_R^S(t) = \lambda_0 \, \varphi_R^S(t) \qquad (2.27)$$

$$L_R^S(t) = \lambda_0 f_0(t_R - t^S) + \lambda_0 (\varphi_{0R} - \varphi_0^S - N_R^S) \qquad (2.28)$$

$$L_R^S(t) = c(t_R - t^S) + \lambda_0 (\varphi_{0R} - \varphi_0^S - N_R^S) \qquad (2.29)$$

$$L_R^S(t) = c(t_R - t^S) + B_R^S \qquad (2.30)$$

The name carrier phase, $L^S{}_R(T_R)$, is in units of meters. This equation is identical to that for the pseudorange, with the exception of the "carrier phase bias," $B^S{}_R$ which is in units of meters:

$$B_R^S = \lambda_0 (\varphi_{0R} - \varphi_0^S - N_R^S) \qquad (2.31)$$

The first term in the carrier phase model is the pseudorange, and the second term is a constant. We have already developed a model for pseudorange, therefore the model for carrier phase as follows:

$$L_R^S(t) = \rho_R^S(t_R, t^S) + c\big(dt_R(t) - dt^S(t)\big) + T_R^S - I_R^S + B_R^S \qquad (2.32)$$

In the above, the delay on the signal due to the troposphere $T^S{}_R$ and the ionosphere $-I^S{}_R$ (the minus sign indicating that the phase velocity actually increases) included to the model.

Additionally, the model for pseudorange can be shown with the small difference that the ionospheric delay has a positive sign. Because, any information, such as the +1 and -1 "chips" which are modulated onto the carrier wave, must travel with the "group velocity" rather than "phase velocity".

$$L_R^S(t) = \rho_R^S(t_R, t^S) + c\big(dt_R(t) - dt^S(t)\big) + T_R^S + I_R^S \qquad (2.33)$$

The true time of signal reception $t_R$ is unknown and needed to be calculated the satellite-receiver range term $\rho^S{}_R(t_R, t^S)$ precisely. The true time of reception can be written:

$$t_R = t - dt_R \qquad (2.34)$$

The epoch $t_R$ is known, as it is the receiver clock time written into the data file with the observation, hence called the "time-tag". However, the receiver clock bias $dt_R$ is not known initially, but could be as large as milliseconds. Due to satellite motion and Earth rotation, the range will change by several meters over the period of a few milliseconds.

End of the process, the received carrier phase gives information regarding the range between satellite and receiver. The measure of the range is obtained and expressed in units of cycles.

## 2.3.5  Measurement challenges

Tropospheric delay, ionospheric delay, multipath, and antenna phase center offset, and variation will be described and modelled in the following section. "GNSS: GPS, GLONASS, Galileo and more" book (Hofman-Wellenhof, Lichtenegger, & Wasle, 2008) used as reference for formulations on the following.

**Tropospheric delay**

The atmosphere of the earth is categorized into different layers according to their physical properties and influences onto the electromagnetic waves. With respect to the electromagnetic structure, the atmosphere is divided into the neutral atmosphere and the ionosphere. While the neutral atmosphere comprises the troposphere and the stratosphere, the GNSS community abbreviates this to the troposphere and calls the delay due to the neutral atmosphere "tropospheric delay".

The troposphere extends from the earth's surface to about 50 km height. The troposphere is nondispersive for frequencies up to 30 GHz. The tropospheric refractive index is a function of temperature, pressure, and partial water vapor pressure. The latter consists of a dry and a wet component.

The tropospheric path delay is defined by

$$\Delta^{Trop} = \int (n-1)\, ds_0 \qquad (2.35)$$

Usually, instead of the refractive index $n$ the refractivity

$$\Delta^{Trop} = \int N^{Trop}\, ds_0 \qquad (2.36)$$

Hopfield (1969) shows the possibility of separating $N^{Trop}$ into a dry and a wet component,

$$N^{Trop} = N_d^{Trop} + N_w^{Trop} \qquad (2.37)$$

and

$$\Delta^{Trop} = \Delta_d^{Trop} + \Delta_w^{Trop} \qquad (2.38)$$

The corresponding dry component on the surface is

$$N_d^{Trop} = c_1 \frac{p}{T} \qquad (2.39)$$

$$c_1 = 77.64\ K\ mb^{-1} \qquad (2.40)$$

where $p$ is the atmospheric pressure in units of millibar (mb) and $T$ is the temperature in kelvin (K). The wet component on the surface was found to be

$$N_w^{Trop} = c_2 \frac{e}{T} + c_3 \frac{e}{T^2} \qquad (2.41)$$

$$c_2 = -12.96\ K\ mb^{-1}, \qquad c_3 = 3.718 * 10^5\ K^2\ mb^{-1} \qquad (2.42)$$

where $e$ is the partial pressure of water vapor in mb and $T$ again the temperature in K. The overbar in the coefficients only stresses that there is absolutely no relationship to the coefficients for the ionosphere.

The values for $c_1$, $c_2$, and $c_3$ are empirically determined and, certainly, cannot fully describe the local situation. An improvement is obtained by measuring meteorological data at the observation site. meteorological surface data can be considered with several models:

1. Hopfield model (Hopfield , 1969),
2. Modified Hopfield models (Goad, 1974), and
3. Saastamoinen model (Saastamoinen, 1973).

In this paper, these models are not mentioned.

**Ionosphere delay**

The ionosphere is the electrically charged component of the higher atmosphere. It is characterized by its free, neutral, and charged particles, where density varies as a function of the time of day. Therefore, the ionospheric refraction is modeled as a function of the electron density represented by the total electron content (TEC). The TEC is influenced by the solar activity, diurnal and seasonal variations, and the earth's magnetic field. TEC can be modeled on a global and continental level. Small-scale variations of TEC inhomogeneities are not yet possible to predict.

Consider a single electromagnetic wave propagating in space with wavelength $\lambda$ and frequency $f$. The velocity of its phase:

$$v_{ph} = \lambda f \tag{2.43}$$

The wave propagation in a medium depends on the refractive index $n$. The phase and group velocity, appropriate formulas for the corresponding refractive index $n_{ph}$:

$$v_{ph} = \frac{c}{n_{ph}} \tag{2.44}$$

and the refractive index $n_{gr}$:

$$v_{gr} = \frac{c}{n_{gr}} \tag{2.45}$$

The ionosphere extends in various layers from about 50 km to 1 000 km above earth. It is a dispersive medium with respect to the GNSS radio signal. Following (Seeber, 2003, p. 54) the series:

$$n_{ph} = 1 + \frac{c_2}{f^2} + \frac{c_3}{f^3} + \frac{c_4}{f^4} + \cdots \tag{2.46}$$

approximates the phase refractive index. The coefficients $c_2$, $c_3$, $c_4$ do not depend on frequency but on the quantity $Ne$ denoting the number of electrons per cubic meter (i.e., the electron density) along the propagation path. Using an approximation by cutting off the series expansion after the term, that is:

$$n_{ph} = 1 + \frac{c_2}{f^2} \qquad\qquad (2.47)$$

differentiating this equation leading to

$$n_{gr} = 1 - \frac{c_2}{f^2} \qquad\qquad (2.48)$$

It can be seen from below that the group and the phase refractive indices deviate from unity with opposite sign. With an estimate for $c_2$ (Seeber, 2003, p. 54),

$$c_2 = -40.3\, N_e \quad [Hz^2] \qquad\qquad (2.49)$$

the relation $n_{gr} > n_{ph}$ and, $v_{gr} < v_{ph}$ follows because the electron density $N_e$ is always positive. As a consequence of the different velocities, a group delay and a phase advance occur. In other words, GNSS ranging codes are delayed and the carrier phases are advanced. Therefore, the measured code pseudoranges are too long and the measured carrier phase pseudoranges are too short compared to the geometric range between the satellite and the receiver. The amount of the difference is the same in both cases.

The difference $\Delta^{Iono}$ between measured and geometric range is called ionospheric refraction. In a good approximation the ionospheric range error is related to the total electron content:

$$\Delta_{ph}^{Iono} = -\frac{40.3}{f^2}\, TEC, \qquad\qquad \Delta_{gr}^{Iono} = \frac{40.3}{f^2}\, TEC \qquad\qquad (2.50)$$

as the final result (in meter). Usually, the TEC is given in TEC units (TECU), where

$$1\, TECU = 10^{16}\ electrons\ per\ m^2 \qquad\qquad (2.51)$$

The geographic variation of TEC is illustrated for Europe and Glob and offered to users ionosphere maps on daily basis and free of cost (see Figure 2.11).
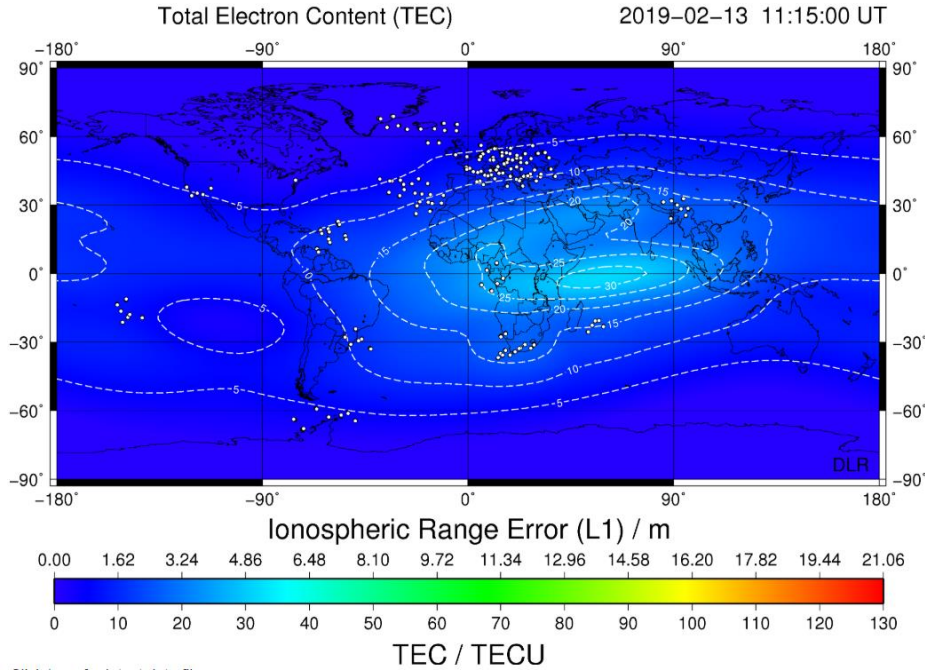
*Figure 2.11: Global Ionosphere map for Feb 13, 2019, at 11:15 UTC*

It is difficult to find a satisfying model for the TEC because of the various time dependent influences. The most efficient method is to eliminate the ionospheric refraction by using two signals with different frequencies. This dual-frequency method is the main reason why the GNSS satellites emit at least two carrier waves.

The ionospheric error is not equal on L1 and L2 and the relation shown as:

$$I_2 = \frac{f_1^2}{f_2^2} \, I_1 \tag{2.52}$$

Moreover, L1 and L2 carrier phases can be combined together that will reduce the ionospheric delay to zero. A new equation L3 is obtained:

$$L3(t) = \frac{f_1^2}{f_1^2 - f_2^2} L1(t) - \frac{f_2^2}{f_1^2 - f_2^2} L2(t) \tag{2.53}$$

By using Equation (2.52), Substituting L1 and L2 with the observation equation for carrier phase and rearranging the terms, ionospheric effect vanishes at the end.

$$\frac{f_1^2}{f_1^2 - f_2^2} I_1(t) - \frac{f_2^2}{f_1^2 - f_2^2} \frac{f_1^2}{f_2^2} \, I_1 = 0 \tag{2.54}$$

41

The advantage of the ionosphere-free combination is the elimination (or more precisely, the reduction) of ionospheric effects. Remembering the derivation, it should be clear that the term "ionosphere-free" is not fully correct because there are some approximations involved, for instance, Equation (2.47).

**Multipath**

Multipath is described by its name: a satellite-emitted signal arrives at the receiver by more than one path (Tawk, 2013). Multipath is mainly caused by reflecting surfaces near the receiver (Figure 2.12). Secondary effects are reflections at the satellite during signal transmission.

As has been seen at Figure 2.12, the satellite signal arrives at the receiver on three different paths, one direct and two indirect ones. As a consequence, the received signals have relative phase offsets and the phase differences are proportional to the differences of the path lengths. There is no general model of the multipath effect because of the time- and location-dependent geometric situation. The influence of the multipath, however, can be estimated by using a combination of f1 and f2 code and carrier phase measurements.
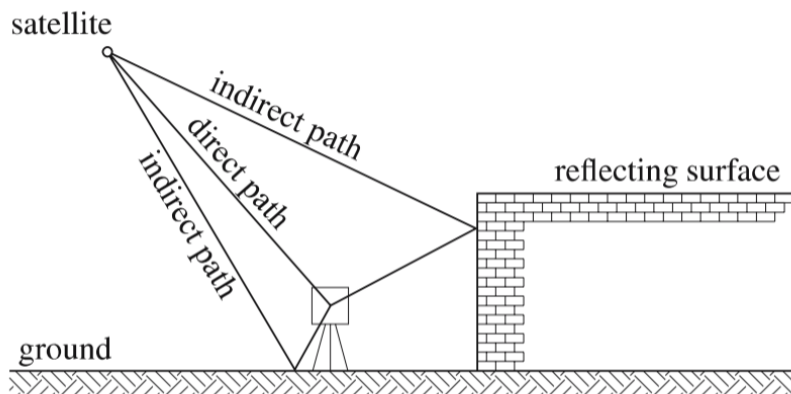


*Figure 2.12: Multipath effect (Hofman-Wellenhof, Lichtenegger, & Wasle, 2008)*

According to "GPS multipath field observations at land and water sites" document (Tranquilla & Carr, 1990/91) group the multipath errors of pseudoranges into three classes:

1. diffuse forward scattering from a distributed area (i.e., the signal passes through a metallic environment),
2. specular reflection from well-defined objects or reflective surfaces in the vicinity of the antenna (i.e., Figure 2.12), and
3. fluctuations of very low frequency (i.e., reflection from the surface of water).

Purely from geometry it is clear that signals received from low satellite elevations are more susceptible to multipath than signals from high elevations. Note also that code ranges are more affected by multipath than carrier phases.

The multipath effects on carrier phases should not be greater than about 2-3 cm (good satellite geometry and a reasonably long observation interval). When performing static surveys where the observation times are relatively long, intermittent periods of multipath contamination are not a problem. Rapid static surveys (i.e., surveys with very short observation times) may be more contaminated in such cases.

In this research u-blox 7P platform was used. It cannot track at the same time two or more satellite systems. Therefore, multipath errors will be more significant than in the case of concurrent GPS and GLONASS acquisition. However, the latest model from u-blox with the eight-generation positioning platform 8M allow the user to enable in the tracking configuration 2 satellite systems: GPS and GLONASS or BeiDou or GLONASS and BeiDou. Although having more satellites in view is of great help in the processing mode, concurrent tracking of more systems is not enough (Grec, 2014/15).

Various methods were developed in order to reduce or estimate the multipath effects,

1. antenna-based mitigation,
2. improved receiver technology, and
3. signal and data processing.

A reduction of the multipath effect can be achieved by digital filtering, wideband antennas, antenna ground planes absorbing radio frequencies, choke ring antennas including the advanced dual-frequency choke ring design (Philippov, Sutiagin, & Ashjaee, 1999).

Multipath on code measurements remains one of the most significant error sources for differential GNSS vehicle navigation. Compared to static applications, the positions of various reflectors are changing rapidly, increasing the difficulty of a proper model.

**Antenna phase center offset and variation**

In an idealized situation, the electrical phase center of the antenna is the point to which the measurements derived from received GNSS signals refer. Usually, this will not be a point which can be measured by a tape measurement. Therefore, a geometrical point on the antenna denoted as antenna reference point (ARP) is introduced in Figure 2.13. The IGS defines the ARP as the intersection of the vertical antenna axis of symmetry with the bottom of the antenna.

However, this idealized situation is not true in the reality because the electrical antenna phase center varies with elevation, azimuth, intensity of the satellite signal, and is also frequency dependent. In other terms, each incoming signal has its own electrical antenna phase center. Therefore, a mean position of the electrical antenna phase center is determined for the purpose of the offset calibration (Hofman-Wellenhof, Lichtenegger, & Wasle, 2008).

The antenna phase center offset (PCO) defines the difference between the ARP and the mean electrical antenna phase center.

The antenna PCO is given by three-dimensional coordinates of the electrical antenna phase center referring to the ARP and it has been provided by the manufacturer. Due to the dependence on frequency the antenna PCO must be given for each carrier frequency.

Comparing the electrical antenna phase center of an individual measurement with the mean electrical antenna phase center, a deviation will arise. These deviations are denoted as antenna phase center variations (PCV). The azimuth- and elevation-dependent PCV define the phase pattern (individually for each carrier frequency).
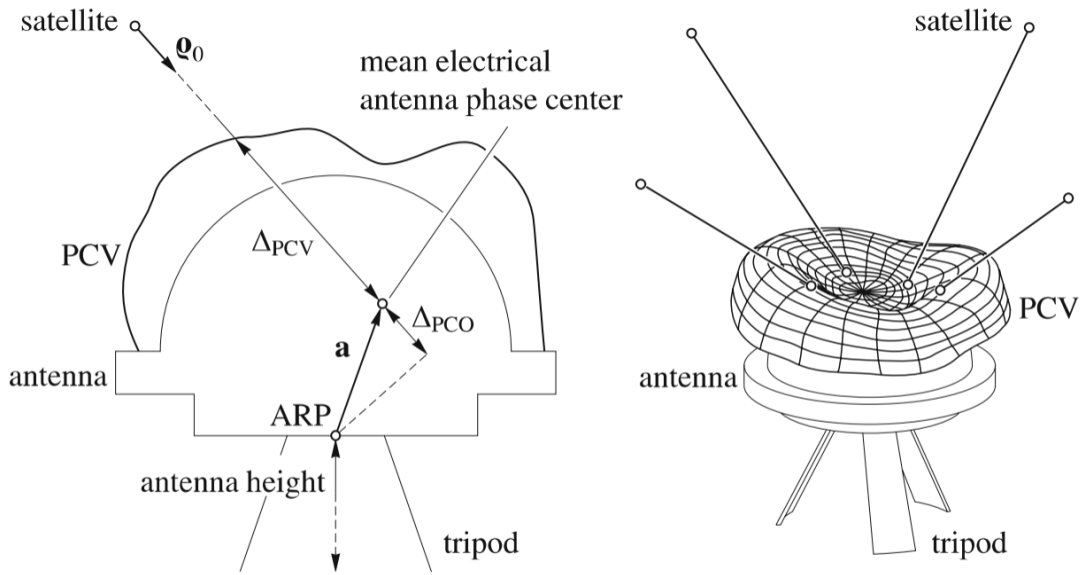
*Figure 2.13: Electrical phase center and antenna reference point (Hofman-Wellenhof, Lichtenegger, & Wasle, 2008)*

Introducing for the PCO the vector $a$ as indicated in Figure 2.13 and the unit vector $\varrho_0$ between the satellite and the receiver, $\Delta_{PCO}$, the influence of the PCO on the phase measurement, can be obtained as the projection of a onto the unit vector $\varrho_0$ between the satellite and the receiver:

$$\Delta_{PCO} = a * \varrho_0 \tag{2.55}$$

The influence of PCV on the phase pseudorange, denoted as $\Delta_{PCV}$, is described by a function depending on the azimuth $\alpha$ and the zenith angle $z$ of the satellite, and of the carrier frequency $f$:

$$\Delta_{PCV} = \Delta_{PCV}(\alpha, z, f) \tag{2.56}$$

The total correction of the phase pseudorange due to PCO and PCV is the combined effect $\Delta PCO + \Delta PCV$. Applying this total correction, the phase pseudoranges refer to the ARP. In other terms, the coordinates of the ARP will result after processing the measured data properly. As seen from Figure 2.13, the resulting height component must still be reduced by the antenna height.

## 2.3.6 Differencing positioning technique

### 2.3.6.1 Single differencing
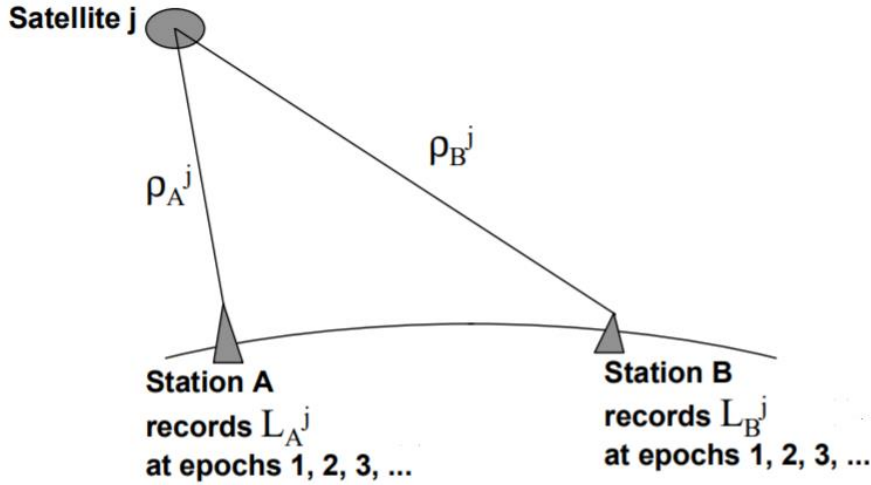


*Figure 2.14: Single differences geometry (Hofman-Wellenhof, Lichtenegger, & Wasle, 2008)*

Two receivers and one satellite are involved to the single differencing. The purpose of single differencing is to eliminate satellite clock bias. The phase equations for the two points are below by denoting the receiver sites "*A and B*", and the satellite "*j*":

$$L_A^j = \rho_A^j + c\left(dt_A - dt^j\right) + T_A^j - I_A^j + B_A^j \tag{2.57}$$

$$L_B^j = \rho_B^j + c\left(dt_B - dt^j\right) + T_B^j - I_B^j + B_B^j \tag{2.58}$$

The single difference phase is defined as the difference between these two:

$$\Delta L_{AB}^j = L_A^j - L_B^j \tag{2.59}$$

$$\Delta L_{AB}^j = (\rho_A^j - \rho_B^j) + c(dt_A - dt_B) - c(dt^j - dt^j) + (T_A^j - T_B^j) - (I_A^j - I_B^j) + (B_A^j - B_B^j)$$

$$\Delta L_{AB}^j = \Delta\rho_{AB}^j + c\Delta t_{AB} + \Delta T_A^j - \Delta I_A^j + \Delta B_A^j \tag{2.60}$$

Equation (2.60) is referred to as single-difference equation. This equation stresses one aspect of the solution for the unknowns on the right side. A system of such equations would lead to a rank deficiency even in the case of an arbitrarily large redundancy. This means that the design matrix

of the adjustment has linearly dependent columns and a rank deficiency exists. Figure 2.14 illustrates the geometry of single differencing.

An assumption has been made, that the satellite clock bias $dt^j$ is identical at the slightly different times that the signal was transmitted to A and to B. The difference in transmission time could be as much as a few milliseconds. So, the satellite clock bias $dt^j$ has canceled at the final formula.

Although the single difference has the advantage that many error sources are eliminated or reduced, the disadvantage is that only relative position can be estimated (unless the network is global scale). Moreover, the receiver clock bias is still unknown, and very unpredictable. (Hofman-Wellenhof, Lichtenegger, & Wasle, 2008).

## 2.3.6.2 Double differencing
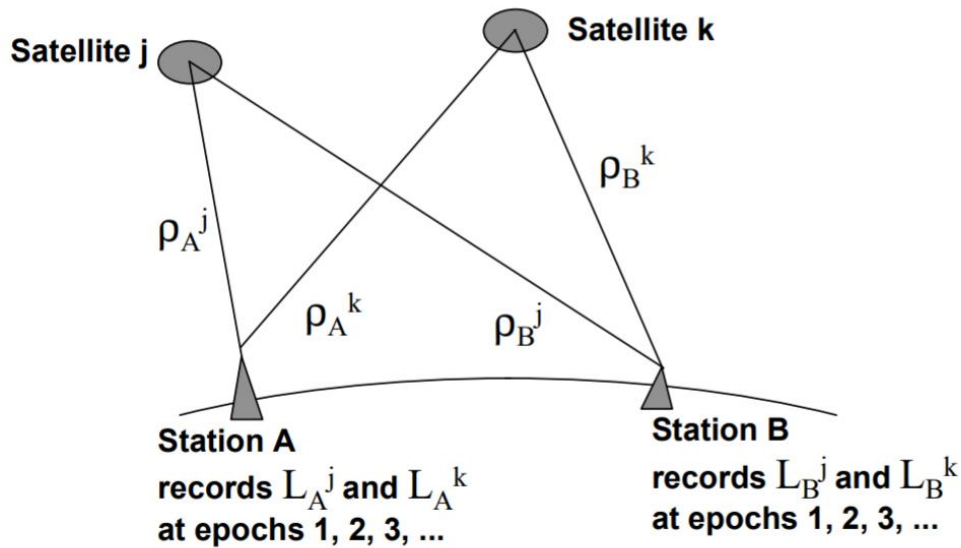


*Figure 2.15: Double differences geometry (Hofman-Wellenhof, Lichtenegger, & Wasle, 2008)*

Two receivers and two satellite are involved to the single differencing. The purpose of double differencing is to eliminate receiver clock bias. The phase equations for the two points are below by denoting the receiver sites "*A and B*", and two satellite "*j and k*":

$$\Delta L_{AB}^{j} = \Delta \rho_{AB}^{j} + c\Delta t_{AB} + \Delta T_{A}^{j} - \Delta I_{A}^{j} + \Delta B_{A}^{j} \qquad (2.61)$$

$$\Delta L_{AB}^k = \Delta \rho_{AB}^k + c\Delta t_{AB} + \Delta T_A^k - \Delta I_A^k + \Delta B_A^k \qquad (2.62)$$

The double difference phase is defined as the difference between these two:

$$\nabla \Delta L_{AB}^{jk} = \Delta L_{AB}^j - \Delta L_{AB}^k \qquad (2.63)$$

$$\nabla \Delta L_{AB}^{jk} = \left(\Delta \rho_{AB}^j - \Delta \rho_{AB}^k\right) + (c\Delta t_{AB} - c\Delta t_{AB}) + \left(\Delta T_A^j - \Delta T_A^k\right) - \left(\Delta I_A^j - \Delta I_A^k\right) + \left(\Delta B_A^j - \Delta B_A^k\right)$$

$$\nabla \Delta L_{AB}^{jk} = \nabla \Delta \rho_{AB}^{jk} + \nabla \Delta T_A^{jk} - \nabla \Delta I_A^{jk} + \nabla \Delta B_A^{jk} \qquad (2.64)$$

The double-superscript is used to denote quantities identified with two satellites, and the upside-down triangular symbol as a mnemonic device, to emphasize that the difference is made between two points in the sky. Figure 2.15 illustrates the geometry of double differencing.

Any systematic effects due to unmodelled atmospheric errors are generally increased slightly by approximately 40% by double differencing as compared to single differencing. Similarly, random errors due to measurement noise and multipath are increased. Overall, random errors are effectively doubled as compared with the undifferenced observation equation. On the other hand, the motivation for double differencing is to remove clock bias, which would create much larger errors (Hofman-Wellenhof, Lichtenegger, & Wasle, 2008).

The double difference combination has an additional advantage, in that the ambiguity is an integer:

$$\nabla \Delta B_{AB}^{jk} = \Delta B_{AB}^j - \Delta B_{AB}^k \qquad (2.65)$$

$$\nabla \Delta B_{AB}^{jk} = \left(B_A^j - B_B^j\right) - \left(B_A^k - B_B^k\right) \qquad (2.66)$$

$$\nabla \Delta B_{AB}^{jk} = \lambda_0 \left(\varphi_{0A} - \varphi_0^j - N_A^j\right) - \lambda_0 \left(\varphi_{0B} - \varphi_0^j - N_B^j\right) - \lambda_0 \left(\varphi_{0A} - \varphi_0^k - N_A^k\right) \\ + \lambda_0 \left(\varphi_{0B} - \varphi_0^k - N_B^k\right)$$

$$\nabla \Delta B_{AB}^{jk} = -\lambda_0 \left(N_A^j - N_B^j - N_A^k + N_B^j\right) \qquad (2.67)$$

$$\nabla \Delta B_{AB}^{jk} = -\lambda_0 \Delta N_{AB}^{jk} \qquad (2.68)$$

Hence, we can write the double differenced phase observation equation:

$$\Delta L_{AB}^{jk} = \Delta \rho_{AB}^{jk} + c\Delta t_{AB} + \Delta T_{AB}^{jk} - \Delta I_{AB}^{jk} + \Delta B_A^j - \lambda_0 \Delta N_{AB}^{jk} \qquad (2.69)$$

From the point of view of estimation, it makes no difference whether we use a minus or plus sign for $N$, so long as the partial derivative has a consistent sign.

# 3  GNSS RECEIVERS AND SOFTWARE PACKAGES

## 3.1  GNSS Receivers

During the time span of research, the following instruments are used:

- 1 geodetic Leica GRX1200 receiver with Antenna type: Leica AX1202GG,
- 1 U-blox LEA-4T module and its default antenna, and
- 1 low-cost GPS receiver Samsung Galaxy S8.

### 3.1.1  Leica GRX1200

As mentioned in Leica GRX1200 Product Description Brochure, the Leica GRX1200 Series is designed specifically for use at reference stations. The measurement engine supports GPS, GLONASS, Galileo and BeiDou. Regarding data management, removable and robust CompactFlash cards up to 1 GB are used for logging data. According to Leica, 1 GB is sufficient for about 7 weeks of 1Hz L1+L2 GPS data. Also, Leica GRX1200 is able to track the new multi-frequency signals from modernized GPS (including L5 and L2C), GLONASS and Galileo. There is no need for power-consuming external memory storage, which typically cannot fulfil in the tough environment conditions to which reference stations are exposed. Files can be logged in raw data and/or RINEX file (Leica Geosystems AG, 2009).

The Leica GRX1200 uses SmartTrack technology. SmartTrack, "the advanced measurement technology", consists in advanced GPS acquisition technique: after switching on the time needed to acquire all satellites is typically 50 seconds; after loss of lock re-acquisition starts typically within 1 second; very high sensitivity, it acquires more than 99% of all possible observations above 10 degrees elevation (Leica Geosystems AG, 2009).

The main characteristics of Leica GRX1200 can be listed:

- Acquisition within seconds,
- Excellent signal strength,
- Reliable tracking to low elevations,

- Suppresses phase and code multipath,

- Jamming resistant,

- Measurements up to 20 Hz, and

- Low power consumption.



*Figure 3.1: Leica GRX1200 and AX1202 GG antenna*

The type of connected antenna directly affects the performance of this sensor. In this research, "AX1202GG" standard geodetic antenna (see Figure 3.1) for Leica GRX1200 used. This antenna will suppress multipath, deliver high-quality observations for single stations and networks. Latest generation of geodetic antenna from Leica includes sub-millimeter phase center accuracy, high quality measurements even from low elevation satellites and have built-in ground plane for multipath suppression.

The built-in File Transfer Protocol (FTP) server feature allows simple and quick manual download of data without the need for special software. Alternatively, FTP Push can be used in order to automatically upload data from the receiver to a remote FTP server.

Leica GRX1200 Series is sheltered inside a strong magnesium housing and is designed to MIL-STD-810 (United States Military Standard) specifications to withstand the roughest use and the most severe environments for protection. These receivers can operate through a wide temperature range, are fully waterproof, rain, sand and dustproof (see Table 3.1 for details) (Leica Geosystems AG, 2009).

*Table 3.1:* Technical data for GRX1200 (courtesy Leica Geosystems).

| Leica GRX1200 | Nominal value of frequency in L1 sub-band, in MHz |
|---|---|
| GNSS technology | SmartTrack+ |
| Measurement precision<br>• carrier phase<br>• code | L1: rms = 0.2 mm ;   L2: rms = 0.2 mm<br>L1: rms = 20 mm  ;   L2: rms = 20 mm |
| Web & FTP services | Yes |
| Optional control software | Leica GPS Spider software |
| Weight | 1.2 kg |
| Temperature range | $-40^0$C to $+65^0$C |
| Waterproof | MIL-STD-810F<br>Temporary submersion to 1 m |
| Shock/drop on hard surface | Withstand 1.0 m drop |
| Supply voltage | Nominal 12V DC |
| Raw data logging | MDB (Leica proprietary format) and RINEX |
| Data streaming | RTCM v2.1/2.2/2.3/3.0<br>NMEA 0183<br>Leica LB2 raw data |
| NTRIP | Integrated NTRIP server |

Table published by Leica under accuracy heading is given in Table 3.2 for interested normal baselines.

| Static | | Kinematic | |
|---|---|---|---|
| Horizontal | Vertical | Horizontal | Vertical |
| 5 mm + 0.5 ppm | 10 mm + 0.5 ppm | 10 mm + 1 ppm | 20 mm + 1 ppm |

### 3.1.2  U-blox LEA-4T receiver

U-blox is a Swiss company and a provider that creates wireless semiconductors and modules for consumer, automotive and industrial markets. U-blox develops and sells chips and modules that support global satellite navigation systems (GNSS), including receivers for GPS, GLONASS, Galileo, BeiDou, and QZSS. The Evaluation Kit with Precision Timing output was developed by u-blox as a low-cost single-frequency RTK technology (ublox, 2007).

Single-frequency GNSS receivers access only L1 frequency. The single-frequency code receiver, is the cheapest and the least accurate type of receivers, also called low-cost GNSS receiver. It measures the pseudoranges with the C/A code only (ublox, 2007).

The accuracy of the time pulse is as good as 50 ns, synchronized to GPS or UTC time. An accuracy of 15 ns is achievable by using the quantization error information to compensate the granularity of the time pulse. Main features:

- 16-channel ANTARIS®4 positioning engine,
- Stationary mode for GPS timing operation,
- 15 ns timing accuracy (error compensated),
- Single Satellite GPS timing,
- 10 Hz raw measurement data output, and
- Supports SBAS: WAAS, EGNOS, MSAS.

### 3.1.3  Samsung Galaxy S8

In this thesis, Samsung Galaxy S8 device is used as a single frequency smartphone which runs Android 7.1. It is visible in Figure 3.2 that the Samsung S8 shows a great transparency in being able to analyze also the navigational message, and trace almost the whole of the GNSS constellations. The table distinguishes the version of the device as "*Exynos*" which is identified for all the devices produced for the market in Europe, the Middle East and Africa.

| Model | Android version | Automatic Gain Control | Navigation messages | Accumulated delta range | HW clock | L5 Support | Global systems |
|---|---|---|---|---|---|---|---|
| Huawei Mate 20 X | 9.0 | no | yes | yes | yes | yes | GPS GLONASS GALILEO QZSS |
| Huawei Mate 20 RS (Porsche Design) | 9.0 | no | no | yes | yes | yes | GPS GLONASS GALILEO BeiDou |
| Huawei Mate 20 Pro | 9.0 | no | no | yes | yes | yes | GPS GLONASS GALILEO BeiDou |
| Huawei Mate 20 | 9.0 | no | no | yes | yes | yes | GPS GLONASS GALILEO BeiDou |
| Huawei Mate 10 | 8.0 | no | yes | yes | yes | no | GPS GLONASS |
| Huawei Mate 10 Pro | 8.0 | no | yes | yes | yes | no | GPS GLONASS QZSS |
| Google Pixel 2 XL | 8.0 | yes | no | no | yes | no | GPS GLONASS GALILEO BeiDou QZSS |
| Google Pixel 2 | 8.0 | yes | no | no | yes | no | GPS GLONASS GALILEO BeiDou QZSS |
| Sony Xperia XZ1 | 8.0 | no | no | no | yes | no | GPS GLONASS GALILEO BeiDou |
| Samsung Note 8 (Exynos) | 7.1 | no | yes | yes | yes | no | GPS GLONASS GALILEO BeiDou |

*Figure 3.2: Devices that support raw GNSS measurements and the data*
*(https://developer.android.com/guide/topics/sensors/gnss)*

The Android operating system has ad-hoc interface called "Application Programming Interface (API)" that allows users to access the systems functionalities. Access to the GNSS measurements in the Android devices were added in API level 24 embedded in Android N using the *GNSSClock, GnssNavigationMessage* and *GnssMeasurement* classes. Before that, researchers had access with API level 23 to the following Android classes:

- **GPS Satellite**, containing such basic satellite information as azimuth, elevation, PRN and C/No. It also flags if the satellite is used in the PVT (position, velocity and time) solution and the availability of almanac and ephemerides.
- **GPS Status** provides information about the status and solution of the GNSS chipset.
- **Location**, indicating if a positional and time solution is provided.
- **NMEA Listener**, providing basic NMEA sentences.
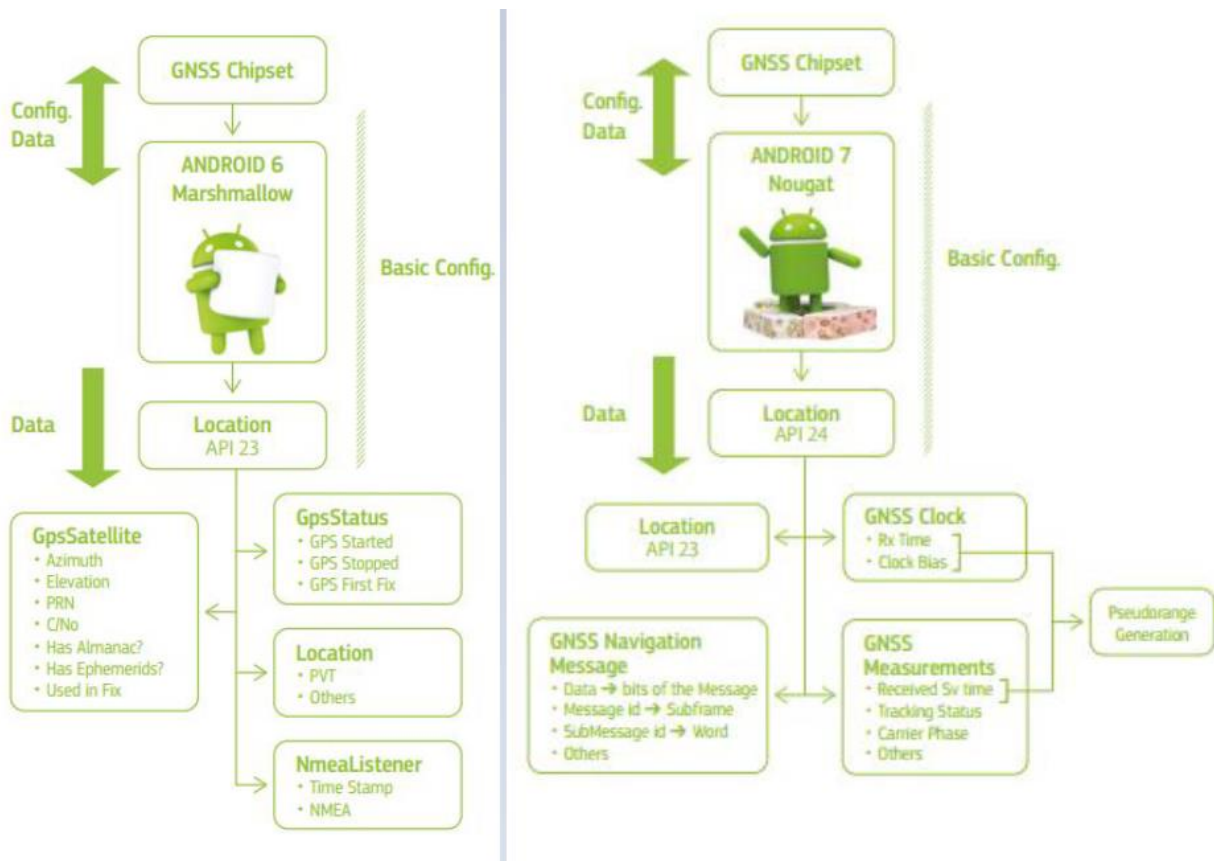


*Figure 3.3: Location API in Android API Level 23 (on the left) and Level 24 (on the right)*

From API level 24 (Android 7), researchers have access to API level 23 and the following GNSS raw and computed information:

- **GNSS Clock**, that contains:
    - Receiver time (used to compute the pseudorange);
    - Clock bias
- **GNSS Navigation Message**, that contains:
    - Navigation message bits (all the constellations);
    - Navigation message status.
- **GNSS Measurements**, that contains:
    - Received satellite time (used to compute the pseudorange);
    - Code;
    - Carrier phase

While data is directly received from the GNSS chipset, researchers do not have direct access to the chipset.
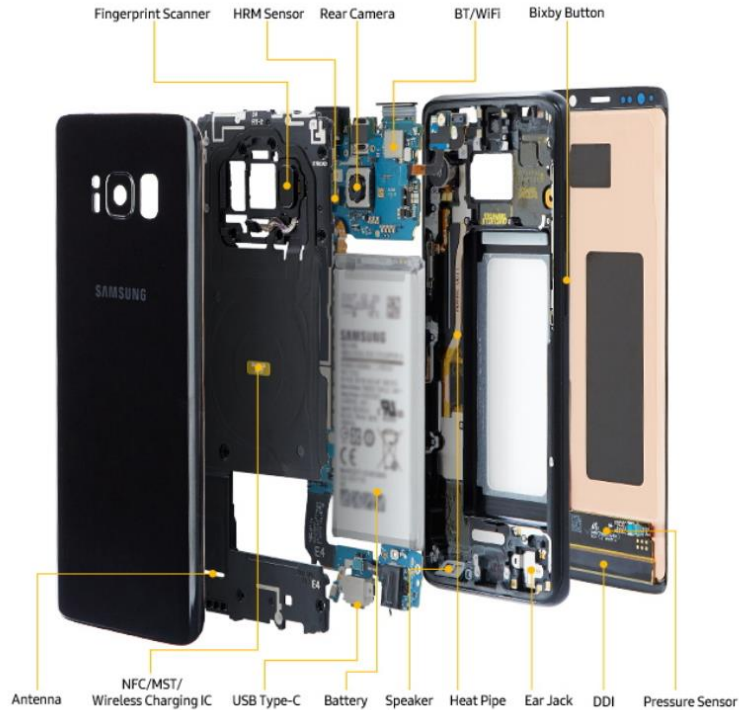


*Figure 3.4: Samsung Galaxy S8 Scheme*

## 3.2   Software Packages

In this thesis, the various software is used to analyze and process the data: Leica Geo Office, MATLAB, QGIS, OruxMaps, GNSS Analysis APP and RTKLIB.

In order to import data to QGIS, the final results from Leica Geo Office are exported as ASCII files. Output data from OruxMaps is .gpx file can be imported by QGIS. Output file is logged by GNSS Logger in Android has to be transformed into a format can be imported by QGIS. For this task, MATLAB may be used.

### 3.2.1   Leica Geo Office

Leica Geo Office (LGO) is a software produced by Leica Geosystems, a Switzerland enterprise that produces instruments for surveying and measurement and the relative software to process the data acquired. LGO is dedicated to process data from GNSS survey and is able to handle many different processing scenarios: static, rapid static, stop-and-go, kinematic. It can process data from multi constellations, GPS, GLONASS and Galileo and can process both single frequency and double frequency data. Many tools to import data from different formats (for example raw data, cad and GIS data), to export data and create report are available (Negretti, 2013/2016).

In present thesis, LGO is used for importing raw data from Leica GRX1200 and process double frequency data for stop-and-go and kinematic surveying scenarios. Final results from LGO are exported in ASCII file.

### 3.2.2   QGIS

QGIS is free and open source desktop GIS. It allows user to create, edit, visualize, analyze and publish geospatial information on Windows, Mac OS, Linux, BSD and Android. The QGIS project is under very active development by an enthusiastic and engaged developer community (OSGeo, 2019). QGIS supports both raster and vector layers; vector data is stored as either point, line, or polygon features. Multiple formats of raster images are supported, and the software can georeference images. Also, QGIS supports shapefiles, coverages, personal geodatabases, .dxf, MapInfo, PostGIS and other formats (QGIS, 2019).

In present thesis, QGIS version 3.0.0 is used for editing, visualizing and analyzing geospatial data.

### 3.2.3 MATLAB

MATLAB is an interpreted language for numerical computation. It allows to perform numerical calculations and visualize the results without the need for complicated and time-consuming programming. MATLAB allows its users to solve problems accurately, produce graphics easily and produce code efficiently (Edurev, 2019). MATLAB has several advantages over languages:

- Its basic data element is the matrix. A simple integer is considered a matrix of one row and one column.
- Vectorized operations. Adding two arrays together needs only one command, instead of a for or while loop.
- The graphical output is optimized for interaction. User can plot your data very easily, and then change colors, sizes, scales, etc., by using the graphical interactive tools.

(York University, 2019).

In present thesis, MATLAB R2018a is used for editing, visualizing, analyzing and processing the data. Some written codes used in processing and analysis are added to Appendix A, B and C.

### 3.2.4 OruxMaps

OruxMaps is a free map viewer for android platform. It can display OpenStreetMap maps (raster tiles and vector maps from Mapsforge) and has tracking and waypoint recording features making it suitable for gathering data. It can be downloaded from (https://www.oruxmaps.com/cs/en/).

In present thesis, OruxMaps is used for Record a track and Export a track in GPX format. The aim is to get a first idea of how much compatible coordinates are generated by android smartphone GPS in comparison with a geodetic receiver when both are used in the same filed condition.

## 3.2.5 GNSS Analysis APP

The GPS Measurement Tools project includes GNSS Logger for android and GNSS Analysis App for desktop. GNSS Logger is a sample application that shows how to log data related to Android location, including raw GNSS measurements. To get GNSS output with the sample app, android device must support raw GNSS measurements.
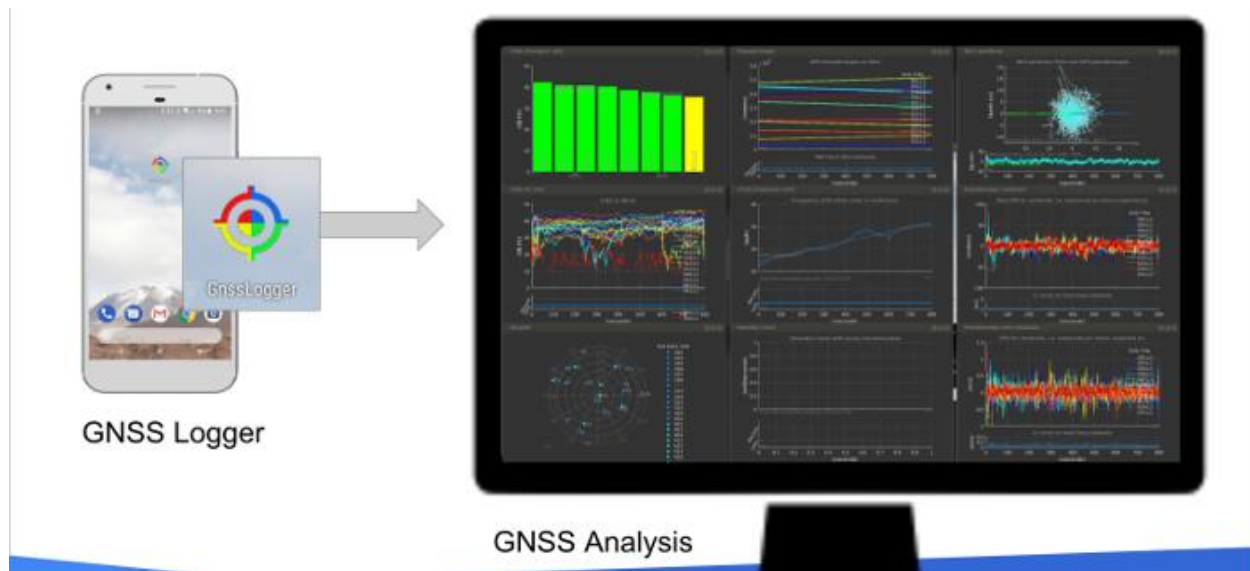


*Figure 3.5: The relation of GNSS Logger and GNSS Analysis: GNSS Logger collects the measurements that can be consumed by GNSS Analysis.*

Once user has captured the GNSS log using the GNSS Logger, user can copy the log files from the device to computer for further analysis with GNSS Analysis App. The GNSS Analysis app reads the GPS/GNSS raw measurements collected by the GNSS Logger and uses them to analyze the GNSS receiver behavior (see Figure 3.5). The GNSS Analysis app is built on MATLAB, but user don't need to have MATLAB to run it. The app is compiled into an executable that installs a copy of the MATLAB Runtime.

Google has publicly released GNSS Analysis Tools to process and analyze GNSS raw measurements from your phone. App-developers, researchers and educators can download and reach more detailed information (https://developer.android.com/guide/topics/sensors/gnss).

Some reports of the end of processing with GNSS Analysis Tool are added to Appendix D.

### 3.2.6  Geo++ RINEX Logger

Geo++ RINEX Logger uses Android API services to log raw GNSS measurement data into a RINEX file including pseudoranges, accumulated delta ranges, doppler frequencies and noise values. It supports GPS / GLONASS / GALILEO / BDS / QZSS for L1 / L5 / E1B / E1C / E5A (as supported by the device). It can be downloaded from:

 (https://play.google.com/store/apps/details?id=de.geopp.rinexlogger&hl=en)



*Figure 3.6: Geo++ RINEX Logger interface*

### 3.2.7  RinexOn

RinexOn utilizes the measurements of the Android Raw Measurements API to produce RINEX Observation and Navigation Message Files from the Android GNSS chipset. The app was written

by NSL as part of the FLAMINGO project (https://www.flamingognss.com/). The application was launched at the GSA (European Global Navigation Satellite System Agency) Raw Measurements Task Force Workshop "GNSS Raw Measurements: From research to commercial use" on 30 May 2018.

Features of the application are presented on below:

- RINEX observation: The app currently produces a RINEX observation file for the GPS, GLONASS and Galileo constellations. The RINEX files are currently only written in version 3.03.
- RINEX navigation message: The app currently produces a RINEX navigation message file for GPS and GLONASS constellations.
- NMEA log: NMEA message log may also be written.
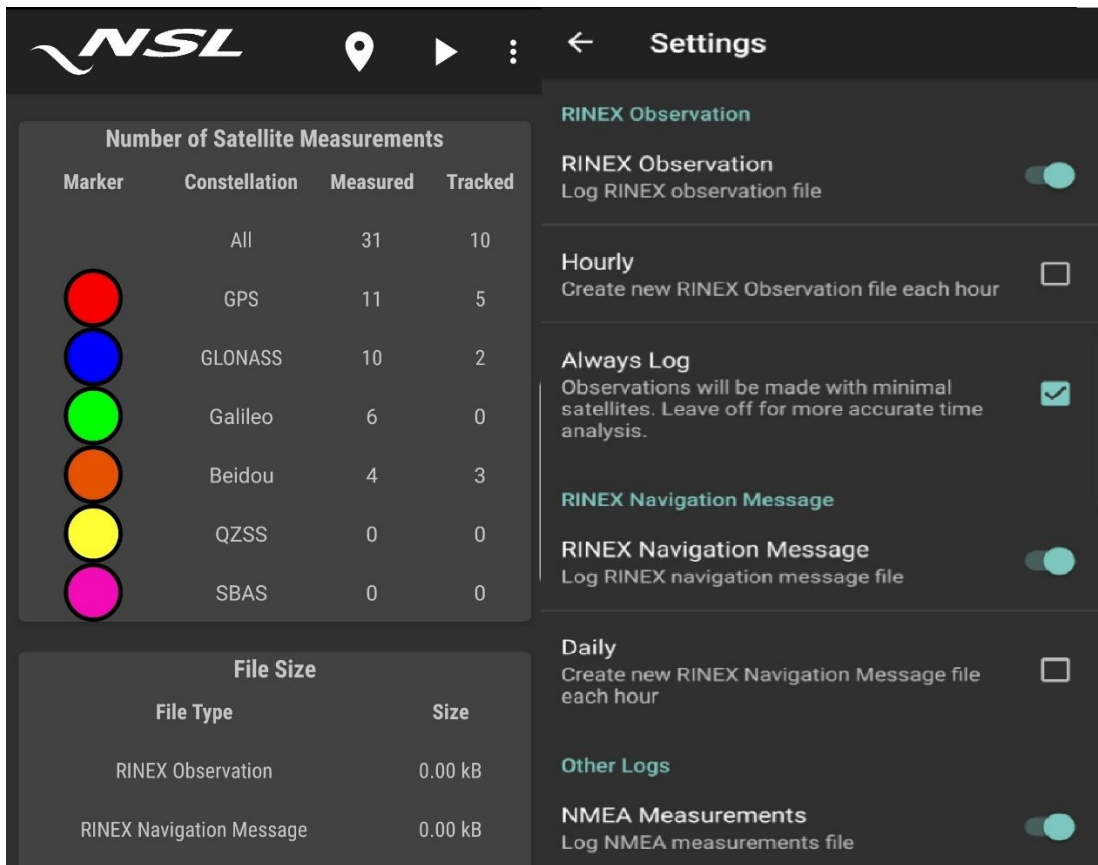


*Figure 3.7: RinexOn interface*

### 3.2.8 RTKLIB

RTKLIB is an open source software written in C language for standard and precise positioning with GNSS. The main developer is Tomoji Takasu of the Tokyo University of Marine Science and Technology. It can be downloaded from (http://www.rtklib.com/).

It supports data from many different systems, like GPS, GLONASS, Galileo, QZSS, BeiDou and SBAS; various positioning modes are available for both real-time and post-processing: Single, Differential GNSS, Kinematic, Static, Moving-Baseline, Fixed, PPP-Kinematic, PPP-Static and PPP-Fixed.

In present thesis, the version 2.4.2 installed for dividing a long observation period into multiple short observation windows and post-processing data (see Chapter 5) from the u-blox.

# 4   RESEARCH APPROACH

In Android Release N ("Nougat"), Google introduced APIs giving access to GNSS raw measurements from android smartphones. After this announcement, users will be able to log GNSS raw measurements such as GPS satellite information (C/No, azimuth, elevation if a particular satellite has been used in the PVT), NMEA sentences and PVT solution with the proper time stamp. This can open many possibilities for the single-frequency GNSS receivers, also called low-cost GNSS receiver, integrated in smartphones.

The single-frequency GNSS receivers are widely used in smart mobile devices: in addition to smartphones, in car navigation system, smartwatch, tablet with navigation applications. The technique used to get up the position is the single point positioning that reach an accuracy of tens meters.

An opportunity to do better and complete research with GNSS raw measurements from the single-frequency GNSS receivers can improve the accuracies for smart mobile devices. Tens meters accuracy could be enough for most of daily navigation purposes, however it could be better to increase it for some particular cases: usages needs higher accuracy (decimeter of accuracy) like navigation for impaired people.

In this aspect, mainly, the research investigates assessment of kinematic and short session static accuracies with single frequency low-cost receivers. Additionally, shares what kind of difficulties are faced, how good the results are evaluated, when the single-frequency GNSS receiver raw measurements are processed and analyzed with well know geodetic software packages.

One of the major challenges to reach better accuracies in the research comes from short period of time (5 – 10 minutes) surveys are not good enough to solve ambiguities most of the time. However, in the research, experiments are performed with short period of time applications with mobile devices. Contrary, in standard procedures, a static positioning is up to 6 hours with geodetic GPS.

Besides, u-blox is a single-frequency GNSS receiver measures the pseudoranges with the C/A code only. For the research, the investigating u-blox data makes sense to see behavior under short period of time surveys. In this aspect, the research contains the processing and analysis of static positioning for short time periods with u-blox either.

Briefly, one reference network with stop-and-go surveying technique, one reference trajectory with kinematic surveying technique were carried out to assess the behavior of the measurements over time with single frequency GNSS receivers. Additionally, an experiment with static surveying technique is studied to create a general impression of single-frequency GNSS receivers.

The chapter will start with brief description of reference networks set-up and continues with detailed explanation of field work and storing data for the reference networks. Also, it explains applied algorithms to generate the reference networks. At the final, created reference networks are presented.

## 4.1   The Reference Network Set-up

The field work was conducted in 2 different locations in Milano, inside Leonardo Campus of Politecnico di Milano with stop-and-go surveying technique and kinematic surveying technique. Each surveying technique is achieved in different chosen location; thus, 2 reference generated:



*Figure 4.1: Research area*

- Reference Network 1: The field experiments with stop-and-go surveying technique is set around fountain in green area in front of Leonardo Campus of Politecnico di Milano.

- Reference Trajectory 2: The field experiments with kinematic surveying technique is set in green area in front of Leonardo Campus of Politecnico di Milano.

The both reference is located in a couple of hundred meters range to the Milano Permanent Station I (see Figure 4.1). During the time span of all field work, a single geodetic Leica GRX1200 receiver (see Chapter 3) with Antenna type: Leica AX1202GG is used.

## 4.2   Reference Network 1: The Fountain

"Reference Network 1" has been set around the fountain in green area in front of Leonardo Campus of Politecnico di Milano in 2017, several days in November and December (see Figure 4.2).



*Figure 4.2: Estimated point locations around the fountain (in red) and estimated starting point location (in yellow)*

Measured points are defined on each joint between stones surrounding the fountain area. Consequently, a hundred joints are defined as measurement points around the fountain. Stones surrounding the fountain area have different sizes and they cover approximately 75 meters round (see Figure 4.3).



*Figure 4.3: Joints between stones and several example points measured with Leica GRX1200*

As it can be seen in Figure 4.1, the location is in the middle of the green area, far from buildings; this should decrease the errors due to multipath. Furthermore, the surveying area is suitable for the receiver can continuously track at least 4 satellites with 15º angle view.

**Surveying for Reference Network 1 -The Fountain-**

"Stop-and-Go GPS Surveying Technique" is performed during the surveying by Leica GRX1200 in order to define Reference Network 1. Leica receiver is used as rover the whole time. At the below, more information about experiment is sorted:

- "Stop-and-Go GPS Surveying Technique" is the kinematic technique, because the user's receiver continues to track satellites while it is in motion. It is known as stop-and-go (or

semi-kinematic) technique because of the coordinates of the receiver are only of the interest when it is stationary (the stop part) but the receiver continues to function while is being moved (the `go' part) from one stationary set up to the next (Rizos).

- Only GPS satellites are considered in processing.

- Elevation mask is defined as 15º.

- No SNR mask is used.

- 5 epochs measured for each point.

Six repetitions are made with Stop-and-Go GPS Surveying around the fountain. Surveys have taken by Leica geodetic receiver uses Milano Permanent Station I on the roof of Department of Architecture building in Politecnico di Milano, in via Edoardo Bonardi, 9. Distance between Milano Permanent Station I and surveying points are under couple hundred meters. True 3-D coordinates of the Milano Permanent Station I are listed in Table 4.1.

*Table 4.1:* True coordinates in UTM32N for Milano Permanent Station I.

| East [meters] | North [meters] | Height [meters] |
|---|---|---|
| 517924.014 | 5036298.544 | 187.262 |

By LGO, the results are obtained in ETRF UTM-32N coordinates (East, North, Height, …) for each repetition. 6 coordinates for each point from 6 repetition of stop-and-go surveying are averaged in order to use reference in comparison with coordinates from low-cost GPS measurements.

**Analysis of Reference Network 1 -The Fountain-**

An analysis of the data is performed in order to show the quality of the reference which is produced by averaging the coordinates. The analysis assesses the repeatability of the data which is the maximum difference between estimated coordinates in Table 4.2.

Reference Network 1 (around the fountain) is used in comparison with kinematic and static surveying by smartphone in Chapter 5.

|  | East [cm] | North [cm] | Height [cm] |
|---|---|---|---|
| Best | 0.3 | 0.5 | 0.4 |
| Worst | 4.2 | 4.3 | 4.5 |
| Mean | 1.9 | 1.9 | 2.2 |

## 4.3  Reference Trajectory 2: Kinematic Trajectory

"Reference Trajectory 2" have been set in green area in front of Leonardo Campus of Politecnico di Milano in 2017, several days in November and December (see Figure 4.4). The area used for kinematic trajectory is near the fountain area (see Figure 4.1) .
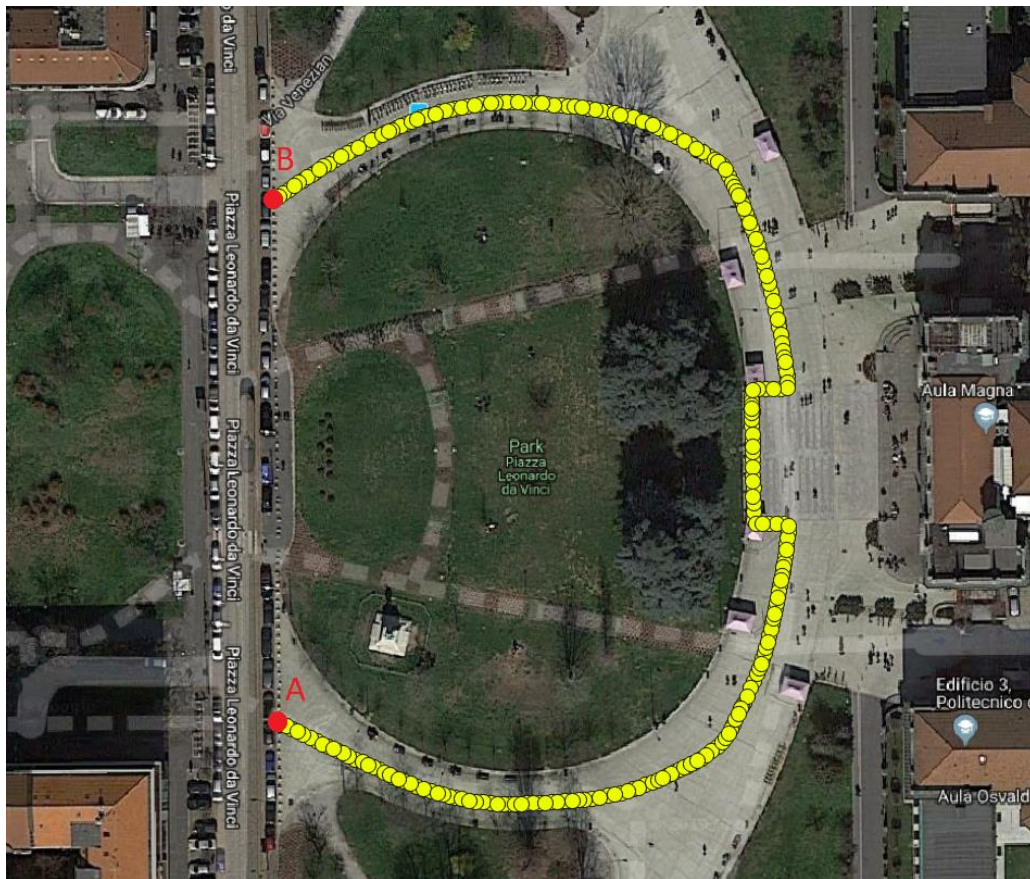


Figure 4.4: Estimated trajectory (in yellow) and estimated end point locations (in red)

68

As seen on Figure 4.4, a visible and repeatable path has been identified on the middle of the green area. Determined track goes through the joints between concrete blocks all the way long on the ground from Point A to Point B. Track mostly follows the center of the path. However, middle of the path there is a marble floor. At that area track goes around the marble floor by following joints. Defined track has approximately 275 meters length.

Endpoints of the track, Point A and B, shown on Figure 4.5:

- Point A has chosen at 13th pillar looking from south to north.
- Point B has chosen at 14th pillar looking from north to south.



*Figure 4.5: The locations of Point A and Point B (on the left point A is presented, on the right point B is presented).*

The estimated 3-D coordinates of the endpoints are listed in Table 4.3.

*Table 4.3: Approximately endpoint coordinates (ETRF UTM-32N).*

| Points | X(East)(meters) | Y(North)(meters) | h(meters) |
|--------|-----------------|------------------|-----------|
| A | 517646.9 | 5036043.9 | 159.9 |
| B | 517646.2 | 5036131.8 | 160.1 |

The defined track for Reference Trajectory 2 is in the same green area applied for Reference Network 1. As we remembered, the location is chosen at the middle of the green area, far from buildings to decrease the errors due to multipath. Furthermore, the surveying area is suitable because the sky is almost open above 15º angle view. However, track (approximately 275 meters track) for kinematic surveys is longer in comparison with fountain area (approximately 75 meters round).

### 4.3.1  Surveying for Reference Trajectory 2 -Kinematic Trajectory-

"Kinematic Surveying Technique" is perform during the surveying by Leica GRX1200 in order to define Reference Trajectory 2. Leica receiver is used as rover the whole time. At the below, more information about experiment is sorted:

- "Kinematic Surveying Technique" is a generalization of stop-and-go technique used while generating Reference Network 1. Instead of only coordinating the stationary points and disregarding the trajectory of the roving antenna as it moves from point-to-point, the intention of kinematic surveying is to determine the position of antenna while it is in motion. In many respects the technique is similar to stop-and-go technique. That is, ambiguities must be resolved before starting the survey, and ambiguities must be reinitialized during the survey when a cycle slip occurs (Rizos).

- Only GPS satellites are considered in processing.

- Elevation mask is defined as 15º.

- No SNR mask is used.

- Sampling rate is defined as 1 HZ (1 observation for each second).

Kinematic surveys by Leica geodetic receiver at Reference Trajectory 2 uses Milano Permanent Station I on the roof of Department of Architecture building in Politecnico di Milano, in via Edoardo Bonardi, 9 as Reference Network 1. The distance between Milano Permanent Station I and surveying points is under couple hundred meters. The 3-D coordinates of the Milano Permanent Station I are listed in Table 4.1.

The positions are collected 4 times by walking with constant speed from Point A to Point B and 4 times from Point B to Point A by Leica GRX1200. In total, eight repetition are made with kinematic surveying on the defined track. By LGO, the results are obtained in ETRF UTM-32N coordinates (East, North, Height, …) for each repetition.

## 4.3.2  The clustering of points from geodetic receiver

The clustering methods are performed for smoothing the point cloud which is obtained by 8 repetition of kinematic survey. Two different clustering method are studied:

- K-means Method, and
- Clustering method implemented by the author.

K-means is studied as one of the popular clustering method. Additionally, a clustering method has been implemented by the author as an alternative.

### *4.3.2.1 K-means method*

K-means is one of the unsupervised learning algorithms that solve the clustering problem. The procedure follows a simple and easy way to classify a given data set through a certain number of clusters (assume $k$ clusters) fixed a priori. The main idea is to define $k$ centroids, one for each cluster. These centroids should be placed in a cunning way because of different location causes different result. So, the better choice is to place them as much as possible far away from each other (MacQueen, 1967).

In present thesis, k-means clustering algorithm is used to create the reference from point cloud in MATLAB. The whole code will be presented in Appendix B.

With k-means clustering algorithm, 4 different reference are created by changing $k$ parameter which defines the number of centroids. $K$ parameter is chosen as 270 and 540 in order to define a centroid for each meter and half meter at approximately 270 meters path. In addition, as an author choice, k-means algorithm is performed with $k=400$ and $k=450$ to see well smoothed centroid spread. Also, *'Replicates'* parameter is defined as 25 which defines the number of times to repeat clustering using new initial cluster centroid positions. Used algorithm initializes centroids and uses squared Euclidean distance by default. K-means returns the solution with the lowest sum value of the point distances to centroids.

In total, four result with different k parameters (270, 400, 450, 540) are shown in Figure 4.6 - Figure 4.13. The statistical comparison between reference and low-cost GPS measurements are only given for references produced with $k=270$ and $k=540$.

The result obtained by k=270 gives the smoothest centroid spread. However, as seen in Figure 4.7, the corners are rounded. By the increase of k parameter, artifacts are started to occur on the corners and some areas which are points have wide spread.
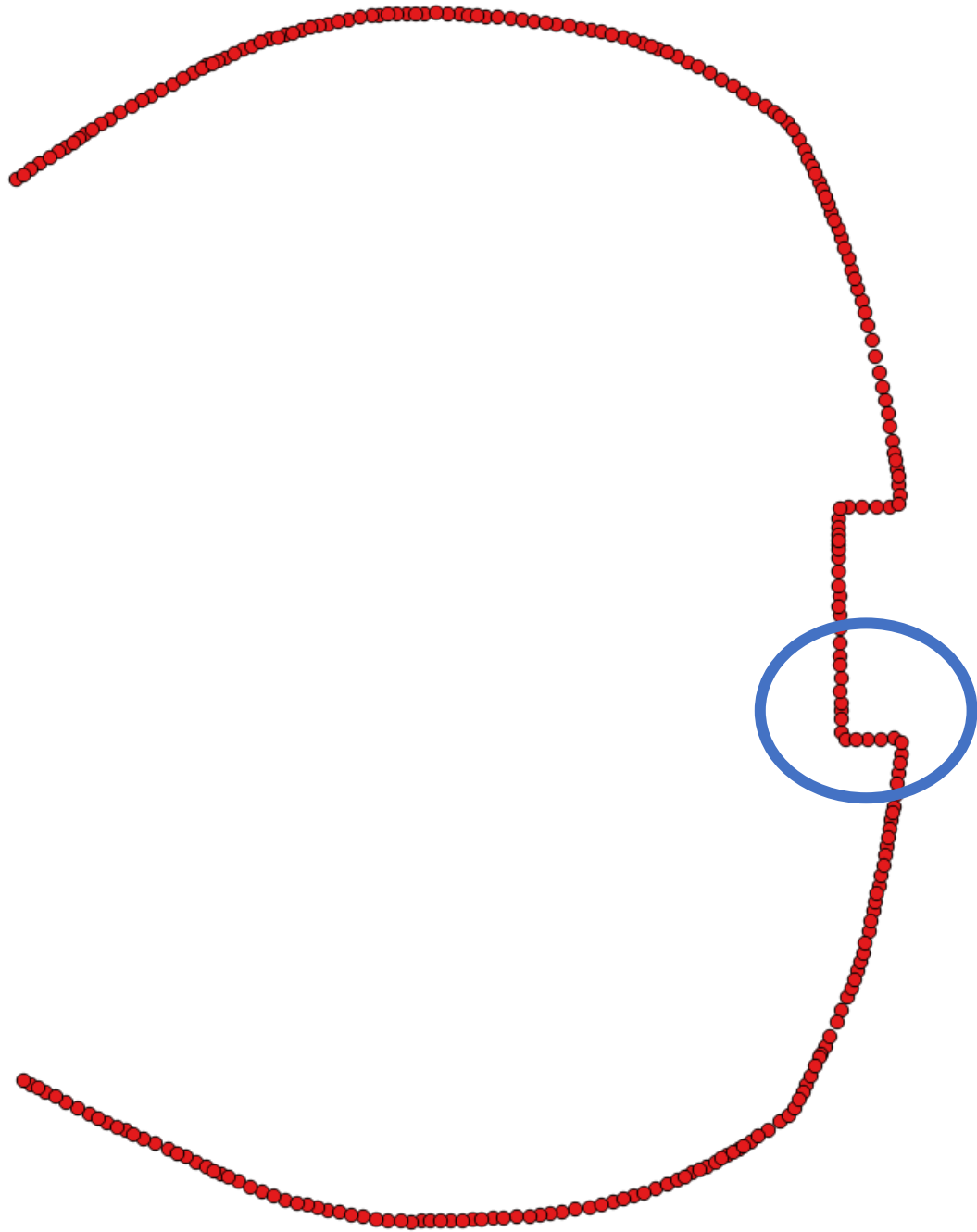
*Figure 4.6: Centroids with k=270 in red (image is generated with QGIS). Blue circle defines zoomed area for the following Figure 4.7.*

*Figure 4.7: Red defines centroids, green defines points measured with Leica GRX1200 at zoom area for "Centroids with k=270" (Figure 4.6)*

*Figure 4.8: Centroids with k=400 in red (image is generated with QGIS). Blue circle defines zoomed area for the following Figure 4.9.*

*Figure 4.9: Red defines centroids, green defines points measured with Leica GRX1200 at zoom area for "Centroids with k=400" (Figure 4.8)*

*Figure 4.10: Centroids with k=450 in red (generated with QGIS). Blue circle defines zoomed area for the following Figure 4.11.*
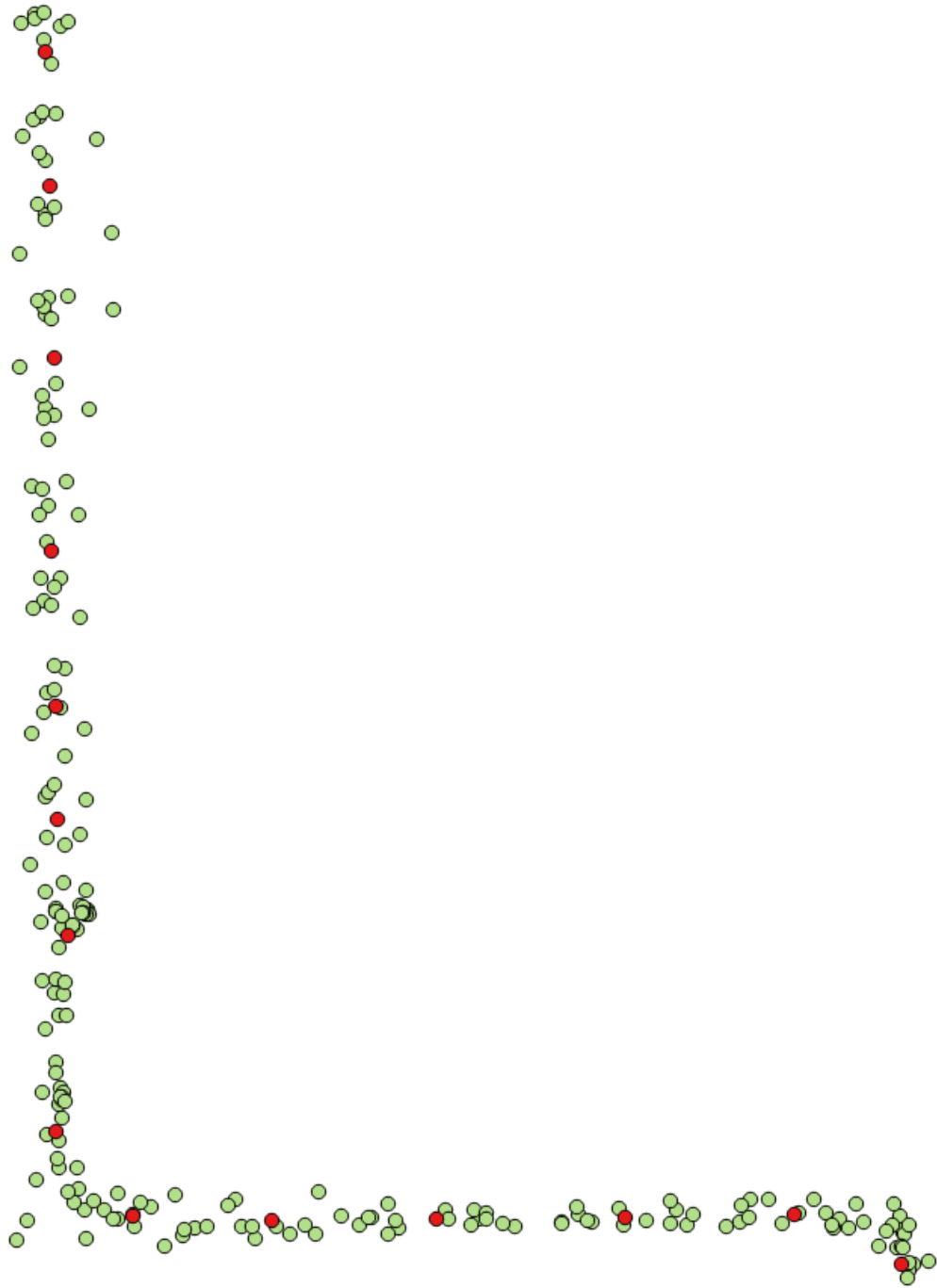
*Figure 4.11: Red defines centroids, green defines points measured with Leica GRX1200 at zoom area for "Centroids with k=450" (Figure 4.10)*

*Figure 4.12: Centroids with k=540 in red (generated with QGIS). Blue circle defines zoomed area for the following Figure 4.13.*
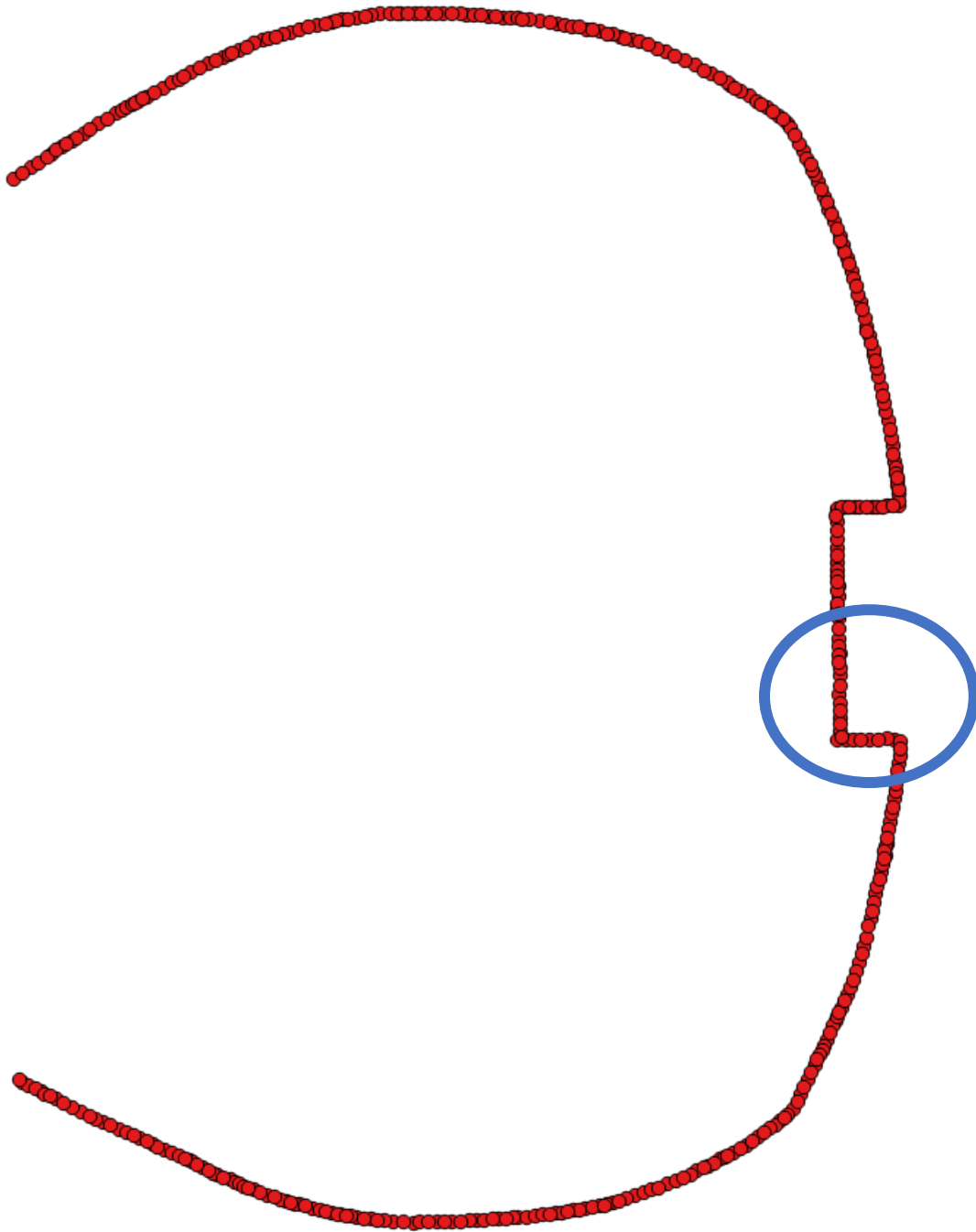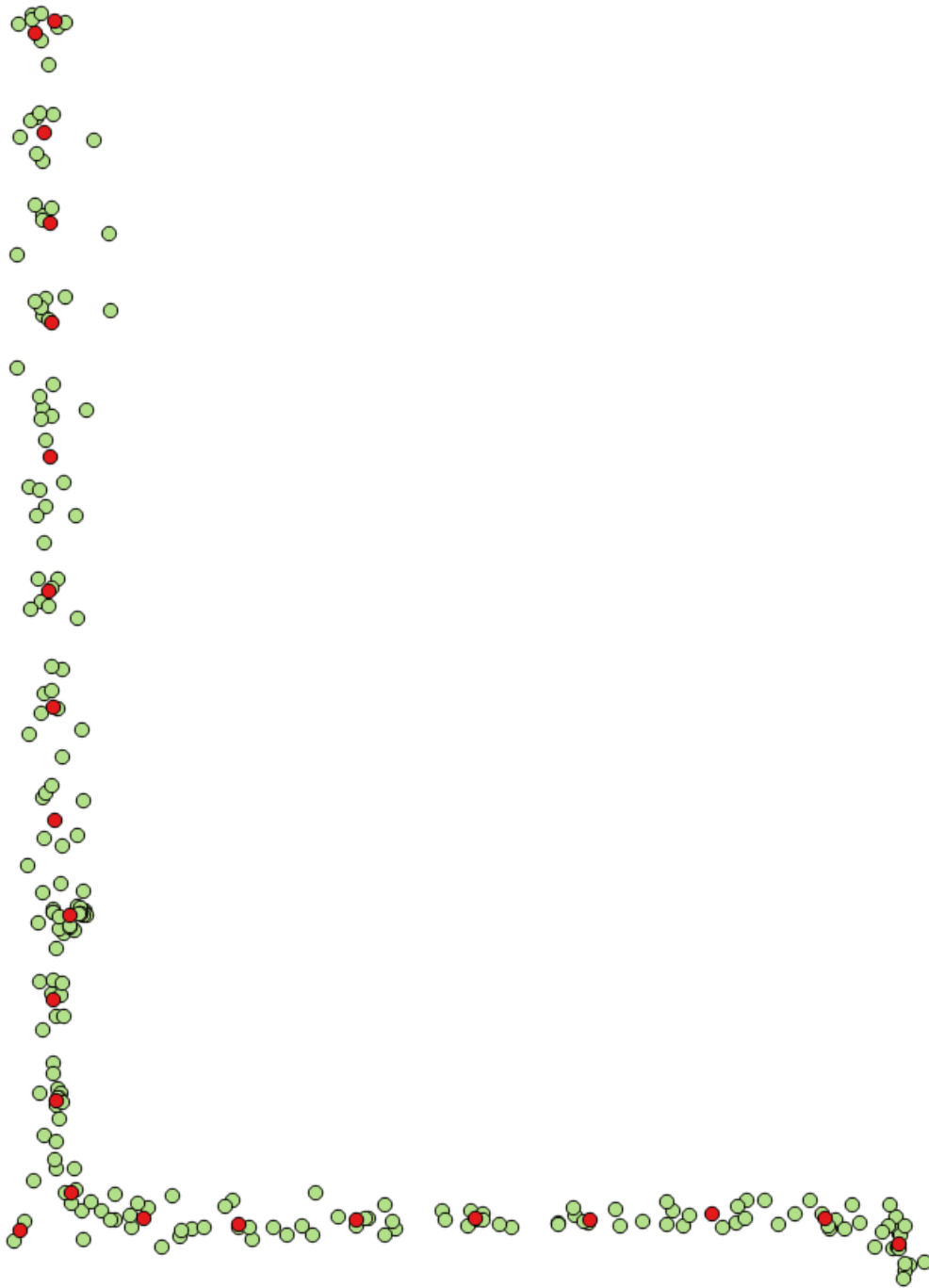
*Figure 4.13: Red defines centroids, green defines points measured with Leica GRX1200 at zoom area for "Centroids with k=540" (Figure 4.12)*
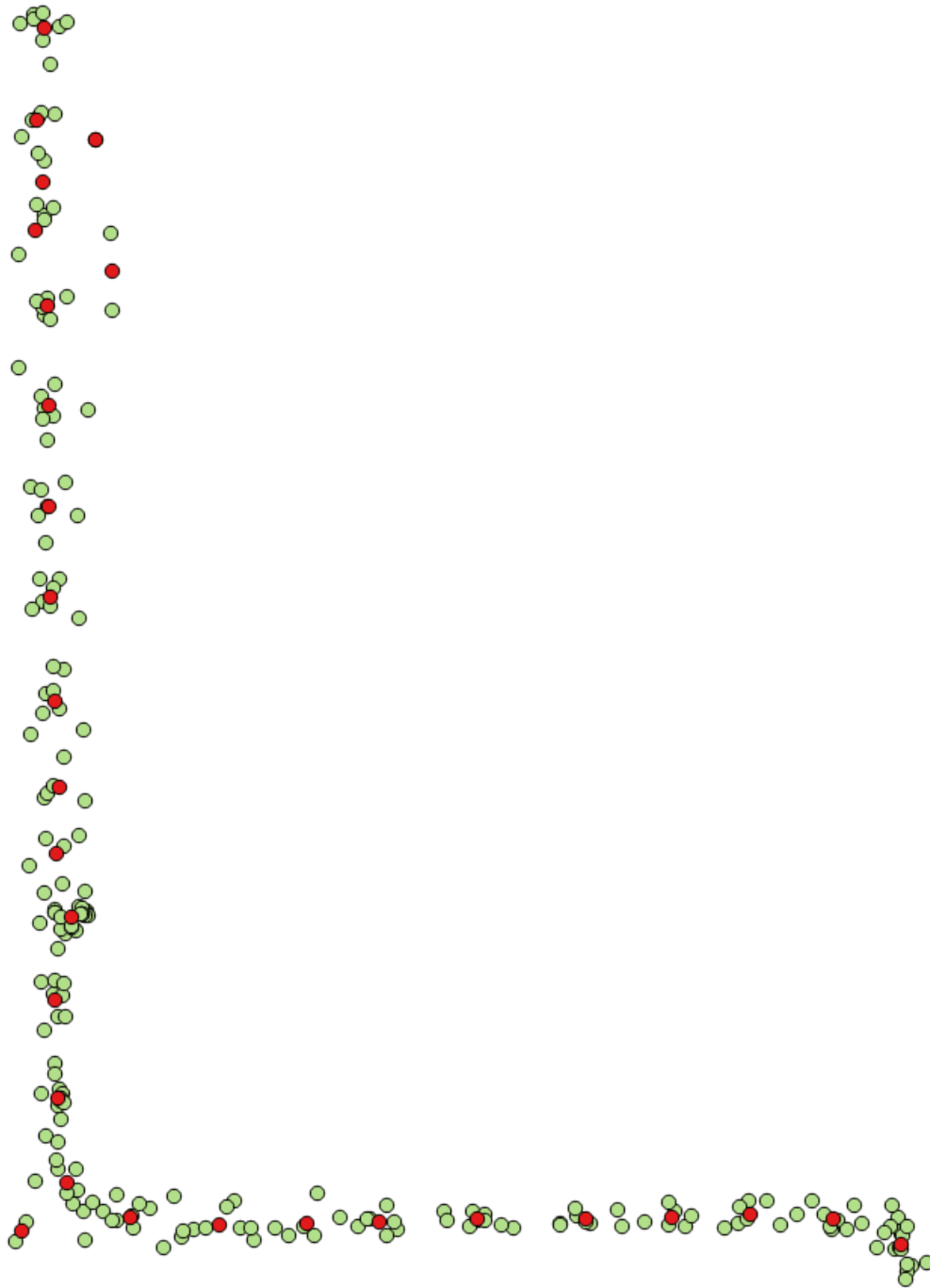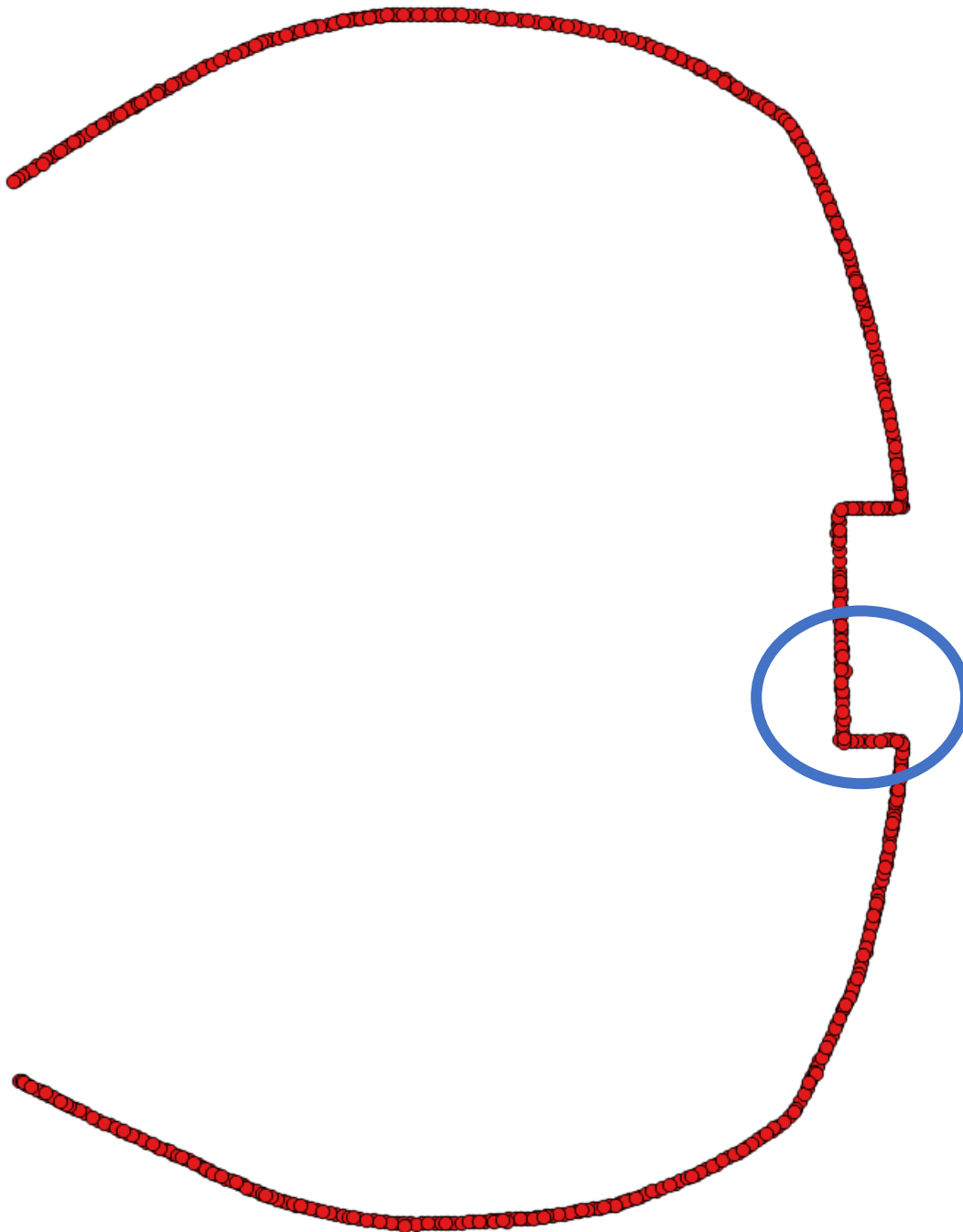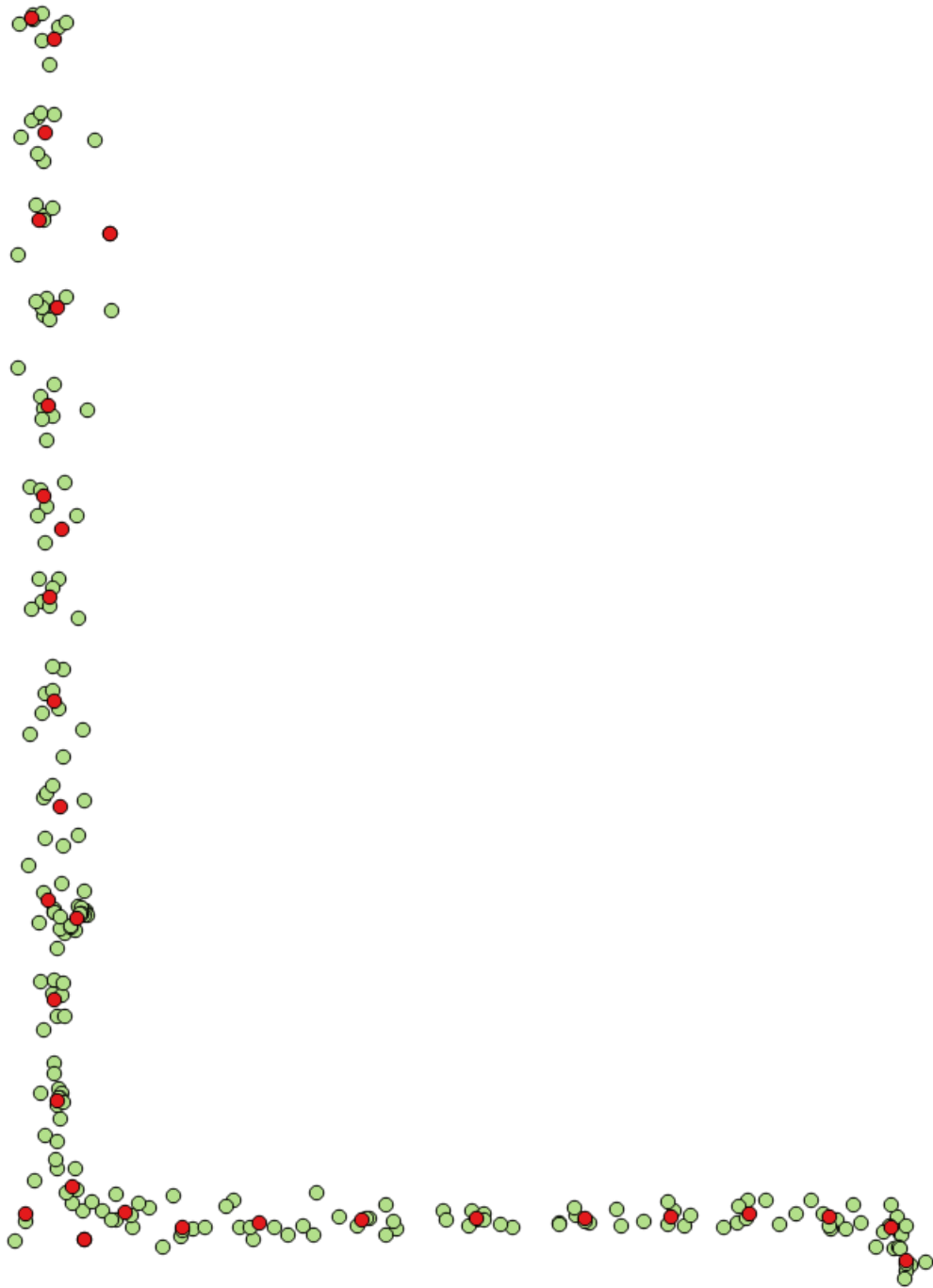
## 4.3.2.2 Clustering method implemented by the author

Beside k-means method, another clustering method is implemented by the author. On the contrary a certain number of clusters (assume $k$ clusters) as fixed a priori in k-means, implemented method classifies a given data set through a distance between centroid and measured points.

In implemented method, $T=25cm$ and $T=50cm$ are defined as a threshold distance (parameter $T$) between centroid of each cluster and measured points in cluster. Thus, point cloud could be clustered in 25cm and 50cm radius circle. This values are corresponding to what $k$ parameters means (number of clusters) in k-means method ($k=270$ one centroid for each meter and $k=540$ one centroid for each half meter).

To explain how algorithm works, a simple example can be shown. At the beginning, a point must be chosen very carefully as the first point. In Figure 4.14, Point 1 chosen as the starting point. As a start, the mean is calculated for the closest point and Point 1 and shown as a blue dot between them in Figure 4.14.
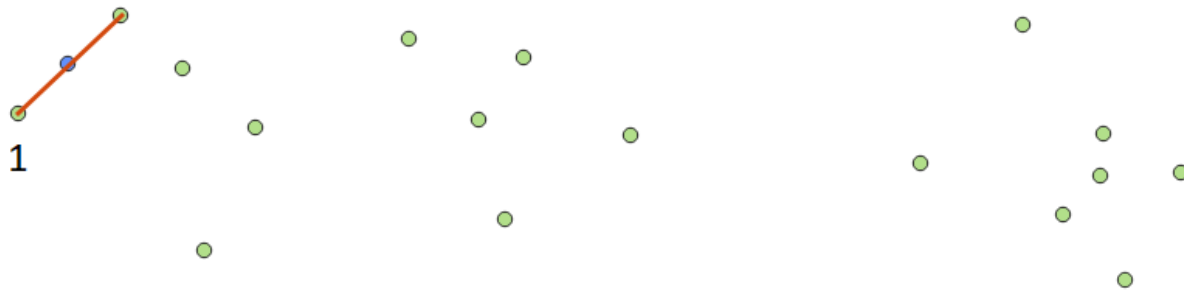


*Figure 4.14: The first step of the example of the clustering method implemented by the author*

In Figure 4.15, the circle has been drawn with red according to defined $T$ parameter as radius. As it is seen, the points are in threshold (in circle – $T$ parameter). In this case, the algorithm continuous to add the closest points.
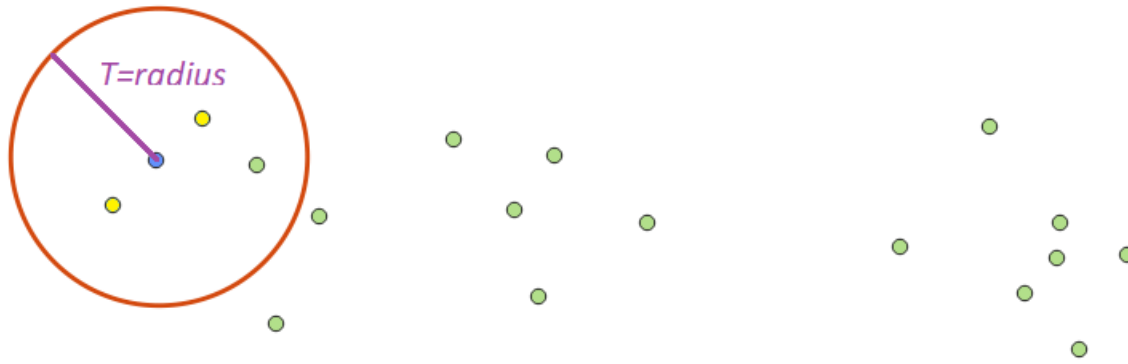
*Figure 4.15: The second step of the example of the clustering method implemented by the author*

After that, the mean is calculated again with adding the second closest point to Point 1 and controlled for $T$ parameter if it fulfills the condition (the distance between centroid and points must be smaller than $T$ parameter) -in Figure 4.16-.
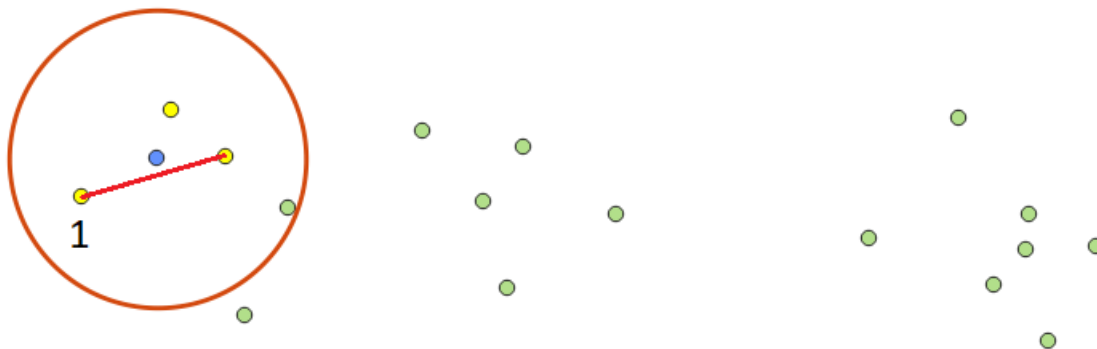


*Figure 4.16: The third step of the example of the clustering method implemented by the author*

The same process continued for the third and fourth closest points in Figure 4.17 and Figure 4.18.
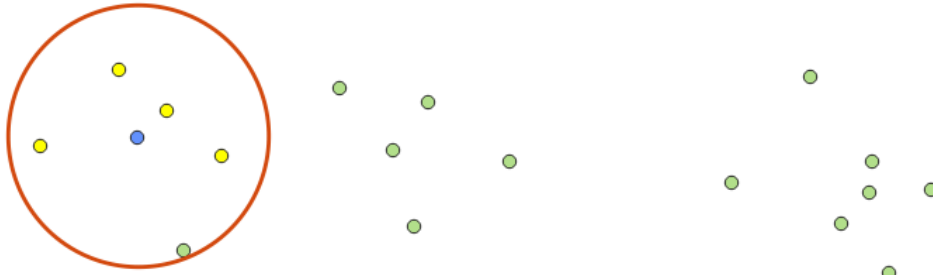
*Figure 4.17: The fourth step of the example of the clustering method implemented by the author*
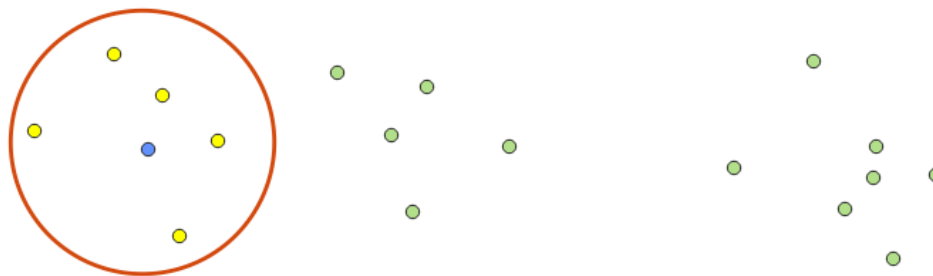


*Figure 4.18: The fifth step of the example of the clustering method implemented by the author*

When $5^{th}$ closest point is added the cluster, the mean of the points (shown in yellow) moved to new location shown in Figure 4.19. This time, the distance between points and mean is greater than the defined threshold ($T$ parameter). This shows the last point (Point 6) belongs to another cluster (see Figure 4.19).
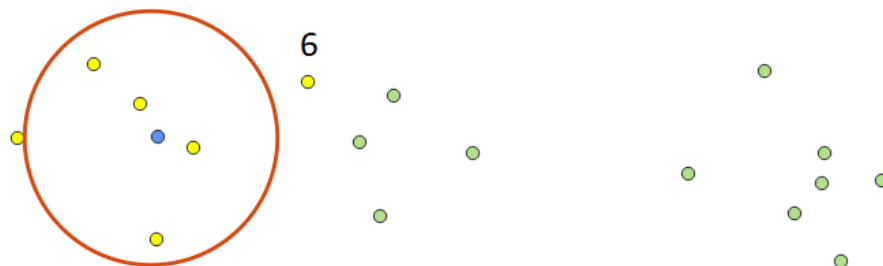


*Figure 4.19: The sixth step of the example of the clustering method implemented by the author*

83

In this case, Points 6 (see Figure 4.19) is removed from the first cluster and then the same process is started for the second cluster with Point 6. After following the same steps of the process, 3 clusters are created for whole point cloud (see Figure 4.20).
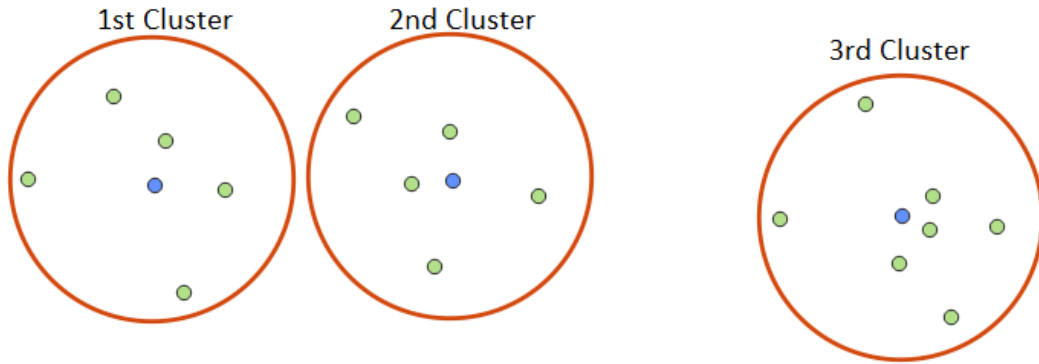


*Figure 4.20: The last step of the example of the clustering method implemented by the author*

In present research, the centroids of the clusters (it can be seen with blue points in Figure 4.20) are used to define the reference. "MATLAB Code" to perform clustering is presented in Appendix C.

With this clustering algorithm, 2 different references are created by changing $T$ parameter ($T=25cm$ and $T=50cm$) which defines the maximum distance of points to the centroid. The outputs from both T parameters are presented in Figure 4.21, Figure 4.22, Figure 4.23 and Figure 4.24 respectively.

The result of clustering with $T=25cm$ can be compared with k-means clustering $k=540$ results. The comparison between both shows that they have similar results, however, implemented clustering method has more artifacts than k-means. Also, the comparison between the result of clustering with $T=50cm$ and k-means clustering k=270 leads to the same conclusion. In the end, implemented clustering method have similar results with a little bit more artifacts.
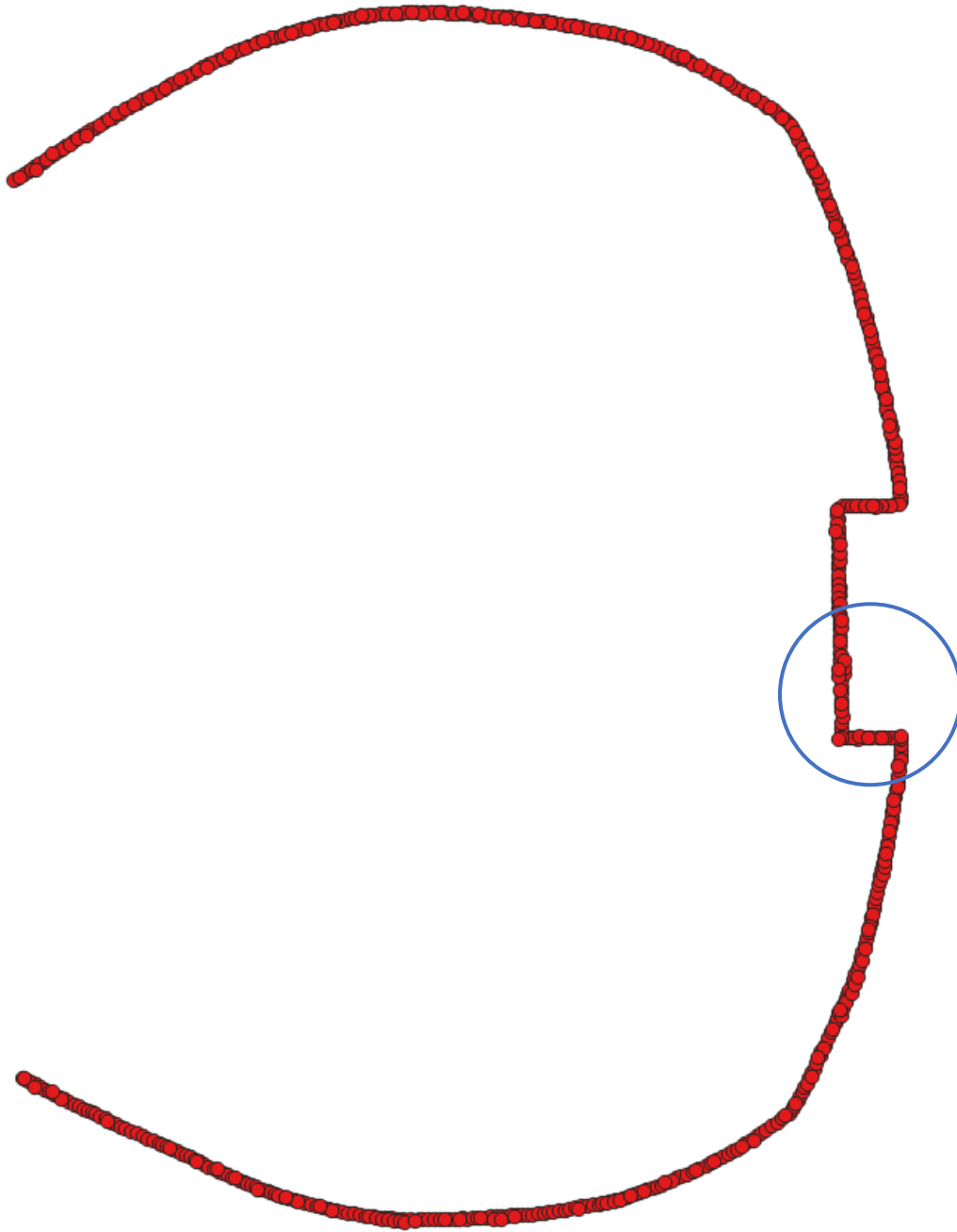
*Figure 4.21: Centroids with T=25cm in red (image is generated with QGIS). Blue circle defines zoomed area for the following Figure 4.22.*
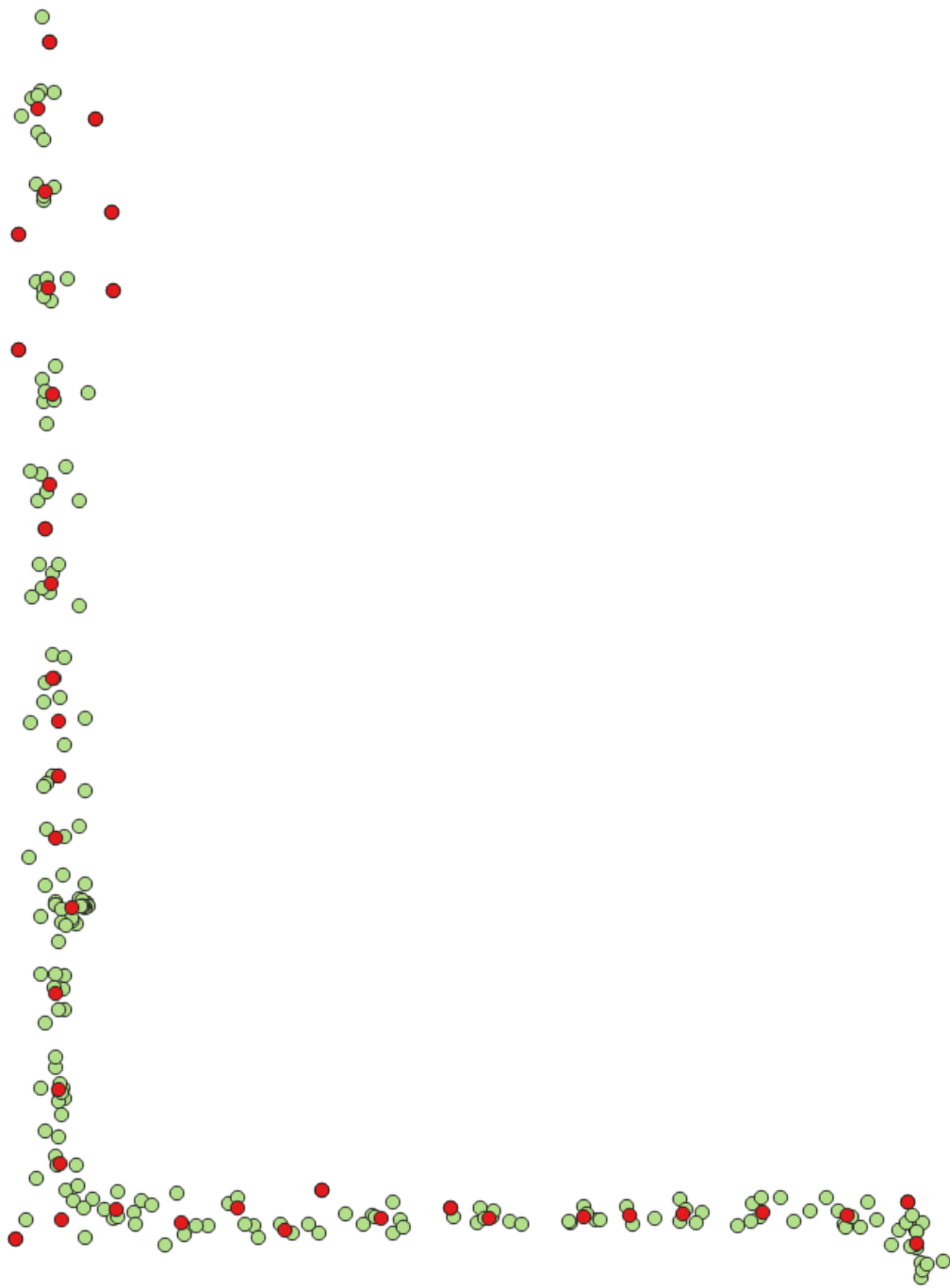
*Figure 4.22: Red defines centroids, green defines points measured with Leica GRX1200 at zoom area for "Centroids with T=25cm" (Figure 4.21)*
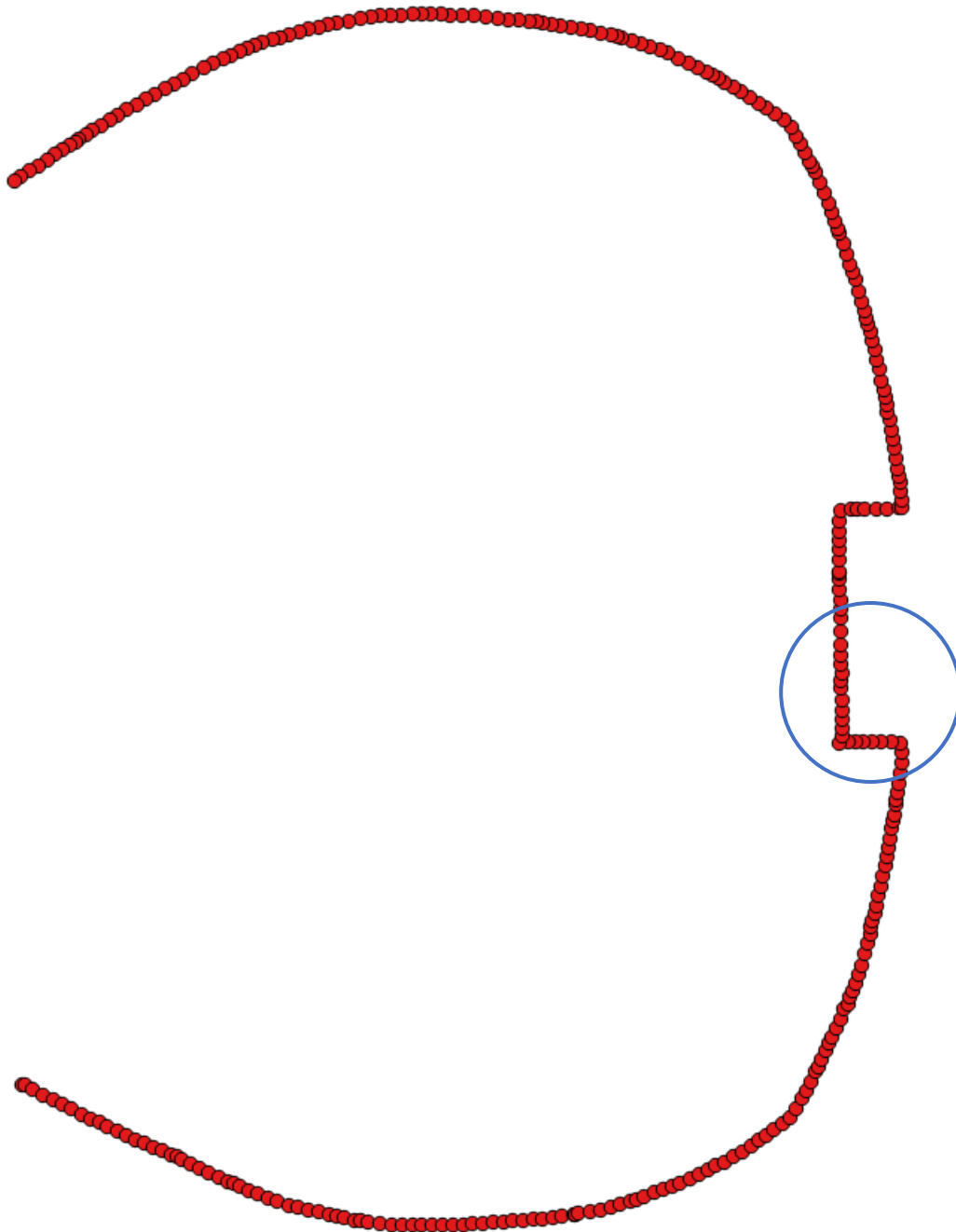
*Figure 4.23: Centroids with T=50cm in red (image is generated with QGIS). Blue circle defines zoomed area for the following Figure 4.24.*
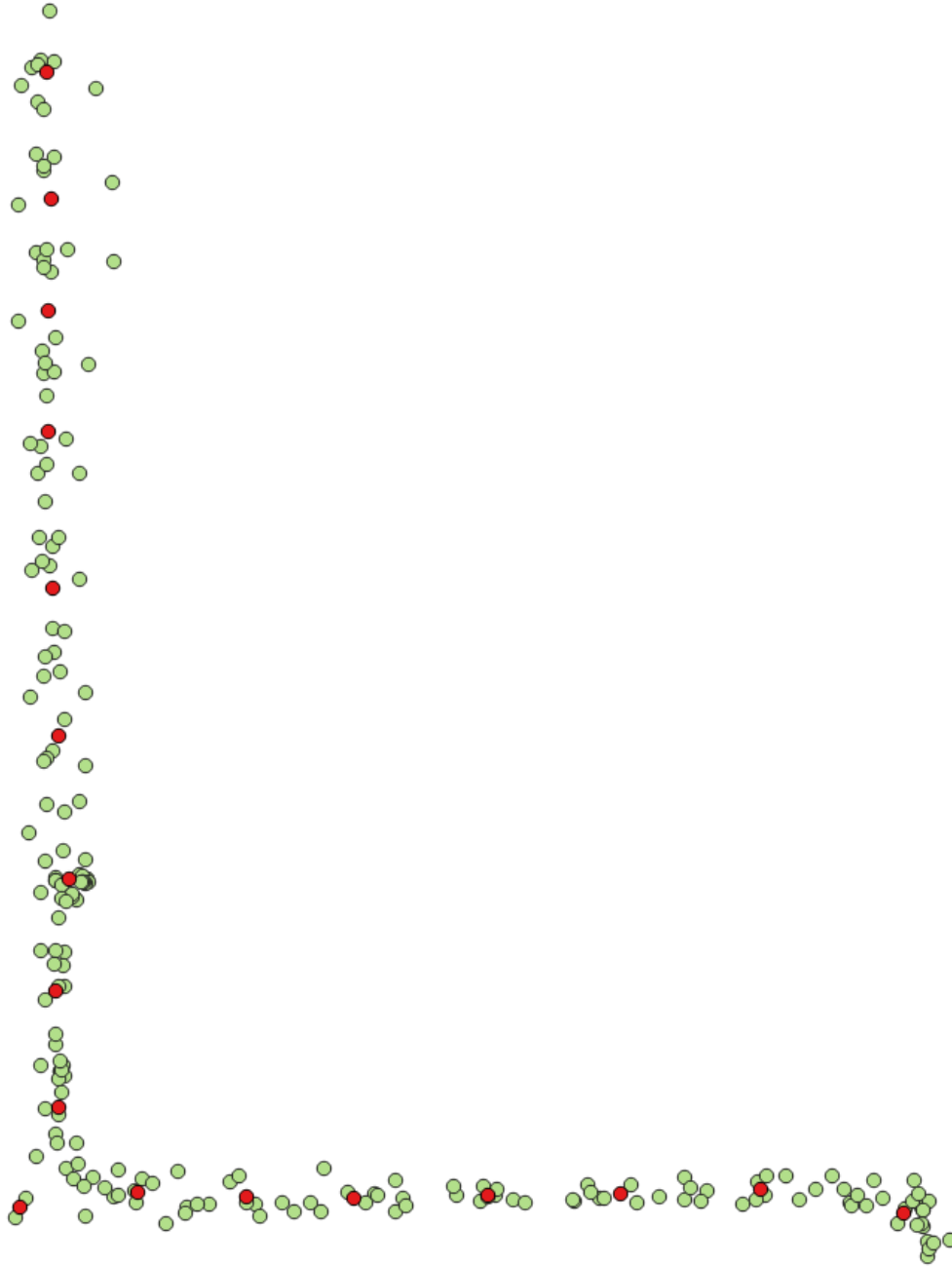
*Figure 4.24: Red defines centroids, green defines points measured with Leica GRX1200 at zoom area for "Centroids with T=50cm" (Figure 4.23)*

# 5  SINGLE FREQUENCY RECEIVER EXPERIMENTS

The chapter is divided into four sections, corresponding to the experiment. First, U-blox data is observed for short observation windows in static mode. Then, two kinematic survey experiments executed with Samsung Galaxy S8 on Reference Network 1 and Reference Trajectory 2. And finally, static survey with smartphone will be discussed. RTKLIB is used as the preferred software package for processing raw GNSS measurements. The research is interested in only GPS satellites while processing the observations.

## 5.1  Experiment 1: Static Survey with U-blox

The data used in this experiment were acquired during a survey made in Milano, took place in 2014, between GPS day 060 and 064 on the roof of Department of Architecture building, Politecnico di Milano, in via Edoardo Bonardi, 9 (see Figure 5.1). The experiment data is set up from February 1$^{st}$, 2014 to March 5$^{th}$, 2014 with a sampling rate of 1 Hz Static Surveying Technique by U-blox LEA-4T. The field part of the experiment is made by another author, but collected data is used in the present research.

In Experiment 1, the aim is the assessment of accuracy of relative static data processing for L1 receivers. In the research, before the smartphone raw GNSS measurement processing, as a single frequency receiver, U-blox LEA-4T data accuracy is studied for the short cuts of time period. For this purposes, U-blox receiver is used as rover with the following observational operating parameters:

- "Static Surveying Technique" is a GNSS survey, the receiver remains fixed during the period of observation, that is usually called occupation time. The occupation time refers to the time for how long the rover unit should be kept static to achieve the desired level of accuracy. Longer occupation times will lead to higher accuracy.

- Only GPS satellites are considered in processing. Because, in the research, author is interested with only GPS.

- Elevation mask defined as 10º.

- No SNR mask is used.

- Sampling rate is defined as 1HZ (1 observation for each second).
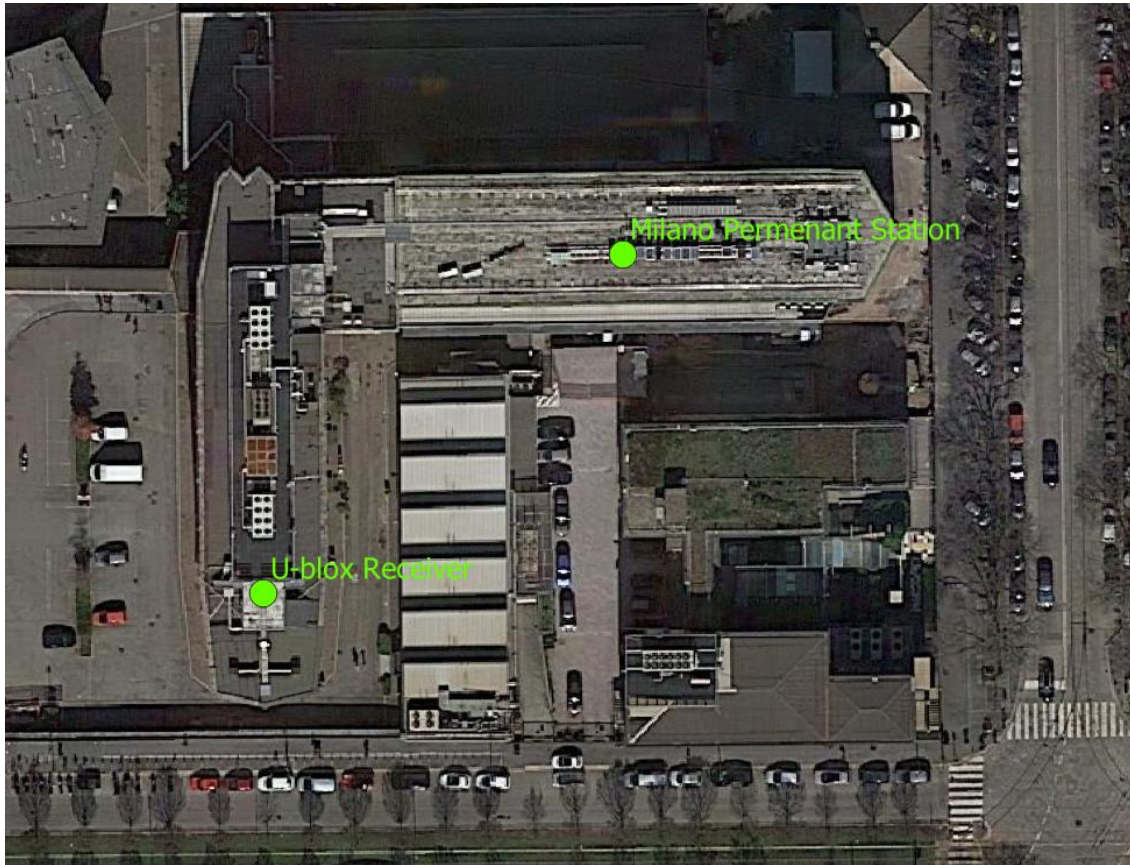
*Figure 5.1: The position of Milano Permanent Station I and the U-blox, the approximate distance is less than 80 meters.*

Milano Permanent Station I has been used as reference while the experiment is placed on the roof of Department of Architecture building (see Figure 5.1). The coordinates of the Milano Permanent Station are listed in Table 5.1.

*Table 5.1: The reference coordinates in UTM32N for Milano Permanent Station I.*

| East [meters] | North [meters] | Height [meters] |
|:---:|:---:|:---:|
| 517924.014 | 5036298.544 | 187.262 |

The flowchart in Figure 5.2, summarizes the overall procedure to identify the differences of each individual part of the whole experiment.

| | |
|---|---|
| The raw data between 28th Feb and 16th Mar | • sample rate of 1HZ<br>• in .ubx file format |
| Daily sessions between 1st-5th Mar (in total: 5 session) | • processed by RTKPOST<br>• averaged for the reference position |
| The hourly sessions of 5 days (in total: 120 session) | • processed by RTKPOST<br>• defining the best and the second best hourly sessions |
| The best and the second best hourly sesions for each day | • two sesions for each five day (in total: 10 sessions) |
| 10 minutes period of time session (in total: 60 session) | • processed by RTKPOST<br>• statistical calculations and analysis |
| 5 minutes period of time session (in total: 120 session) | • processed by RTKPOST<br>• statistical calculations and analysis |

*Figure 5.2: The flowchart of Experiment 1*

## 5.1.1 Define the reference with daily data processing

The raw observation data collected with U-blox LEA-4T in .ubx file format must be transformed to RINEX file format for processing. To do this, several options are available, but the author decided to use RTKCONV function of the RTKLIB software package for the consistency (see Figure 5.3). The raw observation data acquired by U-blox which is continuous from February 1$^{st}$, 2014 to March 5$^{th}$, 2014 is divided to 5 daily smaller sessions.
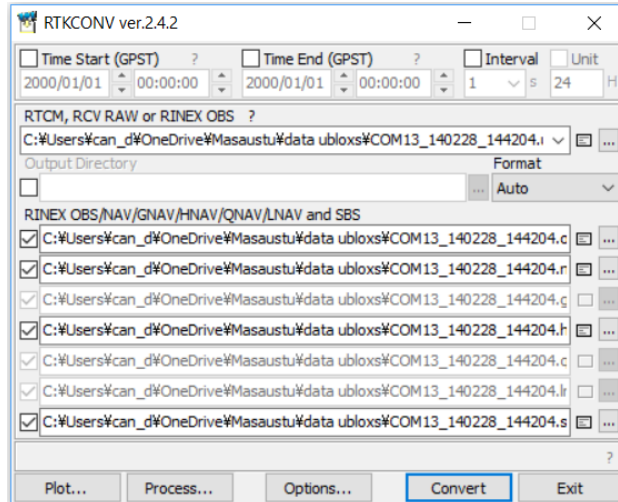
*Figure 5.3: Interface of the RTKCONV function of the RTKLIB software*

By using RTKPOST function of the RTKLIB software, estimated baselines between Milano Permanent Station I and U-blox observations are calculated from the daily observation data with the static mode for each 5 days. Static point positioning by double differencing the carrier phase observations can reach accuracies at sub-centimeter level (literature $0.5 - 1\text{cm}$) in which is detailed according to "Leica User Manual" in Chapter 3. In present research, only single-frequency data from U-blox is available for the processing, therefore, a slight decrease in accuracy is expected. The processing parameters used for processing by RTKLIB are below:

- Processing mode: Static,
- Frequencies: L1 frequency,
- Filter type: Combined,
- Elevation cut-off: 15 degrees,
- No SNR mask,
- Ionosphere correction: Broadcast,
- Troposphere correction: Saastamoinen,
- Satellite ephemerides: Broadcast,
- Ambiguity resolution: Continuous.

The solutions are printed in E/N/U-Baseline format. The estimated baselines are presented for each daily observation is in Table 5.2.

*Table 5.2: The estimated baselines of the daily u-blox observations to Milano Permanent Station.*

| Sessions | East-baseline [m] | North-baseline [m] | Up-baseline [m] |
|---|---|---|---|
| 01/03/2014 | -44.296 | -45.144 | 6.009 |
| 02/03/2014 | -44.290 | -45.149 | 6.013 |
| 03/03/2014 | -44.291 | -45.148 | 6.014 |
| 04/03/2014 | -44.290 | -45.149 | 6.014 |
| 05/03/2014 | -44.288 | -45.153 | 6.016 |

The results of the statistical analysis of the daily observations are given in Table 5.3. Mean baseline from Table 5.3 will be used as a reference baseline on the next calculations for the shorter session observation statistics.

*Table 5.3: The final results of daily observations (E: East, N: North, U: Up).*

| Statistics | E-Baseline | N-Baseline | U-Baseline |
|---|---|---|---|
| Mean [m] | -44.291 | -45.148 | 6.013 |
| Minimum [m] | -44.296 | -45.153 | 6.009 |
| Maximum [m] | -44.288 | -45.144 | 6.016 |
| Standard Deviation [cm] | 0.297 | 0.324 | 0.254 |

## 5.1.2 Processing hourly data and defining the two best hourly session for each day

After processing daily observations, analyzing the result and deciding the reference baseline; daily raw observation data by U-blox is divided to hourly session by RTKCONV function of the RTKLIB software as that was done earlier. With this pre-processing of hourly observation sessions, in total, 120 shorter raw observation data are obtained.

By using the same processing parameters with daily observation data processing, estimated baselines for hourly data are processed from 120 sessions. This processing is made by using RTKPOST function of the RTKLIB software as that was done before for the daily data.

The time series of the residuals (the hourly sessions that were processed to estimate the rover positions) relative to the reference position (average of the daily sessions) were computed with following formula:

$$\delta x_i = x_i - \bar{x} \qquad\qquad (5.1)$$

Where:

- $x$ is the reference position of the rover which is the average of the daily sessions (see Table 5.3)
- $x_i$ is the estimated position for session $i$,
- $\delta x_i$ is the vector of the residuals.

The residuals are presented as local East, North and Up in comparison to the reference position. In total, 116 hourly session out of 120 gave the fixed result which is the 97% of the total number of the sessions. Four Blunders in a form of residuals are listed in a table below.

*Table 5.4: RTKLIB residuals of blundered hourly sessions*

| Day | Starting Time | dE [cm] | dN [cm] | dU [cm] | 3-D [cm] |
|-----|---------------|---------|---------|---------|----------|
| 01/03/2014 | 01:00 AM | -21.8 | -2.6 | -0.3 | 22.0 |
| 02/03/2014 | 00:00 AM | -22.6 | 0.9 | -3.1 | 22.8 |
| 02/03/2014 | 01:00 AM | -24.8 | -1.8 | -1.0 | 24.9 |
| 03/03/2014 | 04:00 AM | -12.4 | -2.2 | 1.8 | 12.7 |

The statistics of the fixed solutions are presented in Table 5.5, also positions errors with respect to the reference (created with hourly data) are shown in Figure 5.4. The results are satisfactory: The Root Mean Square (RMS) error of the solutions is 1 cm for East, 0.5 cm for North and 1.3 cm for Up.
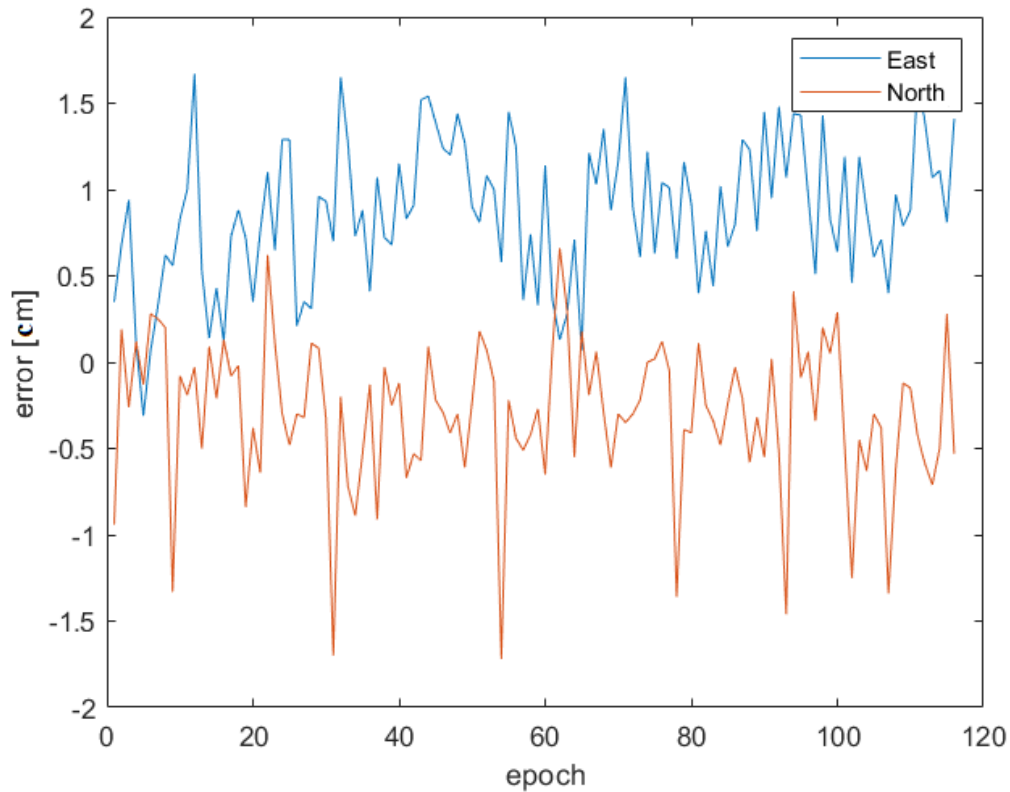
*Figure 5.4: Statistical results for hourly data with respect to reference created from daily data*

*Table 5.5: RTKLIB hourly residuals of final solution (E: East, N: North, U: Up).*

| Statistics | E [cm] | N [cm] | U [cm] |
|:---:|:---:|:---:|:---:|
| Mean | 0.9 | -0.3 | 1.1 |
| Minimum | -0.3 | -1.7 | -0.4 |
| Maximum | 1.7 | 0.7 | 3.4 |
| RMS | 1.0 | 0.5 | 1.3 |

The best two result for each day from hourly sessions are selected for further calculations of 5 minutes and 10 minutes session windows. 3-D distances between hourly observation and reference position which comes daily sessions are considered to define best sessions. These hourly session residuals are presented in Table 5.6.

*Table 5.6: The best two results from hourly observation residuals.*

| Date | Time | dE [cm] | dN [cm] | dU [cm] | 3-D [cm] |
|---|---|---|---|---|---|
| 01/03/2014 | 04:00 AM | 0.1 | 0.1 | 0.3 | 0.4 |
| | 11:00 PM | 0.7 | 0.1 | 0.0 | 0.7 |
| 02/03/2014 | 04:00 AM | 0.2 | -0.3 | 0.5 | 0.6 |
| | 06:00 AM | 0.3 | 0.1 | 0.4 | 0.5 |
| 03/03/2014 | 04:00 PM | 0.4 | 0.1 | 0.4 | 0.6 |
| | 08:00 PM | 0.1 | 0.2 | 0.9 | 0.9 |
| 04/03/2014 | 04:00 AM | 0.6 | -0.2 | -0.1 | 0.7 |
| | 06:00 AM | 0.6 | 0.0 | 0.5 | 0.8 |
| 05/03/2014 | 04:00 AM | 0.5 | -0.3 | 0.3 | 0.7 |
| | 07:00 AM | 0.6 | 0.3 | 0.3 | 0.8 |

### 5.1.3  Processing and analyzing the 10 minutes period data

60 session of 10 minutes period observation data are created by dividing with RTKCONV function of the RTKLIB software as that was done before. By using the same processing parameters with daily and hourly observation data processing, estimated baselines for hourly data is processed from 60 sessions. This processing is made by using RTKPOST function of the RTKLIB software as that was done before for daily and hourly data.

The time series of the residuals (10 minutes time period sessions were processed to estimate the rover positions) relative to the reference position (average of the daily sessions) were computed with the same formula for hourly data (see Equation 5.1)

In total, 31 session out of 60 gave the fixed result which is the 52% of the total. However, the result of 06:10 - 06:19, 02/03/2014 data is unacceptable (farther than 3.5 meters to reference position), nevertheless result is fixed. This session is excluded from statistical calculations. The statistics of the fixed solutions without the unacceptable session are presented in Table 5.7. Also, the table contains the statistics of all solutions (fixed and float). The root mean square (RMS) error of the solutions for fixed is 1.4 cm for East, 0.3 cm for North and 0.7 cm for Up. The errors with respect to reference (created with 10 minutes sessions data) are shown in Figure 5.5.

*Table 5.7: RTKLIB 10 minutes sessions' residuals of final solution for all together fixed and float solutions at the left, and only for fixed solutions at the right (Combined filter type results).*

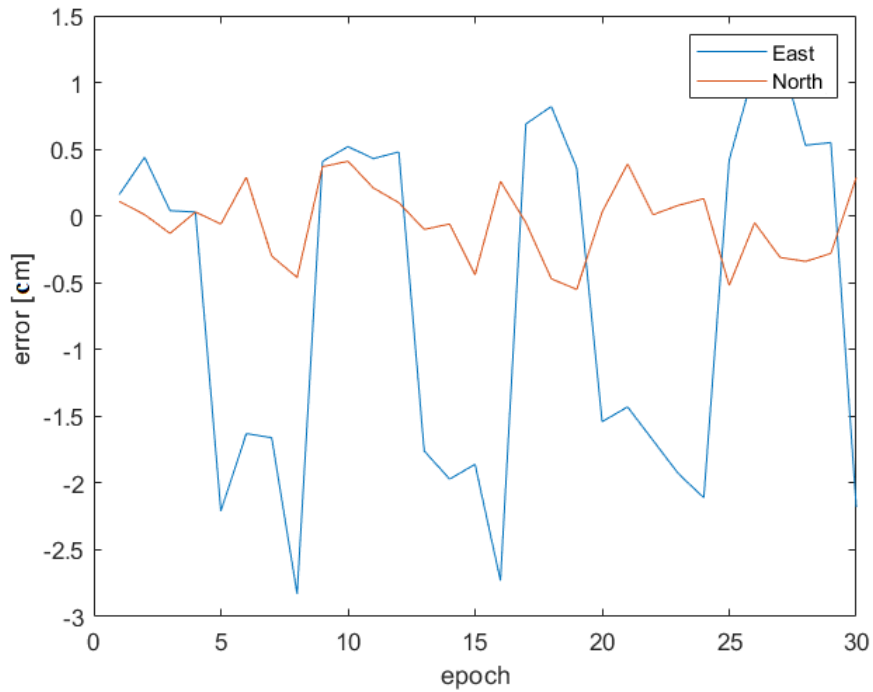| | Combined | | | | | |
|---|---|---|---|---|---|---|
| | Together - fixed and float results | | | Only fixed results | | |
| Statistics | dE [cm] | dN [cm] | dU [cm] | dE [cm] | dN [cm] | dU [cm] |
| Mean | -19.4 | -0.5 | 1.2 | -0.6 | -0.1 | 0.5 |
| Min | -89.6 | -21.0 | -43.3 | -2.8 | -0.6 | -0.4 |
| Max | 14.0 | 29.2 | 45.0 | 1.2 | 0.4 | 1.6 |
| RMS | 33.8 | 8.7 | 14.4 | 1.4 | 0.3 | 0.7 |



*Figure 5.5: Statistical results (from combined) for 10 minutes period data with respect to reference created from daily data*

In addition to the fixed solutions:

➢ 25 session out of 60 gave the float result which is the 42% of the total. Statistics of float results with fixed results are presented in Table 5.7.

➢ 4 session out of 60 didn't give any result which odd situation is. The outputs file of 4 sessions' processing by RTKPOST were not contain neither a result nor error report. These 4 files only had the header part without any result or error message. The reason couldn't be identified, even though the situation was asked to the unofficial RTKLIB forum (which is the only option for users).

After the results obtained with "*Combined*" filter type, additionally, "*Forward*" or "*Backward*" filter type are studied:

- Forward: Kalman is performed forward in time,
- Backward: Kalman is performed backward in time,
- Combined: Combination of the both.

Statistical comparison of the time series for 3 different filter type parameters is presented in Table 5.8 and Table 5.9. The difference of the results from the time series for 3 different filter type parameters are not significant in comparing to instrumental accuracy.

Table 5.8: The statistical comparison of the time series for 3 different filter type parameter (10 minutes session data).

| | | Combined | | | Forward | | | Backward | | |
|---|---|---|---|---|---|---|---|---|---|---|
| | | E-baseline | N-baseline | U-baseline | E-baseline | N-baseline | U-baseline | E-baseline | N-baseline | U-baseline |
| Fixed & Float | Mean[m] | -44.518 | -45.130 | 6.073 | -44.526 | -45.152 | 6.038 | -44.513 | -45.153 | 6.035 |
| | Min [m] | -46.342 | -45.358 | 5.581 | -45.343 | -45.358 | 5.582 | -45.346 | -45.387 | 5.587 |
| | Max [m] | -44.151 | -43.830 | 8.725 | -44.148 | -44.857 | 6.462 | -43.981 | -44.859 | 6.416 |
| | Std [m] | 0.372 | 0.197 | 0.388 | 0.298 | 0.086 | 0.152 | 0.301 | 0.092 | 0.151 |
| Only Fixed | Mean[m] | -44.297 | -45.149 | 6.018 | -44.312 | -45.149 | 6.018 | -44.311 | -45.148 | 6.018 |
| | Min [m] | -44.319 | -45.154 | 6.010 | -44.319 | -45.154 | 6.010 | -44.318 | -45.153 | 6.009 |
| | Max [m] | -44.279 | -45.144 | 6.029 | -44.305 | -45.144 | 6.029 | -44.303 | -45.144 | 6.028 |
| | Std [m] | 0.013 | 0.003 | 0.004 | 0.004 | 0.003 | 0.004 | 0.004 | 0.003 | 0.004 |

Table 5.9: RTKLIB 10 minutes sessions' residuals of final solution for all together fixed and float solutions and only for fixed solutions (Forward and Backward filter type results).

| | Forward | | | | | | Backward | | | | | |
|---|---|---|---|---|---|---|---|---|---|---|---|---|
| | Fixed and float results | | | Only fixed results | | | Fixed and float results | | | Only fixed results | | |
| | dE [cm] | dN [cm] | dU [cm] | dE [cm] | dN [cm] | dU [cm] | dE [cm] | dN [cm] | dU [cm] | dE [cm] | dN [cm] | dU [cm] |
| Mean | -23.5 | -0.3 | 2.5 | -2.1 | -0.1 | 0.5 | -22.2 | -0.4 | 2.1 | -2.0 | 0.0 | 0.5 |
| Min | -105.2 | -21.0 | -43.1 | -2.8 | -0.6 | -0.4 | -105.5 | -23.8 | -42.6 | -2.7 | -0.5 | -0.5 |
| Max | 14.3 | 29.1 | 44.9 | -1.4 | 0.4 | 1.6 | 31.0 | 28.9 | 40.3 | -1.2 | 0.4 | 1.5 |
| RMS | 37.8 | 8.5 | 15.3 | 2.2 | 0.3 | 0.7 | 37.2 | 9.1 | 15.2 | 2.1 | 0.3 | 0.6 |

### 5.1.4 Processing and analyzing the 5 minutes period data

120 session of 5 minutes period observation data are created by dividing with RTKCONV function of the RTKLIB software. By using the same processing parameters with the previous data processing of U-blox, estimated baselines for hourly data is processed from 120 sessions. This processing is made by using RTKPOST function of the RTKLIB software as that was done before.

The time series of the residuals for 5 minutes time period sessions relative to the reference position (average of the daily sessions) were computed with Equation 5.1.

In total, 28 session out of 120 gave the fixed result which is the 23% of the total. However, the results of 3 sessions were unacceptable (farther than a meter to reference position), nevertheless result is fixed:

- The session between 11:35:00 PM – 11:39:59 PM at 01/03/2014
- The session between 06:15:00 AM – 06:19:59 AM at 02/03/2014
- The session between 08:50:00 PM – 08:54:59 PM at 03/03/2014.

These sessions are excluded from statistical calculations. The statistics of the remaining fixed solutions are presented in Table 5.10. Also, the table contains the statistics of all solutions (fixed and float). The root mean square (RMS) error of the solutions for fixed is 1.3 cm for East, 0.3 cm for North and 0.6 cm for Up. The errors with respect to reference (created with 10 minutes sessions data) are shown in Figure 5.6.

*Table 5.10: RTKLIB 5 minutes sessions' residuals of final solution for all together fixed and float solutions at the left, and only for fixed solutions at the right.*

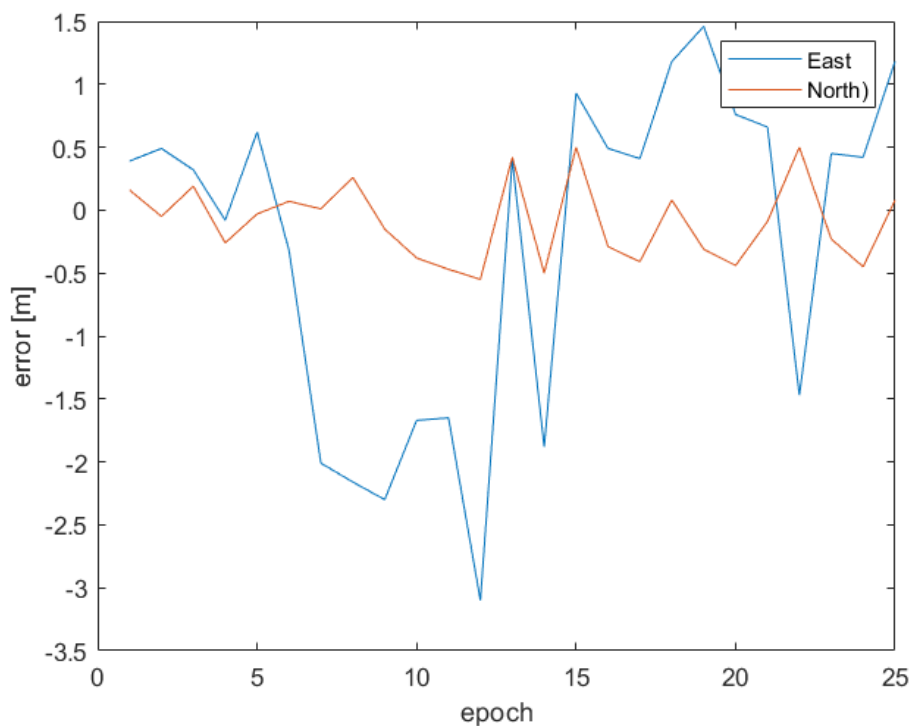| Statistics | Together - fixed and float results | | | Only fixed results | | |
|---|---|---|---|---|---|---|
| | dE [cm] | dN [cm] | dU [cm] | dE [cm] | dN [cm] | dU [cm] |
| Mean | -37.3 | 3.5 | 5.5 | -0.3 | -0.1 | 0.2 |
| Min | -156.5 | -66.5 | -87.7 | -3.1 | -0.6 | -1.1 |
| Max | 134.8 | 48.3 | 89.8 | 1.5 | 0.5 | 1.4 |
| RMS | 61.5 | 19.9 | 32.2 | 1.3 | 0.3 | 0.6 |

*Figure 5.6: Statistical results (from combined) for 5 minutes period data with respect to reference created from daily data*

In addition to the fixed solutions:

➢ 25 session out of 60 gave the float result which is the 42% of the total. Statistics of float results with fixed results are presented in Table 5.7.

➢ 33 session out of 120 didn't give any result which is the same odd situation have been seen with 10 minutes sessions. The outputs file of 33 sessions' processing by RTKPOST were not contain neither a result nor error report. These 33 files only had the header part without any result or error message.

In addition to "*Combined*" filter type, "*Forward*" or "*Backward*" filter type are studied as that was done with 5 minutes sessions. Statistical comparison of the time series for 3 different filter type parameters is presented in Table 5.11 and Table 5.12. The difference of the results from the time series for 3 different filter type parameters are not significant in comparing to instrumental accuracy.

101

Table 5.11: The statistical comparison of the time series for 3 different filter type parameter (5 minutes session data).

| | | Combined | | | Forward | | | Backward | | |
|---|---|---|---|---|---|---|---|---|---|---|
| | | E-baseline | N-baseline | U-baseline | E-baseline | N-baseline | U-baseline | E-baseline | N-baseline | U-baseline |
| Fixed & Float | Mean[m] | -44.6709 | -45.0913 | 6.0948 | -44.7977 | -45.1111 | 6.0833 | -44.7965 | -45.1135 | 6.0860 |
| | Min [m] | -46.3417 | -45.8131 | 4.9592 | -46.1214 | -45.8113 | 4.9592 | -46.1287 | -45.8632 | 4.9610 |
| | Max [m] | -42.7492 | -43.8295 | 8.7250 | -42.9417 | -44.3395 | 7.0697 | -42.9416 | -44.3400 | 7.0736 |
| | Std [m] | 0.5634 | 0.2514 | 0.4491 | 0.5511 | 0.2311 | 0.3645 | 0.5548 | 0.2341 | 0.3666 |
| Only Fixed | Mean[m] | -44.2936 | -45.1493 | 6.0155 | -44.3126 | -45.1493 | 6.0155 | -44.3122 | -45.1490 | 6.0162 |
| | Min [m] | -44.3220 | -45.1539 | 6.0026 | -44.3222 | -45.1539 | 6.0026 | -44.3221 | -45.1555 | 6.0012 |
| | Max [m] | -44.2764 | -45.1434 | 6.0269 | -44.3044 | -45.1434 | 6.0269 | -44.3044 | -45.1437 | 6.0274 |
| | Std [m] | 0.0132 | 0.0032 | 0.0056 | 0.0046 | 0.0032 | 0.0056 | 0.0046 | 0.0032 | 0.0057 |

Table 5.12: RTKLIB 5 minutes sessions' residuals of final solution for all together fixed and float solutions and only for fixed solutions (Forward and Backward filter type results).

| | Forward | | | | | | Backward | | | | | |
|---|---|---|---|---|---|---|---|---|---|---|---|---|
| | Fixed and float results | | | Only fixed results | | | Fixed and float results | | | Only fixed results | | |
| | dE [cm] | dN [cm] | dU [cm] | dE [cm] | dN [cm] | dU [cm] | dE [cm] | dN [cm] | dU [cm] | dE [cm] | dN [cm] | dU [cm] |
| Mean | -50.7 | 3.7 | 7.0 | -2.2 | -0.1 | 0.2 | -50.6 | 3.5 | 7.3 | -2.1 | -0.1 | 0.3 |
| Min | -183.0 | -66.3 | -105.4 | -3.1 | -0.6 | -1.1 | -183.8 | -71.5 | -105.2 | -3.1 | -0.7 | -1.2 |
| Max | 134.9 | 80.9 | 105.6 | -1.3 | 0.5 | 1.4 | 134.9 | 80.8 | 106.0 | -1.3 | 0.5 | 1.4 |
| RMS | 74.7 | 23.3 | 37.0 | 2.2 | 0.3 | 0.6 | 74.9 | 23.6 | 37.2 | 2.2 | 0.3 | 0.6 |

## 5.2   Experiment 2: Kinematic Survey with Smartphone on the Fountain

Experiment 2 have been set around the fountain in green area in front of Leonardo Campus of Politecnico di Milano in 2019, for several days in May. The experiment is performed on Reference Network 1 (see Chapter 4), and coordinated are generated with a sampling rate of 1 HZ in motion by using OruxMaps application of Samsung Galaxy S8.

In Experiment 2, the aim is the assessment of accuracy of the single frequency smartphone receiver for kinematic approach. During the whole experiment, OruxMaps application is used as a map viewer which had access to API level 23. This means, in Experiment 2, raw GNSS measurements are not collected. The coordinates are generated by Samsung Galaxy S8 chipset.

As remembered, a hundred point surrounding the fountain are measured with Leica Geodetic receiver by 6 repetition. By using OruxMaps, the coordinates are collected by counterclockwise walking with a constant speed on the path defined by Reference Network 1.

Five repetition is made with OruxMaps application around the fountain. OruxMaps can store and transform the output to several file formats. In present research, the outputs from OruxMaps are taken as .gpx file. Output file represents the coordinates in units of geographic coordinate system (latitude, longitude and elevation). These coordinates are converted to ETRF UTM-32N coordinates (east, north and height) by using QGIS.

The point positions from five repetition of smartphone measurements are compared one by one with reference which is produced from 6 repetition of geodetic receiver measurements. The comparison can be seen visually in Figure 5.7.
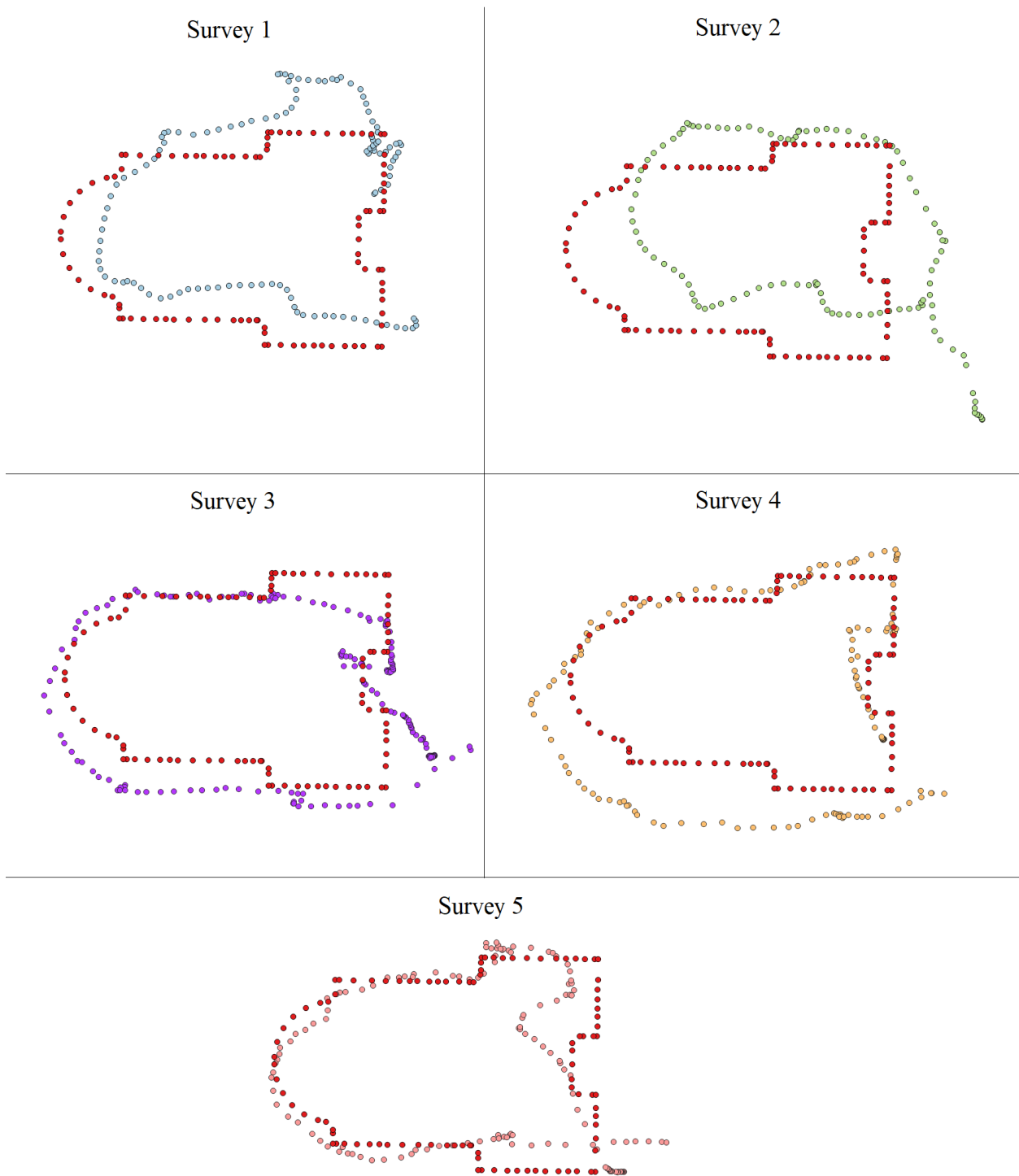
*Figure 5.7: Low-cost receiver coordinates generated by android smartphone chipset in comparison to reference (in red). Survey 1=light blue, Survey 2=light green, Survey 3=purple, Survey 4=orange and Survey 5=pink (produced by QGIS).*

The residuals are calculated for statistical analysis with the following formula:

$$\delta x_i = x_i - \bar{x}$$ (5.2)

Where:

- $x$ is the reference position of the rover which is defined as the closest reference point to the estimated position ($x_i$),
- $x_i$ is the estimated position for session $i$, and
- $\delta x_i$ is the vector of the residuals.

The statistical calculations of the comparison are made by MATLAB. The results are presented in Table 5.13. The distances between estimated points and references reach to 8 meters. Related distances' graphs are presented Figure 5.8 - Figure 5.12 respectively.

*Table 5.13: Statistical results for kinematic surveys with smartphone around the fountain (only OruxMaps). The distances between reference and estimated positions are calculated by Equation above*

| Survey ID | Mean [meters] | Max [meters] | STD [meters] |
|-----------|---------------|--------------|--------------|
| Survey 1  | 1.8           | 4.2          | 1.1          |
| Survey 2  | 2.9           | 8.0          | 2.0          |
| Survey 3  | 1.6           | 6.0          | 1.1          |
| Survey 4  | 1.6           | 4.5          | 1.2          |
| Survey 5  | 1.3           | 5.0          | 1.0          |
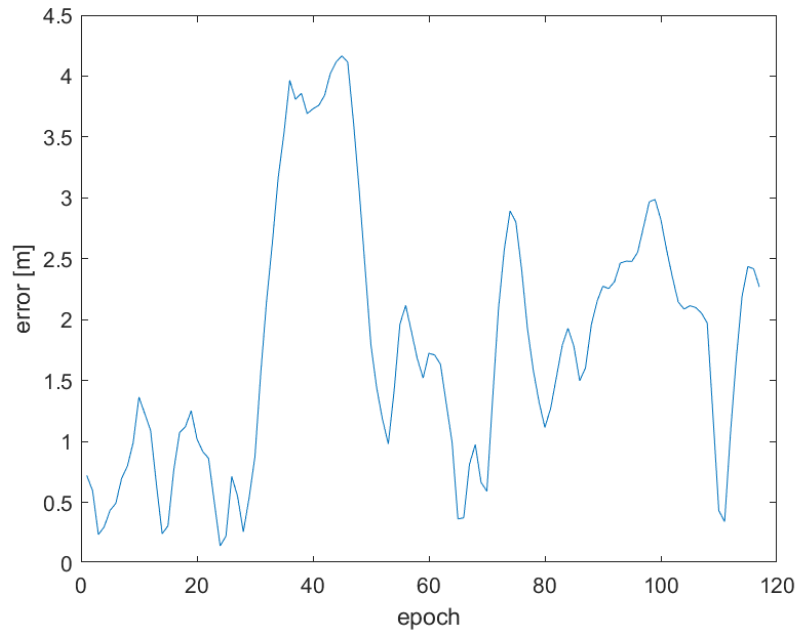
*Figure 5.8: Statistical results for Survey 1 with respect to reference created by average of Stop-and-Go surveying (Reference Network 1).*
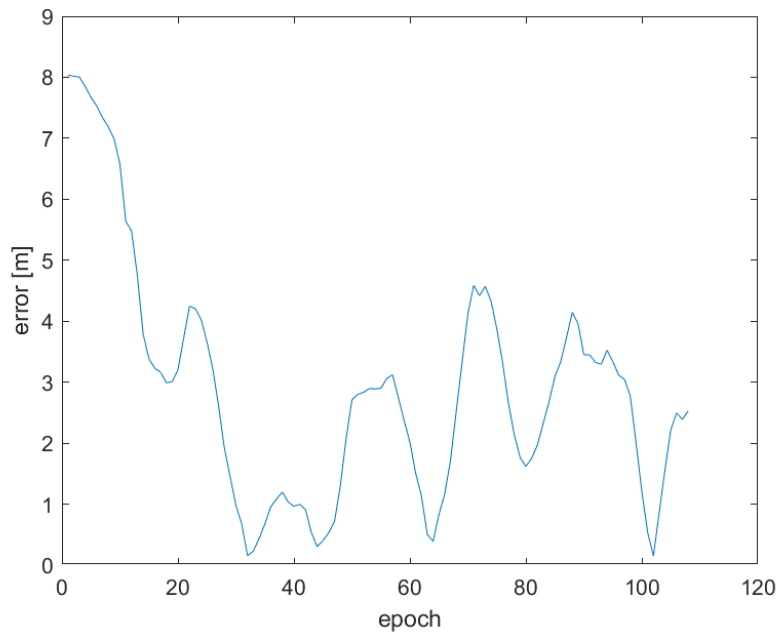


*Figure 5.9: Statistical results for Survey 2 with respect to reference created by average of Stop-and-Go surveying (Reference Network 1).*
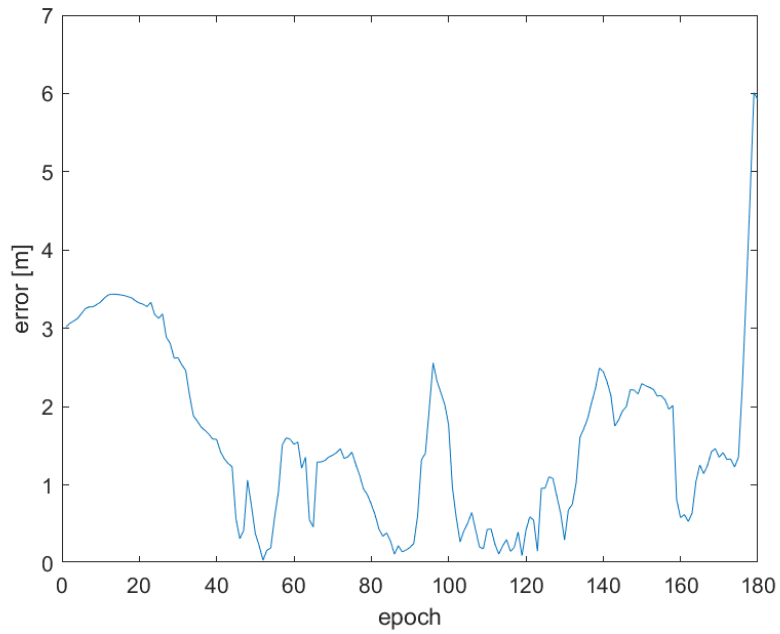
*Figure 5.10: Statistical results for Survey 3 with respect to reference created by average of Stop-and-Go surveying (Reference Network 1).*
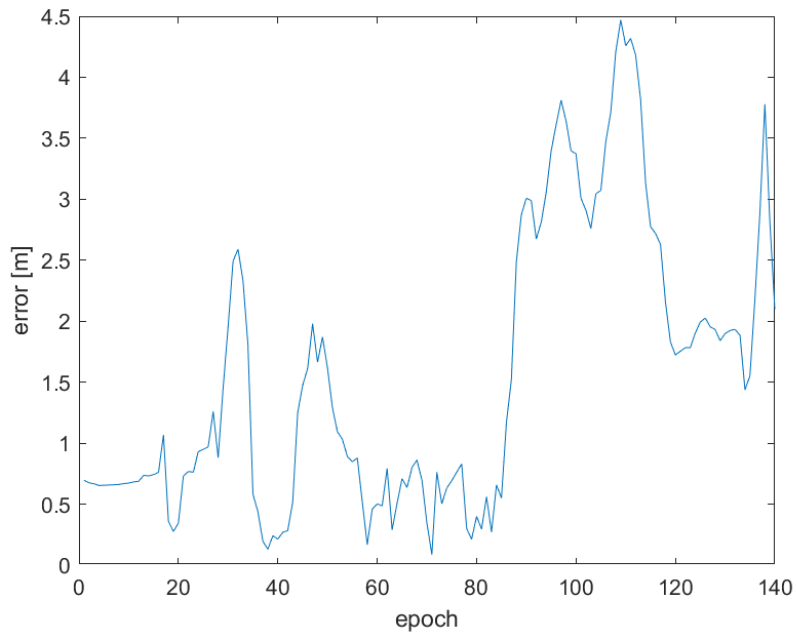


*Figure 5.11: Statistical results for Survey 4 with respect to reference created by average of Stop-and-Go surveying (Reference Network 1).*
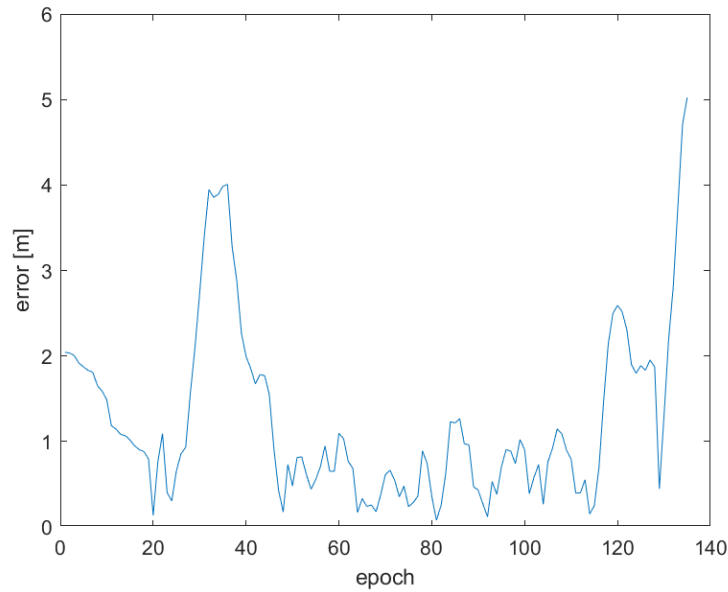
*Figure 5.12: Statistical results for Survey 5 with respect to reference created by average of Stop-and-Go surveying (Reference Network 1).*

## 5.3 Experiment 3: Kinematic Survey with Smartphone on the Kinematic Trajectory

The tests have been set on Reference Trajectory 2 in green area in front of Leonardo Campus of Politecnico di Milano in 2017, for several days in November and December. With Samsung Galaxy S8, points are measured with a sampling rate of 1 HZ.

The flowchart in Figure 5.13, summarizes the overall procedure to identify the differences of each individual part of the whole experiment.



| Field experiment | •14 repetition with OruxMaps in smartphoneS<br>•14 repetition with GNSS Logger in smartphone |
| Processing | •No need with OruxMap<br>•GNSS Logger data processed with GNSS Analsis Tool |
| Result discussion | •Statistics and analysis<br>•Tables |
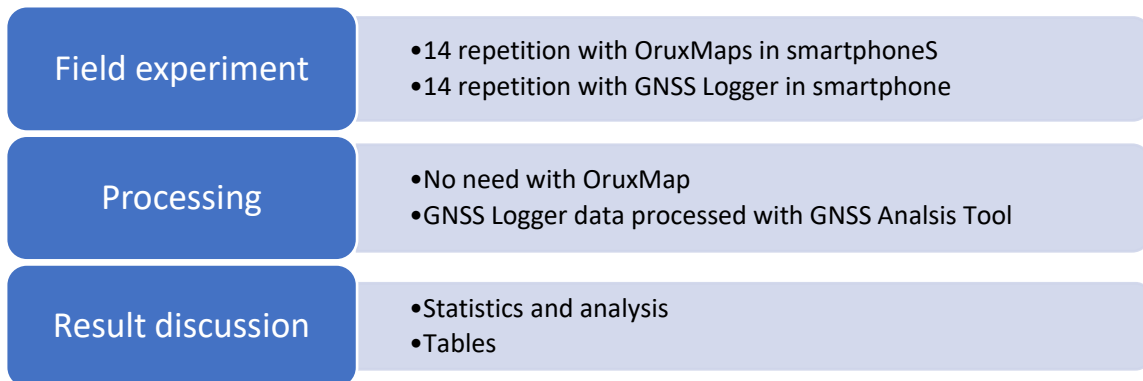
*Figure 5.13: The flowchart of Experiment 3.*

Kinematic surveys with Leica geodetic receiver and clustering methods are explained in detail in Chapter 4. End of these surveys, four reference trajectories are created:

- k-means: *k=270*,
- k-means: *k=540*,
- implemented clustering method: *T=25cm*,
- implemented clustering method: *T=50cm*.

These reference trajectories are compared with the measurement obtained by android smartphone receiver on the following.

In Experiment 3, the aim is the assessment of the accuracy of the single frequency smartphone receiver for kinematic approach. In the experiment, this time raw smartphone measurements are collected and processed by GNSS Analysis Tools in order to compare post-processing results with the coordinates produced by the smartphone chipset.

Two different application are used simultaneously with smartphone:

- OruxMaps: Map viewer application is used to collect positions proved by Samsung Galaxy S8 chipset,
- GNSS Analysis Tool: GNSS Logger to log raw GNSS measurements which are collected by Samsung Galaxy S8 receivers.

## 5.3.1 OruxMaps

The aim of the survey with OruxMaps is to get a first idea about the accuracy of coordinates which are generated by smartphone chipset as that was done in Experiment 2. This time around, comparison is done with Reference Trajectory 2.

In total 14 repetitions of surveys are performed:

- Surveys which are labeled with odd numbers (Survey 1, 3, 5,…) are performed by walking with constant speed from Point A to Point B.
- Surveys which are labeled with even numbers (Survey 2, 4, 6,…) are performed from Point B to Point A as a sequence of previous one.

Observations are stored for each second (1HZ). Output file which is executed in .gpx file by OruxMaps represents the coordinates in units of geographic coordinate system (latitude, longitude and elevation). These coordinates are converted to ETRF UTM-32N coordinates (east, north and height) by QGIS that was done in the previous experiment.

The distances from each estimated point to the closest reference points (generated by k-means *k=270*) calculated by Equation 5.2 as Experiment 2. Mean distance, maximum distance and standard deviation of distances for each survey presented in Table 5.14.

*Table 5.14: Statistics of the distances between estimated points and the closest reference points for k-means k=270.*

| Survey ID | Mean [meters] | Max [meters] | STD [meters] |
|-----------|---------------|--------------|--------------|
| Survey 1  | 1.9           | 5.9          | 1.3          |
| Survey 2  | 2.5           | 7.2          | 1.6          |
| Survey 3  | 2.1           | 5.6          | 1.3          |
| Survey 4  | 6.6           | 15.3         | 3.9          |
| Survey 5  | 4.9           | 12.3         | 3.8          |
| Survey 6  | 4.1           | 9.9          | 2.4          |
| Survey 7  | 1.9           | 3.8          | 1.0          |
| Survey 8  | 3.5           | 9.0          | 1.8          |
| Survey 9  | 3.2           | 10.5         | 2.4          |
| Survey 10 | 4.0           | 13.2         | 2.7          |
| Survey 11 | 3.1           | 7.6          | 1.6          |
| Survey 12 | 3.0           | 8.8          | 1.9          |
| Survey 13 | 2.6           | 6.8          | 1.6          |
| Survey 14 | 4.2           | 13.0         | 3.2          |

High difference between sequence surveys are noticed. For example: the differences between Survey 3 and Survey 4 are quite high take in consideration they is 6 minutes time difference between them.

A simple analysis is performed in order to see difference between 4 reference trajectories (two of them by k-means, two of them by implemented clustering method) on the first 2 surveys. Therefore, the distances to the closest reference points for each epoch are evaluated. Statistics of results are presented in Table 5.15.

*Table 5.15: Statistics of the distances between estimated points and the closest reference points for k-means k=270 and k=540, implemented clustering method T=25cm and T=50cm (Survey 1 and Survey 2 by OruxMaps)*

| References | Survey 1 | | | Survey 2 | | |
|---|---|---|---|---|---|---|
| | **Mean [meters]** | **Max [meters]** | **STD [meters]** | **Mean [meters]** | **Max [meters]** | **STD [meters]** |
| k=270 | 1.9 | 5.9 | 1.3 | 2.5 | 7.2 | 1.6 |
| k=540 | 1.8 | 5.6 | 1.3 | 2.4 | 6.9 | 1.5 |
| T=25cm | 1.8 | 5.6 | 1.3 | 2.4 | 7.1 | 1.6 |
| T=50cm | 1.9 | 5.9 | 1.3 | 2.5 | 7.2 | 1.5 |

As is seen in Table 5.15, there is no significant difference between different reference trajectories. This is expected that there was no big difference between reference trajectories.

As an example; statistics of the comparison between Survey 1 and Survey 2 with reference trajectory (k-means, k=270) are detailed on the following (see Figure 5.14). Epoch by epoch, distances to the reference trajectory (k-means, k=270) graphs are presented in Figure 5.15 and Figure 5.16.

.
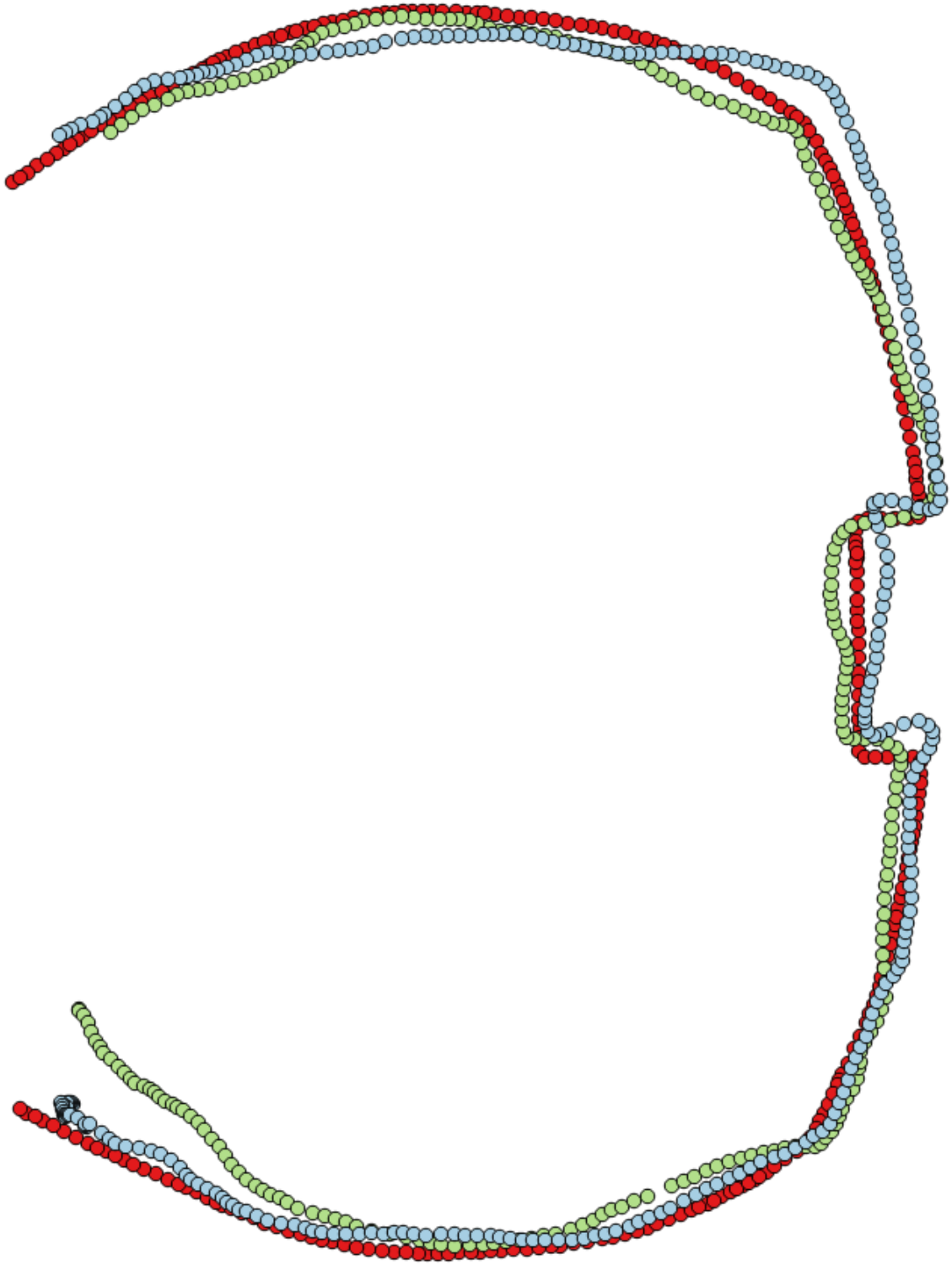
*Figure 5.14: The comparison between Survey 1 and Survey 2 with respect to the reference trajectory k-means k=270. Survey 1 = light green, Survey 2 = light blue and Reference Trajectory 2 = red.*
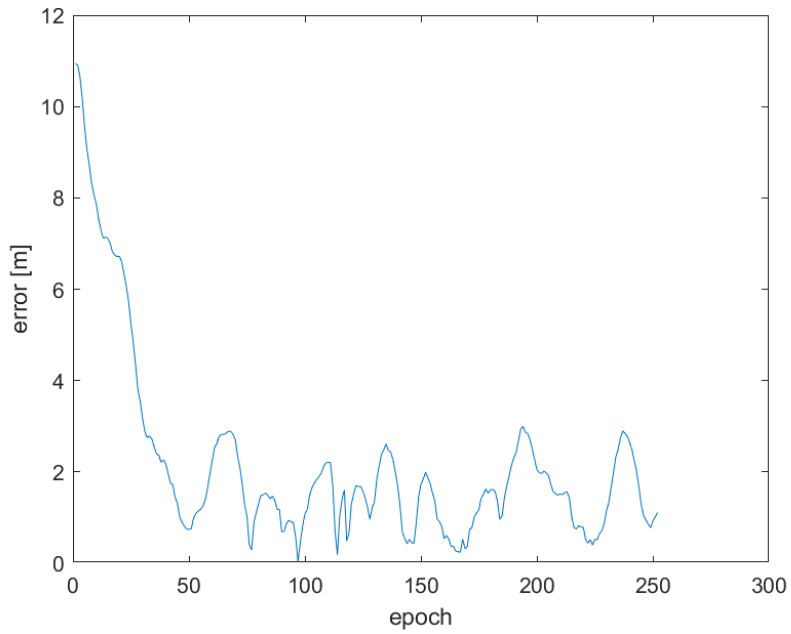
*Figure 5.15: Statistical results for Survey 1 with respect to reference created with K-means clustering method k=270cm (OruxMaps).*
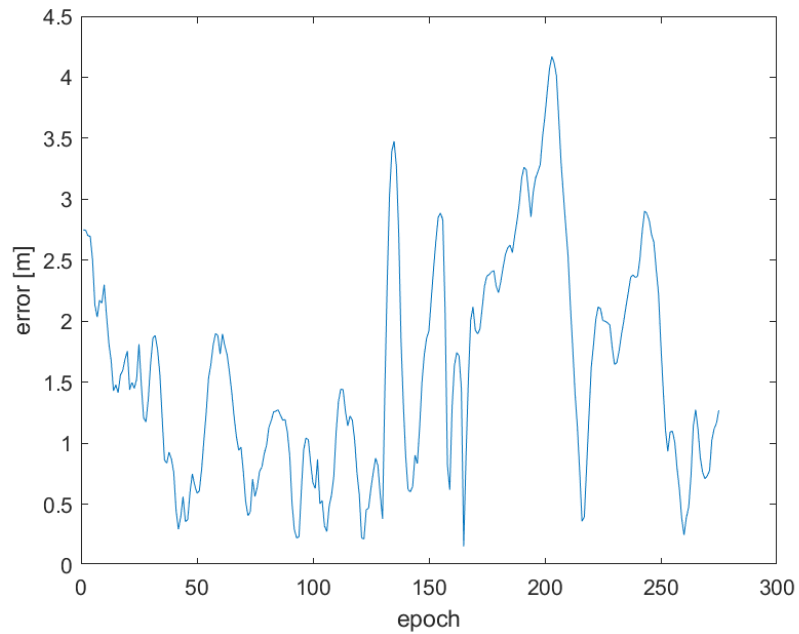


*Figure 5.16: Statistical results for Survey 2 with respect to reference created with K-means clustering method k=270cm (OruxMaps).*

113

## 5.3.2 GNSS Analysis Tools

In Android Release N ("Nougat"), Google introduced APIs giving access to GNSS raw measurements from smartphones. After that, Google has publicly released Analysis Tools to process and analyze these measurements. Analysis Tools includes GNSS Logger APK for android and GNSS Analysis App for desktop. In present research, the aim of the use of the Analysis Tools is to investigate and analyze these raw measurements.

GNSS Logger APK is a sample application that shows how to log data related to Android location, including raw GNSS measurements. This application can create output file with .txt extension for GNSS Analysis Tool in Desktop which can process and analyze GNSS raw measurements from your phone. GNSS Analysis Tool is released by Google in order to see in detail how well the GNSS receivers are working in each particular phone design and thus improve the GNSS design and performance in their phones. GNSS Logger APK and GNSS Analysis Tool are publicly available for app-developers, researchers and educators.



*Figure 5.17: GNSS Logger APK output.*

By using GNSS Logger APK, 14 surveys are made simultaneously with OruxMaps. As mentioned before, surveys labeled with odd numbers are made by walking from Point A to Point B and the even numbered surveys are from Point B to Point A. Data is stored for each second (1HZ). The outputs from GNSS Logger APK are taken in unique format which can be analyzed and processed by GNSS Analysis Tool in Desktop. The unique format (see Figure 5.17) is not readable by well-known GNSS processing packages which are able to read RINEX format.

14 GNSS Logger output are processed by GNSS Analysis Tool in Desktop which uses Weighted Least Square Estimation to compute positions. Table 5.16 presents the statistical results for 14 Survey processed by GNSS Analysis Tool.

*Table 5.16: Statistics of the distances between estimated points and the closest reference points for k-means k=270 (GNSS Analysis Tool).*

| Survey ID | Mean [meters] | Max [meters] | STD [meters] |
|-----------|---------------|--------------|--------------|
| Survey 1  | 3.7           | 22.3         | 3.2          |
| Survey 2  | 5.3           | 19.4         | 4.1          |
| Survey 3  | 5.0           | 30.7         | 5.2          |
| Survey 4  | 4.2           | 23.3         | 3.8          |
| Survey 5  | 4.0           | 22.5         | 3.5          |
| Survey 6  | 4.8           | 23.8         | 4.2          |
| Survey 7  | 4.7           | 22.8         | 4.1          |
| Survey 8  | 4.3           | 28.0         | 3.5          |
| Survey 9  | 3.8           | 20.8         | 3.4          |
| Survey 10 | 6.1           | 51.2         | 6.5          |
| Survey 11 | 3.8           | 18.6         | 3.1          |
| Survey 12 | 6.6           | 39.9         | 6.0          |
| Survey 13 | 3.9           | 17.0         | 3.1          |
| Survey 14 | 4.9           | 32.1         | 4.3          |

Addition to the processing raw GNSS measurements, GNSS Analysis Tool prepares reports for the data. According to the reports, the expected Weighted Least Squares horizontal scatter is about 10 to 20 meters in open sky. It is smaller when clock is continuous, larger when they are near buildings. In the reports, there is no clock discontinuity reported for any log files (see the example reports in Appendix C).

The results (see Table 5.16) shows that post-processed GNSS raw measurements by GNSS Analysis Tool provide less accuracy than the position generated by Samsung Galaxy S8 chipset (see Table 5.14). Probably, by using additional instruments such as echo sounder, sonars, anemometer, gyrocompass, smartphone chipset provides higher accuracy and smother results could been caused. Additionally, the smartphone chipset could be oweing the better results to the stronger filtering than Weighted Least Square Estimation which GNSS Analysis Tool uses.

The same analysis is performed in order to see difference between 4 reference trajectories (two of them by k-means, two of them by implemented clustering method) on the first 2 surveys. Therefore, the distances to the closest reference points for each epoch are evaluated. Statistics of results are presented in Table 5.17.

*Table 5.17: Statistics of the distances between estimated points and the closest reference points for k-means k=270 and k=540, implemented clustering method T=25cm and T=50cm (Survey 1 and Survey 2 by GNSS Analysis Tool)*

| | Survey 1 | | | Survey 2 | | |
|---|---|---|---|---|---|---|
| **References** | **Mean [meters]** | **Max [meters]** | **STD [meters]** | **Mean [meters]** | **Max [meters]** | **STD [meters]** |
| k=270 | 3.7 | 22.3 | 3.2 | 5.3 | 19.4 | 4.1 |
| k=540 | 3.6 | 22.3 | 3.2 | 5.3 | 19.4 | 4.1 |
| T=25cm | 3.6 | 22.2 | 3.2 | 5.3 | 19.4 | 4.1 |
| T=50cm | 3.7 | 22.3 | 3.2 | 5.3 | 19.4 | 4.1 |

As an example; Survey 1 and Survey 2 point positions obtained by Samsung Galaxy S8 chipsets and raw GNSS measurement processing on Desktop are visualized with respect to reference trajectory (k-means, *k=270*) in Figure 5.18 and Figure 5.19. Error graphs are presented for Survey 1 and Survey 2 GNSS Analysis results on the following.
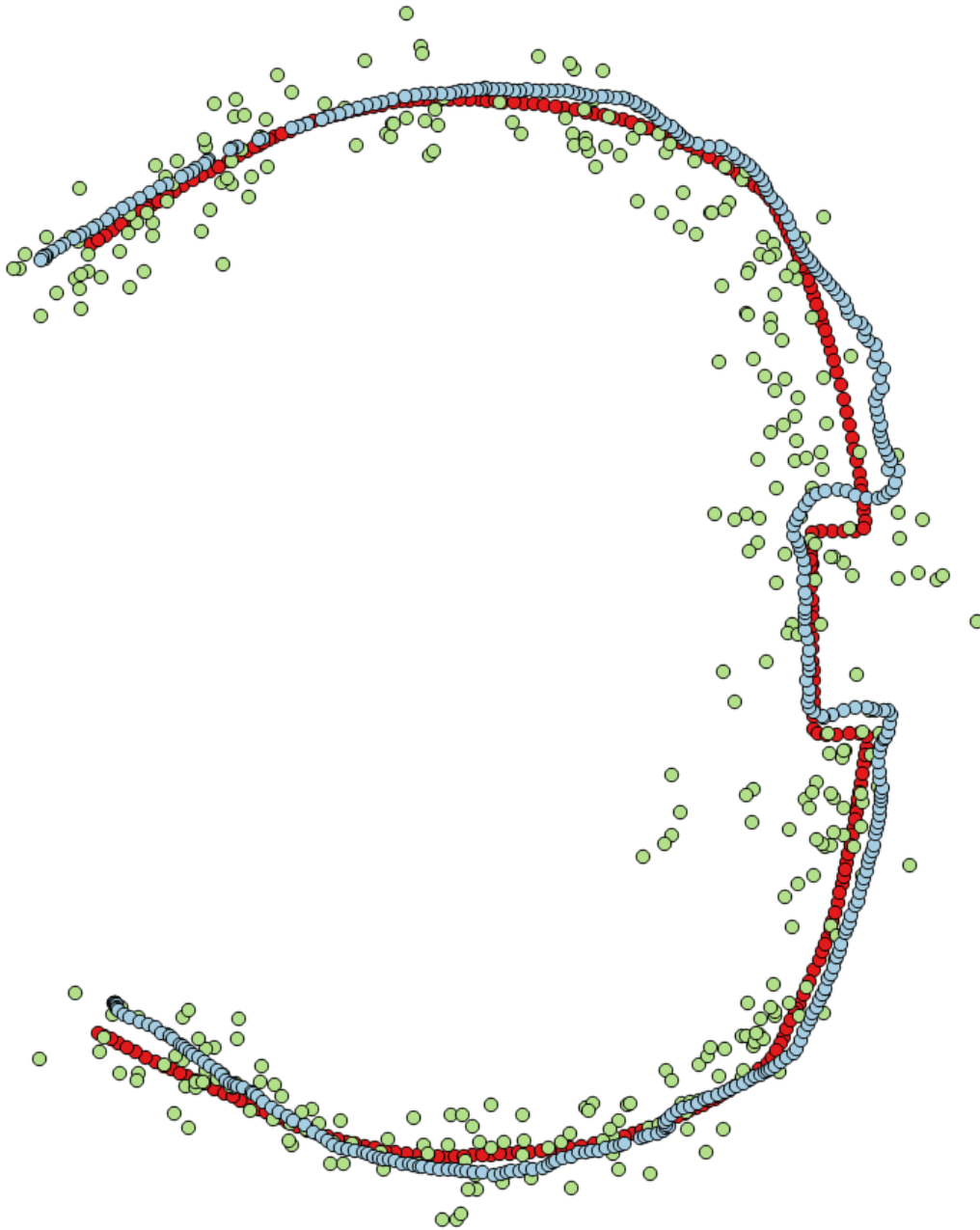


*Figure 5.18: Reference trajectory created with K-means clustering method k=270 in red, OruxMap output in blue, GNSS Analysis Tool output in green is presented for Survey 1.*
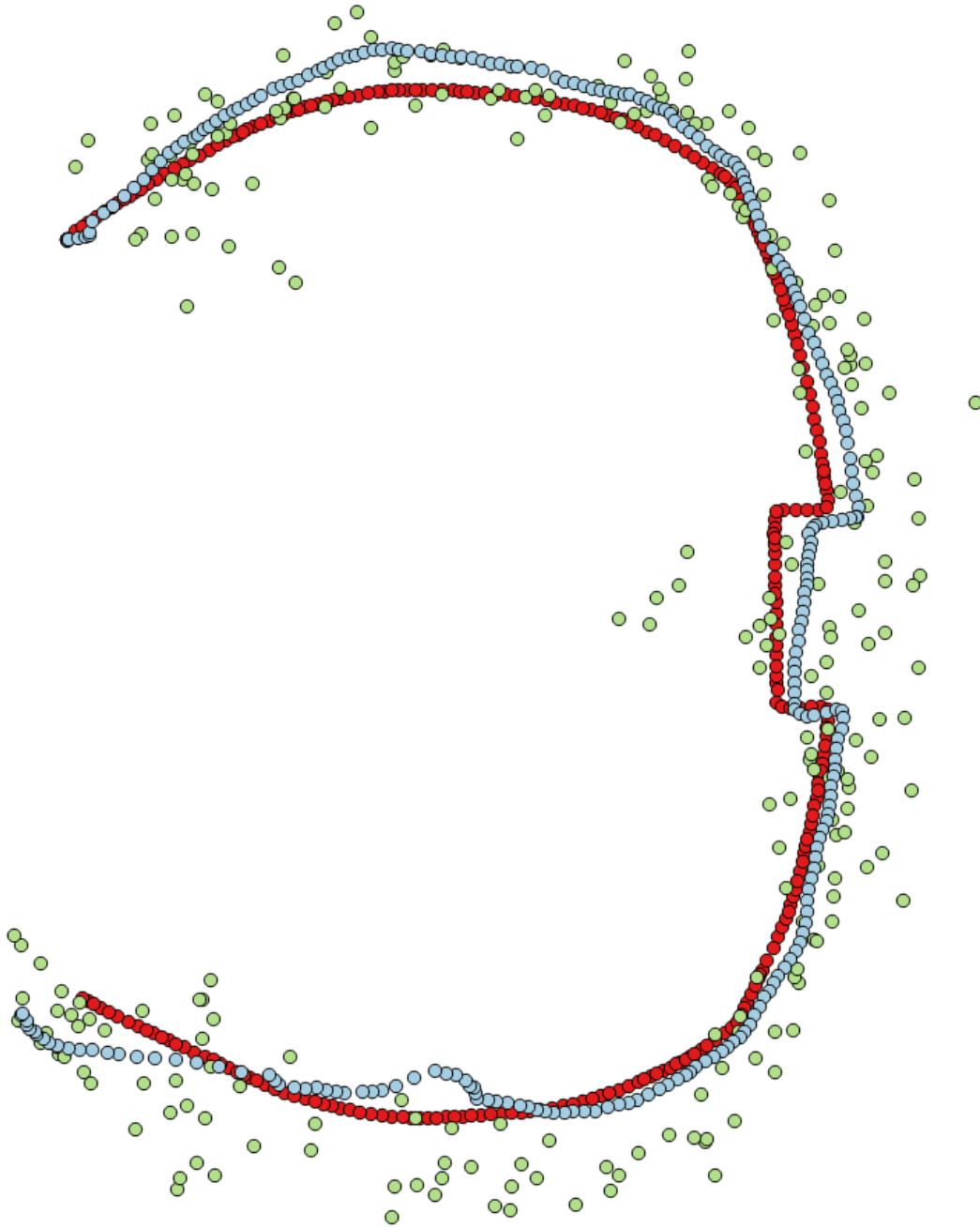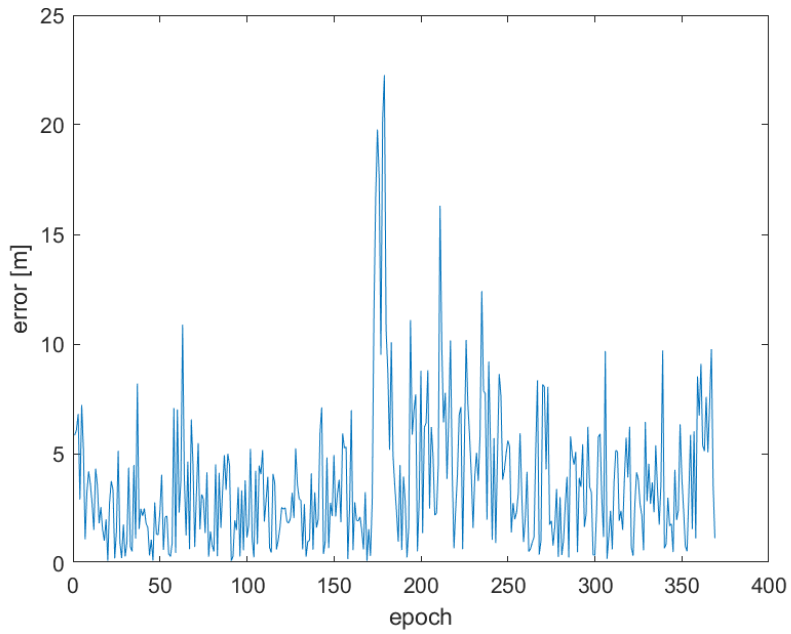
*Figure 5.19: Reference trajectory created with K-means clustering method k=270 in red, OruxMap output in blue, GNSS Analysis Tool output in green is presented for Survey 2.*

*Figure 5.20: Statistical results for Survey 1 by GNSS Analysis Tool with respect to reference created with K-means clustering method k=270.*
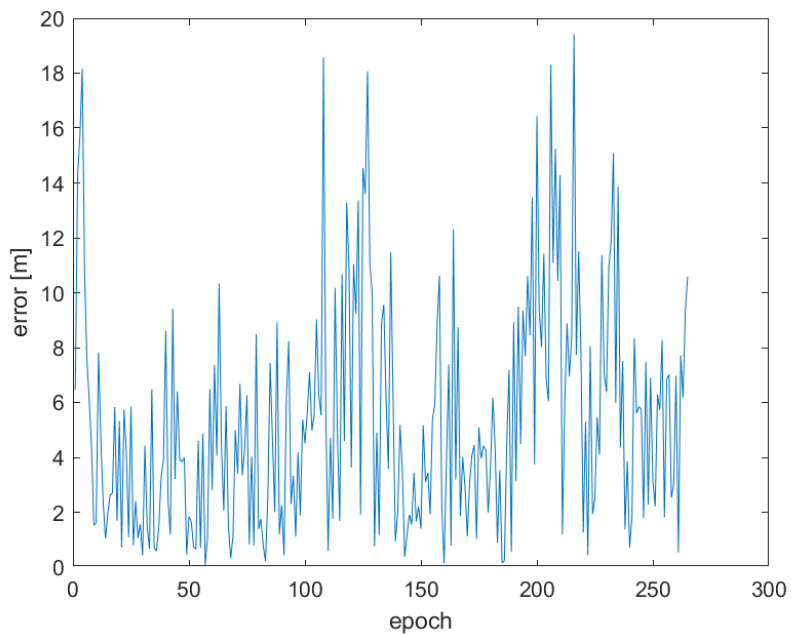


*Figure 5.21: Statistical results for Survey 2 by GNSS Analysis Tool with respect to reference created with K-means clustering method k=270.*

119

## 5.4 Experiment 4: Static Survey with Smartphone

Experiment 4 have been set around the fountain in green area in front of Leonardo Campus of Politecnico di Milano in 2019, for several days in May and June, as Experiment 2. While whole experiment, only corner points are used for static test. 8 points used in Experiment 4 are shown in Figure 5.23 with all measured points cover approximately 75 meters round (Reference Network 1). To put it all in simple terms, 8 corner points are formed by a geodetic receiver and android smartphone in order to asses to accuracy.

Surveying by Leica GRX1200 is done with stop-and-go method by taking 5 epoch measurement from each point. These measurements are used to create Reference Network 1 as mentioned before in Chapter 4. With android smartphone, raw measurements are stored with Geo++ RINEX Logger and RinexOn applications. While using Geo++ RINEX Logger or RinexOn, all coordinates generated by smartphone chipset are stored by OruxMaps as in previous experiments. With android smartphone, 10 minutes surveys are done for each point with a sampling rate of 1 HZ.

The flowchart in Figure 5.22, summarizes the overall procedure to identify the differences of each individual part of the whole experiment.
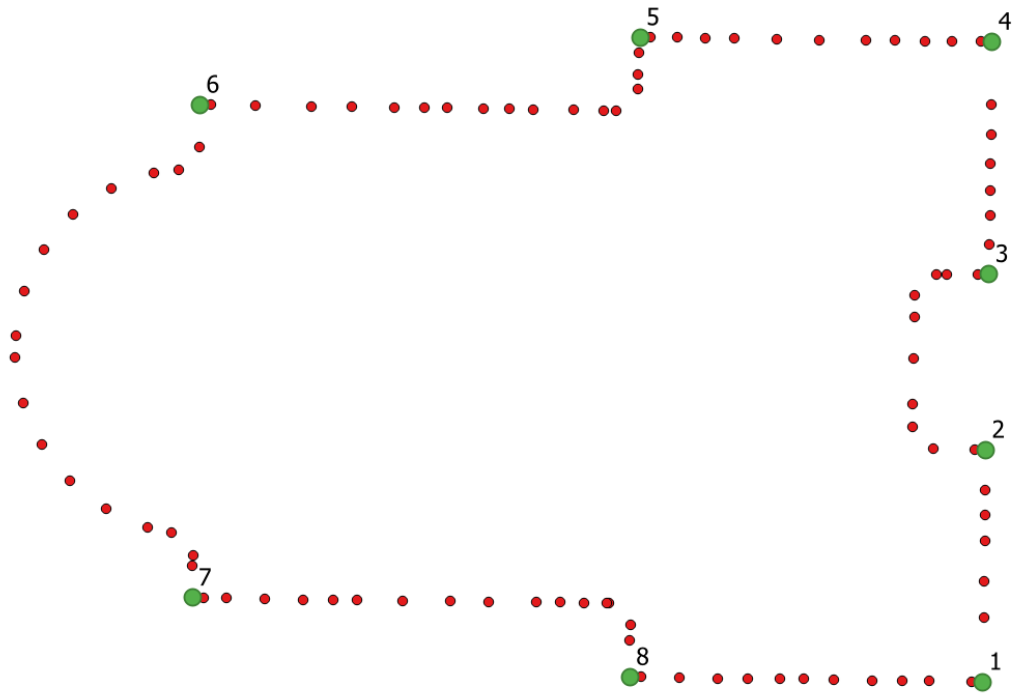
**Field experiment**
- 10 minutes surveying of each point with Geo++ RINEX Logger and OruxMaps in smartphone
- 10 minutes surveying of each point with RinexOn and OruxMaps in smartphone

**Processing**
- No need with OruxMap
- Raw measurements from Geo++ RINEX Logger processed with RTKlib 2.4.3
- Raw measurements from RinexOn processed with RTKlib 2.4.3

**Result discussion**
- Statistics and analysis
- Tables
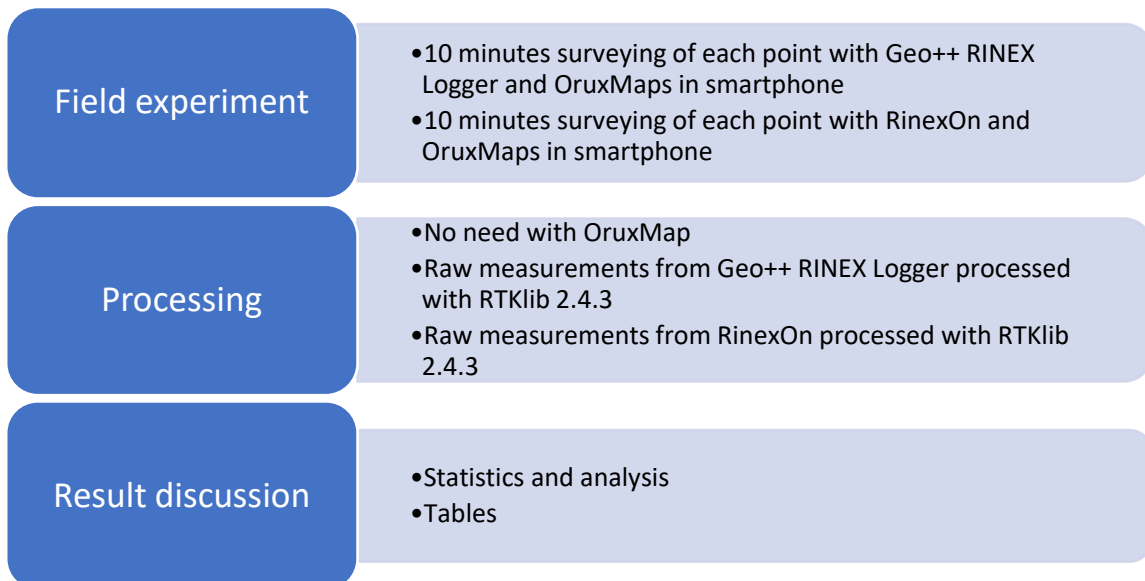
*Figure 5.22: Flowchart o Experiment 4*

*Figure 5.23: Reference points in green*

In Experiment 4, the aim is the assessment of the accuracy of the single frequency smartphone receiver for the static approach. In the experiment, all points (see Figure 5.23) are measured with 10 minutes sessions in static mode by Geo++ RINEX Logger and RinexOn. The sessions by Geo++ RINEX Logger and the sessions by RinexOn are measured in different days. Both applications store the data in RINEX 3.03 file format. In order to process the collected data, RTKLIB 2.4.3 b32 is used and results are presented in the research. Also, several different software are tested for processing, however, they could not reach to successful results.

While processing, Milano Permanent Station II which is new permanent station after replacement of the Milano Permanent Station I is used. Milano Permanent Station II is replaced on the roof of Department of Chemistry building Politecnico di Milano, in Piazza Leonardo da Vinci, 32, because of the renovation on the roof of Department of Architecture building. The distance between Milano Permanent Station II and surveying points are still under couple hundred meters. The coordinates

of the Milano Permanent Station II are listed in Table 5.18. They were needed for DGPS and static point positioning.

*Table 5.18: The reference coordinates in UTM32N for Milano Permanent Station II.*

| East [meters] | North [meters] | Height [meters] |
|---|---|---|
| 517914.526 | 5036118.876 | 191.11 |

### 5.4.1 Geo++ RINEX Logger

Geo++ RINEX Logger uses Android API Level 24 services to log raw GNSS measurement data into a RINEX file version 3.03 including pseudoranges, accumulated delta ranges, doppler frequencies and noise values.

A simple analysis of the data acquired from Geo++ RINEX Logger shows an incorrect reconstruction for different periods of Galileo and BeiDou observations compatible with an incorrect decoding of the observations in Figure 5.24. Highlighted lines in the example shows the Galileo and BeiDou observations are shifted and the values are incorrectly decoded as huge numbers. However, in a processing of only GPS observations these errors have no impact.

```
> 2019  5 17 11 47  4.0003653  3  1
Geo++                                                   MARKER NAME
> 2019  5 17 11 47  4.0003653  0 17
C13  38407966.818  200000361.2191     -269.383     33.946
C29  21937193.197  114232721.3081     -886.159     37.053
C304535682522.160                    -2881.865     27.681
E24                                          8730947437.200                      -1966.637       31.949
E25                                          8729831356.940  747417019913544.1001     183.648       32.226
S02  23421104.407  123078733.8531    -1711.110     35.715
G12  22494366.474  118208693.6631    -2483.734     37.073
G14  23439834.840  123177162.5601    -1670.722     31.237
G24  25857636.731                    -3516.094     12.000
G25  20601682.852  108262573.6071     -729.034     39.450
G29  20144877.392  105862044.5381      612.096     34.685
G31  21531177.676                     1848.057     23.400
G32  24167621.804                    -2586.485     25.825
R09  19257858.962                     1242.397     24.240
R16  21274472.589                    -2907.031     29.191
R18  21588871.835  115242863.1331    -3396.004     35.176
R20  21653389.570  115790404.7811     4058.657     30.176
> 2019  5 17 11 47  5.0003654  0 16
C13  38408046.563  200000786.918      -269.699     34.919
C29  21937394.058  114233763.842      -886.560     37.461
C304835475548.280                    -2881.150     27.960
E24                                          9030740292.720  747418601200674.6001    -1964.421       32.843
E25                                          9029623802.970  747418595333481.600      183.000       32.746
G02  23421464.757  123080603.356     -1712.135     36.405
```

*Figure 5.24: Example of a reconstruction problem observed in data acquired from Geo++ RINEX Logger for Point 1.*

An analysis on the continuity of the observations highlights the significant discontinuity of the phase observations acquired by Geo++ RINEX Logger in Figure 5.25. The problem occurred on some sessions, the reason of the anomalous behavior could not be defined.



*Figure 5.25: Discontinuity problem in the L1 phase observations present in data acquired from Geo++ RINEX Logger for Point 1.*

123

## 5.4.1.1 Processing with RTKLIB

Data processing was reproduced with RTKLIB v. 2.4.3 b28. All solution files are obtained with the respective configuration parameters. The parameters and the main considerations about the choices made are represented below:

- Only GPS satellites are used in processing (research limitations). During whole research only GPS satellites are used in processing.

- Cut-off $= 15°$ depending on the observed SNR values. For satellites with an elevation lower than 15 degrees the SNR values are lower than 25 dBHz.

- SNR mask $= 0$ dBHz since the use of a 15° cut-off angle allows to remove the observations that have a higher probability of being affected by signal disturbances.

- RAIM FDE not applied due to the limited number of satellites in view when processing using only GPS.

- Code / Carrier-Phase Error Ratio L1 equal to 300 in place of the standard value of 100, because smartphone observations are noisier than the observations acquired by other GNSS receivers.

- Carrier-Phase Bias equal to 100 instead of $10^{-4}$ since the initialization of the uncertainties of phase ambiguity, which is based on a difference between code and phase observations within RTKLIB, is affected by the different noise of the observations. Too low value could cause instability in the Kalman filter.

- Integer Ambiguity Resolution Algorithm $=$ OFF. Based on experience on processing raw GNSS data acquired from smartphone, the phase ambiguity fixing algorithms often leads to false fixes in the final solution. This is certainly a technological problem that surely can be overcome in the future.

- Combined filter type provides smoother solution with combining forward and backward filter solutions. All filter types are tested to make the best choice.

All session presented in the research for Geo++ RINEX Logger are measured on May 17th, 2019. These smartphone observations are processed with 3 different position mode by RTKLIB: Single Point Positioning, DGPS and Static. RTKLIB settings interface is presented in Figure 5.26.
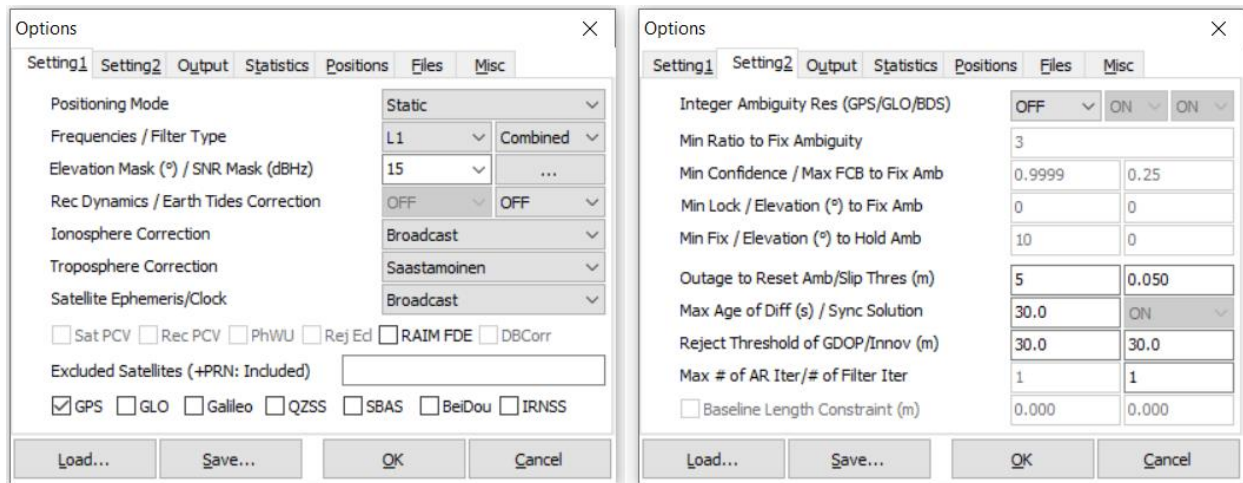
*Figure 5.26: RTKLIB settings window*

## 5.4.1.2 Single Point Positioning for Geo++ RINEX Logger

RTKLIB employs an iterated weighted LSE (least square estimation) for the ″Single″ (single point positioning) mode with or without SBAS corrections. SBAS corrections are not used in the research for smartphone observations.

By using single point positioning mode, 600 positions are computed for each 10 minutes session. Obtained files from RTKLIB represents the coordinates in units of geographic coordinate system (latitude, longitude and height). These coordinates are converted to ETRF UTM-32N coordinates (east, north and height) by using QGIS that was done in the previous experiment.

The results obtained for each point are shown epoch by epoch in Figure 5.27 and Figure 5.28. Statistics of single point positioning results are calculated by MATLAB code and presented in Table 5.19. All related statistical error graphs are presented Figure 5.29 - Figure 5.44 respectively. Final results for each point are calculated by averaging all epochs and presented in Figure 5.45.
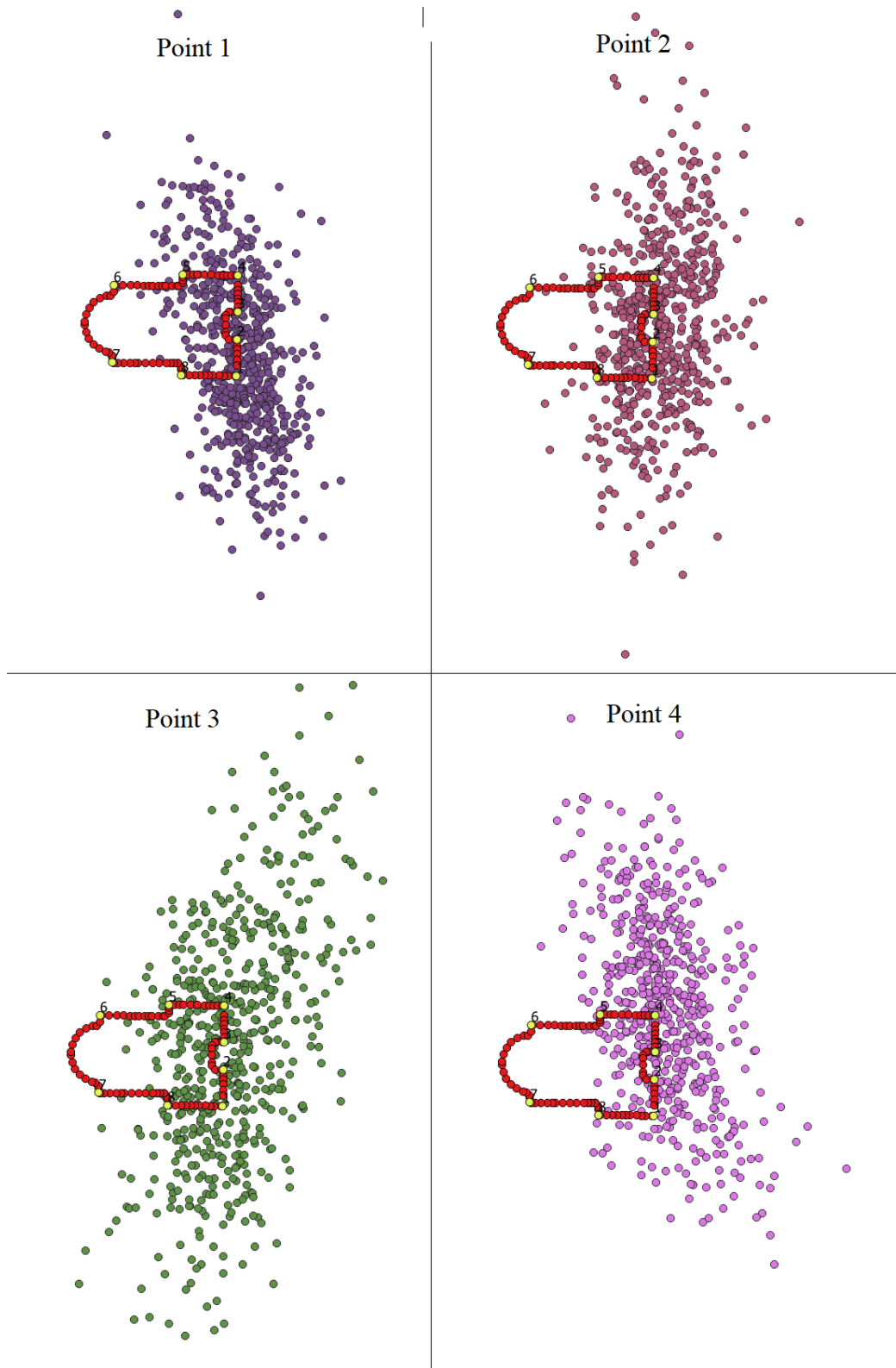
*Figure 5.27: Example of the single point position mode results (Point 1, Point 2, Point 3 and Point 4) (Geo++ RINEX Logger).*

126
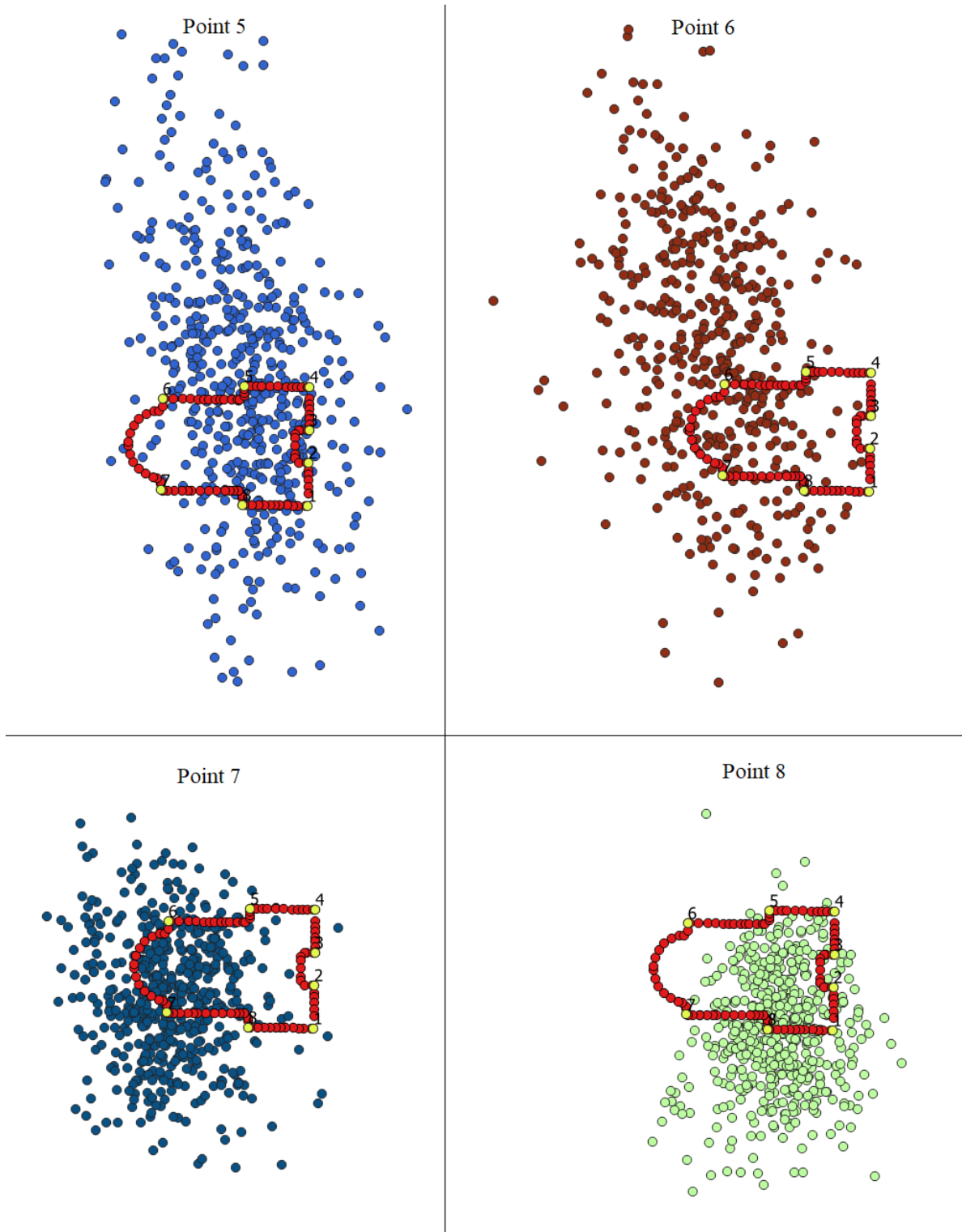
*Figure 5.28: Example of the single point position mode results (Point 5, Point 6, Point 7 and Point 8) (Geo++ RINEX Logger).*

*Table 5.19: Statistics of single point positioning results (Geo++ RINEX Logger).*

| Point ID | | East [m] | North [m] | Height [m] | ΔE [m] | ΔN [m] | ΔH [m] |
|---|---|---|---|---|---|---|---|
| Point 1 | MIN | 517531.836 | 5036051.257 | 122.593 | -19.438 | -32.878 | -37.574 |
| | MAX | 517566.888 | 5036138.156 | 199.985 | 15.614 | 54.020 | 39.817 |
| | Mean | 517551.651 | 5036087.264 | 157.545 | 0.377 | 3.129 | -2.622 |
| | Median | 517551.999 | 5036086.891 | 157.593 | 0.725 | 2.756 | -2.574 |
| | STD | 5.118 | 12.340 | 11.809 | 5.128 | 12.721 | 12.087 |
| Point 2 | MIN | 517535.171 | 5036042.894 | 84.351 | -16.168 | -46.686 | -75.852 |
| | MAX | 517573.253 | 5036138.144 | 202.385 | 21.913 | 48.563 | 42.181 |
| | Mean | 517552.385 | 5036092.189 | 155.915 | 1.045 | 2.608 | -4.289 |
| | Median | 517552.385 | 5036091.655 | 155.732 | 1.045 | 2.075 | -4.472 |
| | STD | 5.463 | 13.323 | 14.917 | 5.558 | 13.566 | 15.510 |
| Point 3 | MIN | 517508.338 | 5035806.973 | 100.843 | -43.085 | -286.734 | -59.371 |
| | MAX | 517594.797 | 5036325.141 | 217.594 | 43.374 | 231.434 | 57.380 |
| | Mean | 517552.391 | 5036092.903 | 158.120 | 0.968 | -0.805 | -2.094 |
| | Median | 517552.032 | 5036093.881 | 158.165 | 0.609 | 0.173 | -2.050 |
| | STD | 8.468 | 29.532 | 17.570 | 8.516 | 29.519 | 17.680 |
| Point 4 | MIN | 517534.366 | 5036061.865 | 107.837 | -17.127 | -37.297 | -52.349 |
| | MAX | 517580.136 | 5036148.982 | 201.368 | 28.643 | 49.821 | 41.183 |
| | Mean | 517552.873 | 5036100.425 | 157.733 | 1.380 | 1.263 | -2.453 |
| | Median | 517552.318 | 5036100.744 | 157.867 | 0.825 | 1.583 | -2.318 |
| | STD | 6.244 | 13.686 | 14.180 | 6.390 | 13.732 | 14.379 |
| Point 5 | MIN | 517525.662 | 5036014.478 | 63.393 | -17.569 | -84.792 | -96.808 |
| | MAX | 517572.342 | 5036171.504 | 209.669 | 29.110 | 72.235 | 49.468 |
| | Mean | 517543.315 | 5036100.088 | 157.584 | 0.083 | 0.819 | -2.617 |
| | Median | 517543.461 | 5036099.007 | 156.471 | 0.229 | -0.263 | -3.730 |
| | STD | 7.018 | 17.660 | 19.845 | 7.012 | 17.662 | 19.999 |
| Point 6 | MIN | 517503.706 | 5036051.544 | 95.583 | -29.192 | -46.141 | -64.611 |
| | MAX | 517551.108 | 5036146.491 | 230.740 | 18.210 | 48.807 | 70.546 |
| | Mean | 517531.472 | 5036102.482 | 165.976 | -1.427 | 4.797 | 5.782 |
| | Median | 517531.836 | 5036102.675 | 166.246 | -1.063 | 4.990 | 6.052 |
| | STD | 7.590 | 15.452 | 23.397 | 7.715 | 16.164 | 24.077 |
| Point 7 | MIN | 517517.495 | 5036066.582 | 99.760 | -15.220 | -19.529 | -60.440 |
| | MAX | 517554.404 | 5036110.726 | 213.264 | 21.689 | 24.615 | 53.064 |
| | Mean | 517533.307 | 5036088.304 | 157.462 | 0.593 | 2.192 | -2.737 |
| | Median | 517532.856 | 5036088.094 | 156.584 | 0.142 | 1.982 | -3.616 |
| | STD | 5.992 | 8.101 | 16.485 | 6.015 | 8.385 | 16.695 |
| Point 8 | MIN | 517528.404 | 5036063.758 | 118.127 | -14.586 | -20.489 | -42.054 |
| | MAX | 517559.954 | 5036111.489 | 198.641 | 16.964 | 27.242 | 38.460 |
| | Mean | 517544.396 | 5036084.114 | 157.310 | 1.406 | -0.134 | -2.871 |
| | Median | 517544.487 | 5036084.217 | 156.394 | 1.497 | -0.030 | -3.787 |
| | STD | 5.101 | 7.445 | 13.937 | 5.286 | 7.440 | 14.217 |
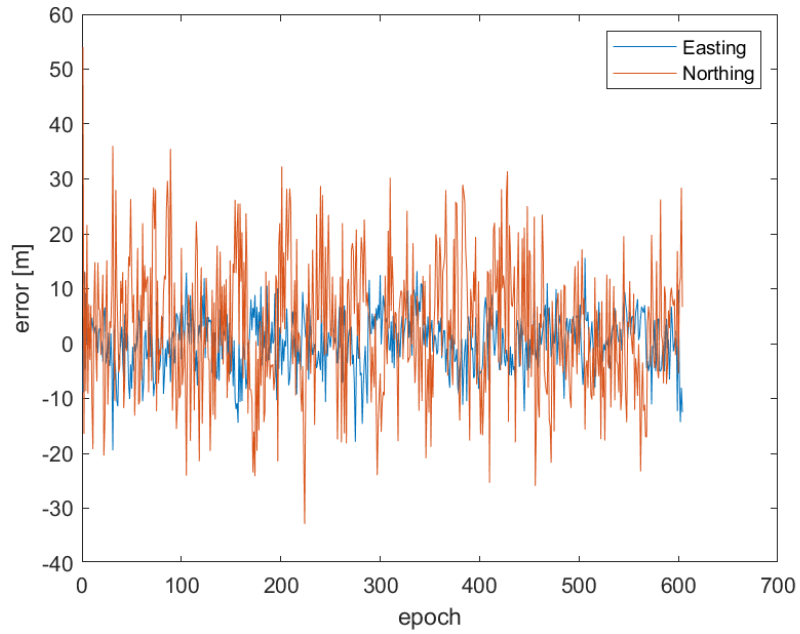
*Figure 5.29: Horizontal errors of single point positioning for each epoch on Point 1 with respect to reference. (Geo++ RINEX Logger data obtained on May 17th, 2019)*
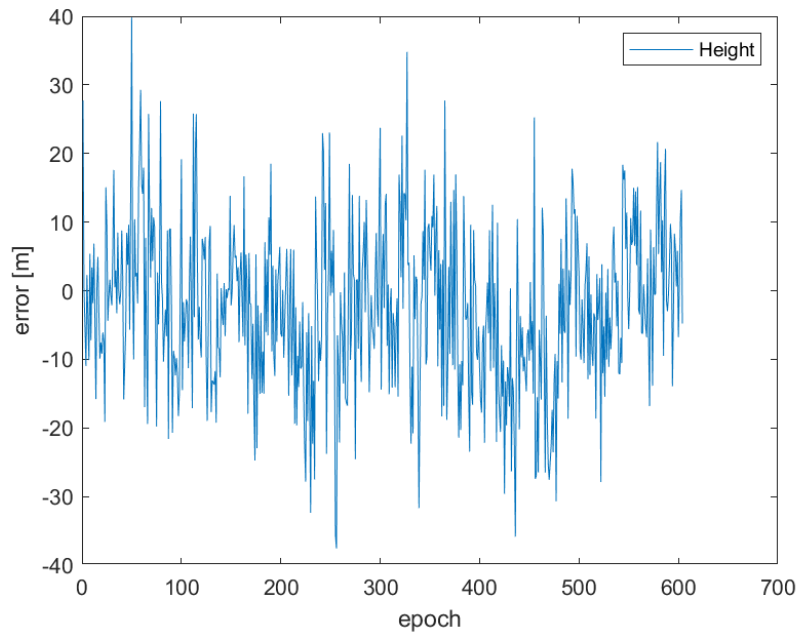


*Figure 5.30: Vertical errors of single point positioning for each epoch on Point 1 with respect to reference. (Geo++ RINEX Logger data obtained on May 17th, 2019)*
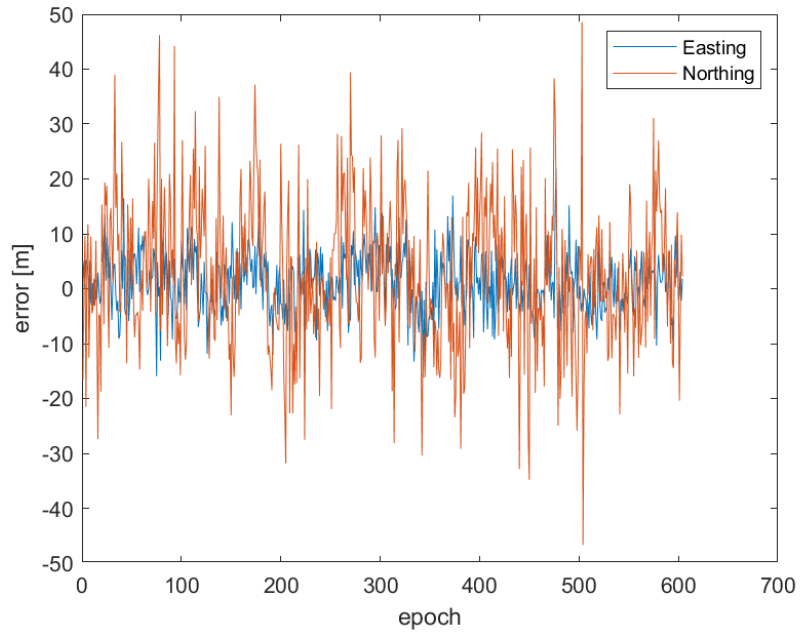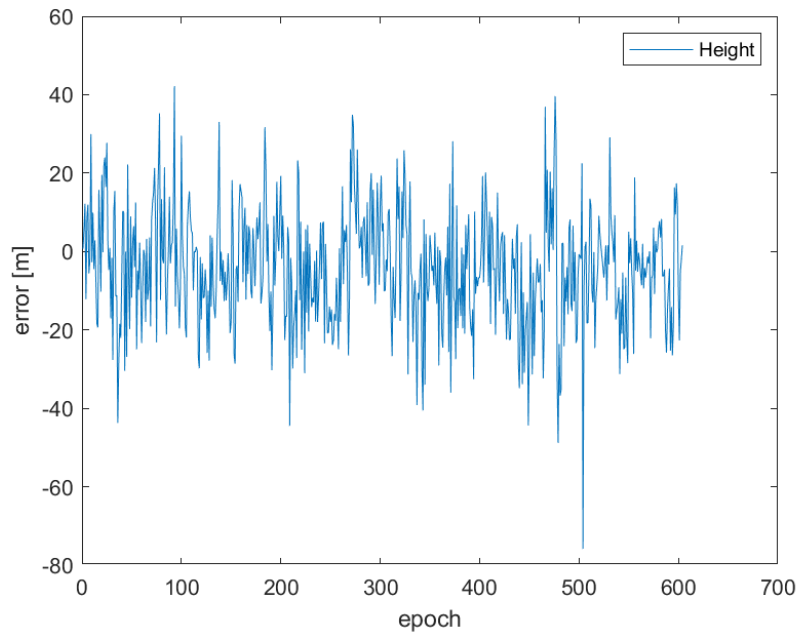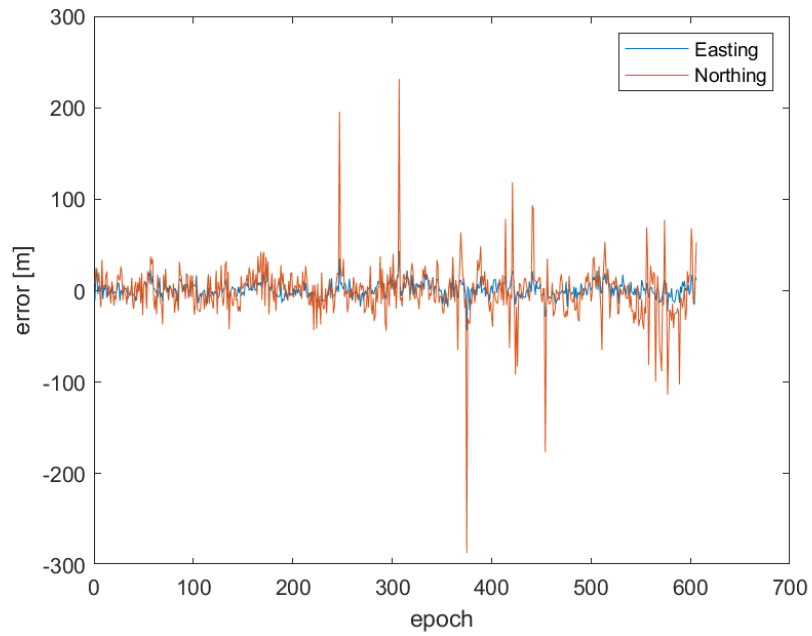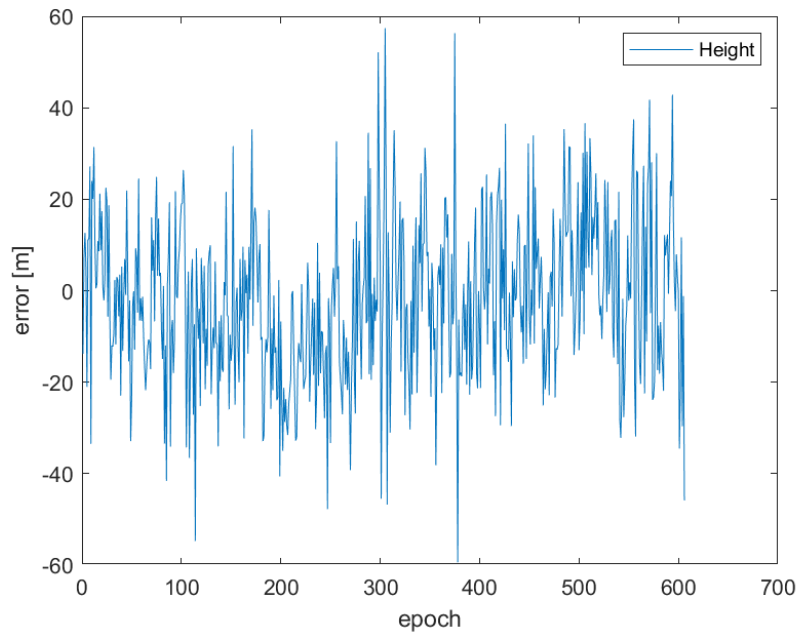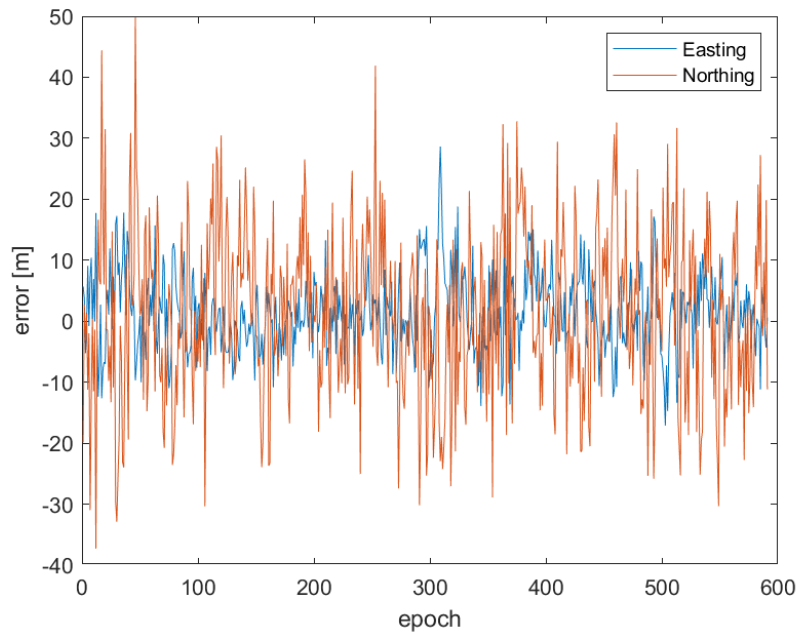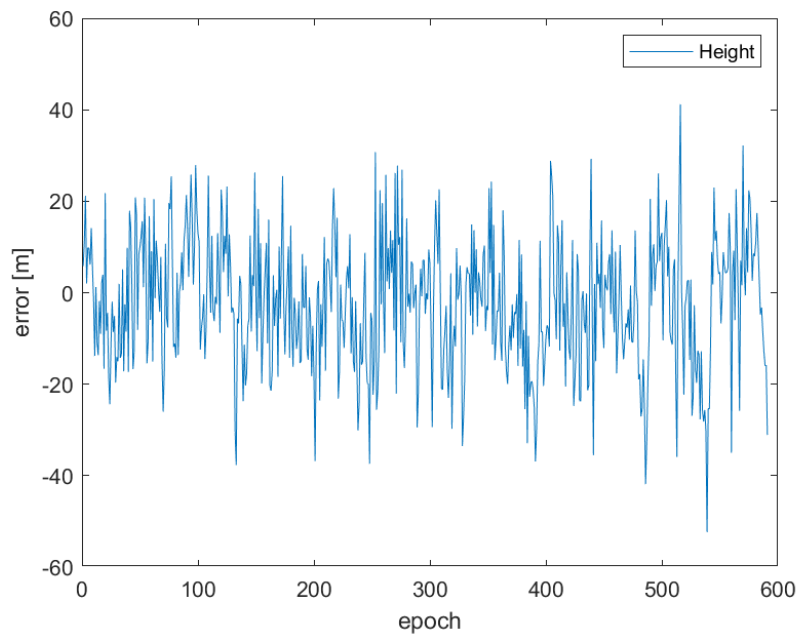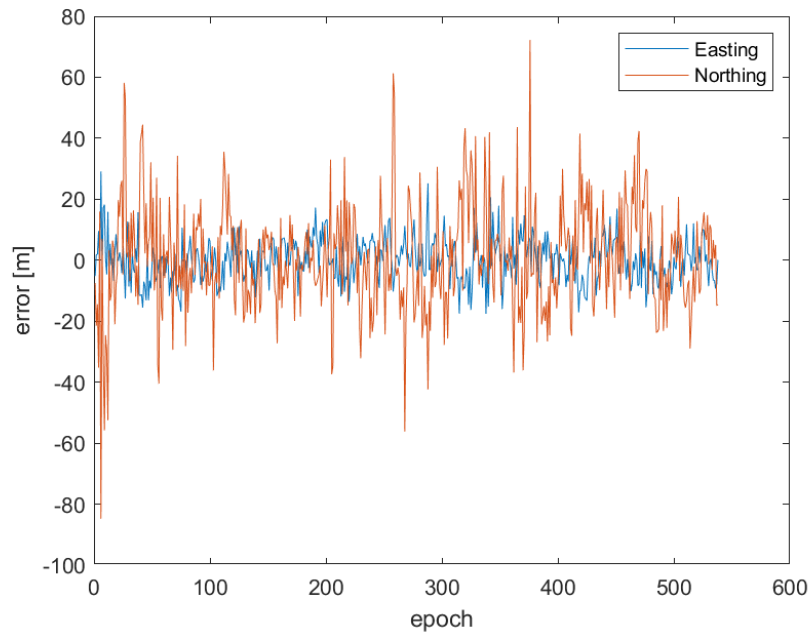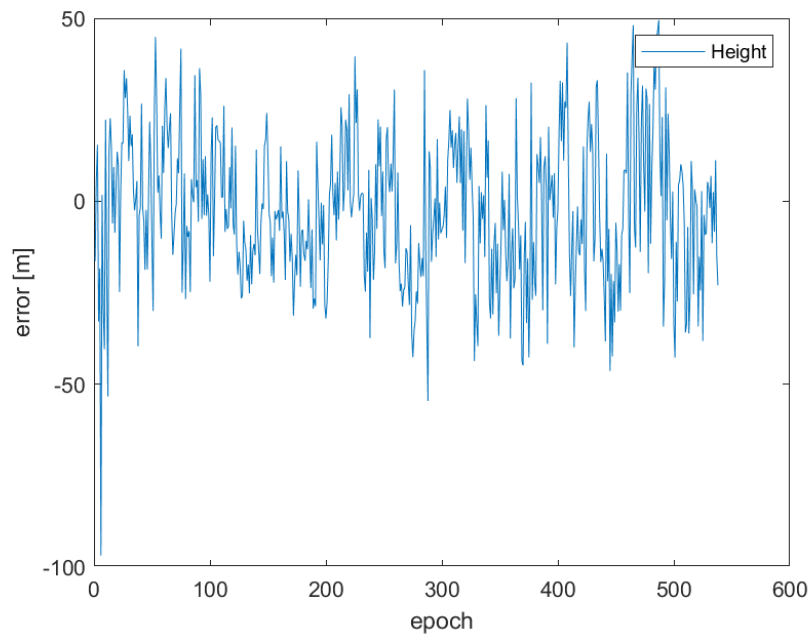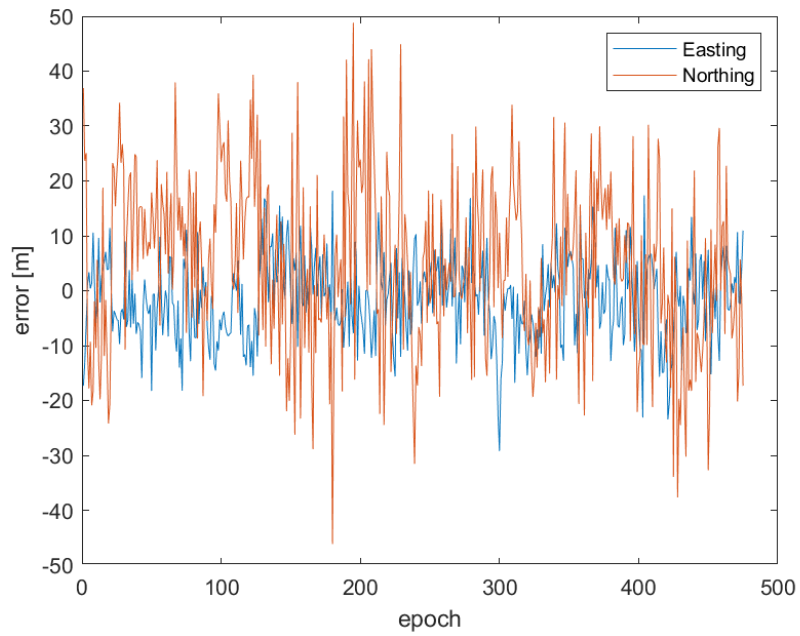
129

*Figure 5.31: Horizontal errors of single point positioning for each epoch on Point 2 with respect to reference. (Geo++ RINEX Logger data obtained on May 17th, 2019)*
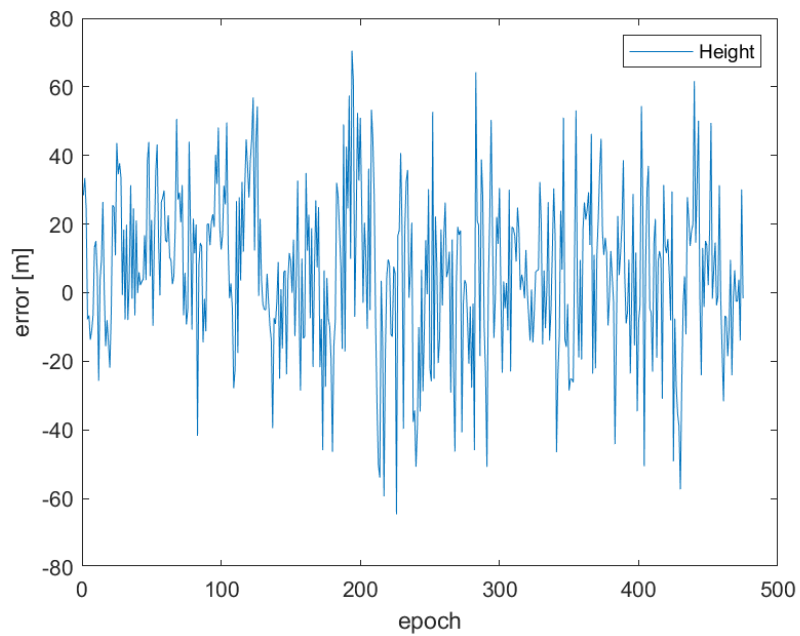


*Figure 5.32: Vertical errors of single point positioning for each epoch on Point 2 with respect to reference. (Geo++ RINEX Logger data obtained on May 17th, 2019)*

130

*Figure 5.33: Horizontal errors of single point positioning for each epoch on Point 3 with respect to reference. (Geo++ RINEX Logger data obtained on May 17th, 2019)*



*Figure 5.34: Vertical errors of single point positioning for each epoch on Point 3 with respect to reference. (Geo++ RINEX Logger data obtained on May 17th, 2019)*
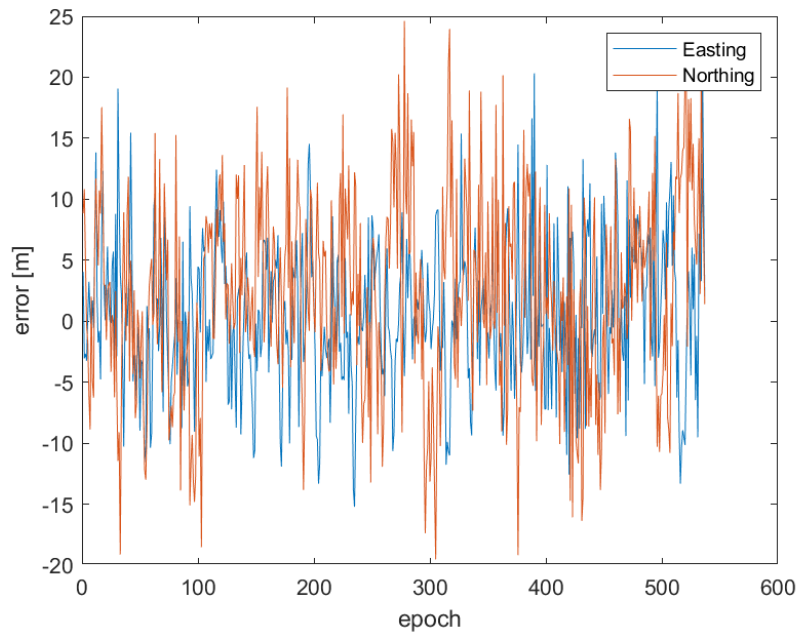
131

*Figure 5.35: Horizontal errors of single point positioning for each epoch on Point 4 with respect to reference. (Geo++ RINEX Logger data obtained on May 17th, 2019)*
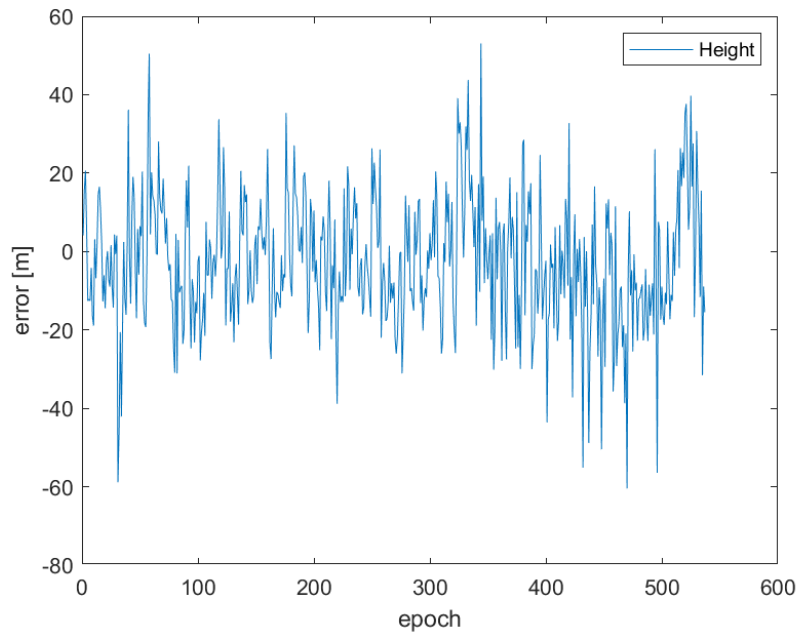


*Figure 5.36: Vertical errors of single point positioning for each epoch on Point 4 with respect to reference. (Geo++ RINEX Logger data obtained on May 17th, 2019)*
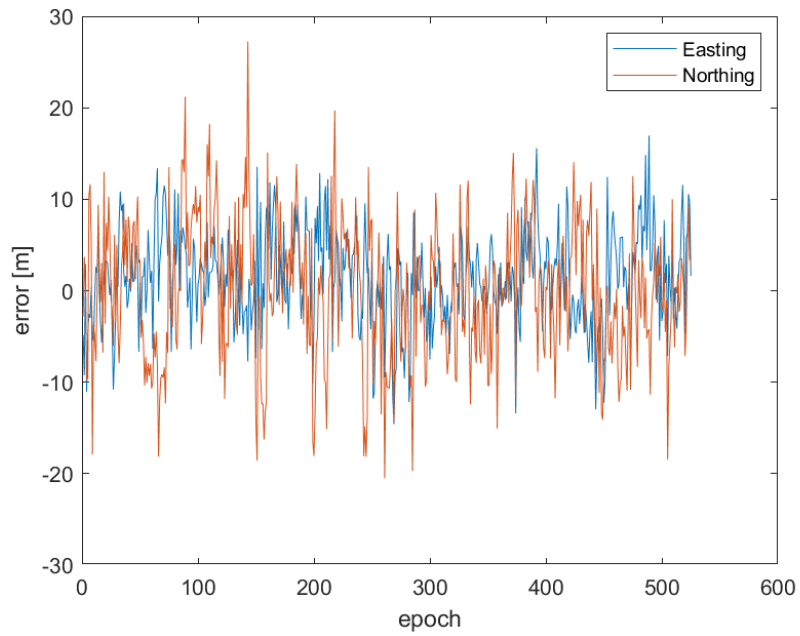
132

*Figure 5.37: Horizontal errors of single point positioning for each epoch on Point 5 with respect to reference. (Geo++ RINEX Logger data obtained on May 17th, 2019)*



*Figure 5.38: Vertical errors of single point positioning for each epoch on Point 5 with respect to reference. (Geo++ RINEX Logger data obtained on May 17th, 2019)*

133

*Figure 5.39: Horizontal errors of single point positioning for each epoch on Point 6 with respect to reference. (Geo++ RINEX Logger data obtained on May 17th, 2019)*
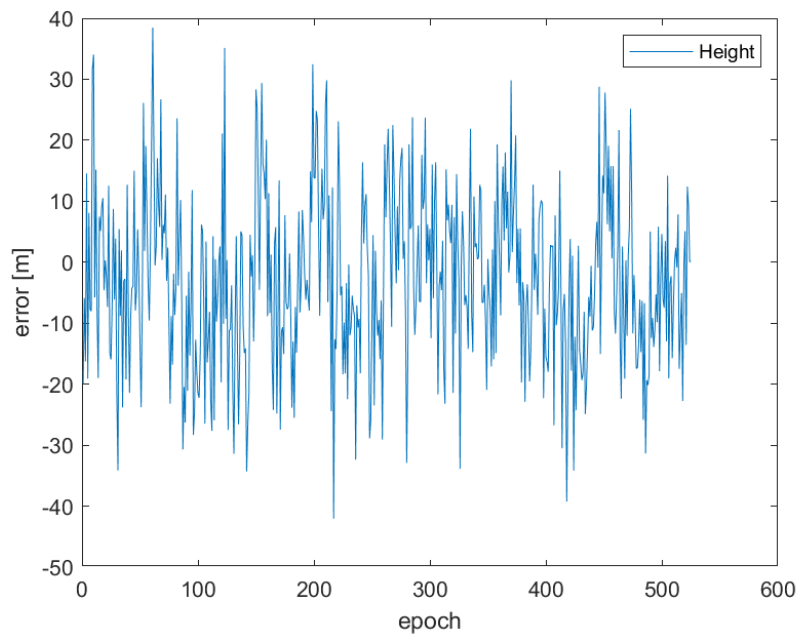


*Figure 5.40: Vertical errors of single point positioning for each epoch on Point 6 with respect to reference. (Geo++ RINEX Logger data obtained on May 17th, 2019)*

134

*Figure 5.41: Horizontal errors of single point positioning for each epoch on Point 7 with respect to reference. (Geo++ RINEX Logger data obtained on May 17th, 2019)*



*Figure 5.42: Vertical errors of single point positioning for each epoch on Point 7 with respect to reference. (Geo++ RINEX Logger data obtained on May 17th, 2019)*

135

*Figure 5.43: Horizontal errors of single point positioning for each epoch on Point 8 with respect to reference. (Geo++ RINEX Logger data obtained on May 17th, 2019)*



*Figure 5.44: Vertical errors of single point positioning for each epoch on Point 8 with respect to reference. (Geo++ RINEX Logger data obtained on May 17th, 2019)*

136

*Table 5.20: Averaged the single point positions by Geo++ RINEX Logger as a final results.*

| Point ID | Geo++ RINEX Logger | | | | | |
| --- | --- | --- | --- | --- | --- | --- |
| | East [m] | North [m] | Height [m] | ΔE [m] | ΔN [m] | ΔH [m] |
| 1 | 517551.651 | 5036087.264 | 157.545 | 0.377 | 3.129 | -2.622 |
| 2 | 517552.385 | 5036092.189 | 155.915 | 1.045 | 2.608 | -4.289 |
| 3 | 517552.391 | 5036092.903 | 158.120 | 0.968 | -0.805 | -2.094 |
| 4 | 517552.873 | 5036100.425 | 157.733 | 1.380 | 1.263 | -2.453 |
| 5 | 517543.315 | 5036100.088 | 157.584 | 0.083 | 0.819 | -2.617 |
| 6 | 517531.472 | 5036102.482 | 165.976 | -1.427 | 4.797 | 5.782 |
| 7 | 517533.307 | 5036088.304 | 157.462 | 0.593 | 2.192 | -2.737 |
| 8 | 517544.396 | 5036084.114 | 157.310 | 1.406 | -0.134 | -2.871 |
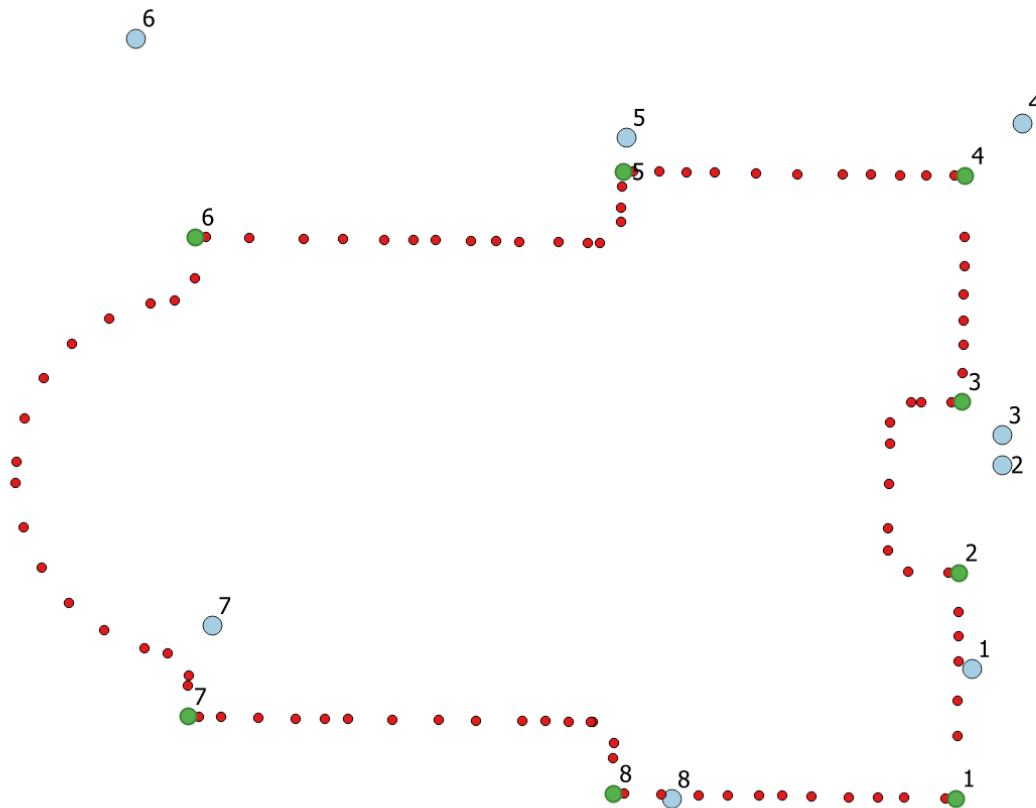


*Figure 5.45: Final results of the single point positioning in blue (Geo++ RINEX Logger).*
*Reference in green.*

The final results for single point positioning are presented on above. The statistics are presented in Table 5.21.

*Table 5.21: Statistics of the results for single point positioning by Geo++ RINEX Logger.*

| Statistics | East [m] | North [m] | Height [m] |
|---|---|---|---|
| Min [m] | -1.118 | -3.027 | -1.445 |
| Max [m] | 1.434 | 2.561 | 5.748 |
| Mean [m] | 0.296 | 0.179 | 1.293 |
| Median [m] | 0.435 | 0.378 | 0.261 |
| STD [m] | 0.983 | 1.713 | 2.605 |
| RMS [m] | 0.966 | 1.612 | 2.758 |

## 5.4.1.3 DGPS for Geo++ RINEX Logger

RTKLIB employs EKF (extended Kalman filter) in order to obtain the final solutions in DGPS/DGNSS mode in conjunction with the GNSS signal measurement models, and the troposphere and ionosphere models.

Theoretically, by using DGPS mode, 600 positions are computed for each 10 minutes session as it is done by simple point positioning mode. However, some sessions have less, because of probably some problems with RTKLIB. Point 8 is a good example in Figure 5.47. Only 9 epoch has a final result in output file from RTKLIB.

Obtained files from RTKLIB represents the coordinates in units of geographic coordinate system (latitude, longitude and height). These coordinates are converted to ETRF UTM-32N coordinates (east, north and height) by using QGIS that was done in the previous experiment.

The results obtained for each point are shown epoch by epoch in Figure 5.46 and Figure 5.47. Statistics of DGPS results are calculated by MATLAB code and presented in Table 5.22. All related statistical error graphs are presented Figure 5.48 - Figure 5.63 respectively. Final results for each point are calculated by averaging all epochs and presented in Figure 5.64.
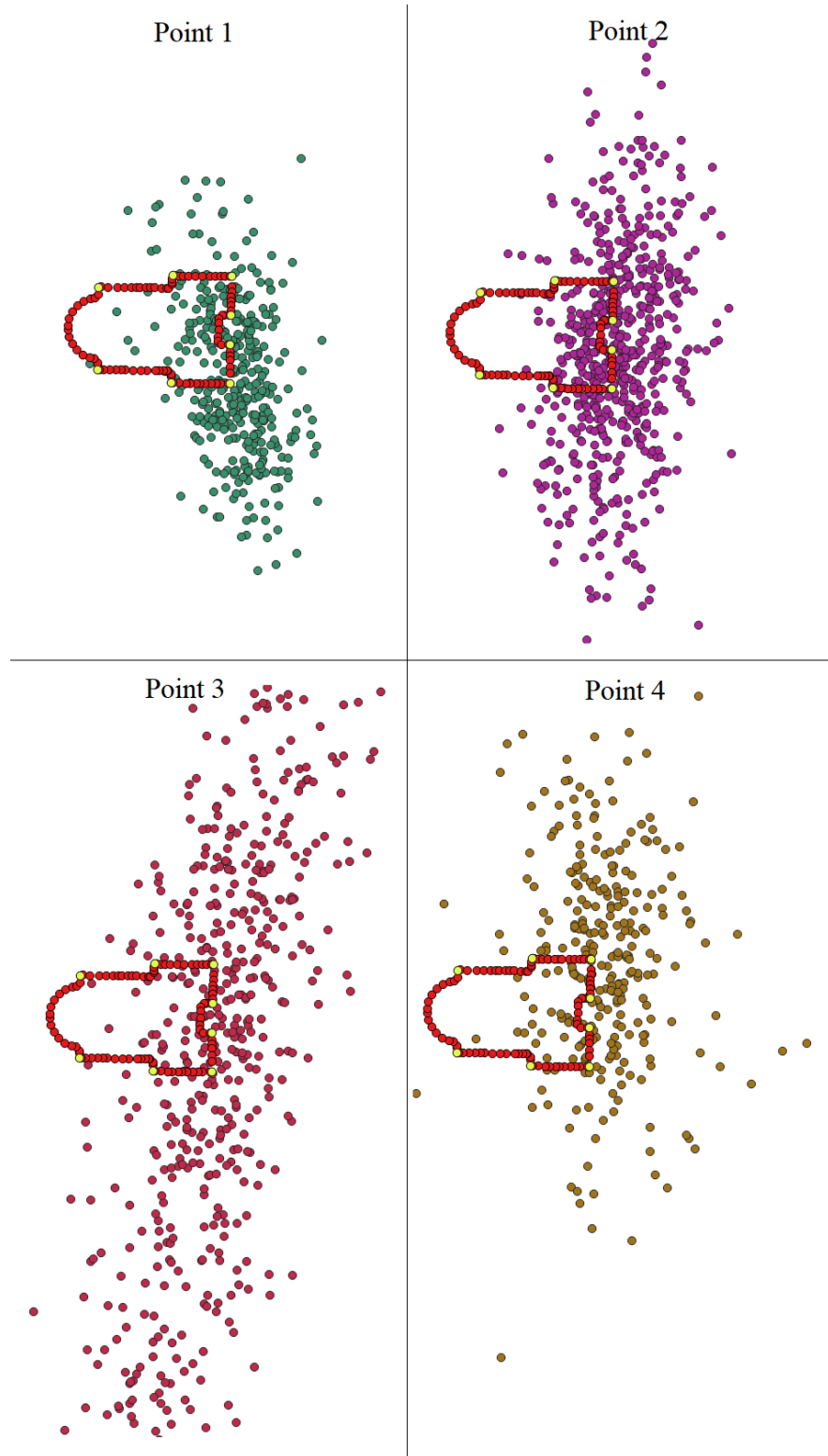
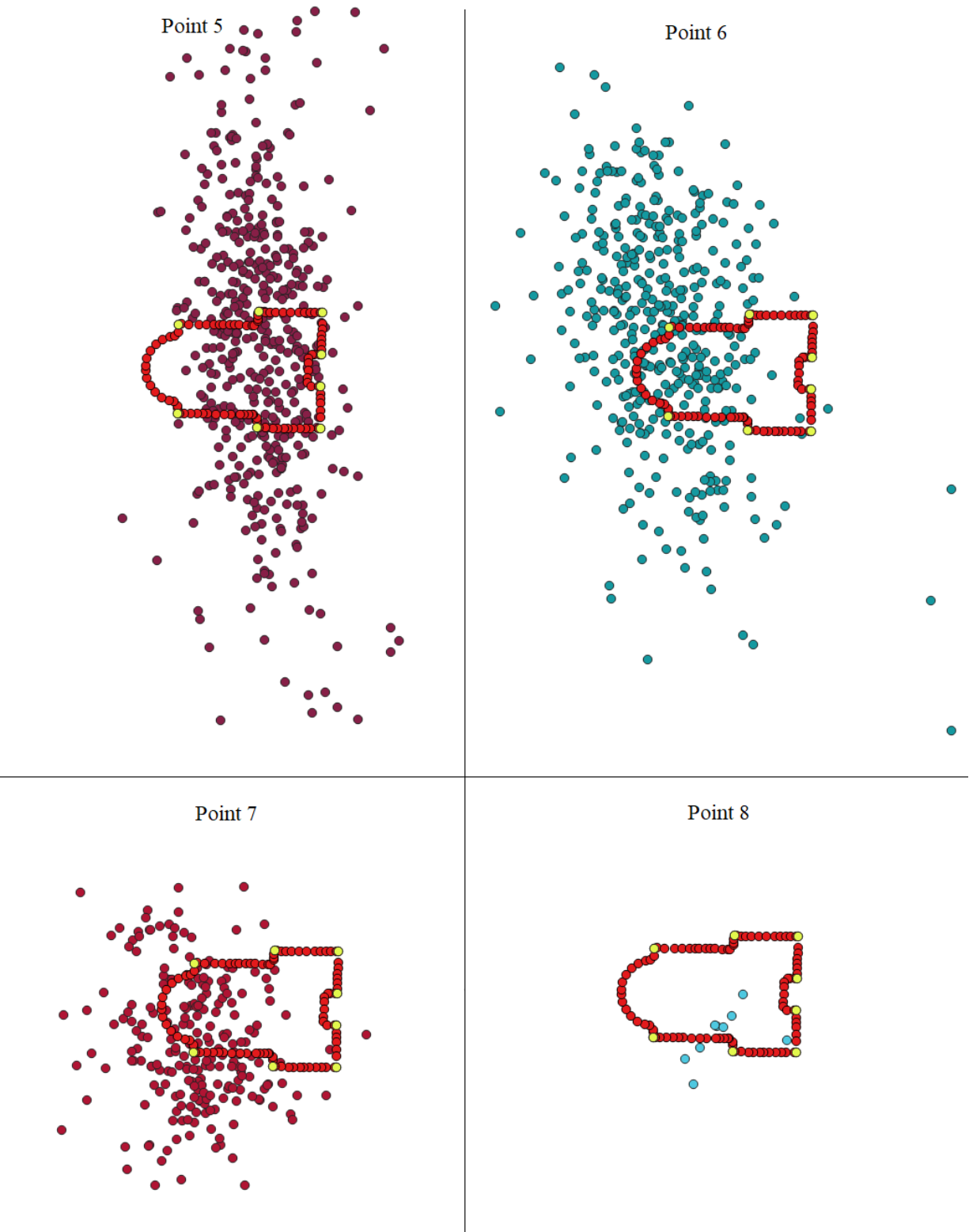*Figure 5.46: Example of DGPS mode results (Point 1, Point 2, Point 3 and Point 4) (Geo++ RINEX Logger).*

*Figure 5.47: Example of DGPS mode results (Point 5, Point 6, Point 7 and Point 8) (Geo++ RINEX Logger).*

*Table 5.22: Statistics of DGPS (Geo++ RINEX Logger).*

| Point ID | | East [m] | North [m] | Height [m] | ΔE [m] | ΔN [m] | ΔH [m] |
|---|---|---|---|---|---|---|---|
| Point 1 | MIN | 517531.590 | 5036058.033 | 127.149 | -19.684 | -26.102 | -33.018 |
| | MAX | 517564.176 | 5036141.323 | 206.925 | 12.902 | 57.187 | 46.758 |
| | Mean | 517551.898 | 5036085.318 | 160.487 | 0.624 | 1.183 | 0.320 |
| | Median | 517552.295 | 5036084.153 | 160.268 | 1.021 | 0.017 | 0.101 |
| | STD | 4.844 | 11.019 | 10.569 | 4.877 | 11.068 | 10.560 |
| Point 2 | MIN | 517535.489 | 5035999.847 | 89.902 | -15.851 | -89.734 | -70.302 |
| | MAX | 517568.035 | 5036166.910 | 221.216 | 16.695 | 77.329 | 61.012 |
| | Mean | 517551.974 | 5036089.360 | 158.137 | 0.634 | -0.221 | -2.067 |
| | Median | 517551.985 | 5036089.255 | 158.194 | 0.645 | -0.325 | -2.010 |
| | STD | 5.489 | 15.143 | 17.762 | 5.521 | 15.132 | 17.867 |
| Point 3 | MIN | 517508.931 | 5035809.083 | 115.627 | -42.493 | -284.625 | -44.587 |
| | MAX | 517595.438 | 5036327.479 | 219.329 | 44.014 | 233.772 | 59.114 |
| | Mean | 517552.769 | 5036092.068 | 163.278 | 1.346 | -1.639 | 3.063 |
| | Median | 517552.442 | 5036091.656 | 163.480 | 1.019 | -2.052 | 3.266 |
| | STD | 10.291 | 42.795 | 16.027 | 10.369 | 42.789 | 16.303 |
| Point 4 | MIN | 517508.126 | 5036043.480 | 88.558 | -43.367 | -55.681 | -71.628 |
| | MAX | 517581.743 | 5036136.026 | 224.715 | 30.249 | 36.864 | 64.529 |
| | Mean | 517552.754 | 5036098.790 | 159.824 | 1.261 | -0.372 | -0.362 |
| | Median | 517552.651 | 5036099.268 | 159.678 | 1.157 | 0.107 | -0.508 |
| | STD | 7.729 | 14.278 | 16.312 | 7.818 | 14.259 | 16.288 |
| Point 5 | MIN | 517525.618 | 5036036.928 | 104.464 | -17.614 | -62.342 | -55.738 |
| | MAX | 517561.508 | 5036165.939 | 208.694 | 18.277 | 66.669 | 48.492 |
| | Mean | 517543.449 | 5036096.414 | 158.364 | 0.217 | -2.855 | -1.837 |
| | Median | 517543.507 | 5036096.560 | 158.711 | 0.275 | -2.709 | -1.490 |
| | STD | 5.416 | 19.231 | 17.476 | 5.415 | 19.421 | 17.553 |
| Point 6 | MIN | 517476.458 | 5036045.411 | 71.840 | -56.441 | -52.273 | -88.354 |
| | MAX | 517569.491 | 5036138.963 | 257.634 | 36.592 | 41.279 | 97.440 |
| | Mean | 517531.891 | 5036097.637 | 165.362 | -1.008 | -0.048 | 5.168 |
| | Median | 517531.595 | 5036098.008 | 165.573 | -1.303 | 0.323 | 5.379 |
| | STD | 8.163 | 14.311 | 22.637 | 8.216 | 14.294 | 23.193 |
| Point 7 | MIN | 517515.652 | 5036068.868 | 109.800 | -17.063 | -17.243 | -50.400 |
| | MAX | 517568.558 | 5036107.630 | 216.364 | 35.843 | 21.518 | 56.165 |
| | Mean | 517533.201 | 5036087.530 | 160.421 | 0.486 | 1.418 | 0.222 |
| | Median | 517533.214 | 5036086.563 | 157.666 | 0.500 | 0.452 | -2.533 |
| | STD | 6.713 | 8.225 | 19.790 | 6.715 | 8.328 | 19.747 |
| Point 8 | MIN | 517536.862 | 5036080.082 | 151.604 | -6.128 | -4.166 | -8.577 |
| | MAX | 517550.087 | 5036091.736 | 186.991 | 7.097 | 7.489 | 26.810 |
| | Mean | 517541.611 | 5036086.374 | 163.721 | -1.379 | 2.126 | 3.540 |
| | Median | 517540.966 | 5036087.494 | 162.540 | -2.024 | 3.247 | 2.359 |
| | STD | 3.982 | 3.381 | 11.296 | 3.999 | 3.832 | 11.223 |
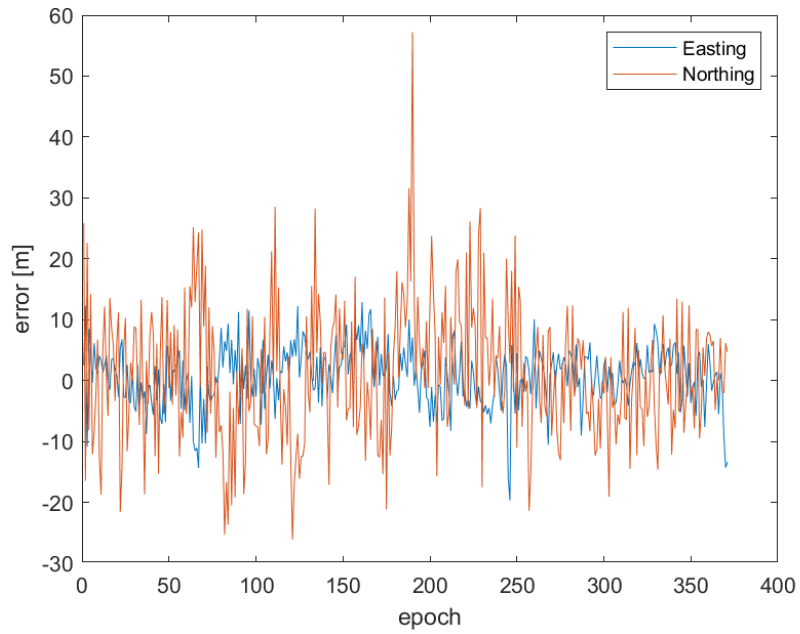
*Figure 5.48: Horizontal errors of DGPS for each epoch on Point 1 with respect to reference. (Geo++ RINEX Logger data obtained on May 17th, 2019)*
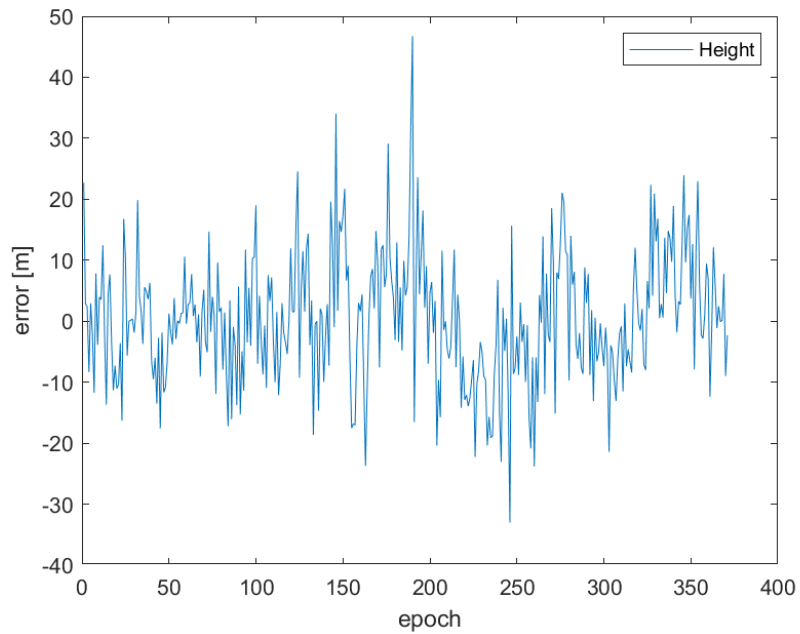


*Figure 5.49: Vertical errors of DGPS for each epoch on Point 1 with respect to reference. (Geo++ RINEX Logger data obtained on May 17th, 2019)*
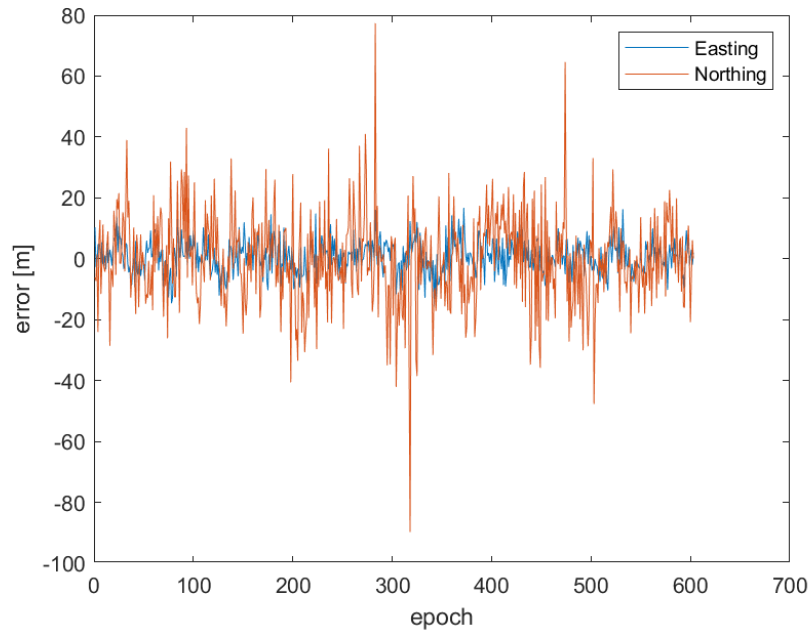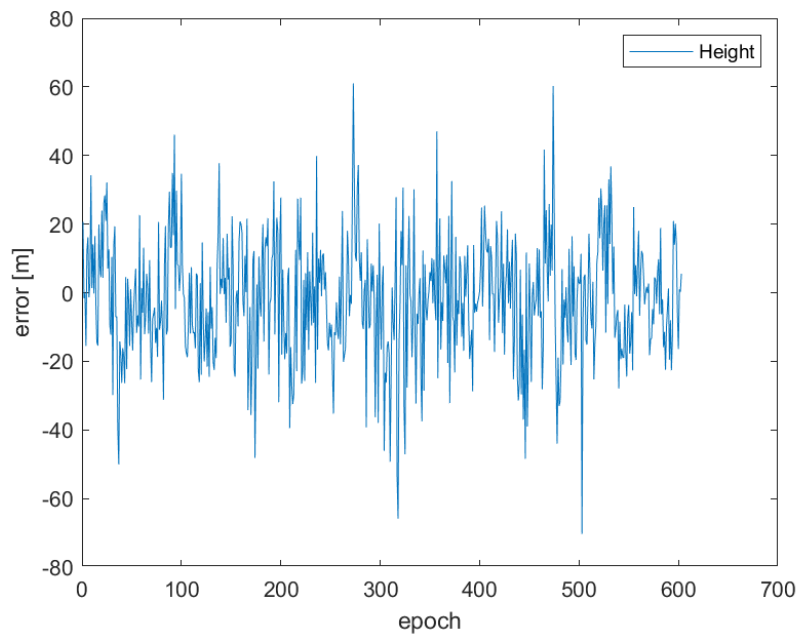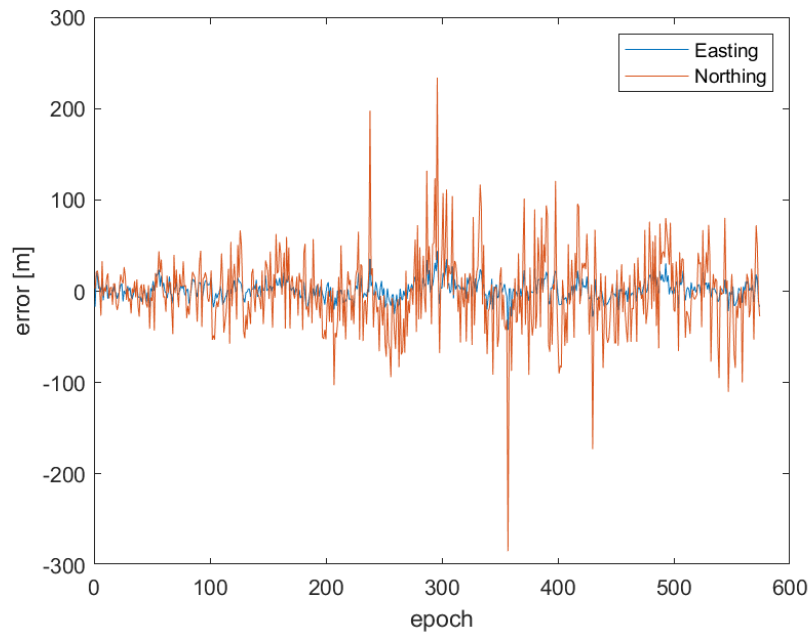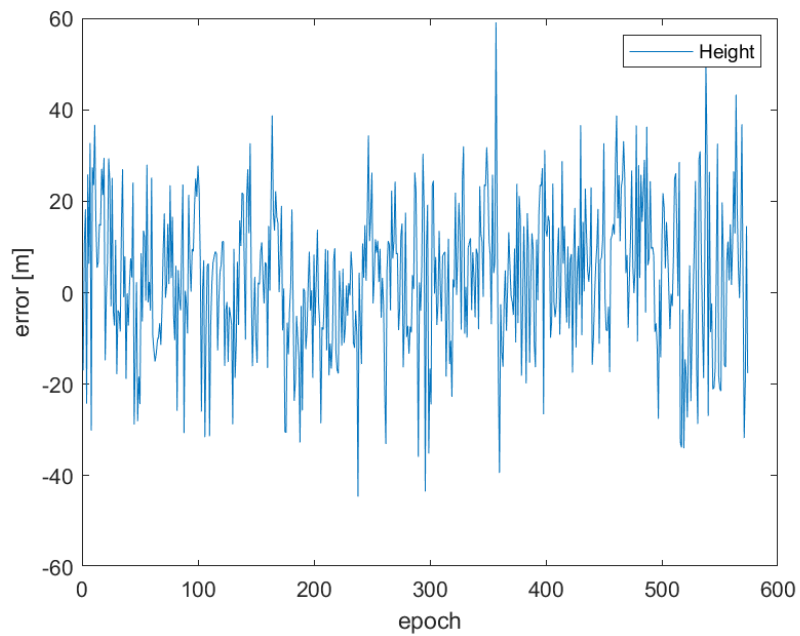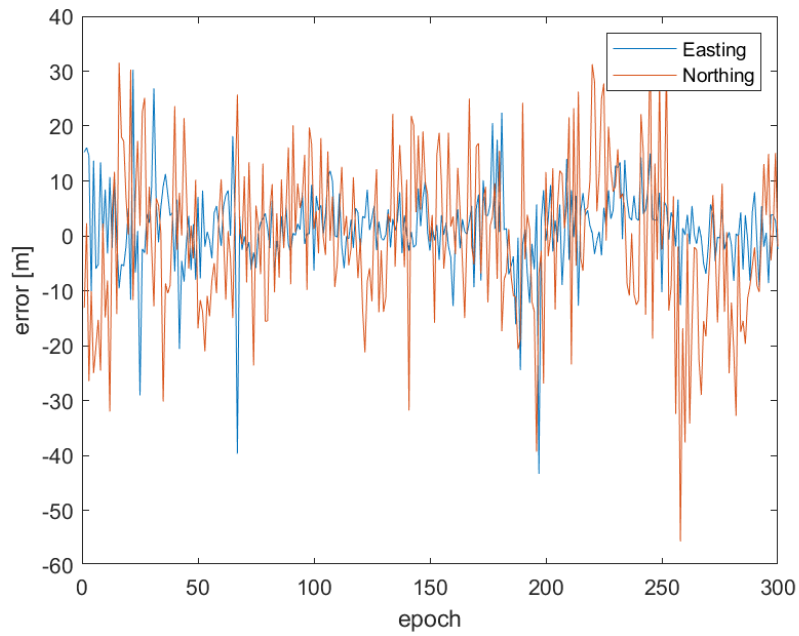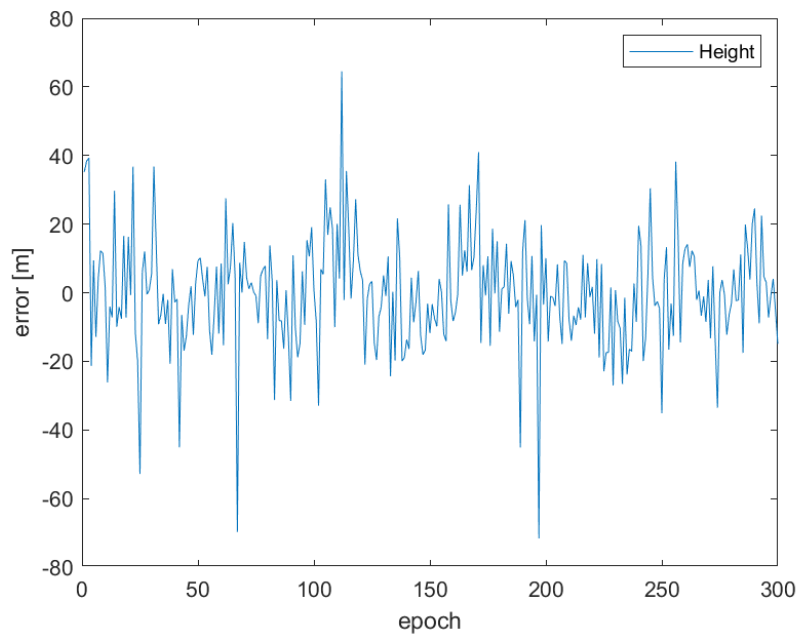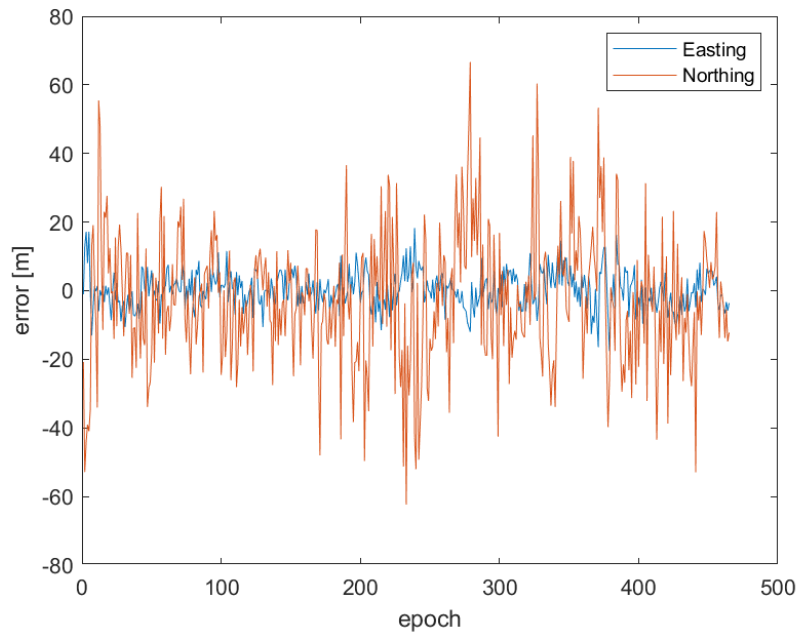
*Figure 5.50: Horizontal errors of DGPS for each epoch on Point 2 with respect to reference. (Geo++ RINEX Logger data obtained on May 17th, 2019)*
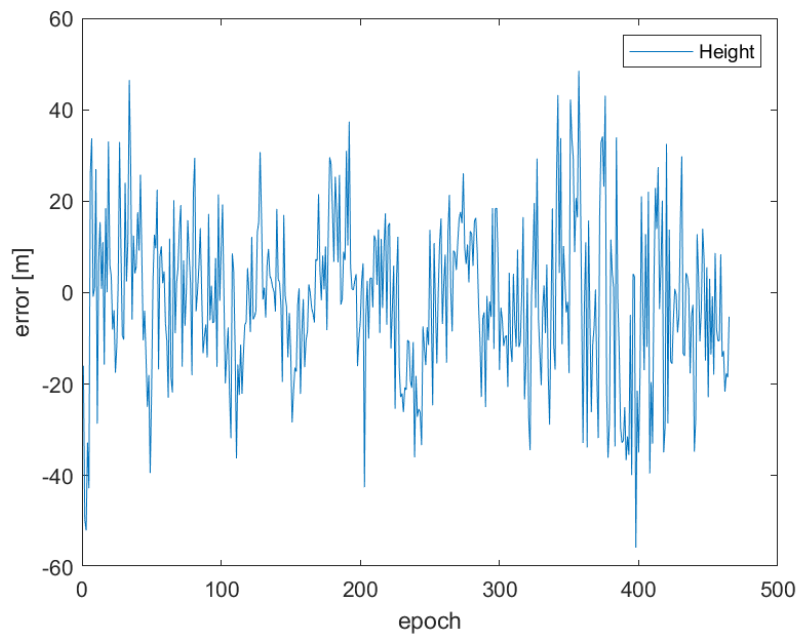


*Figure 5.51: Vertical errors of DGPS for each epoch on Point 2 with respect to reference. (Geo++ RINEX Logger data obtained on May 17th, 2019)*
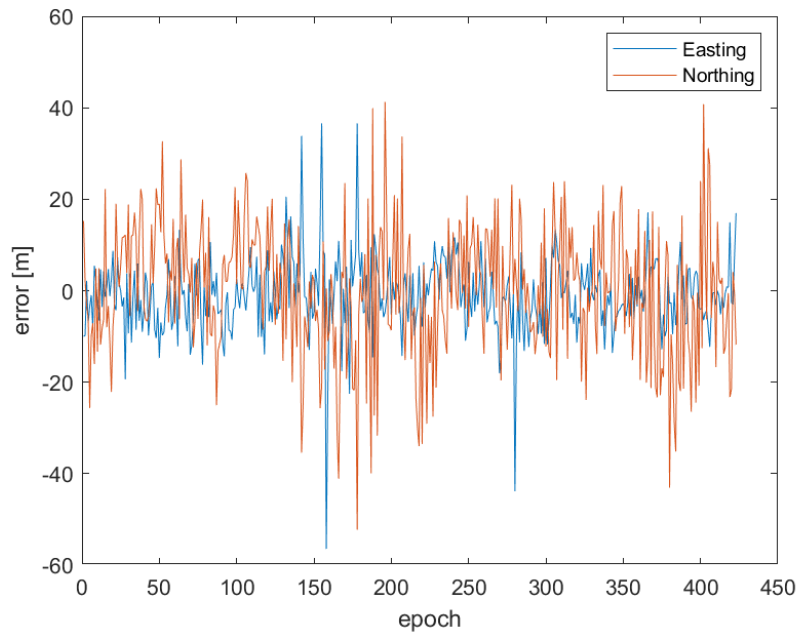
143

*Figure 5.52: Horizontal errors of DGPS for each epoch on Point 3 with respect to reference. (Geo++ RINEX Logger data obtained on May 17th, 2019)*



*Figure 5.53: Vertical errors of DGPS for each epoch on Point 3 with respect to reference. (Geo++ RINEX Logger data obtained on May 17th, 2019)*

*Figure 5.54: Horizontal errors of DGPS for each epoch on Point 4 with respect to reference. (Geo++ RINEX Logger data obtained on May 17th, 2019)*
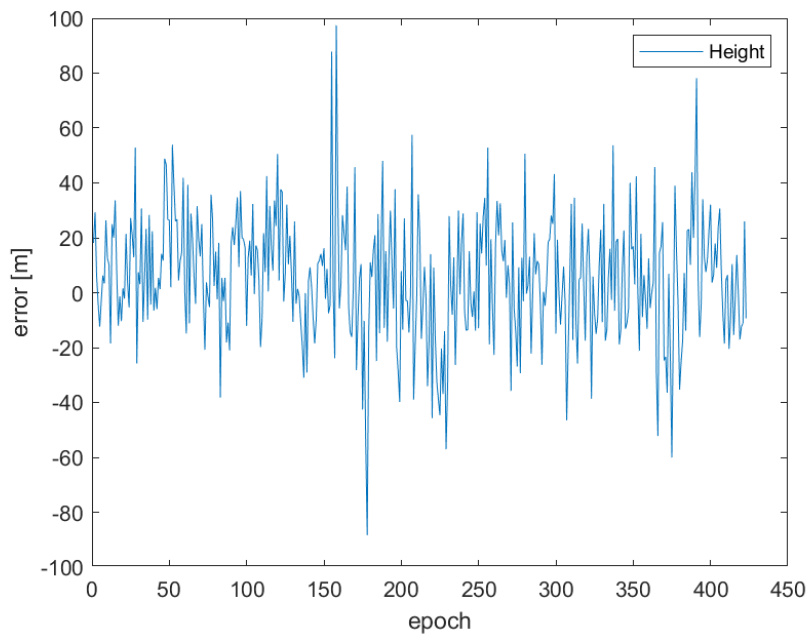


*Figure 5.55: Vertical errors of DGPS for each epoch on Point 4 with respect to reference. (Geo++ RINEX Logger data obtained on May 17th, 2019)*
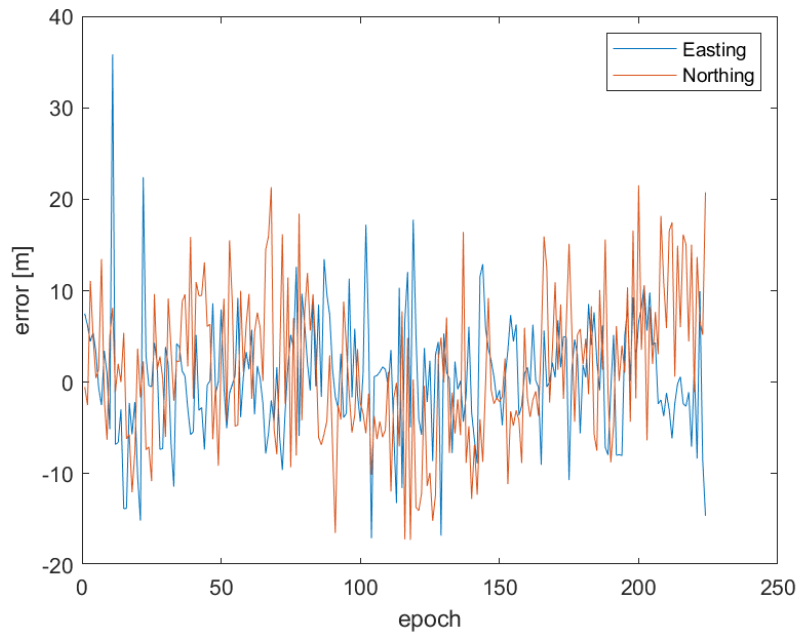
*Figure 5.56: Horizontal errors of DGPS for each epoch on Point 5 with respect to reference. (Geo++ RINEX Logger data obtained on May 17th, 2019)*



*Figure 5.57: Vertical errors of DGPS for each epoch on Point 5 with respect to reference. (Geo++ RINEX Logger data obtained on May 17th, 2019)*

*Figure 5.58: Horizontal errors of DGPS for each epoch on Point 6 with respect to reference. (Geo++ RINEX Logger data obtained on May 17th, 2019)*
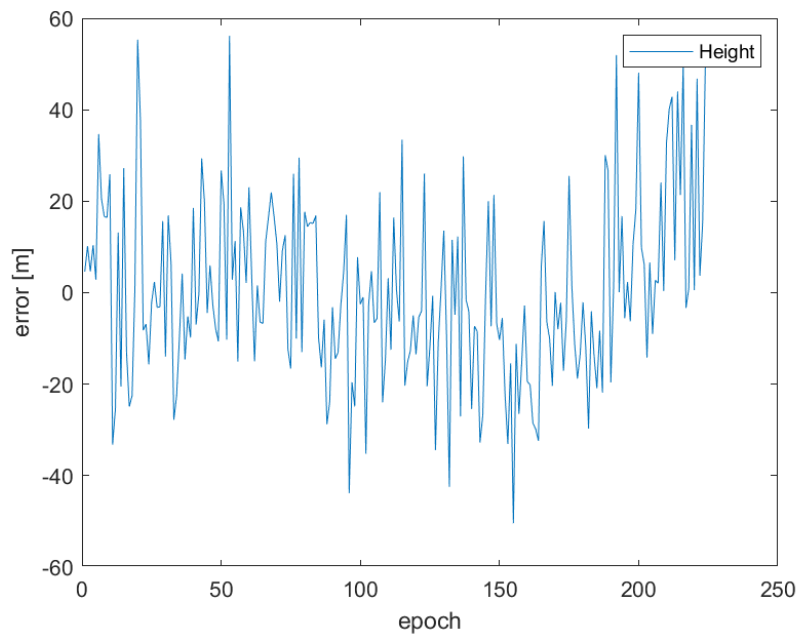


*Figure 5.59: Vertical errors of DGPS for each epoch on Point 6 with respect to reference. (Geo++ RINEX Logger data obtained on May 17th, 2019)*
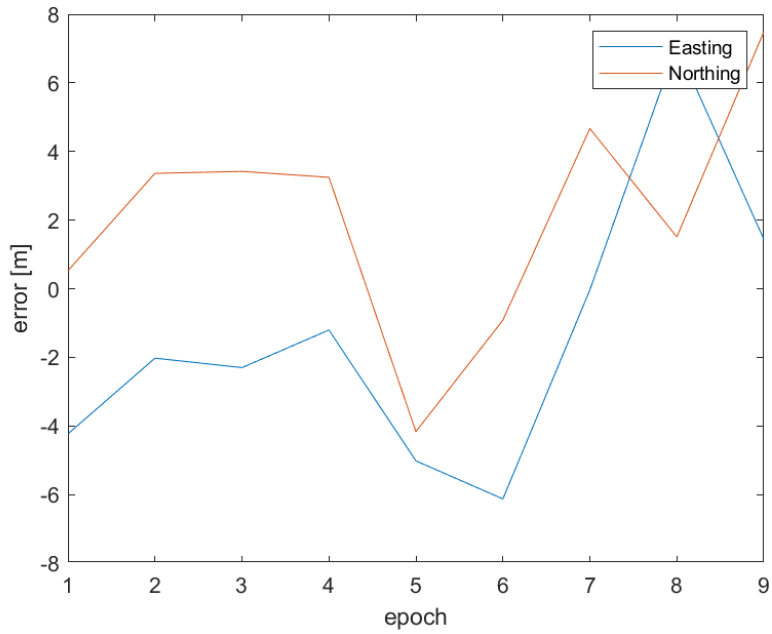
*Figure 5.60: Horizontal errors of DGPS for each epoch on Point 7 with respect to reference. (Geo++ RINEX Logger data obtained on May 17th, 2019)*



*Figure 5.61: Vertical errors of DGPS for each epoch on Point 7 with respect to reference. (Geo++ RINEX Logger data obtained on May 17th, 2019)*

*Figure 5.62: Horizontal errors of DGPS for each epoch on Point 8 with respect to reference.
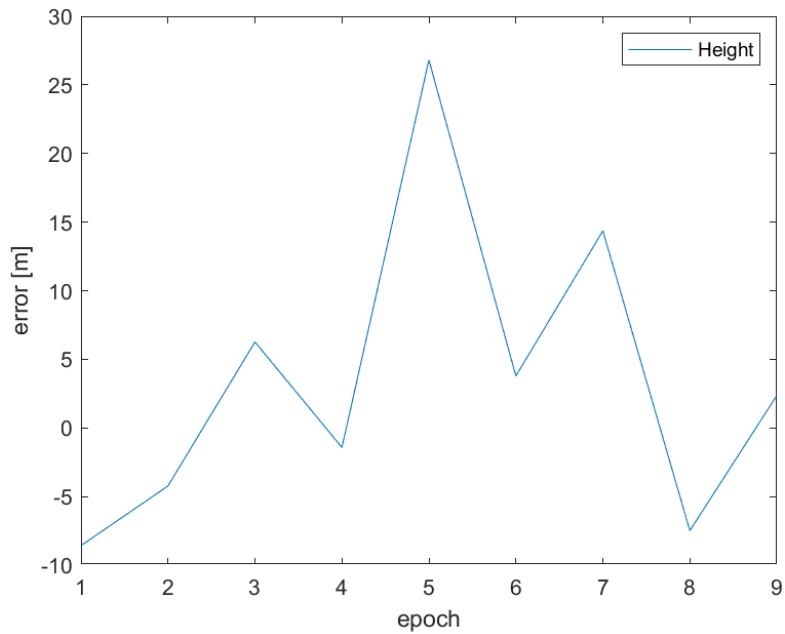(Geo++ RINEX Logger data obtained on May 17th, 2019)*



*Figure 5.63: Vertical errors of DGPS for each epoch on Point 8 with respect to reference.
(Geo++ RINEX Logger data obtained on May 17th, 2019)*

*Table 5.23: Averaged the DGPS results by Geo++ RINEX Logger as a final results.*

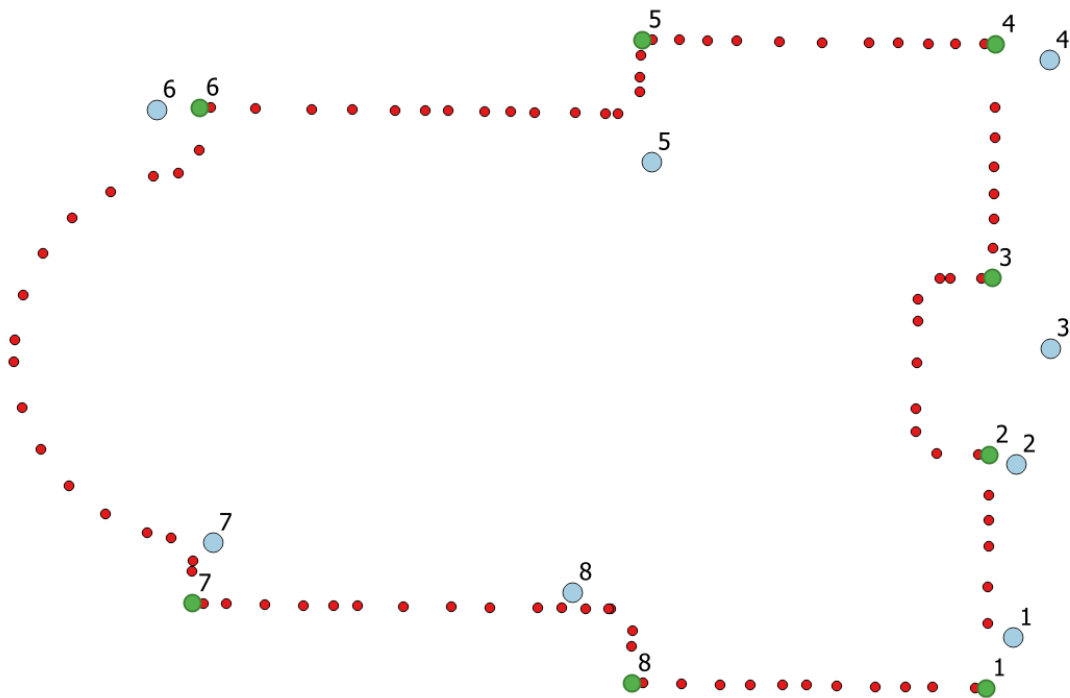| Point ID | Geo++ RINEX Logger | | | | | |
|---|---|---|---|---|---|---|
| | East [m] | North [m] | Height [m] | ΔE [m] | ΔN [m] | ΔH [m] |
| 1 | 517551.898 | 5036085.318 | 160.487 | 0.624 | 1.183 | 0.320 |
| 2 | 517551.974 | 5036089.360 | 158.137 | 0.634 | -0.221 | -2.067 |
| 3 | 517552.769 | 5036092.068 | 163.278 | 1.346 | -1.639 | 3.063 |
| 4 | 517552.754 | 5036098.790 | 159.824 | 1.261 | -0.372 | -0.362 |
| 5 | 517543.449 | 5036096.414 | 158.364 | 0.217 | -2.855 | -1.837 |
| 6 | 517531.891 | 5036097.637 | 165.362 | -1.008 | -0.048 | 5.168 |
| 7 | 517533.201 | 5036087.530 | 160.421 | 0.486 | 1.418 | 0.222 |
| 8 | 517541.611 | 5036086.374 | 163.721 | -1.379 | 2.126 | 3.540 |



*Figure 5.64: Final results of DGPS by Geo++ RINEX Logger in blue, reference in red are presented.*

150

The final results for DGPS are presented on above. The statistics are presented in Table 5.24. There is slightly improvement on North 0.9 meters, on Height 0.7 meters. There is no improvement noticed on East with respect to single point positioning.

*Table 5.24: Statistics of the results for single point positioning by Geo++ RINEX Logger.*

| Statistics | East [m] | North [m] | Height [m] |
|---|---|---|---|
| Min [m] | -1.379 | -2.855 | -2.067 |
| Max [m] | 1.346 | 2.126 | 5.168 |
| Mean [m] | 0.273 | -0.051 | 1.006 |
| Median [m] | 0.555 | -0.134 | 0.271 |
| STD [m] | 0.985 | 1.645 | 2.631 |
| RMS [m] | 0.961 | 1.540 | 2.659 |

## 5.4.1.4 Static for Geo++ RINEX Logger

RTKLIB employs EKF (extended Kalman filter) in order to obtain the final solutions in static mode in conjunction with the GNSS signal measurement models, and the troposphere and ionosphere models.

Theoretically, by using static mode, 600 iterations on epochs have to be done for each 10 minutes session. However, some sessions have less, because of discontinuity problem in the L1 phase observations which is caused the same problem with DGPS mode. Again, Point 8 could be show as a good example in Figure 5.66. Only 9 epoch has a final result in output file from RTKLIB.

Obtained files from RTKLIB represents the coordinates in units of geographic coordinate system (latitude, longitude and height). These coordinates are converted to ETRF UTM-32N coordinates (east, north and height) by using QGIS that was done in the previous experiment.

All results obtained for the iterations are shown epoch by epoch in Figure 5.65 and Figure 5.66. It can be easily noticed on the Figures that iterations are tightly spread. Statistics of static results are calculated by MATLAB code and presented in Table 5.25 and Table 5.26. All related statistical error graphs are presented Figure 5.67 - Figure 5.74 respectively. Final results for each point are presented in Figure 5.75.
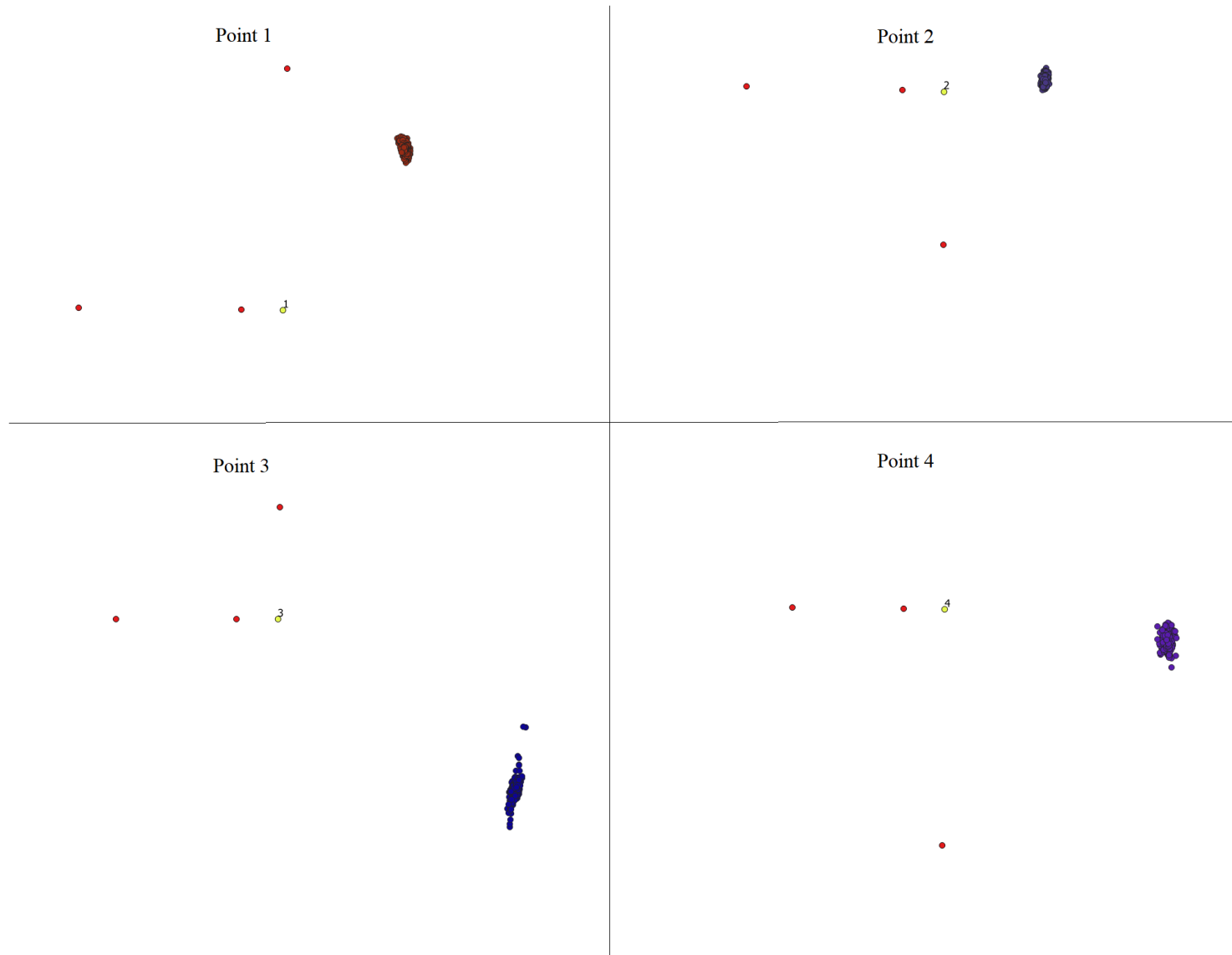
*Figure 5.65: The all results from RTKLIB for static mode (Point 1, Point 2, Point 3 and Point 4) (Geo++ RINEX Logger).*
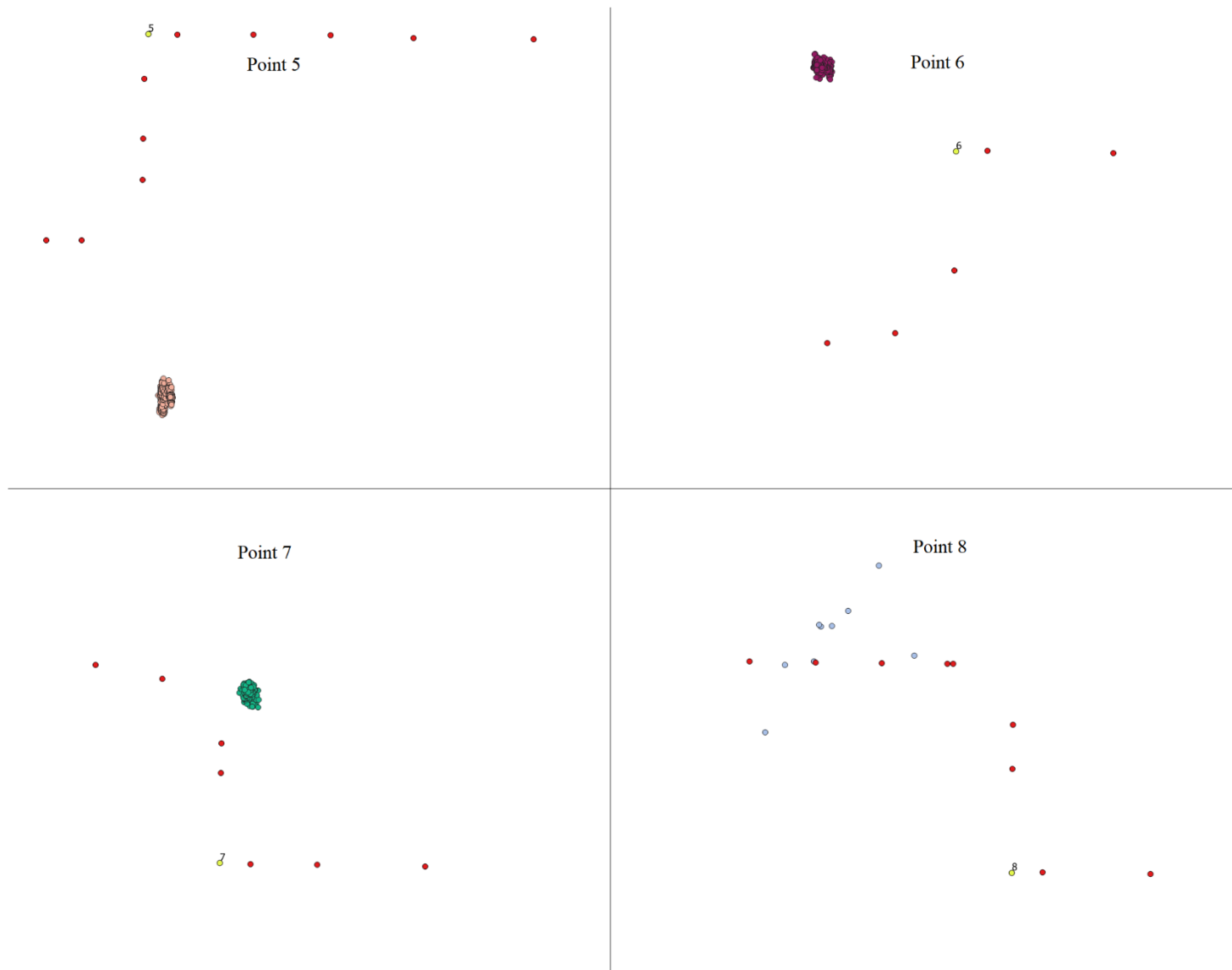
*Figure 5.66: The all results from RTKLIB for static mode (Point 5, Point 6, Point 7 and Point 8) (Geo++ RINEX Logger)*

*Table 5.25: The final results of static mod for Geo++ RINEX Logger observations.*

| Point ID | Reference | | | Geo++ RINEX Logger | | | ΔE [m] | ΔN [m] | ΔH [m] |
|---|---|---|---|---|---|---|---|---|---|
| | East [m] | North [m] | Height [m] | East [m] | North [m] | Height [m] | | | |
| 1 | 517551.274 | 5036084.135 | 160.167 | 517552.009 | 5036085.116 | 160.518 | 0.735 | 0.981 | 0.351 |
| 2 | 517551.340 | 5036089.580 | 160.204 | 517551.970 | 5036089.636 | 158.759 | 0.630 | 0.056 | -1.445 |
| 3 | 517551.423 | 5036093.707 | 160.214 | 517552.857 | 5036092.558 | 162.954 | 1.434 | -1.149 | 2.740 |
| 4 | 517551.493 | 5036099.161 | 160.186 | 517552.870 | 5036098.971 | 160.356 | 1.377 | -0.190 | 0.171 |
| 5 | 517543.232 | 5036099.269 | 160.201 | 517543.414 | 5036096.242 | 158.814 | 0.183 | -3.027 | -1.388 |
| 6 | 517532.899 | 5036097.684 | 160.194 | 517531.780 | 5036098.384 | 165.942 | -1.118 | 0.700 | 5.748 |
| 7 | 517532.715 | 5036086.111 | 160.199 | 517532.955 | 5036087.616 | 160.350 | 0.240 | 1.505 | 0.150 |
| 8 | 517542.990 | 5036084.247 | 160.181 | 517541.879 | 5036086.808 | 164.198 | -1.111 | 2.561 | 4.017 |

*Table 5.26: Statistics of static mod solutions for Geo++ RINEX Logger.*

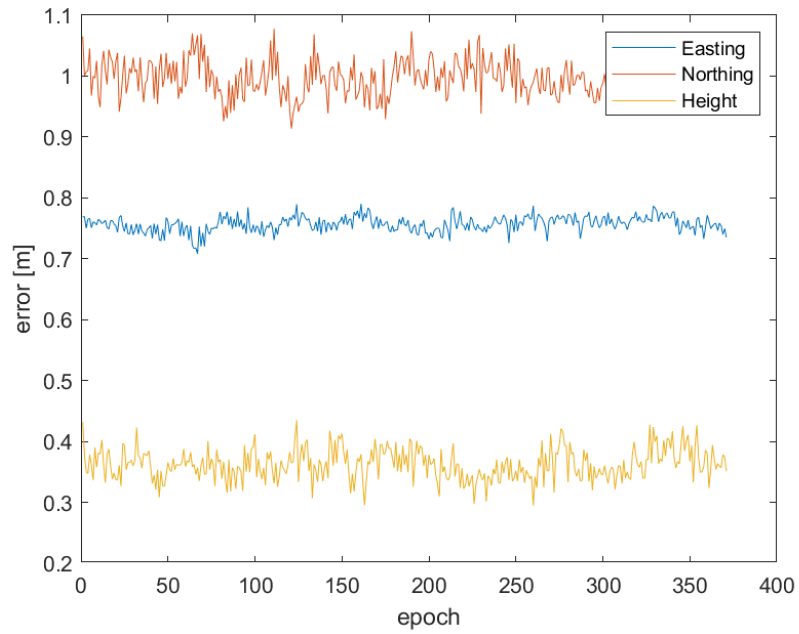| Statistics | East [m] | North [m] | Height [m] |
|---|---|---|---|
| Min [m] | -1.118 | -3.027 | -1.445 |
| Max [m] | 1.434 | 2.561 | 5.748 |
| Mean [m] | 0.296 | 0.179 | 1.293 |
| Median [m] | 0.435 | 0.378 | 0.261 |
| STD [m] | 0.983 | 1.713 | 2.605 |
| RMS [m] | 0.966 | 1.612 | 2.758 |

*Figure 5.67: Errors of static for each epoch on Point 1 with respect to reference. (Geo++ RINEX Logger data obtained on May 17th, 2019)*
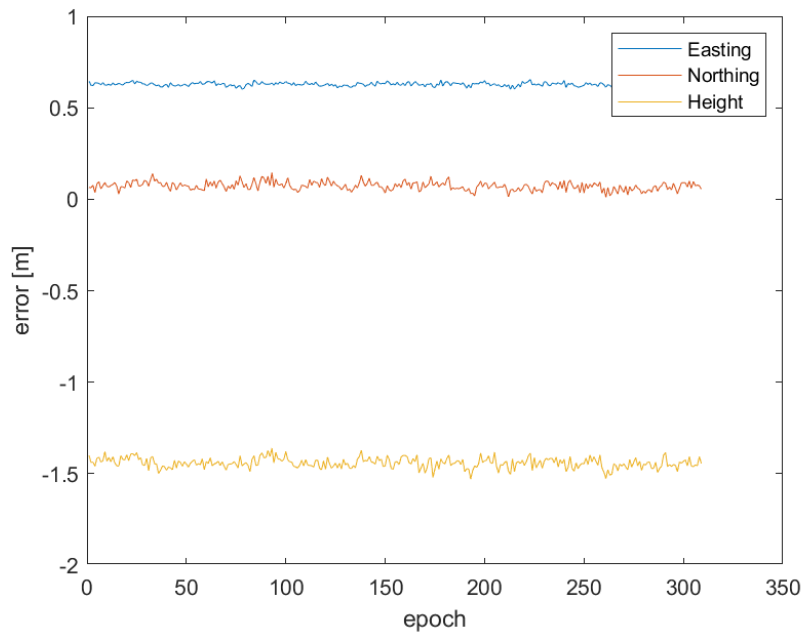


*Figure 5.68: Errors of static for each epoch on Point 2 with respect to reference. (Geo++ RINEX Logger data obtained on May 17th, 2019)*
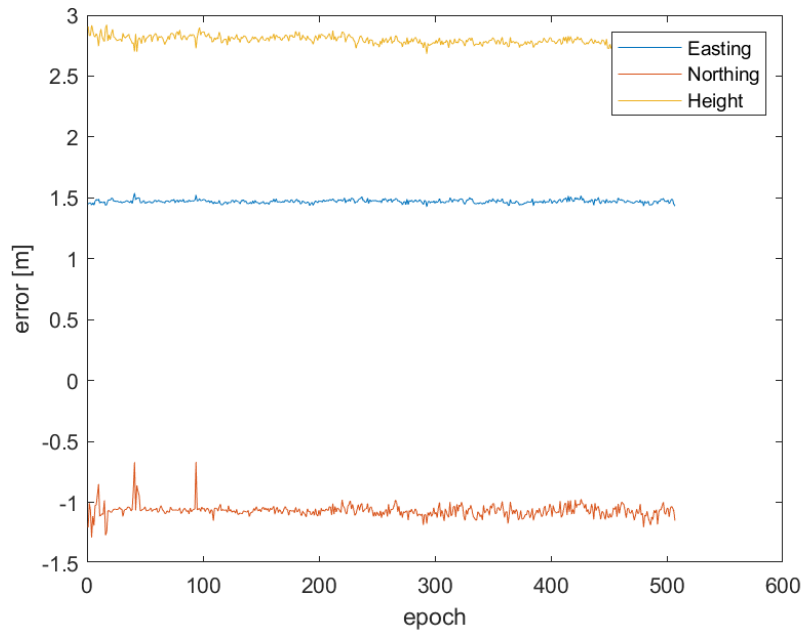
*Figure 5.69: Errors of static for each epoch on Point 3 with respect to reference. (Geo++ RINEX Logger data obtained on May 17th, 2019)*
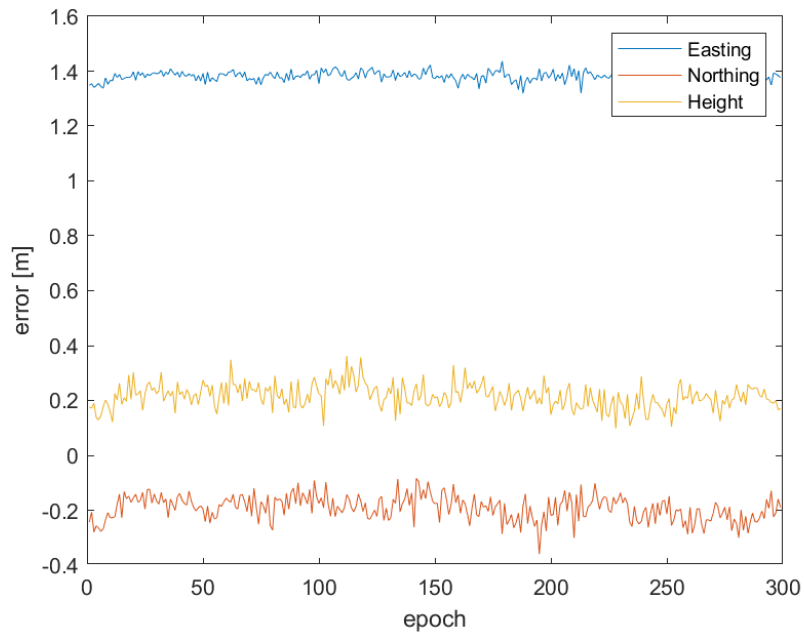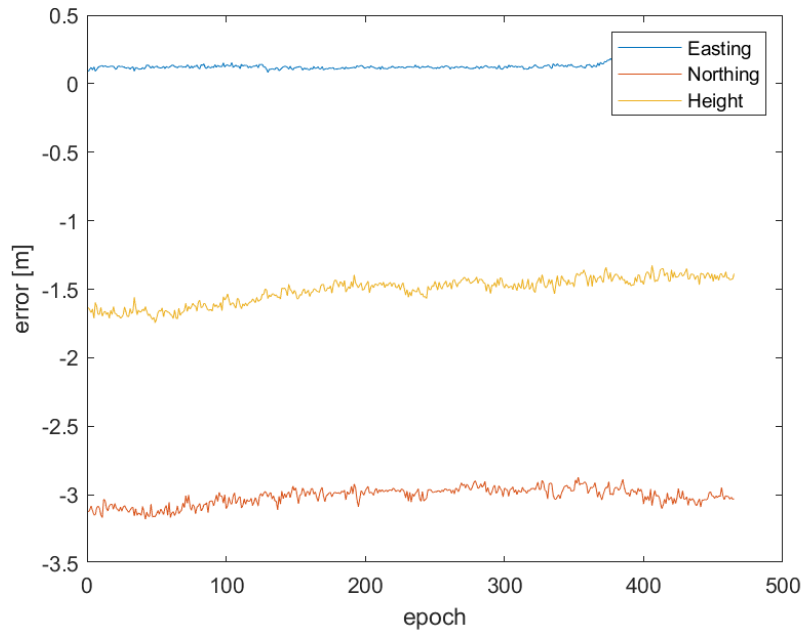


*Figure 5.70: Errors of static for each epoch on Point 4 with respect to reference. (Geo++ RINEX Logger data obtained on May 17th, 2019)*

*Figure 5.71: Errors of static for each epoch on Point 5 with respect to reference. (Geo++ RINEX Logger data obtained on May 17th, 2019)*
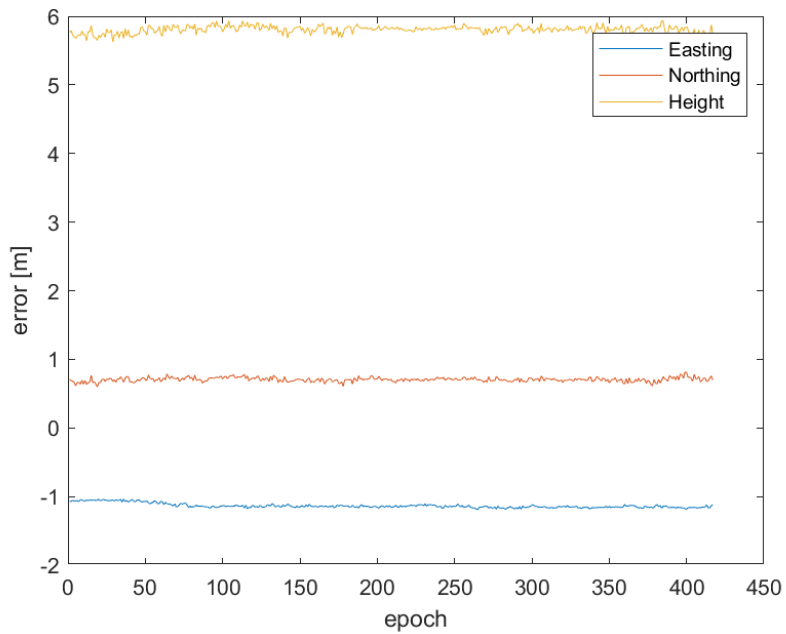


*Figure 5.72: Errors of static for each epoch on Point 6 with respect to reference. (Geo++ RINEX Logger data obtained on May 17th, 2019)*
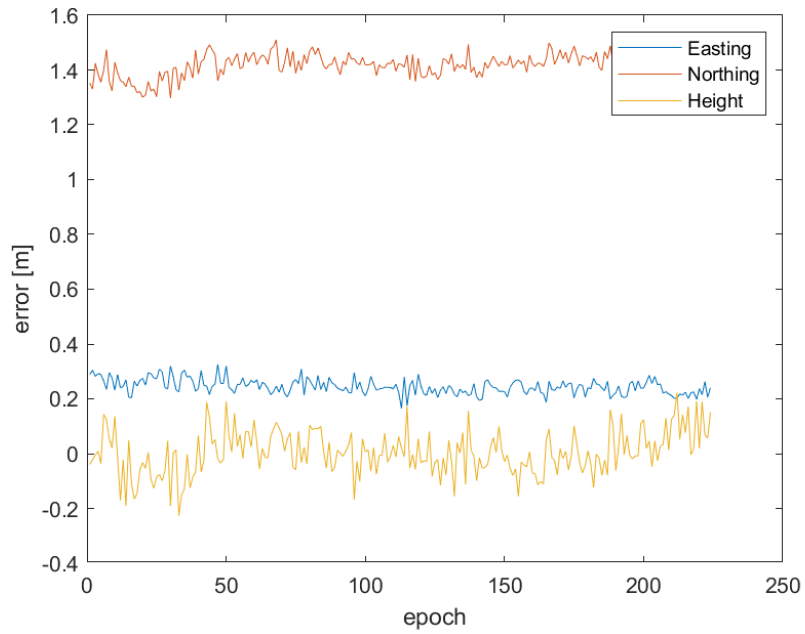
*Figure 5.73: Errors of static for each epoch on Point 7 with respect to reference. (Geo++ RINEX Logger data obtained on May 17th, 2019)*
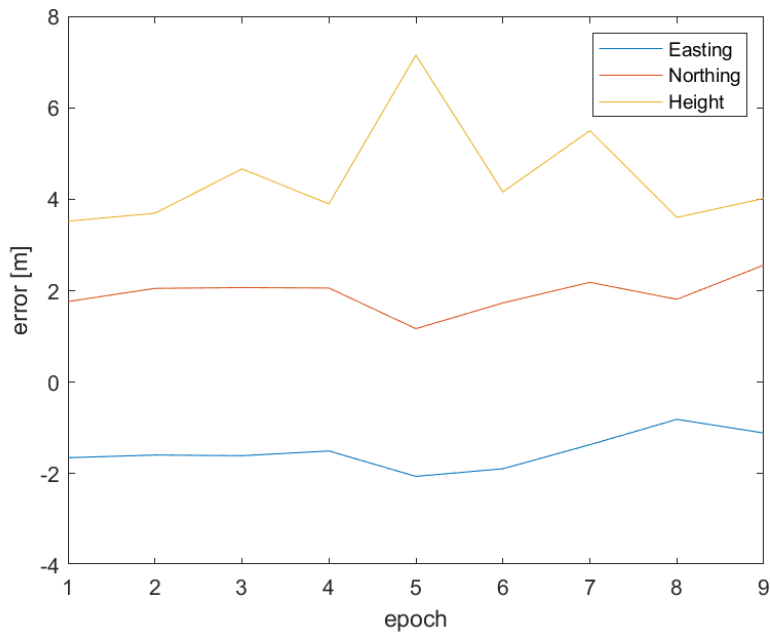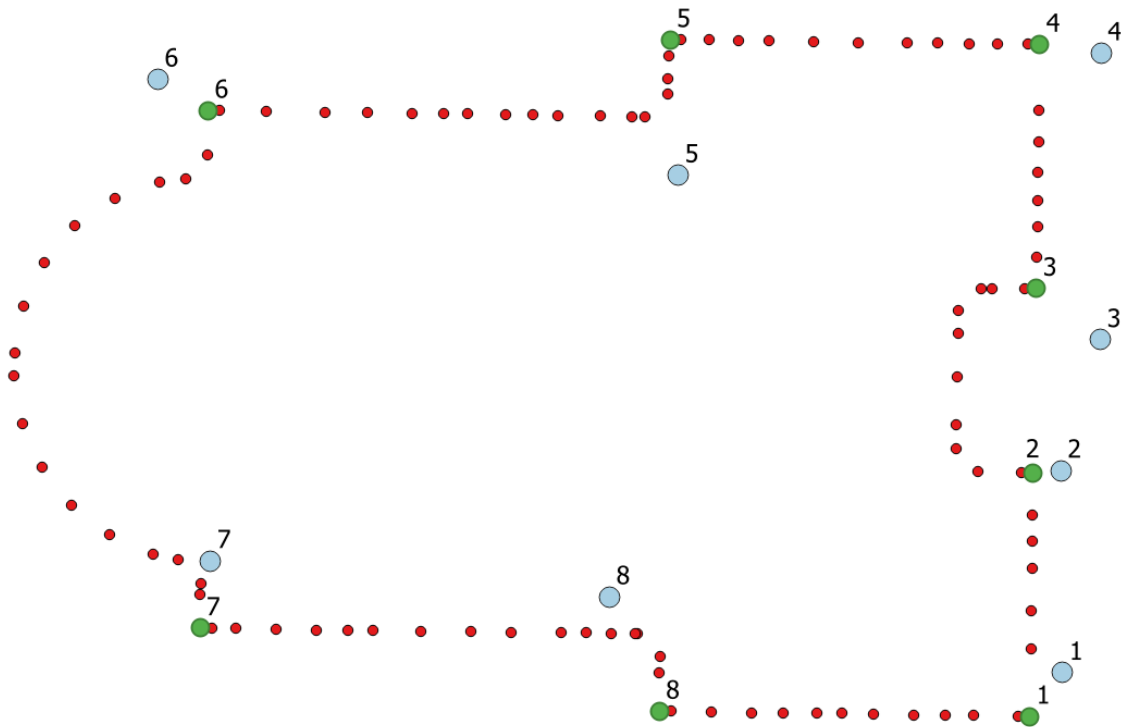


*Figure 5.74: Errors of static for each epoch on Point 8 with respect to reference. (Geo++ RINEX Logger data obtained on May 17th, 2019)*

158

*Figure 5.75: Final results of static (Geo++ RINEX Logger).*

The comparison between single point positioning (see Table 5.21) and static (see Table 5.26) shows that the similar improvement exist for static on North 0.8 meters, on Height 0.6 meters.

## 5.4.2 RinexOn

RinexOn uses Android API Level 24 services to log raw GNSS measurement data into a RINEX file version 3.03 including pseudoranges, accumulated delta ranges, doppler frequencies and noise values. Besides, RinexOn can utilize the measurements of the Android Raw Measurements API produce Navigation Message Files.

Analysis of the data acquired from RinexOn shows that it has better reconstruction of RINEX than Geo++ RINEX Logger shows. Besides, incorrect decoding of the observations has never be seen with any sessions measured. The observation continuity analysis shows that there is no discontinuity of the observations acquired by RinexOn. However, sometimes produced Navigation

Message Files end up empty in Figure 5.76. No reason is identified for empty Navigation Message Files.



```
1      3.03           NAVIGATION DATA    M: Mixed             RINEX VERSION / TYPE[LF]
2  rinex ON           NSL                20190611 203209 UTC  PGM / RUN BY / DATE[LF]
3                                                             END OF HEADER[LF]
4
```

*Figure 5.76: Example of an empty Navigation Message File observed.*

Data processing was reproduced with RTKLIB v. 2.4.3 b28 as it is done with Geo++ RINEX Logger. All solution files are obtained with the same configuration parameters which are defined for Geo++ RINEX Logger in Section 5.3.1.

All session presented in the research for RinexOn are measured on June 11th, 2019, 25 day later than Geo++ RINEX Logger presented sessions. Then, these smartphone observations are processed with 3 different position mode by RTKLIB: Single Point Positioning, DGPS and Static.

### 5.4.2.1 Single Point Positioning for RinexOn

By using single point positioning mode, 600 positions are computed for each 10 minutes session. Obtained files from RTKLIB represents the coordinates in units of geographic coordinate system (latitude, longitude and height). These coordinates are converted to ETRF UTM-32N coordinates (east, north and height) by using QGIS that was done in the previous experiment.

The results obtained for each point are shown epoch by epoch in Figure 5.77 and Figure 5.78. Statistics of single point positioning results are calculated by MATLAB code and presented in Table 5.27. All related statistical error graphs are presented Figure 5.79 - Figure 5.94 respectively. Final results for each point are calculated by averaging all epochs and presented in Figure 5.95.
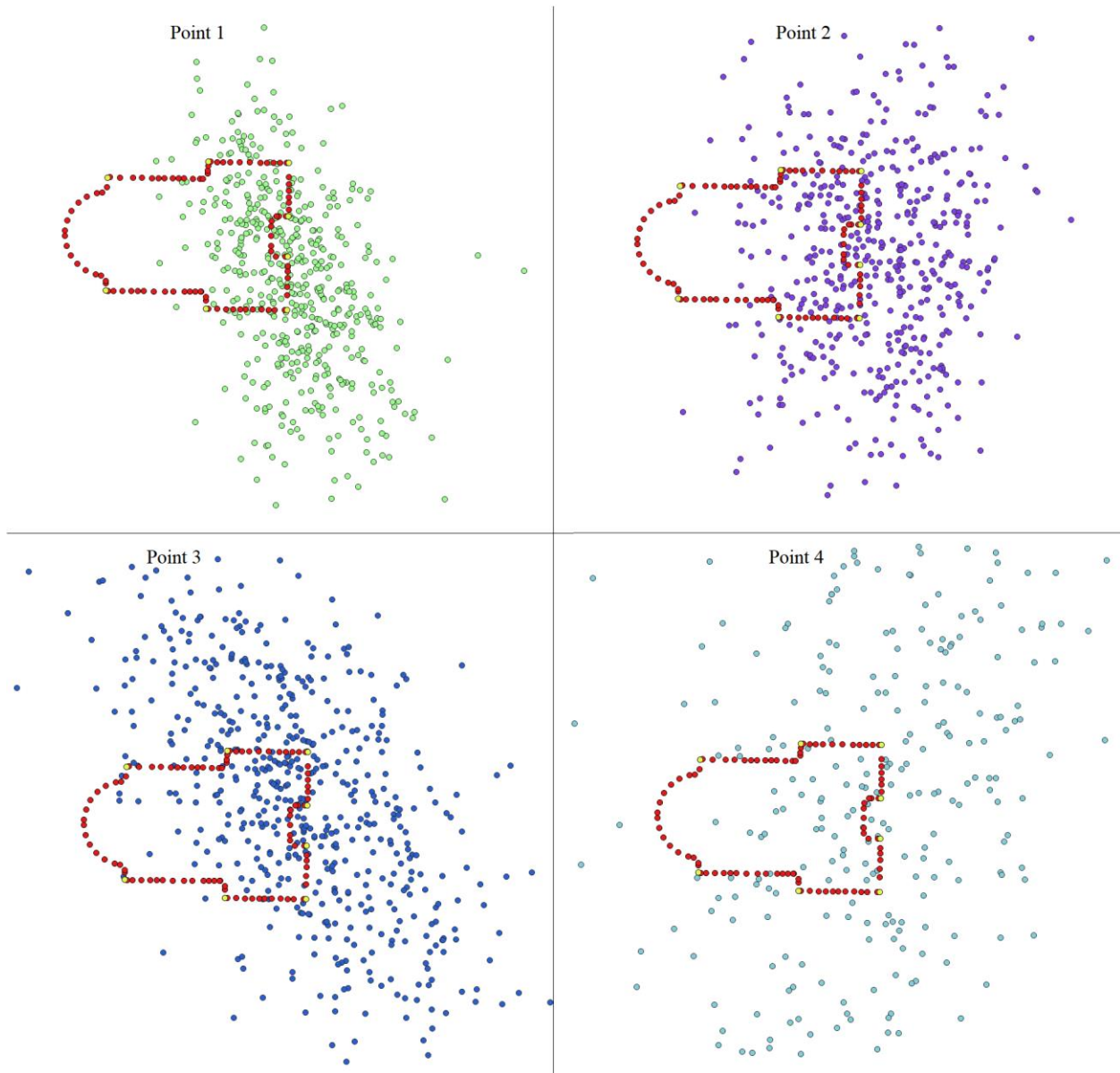
*Figure 5.77: Example of single point positioning mode results (Point 1, Point 2, Point 3 and Point 4) (RinexOn).*
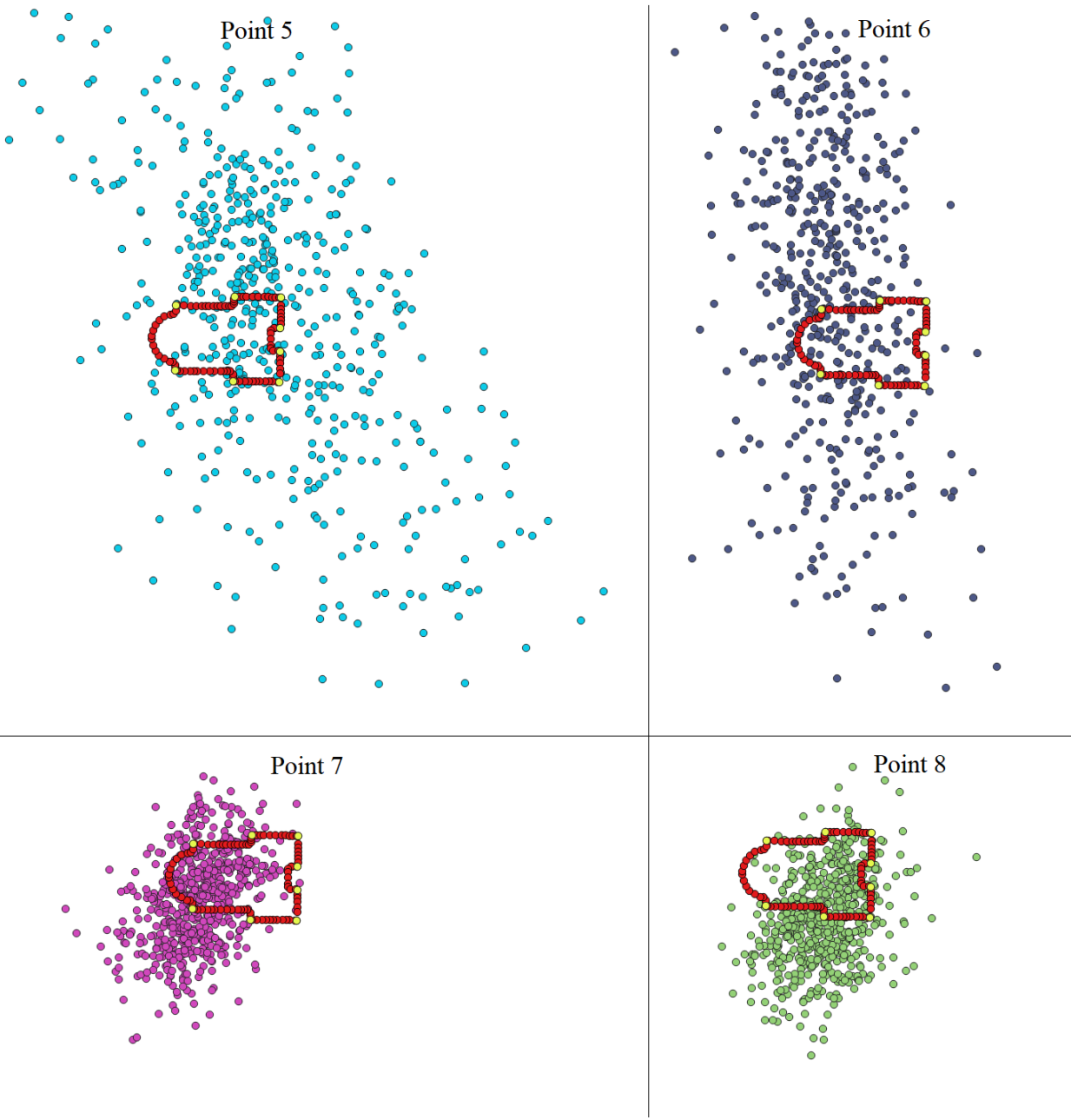
*Figure 5.78: Example of single point positioning mode results (Point 5, Point 6, Point 7 and Point 8) (RinexOn).*

*Table 5.27: Statistics of single point positioning results (RinexOn)*

| Point ID | | East [m] | North [m] | Height [m] | ΔE [m] | ΔN [m] | ΔH [m] |
|---|---|---|---|---|---|---|---|
| Point 1 | MIN | 517537.874 | 5036061.250 | 109.855 | -13.400 | -22.886 | -50.312 |
| | MAX | 517575.513 | 5036121.242 | 214.200 | 24.238 | 37.106 | 54.033 |
| | Mean | 517551.966 | 5036087.142 | 159.757 | 0.691 | 3.007 | -0.410 |
| | Median | 517551.762 | 5036086.938 | 160.200 | 0.487 | 2.802 | 0.033 |
| | STD | 5.318 | 9.348 | 17.145 | 5.357 | 9.811 | 17.133 |
| Point 2 | MIN | 517533.211 | 5036053.873 | 99.329 | -18.129 | -35.708 | -60.874 |
| | MAX | 517572.942 | 5036124.177 | 225.390 | 21.602 | 34.596 | 65.186 |
| | Mean | 517552.884 | 5036090.537 | 159.716 | 1.545 | 0.957 | -0.488 |
| | Median | 517553.093 | 5036090.449 | 158.540 | 1.753 | 0.868 | -1.663 |
| | STD | 6.743 | 10.892 | 20.643 | 6.911 | 10.924 | 20.629 |
| Point 3 | MIN | 517518.517 | 5036060.531 | 49.669 | -32.906 | -33.176 | -110.545 |
| | MAX | 517578.606 | 5036133.693 | 276.149 | 27.183 | 39.985 | 115.935 |
| | Mean | 517550.247 | 5036095.433 | 150.654 | -1.176 | 1.725 | -9.560 |
| | Median | 517550.203 | 5036095.235 | 151.798 | -1.221 | 1.527 | -8.416 |
| | STD | 9.360 | 12.413 | 32.053 | 9.425 | 12.521 | 33.421 |
| Point 4 | MIN | 517502.933 | 5036031.146 | 75.439 | -48.560 | -68.016 | -84.747 |
| | MAX | 517582.253 | 5036194.033 | 215.839 | 30.760 | 94.872 | 55.653 |
| | Mean | 517550.885 | 5036095.699 | 158.511 | -0.609 | -3.462 | -1.675 |
| | Median | 517551.567 | 5036094.921 | 158.787 | 0.074 | -4.241 | -1.399 |
| | STD | 11.871 | 23.801 | 20.938 | 11.869 | 24.017 | 20.974 |
| Point 5 | MIN | 517502.057 | 5036002.494 | 68.035 | -41.175 | -96.775 | -92.166 |
| | MAX | 517608.860 | 5036169.967 | 277.262 | 65.628 | 70.697 | 117.061 |
| | Mean | 517550.037 | 5036096.263 | 163.919 | 6.805 | -3.007 | 3.718 |
| | Median | 517548.405 | 5036098.091 | 162.352 | 5.173 | -1.179 | 2.151 |
| | STD | 16.804 | 26.801 | 32.017 | 18.115 | 26.945 | 32.202 |
| Point 6 | MIN | 517506.788 | 5035975.050 | 27.542 | -26.111 | -122.635 | -132.653 |
| | MAX | 517564.386 | 5036188.809 | 332.531 | 31.488 | 91.125 | 172.337 |
| | Mean | 517534.192 | 5036105.456 | 157.795 | 1.293 | 7.771 | -2.399 |
| | Median | 517534.026 | 5036105.899 | 156.912 | 1.127 | 8.214 | -3.282 |
| | STD | 8.805 | 29.790 | 39.106 | 8.892 | 30.760 | 39.143 |
| Point 7 | MIN | 517510.205 | 5036062.908 | 82.759 | -22.510 | -23.203 | -77.441 |
| | MAX | 517551.713 | 5036109.737 | 232.353 | 18.998 | 23.625 | 72.154 |
| | Mean | 517533.640 | 5036087.776 | 157.981 | 0.925 | 1.664 | -2.218 |
| | Median | 517533.424 | 5036088.366 | 157.388 | 0.709 | 2.254 | -2.812 |
| | STD | 6.194 | 8.133 | 23.332 | 6.258 | 8.295 | 23.418 |
| Point 8 | MIN | 517524.903 | 5036059.543 | 89.814 | -18.087 | -24.704 | -70.366 |
| | MAX | 517570.166 | 5036110.783 | 247.729 | 27.176 | 26.535 | 87.548 |
| | Mean | 517543.067 | 5036083.842 | 159.398 | 0.077 | -0.406 | -0.783 |
| | Median | 517543.184 | 5036083.673 | 159.340 | 0.194 | -0.574 | -0.841 |
| | STD | 6.077 | 8.129 | 27.557 | 6.072 | 8.132 | 27.545 |
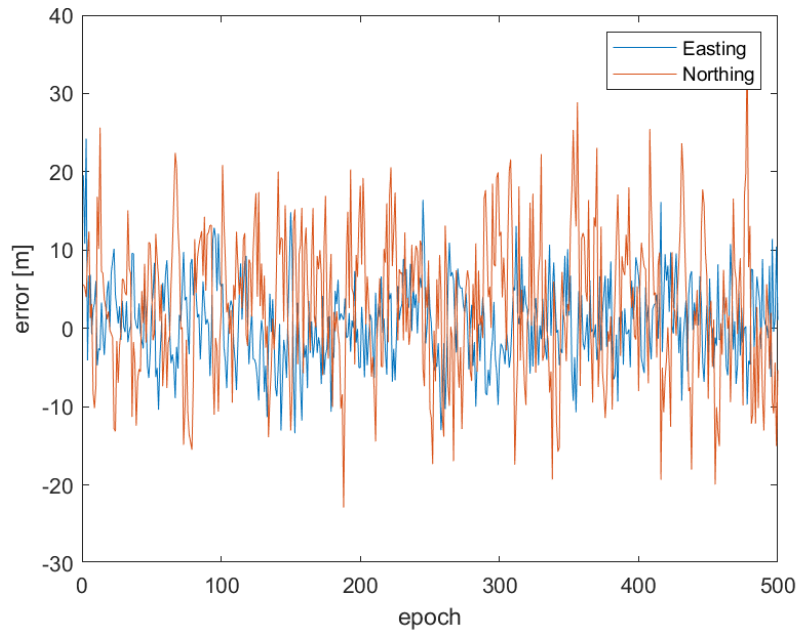
*Figure 5.79: Horizontal errors of static for each epoch on Point 1 with respect to reference. (RinexOn data obtained on June 11th, 2019).*
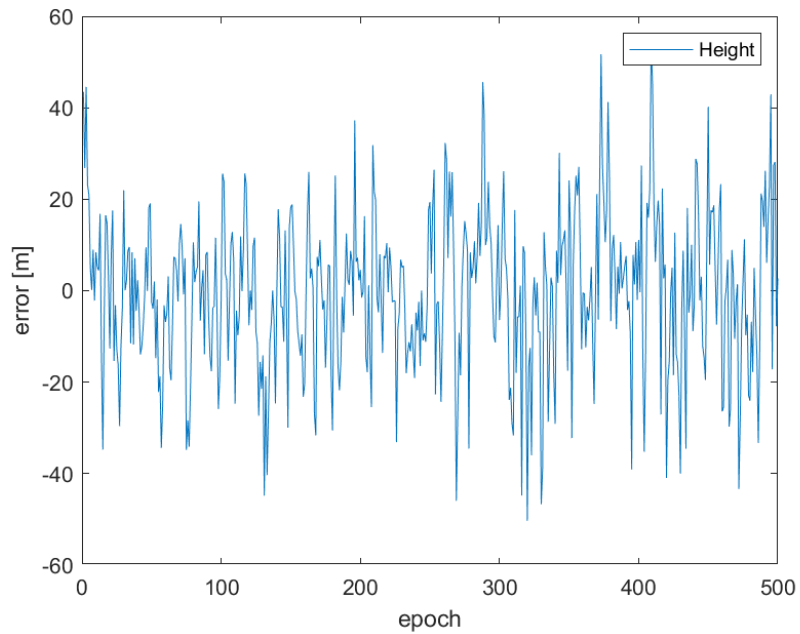


*Figure 5.80: Vertical errors of static for each epoch on Point 1 with respect to reference. (RinexOn data obtained on June 11th, 2019).*
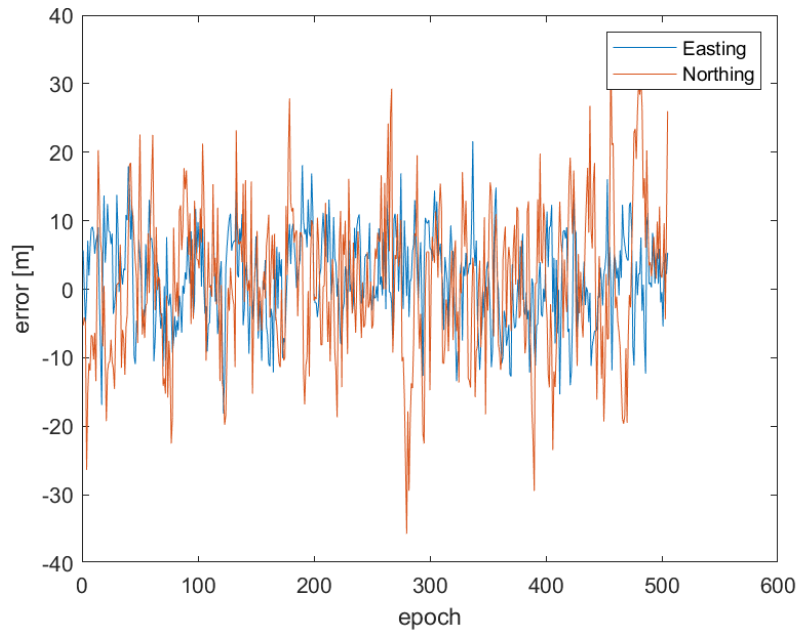
*Figure 5.81: Horizontal errors of static for each epoch on Point 2 with respect to reference. (RinexOn data obtained on June 11th, 2019).*
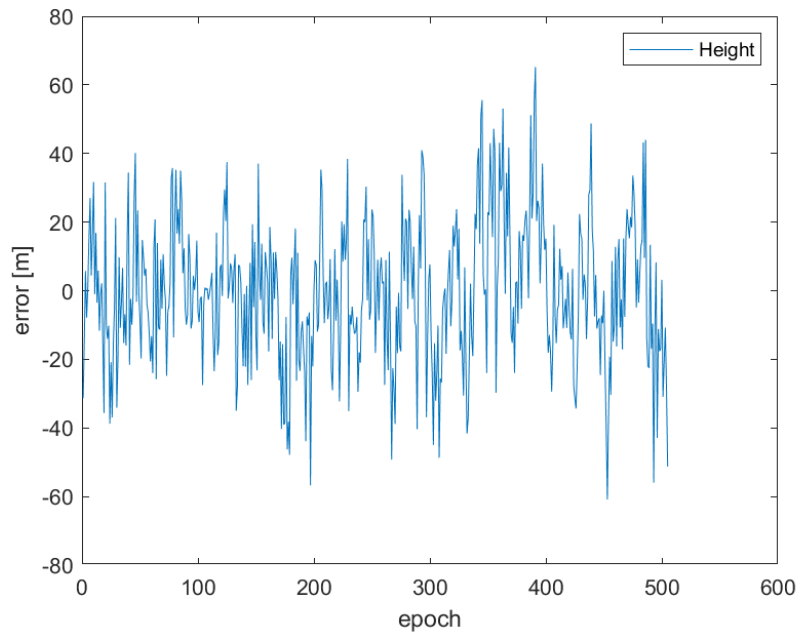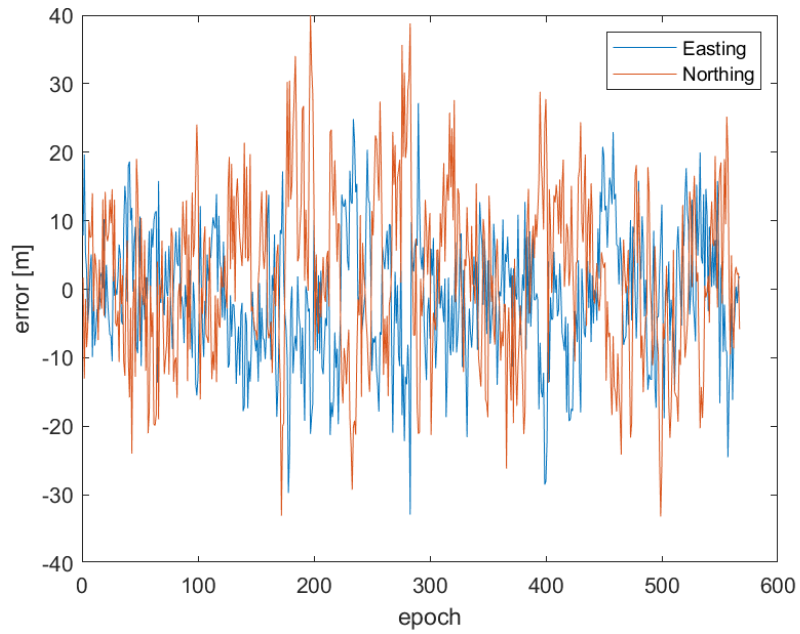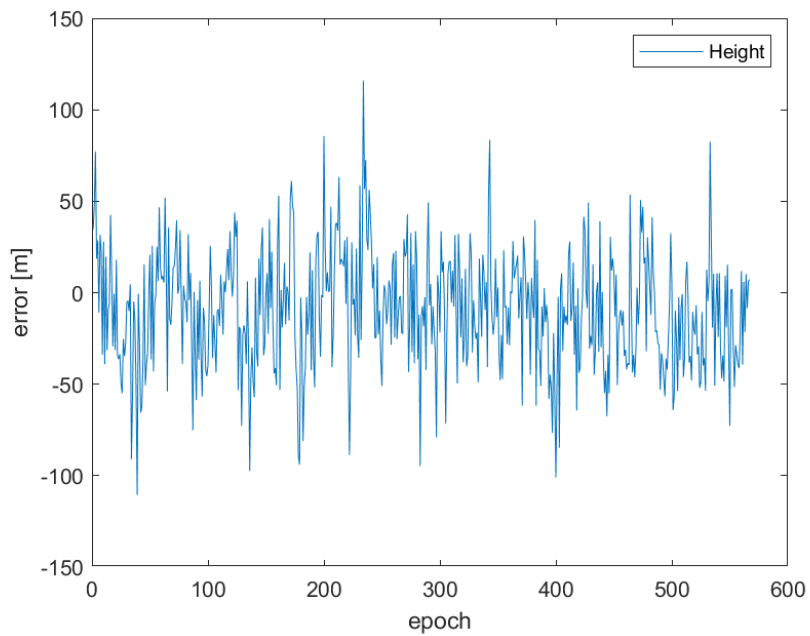


*Figure 5.82: Vertical errors of static for each epoch on Point 2 with respect to reference. (RinexOn data obtained on June 11th, 2019).*

*Figure 5.83: Horizontal errors of static for each epoch on Point 3 with respect to reference. (RinexOn data obtained on June 11th, 2019).*



*Figure 5.84: Vertical errors of static for each epoch on Point 3 with respect to reference. (RinexOn data obtained on June 11th, 2019).*
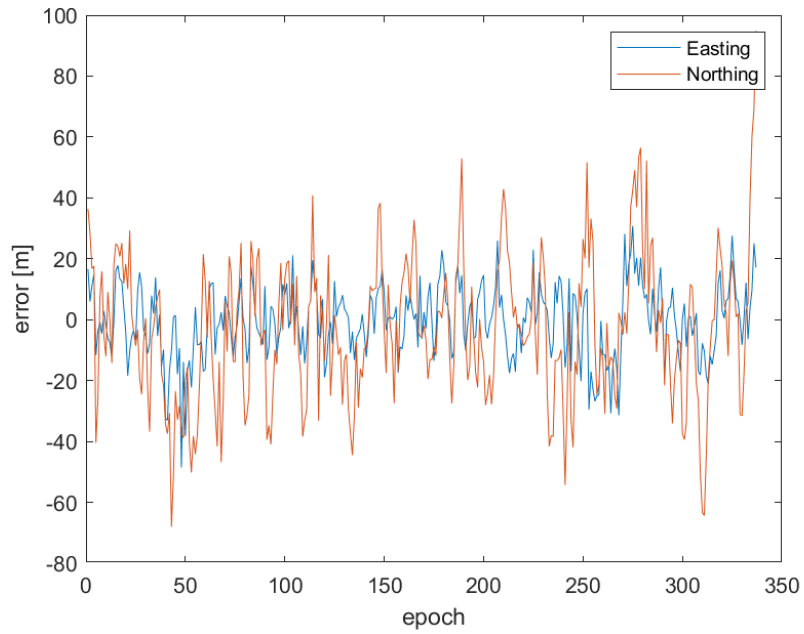
*Figure 5.85: Horizontal errors of static for each epoch on Point 4 with respect to reference. (RinexOn data obtained on June 11th, 2019).*
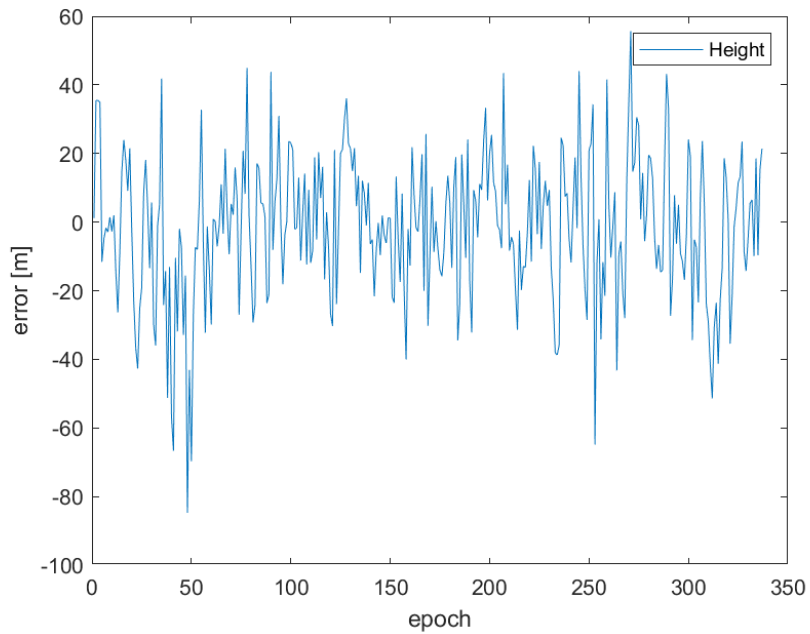


*Figure 5.86: Vertical errors of static for each epoch on Point 4 with respect to reference. (RinexOn data obtained on June 11th, 2019).*
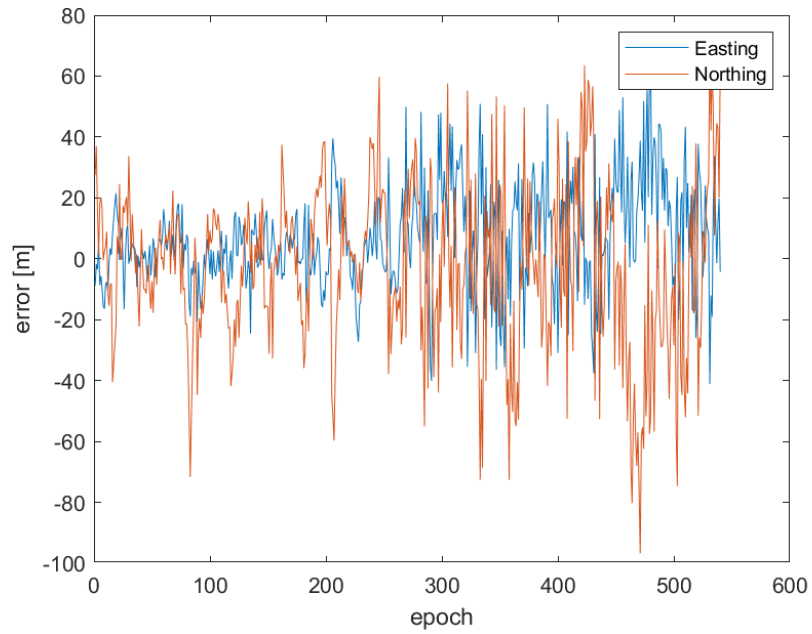
*Figure 5.87: Horizontal errors of static for each epoch on Point 5 with respect to reference. (RinexOn obtained on June 11th, 2019).*
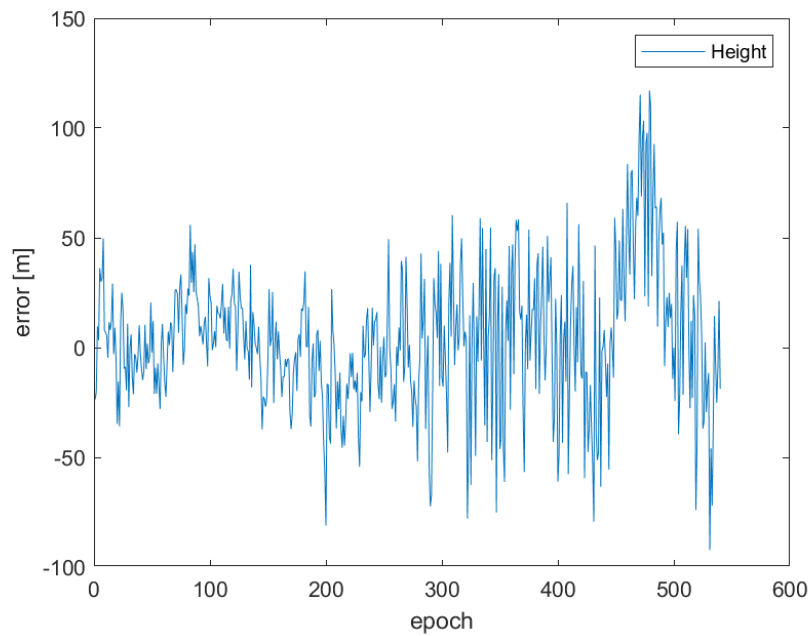


*Figure 5.88: Vertical errors of static for each epoch on Point 5 with respect to reference. (RinexOn data obtained on June 11th, 2019).*

*Figure 5.89: Horizontal errors of static for each epoch on Point 6 with respect to reference. (RinexOn data obtained on June 11th, 2019).*



*Figure 5.90: Vertical errors of static for each epoch on Point 6 with respect to reference. (RinexOn data obtained on June 11th, 2019).*
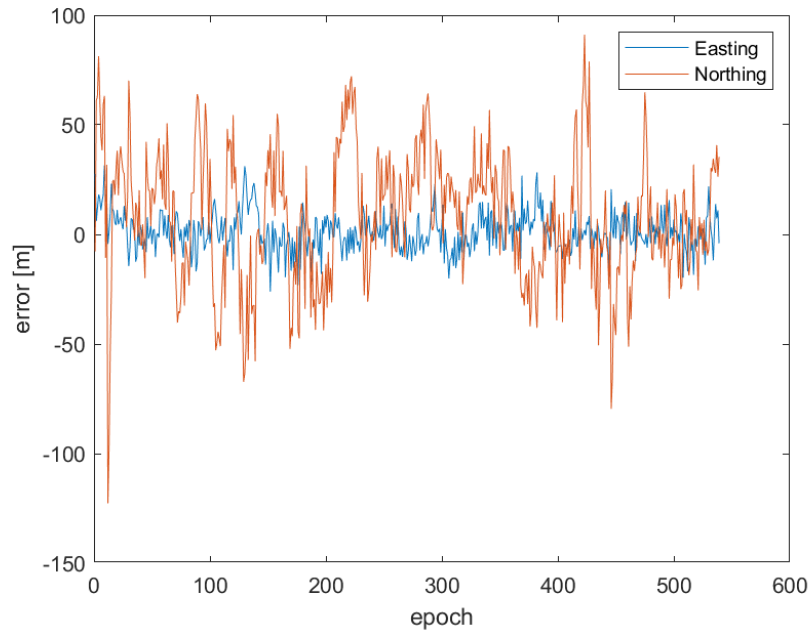
*Figure 5.91: Horizontal errors of static for each epoch on Point 7 with respect to reference. (RinexOn data obtained on June 11th, 2019).*
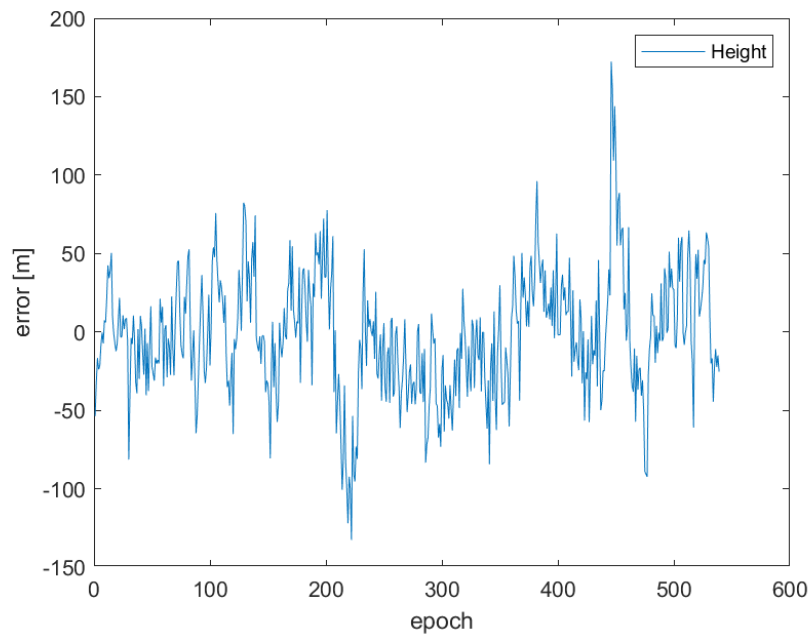


*Figure 5.92: Vertical errors of static for each epoch on Point 7 with respect to reference. (RinexOn data obtained on June 11th, 2019).*
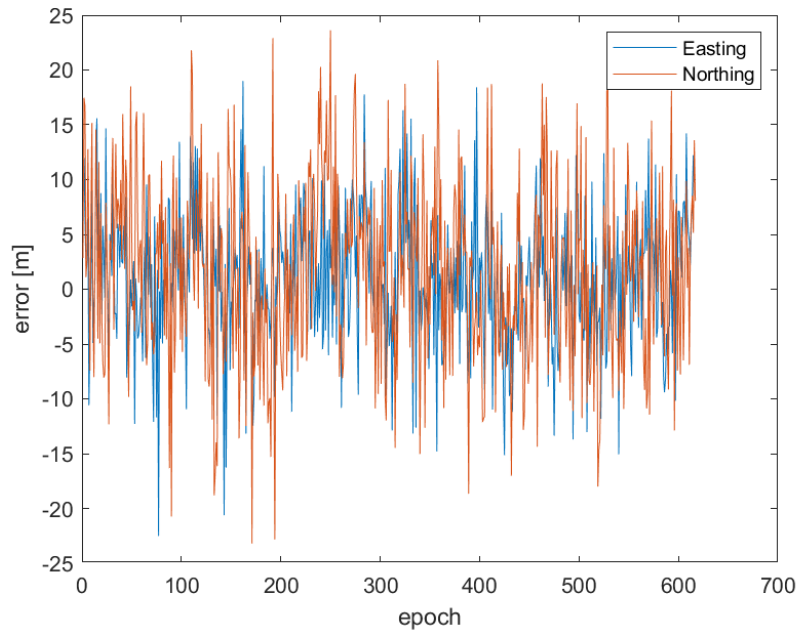
170

*Figure 5.93: Horizontal errors of static for each epoch on Point 8 with respect to reference. (RinexOn data obtained on June 11th, 2019).*
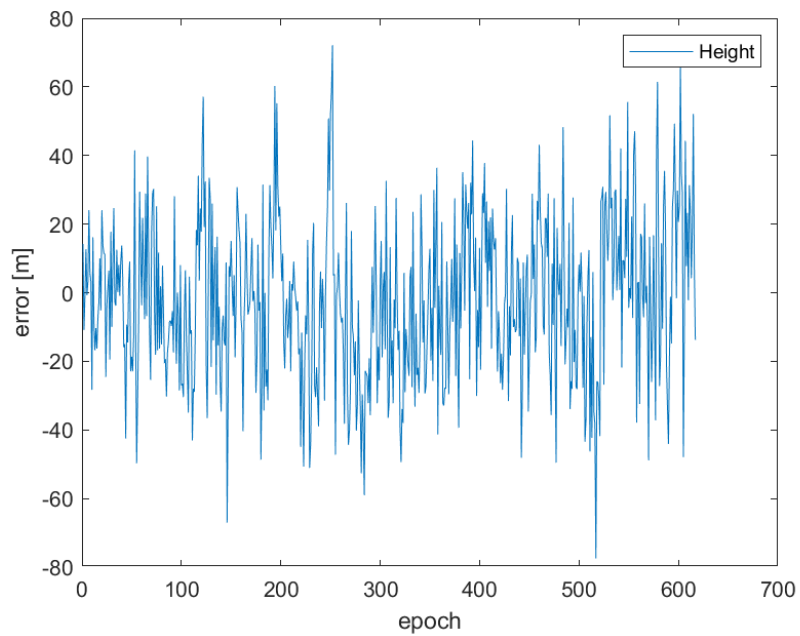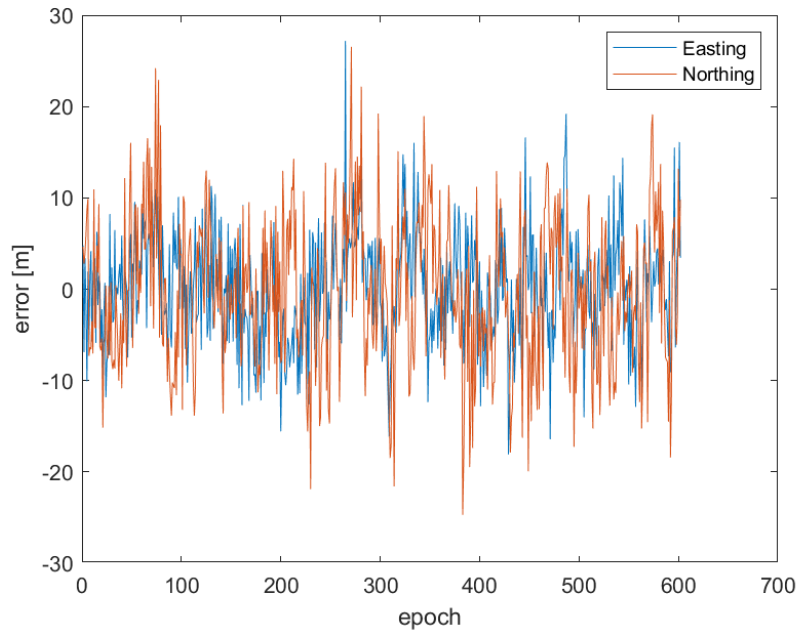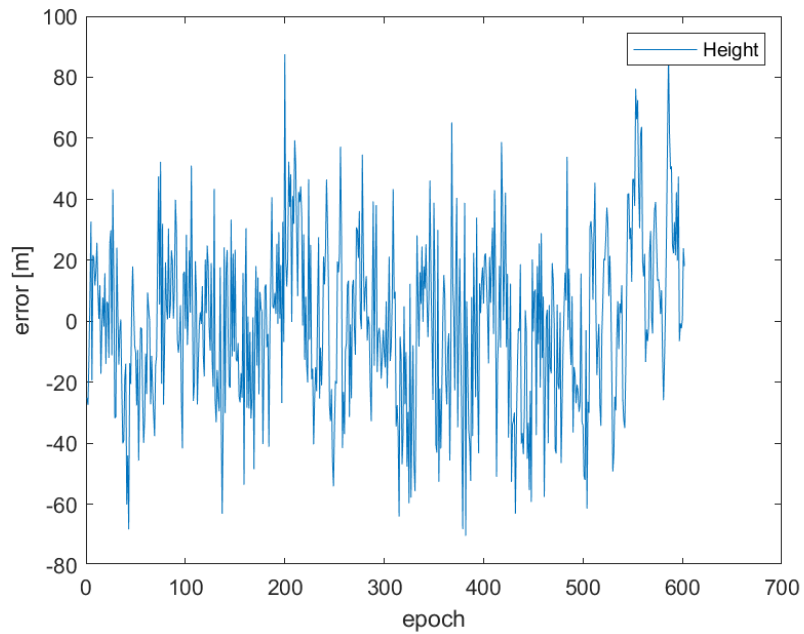


*Figure 5.94: Vertical errors of static for each epoch on Point 8 with respect to reference. (RinexOn data obtained on June 11th, 2019).*

*Table 5.28: Averaged the single point positions by RinexOn as a final results.*

| Point ID | East [m] | North [m] | Height [m] | ΔE [m] | ΔN [m] | ΔH [m] |
|----------|----------|-----------|------------|--------|--------|--------|
| | **RinexON** | | | | | |
| 1 | 517551.966 | 5036087.142 | 159.757 | 0.691 | 3.007 | -0.410 |
| 2 | 517552.884 | 5036090.537 | 159.716 | 1.545 | 0.957 | -0.488 |
| 3 | 517550.247 | 5036095.433 | 150.654 | -1.176 | 1.725 | -9.560 |
| 4 | 517550.885 | 5036095.699 | 158.511 | -0.609 | -3.462 | -1.675 |
| 5 | 517550.037 | 5036096.263 | 163.919 | 6.805 | -3.007 | 3.718 |
| 6 | 517534.192 | 5036105.456 | 157.795 | 1.293 | 7.771 | -2.399 |
| 7 | 517533.640 | 5036087.776 | 157.981 | 0.925 | 1.664 | -2.218 |
| 8 | 517543.067 | 5036083.842 | 159.398 | 0.077 | -0.406 | -0.783 |
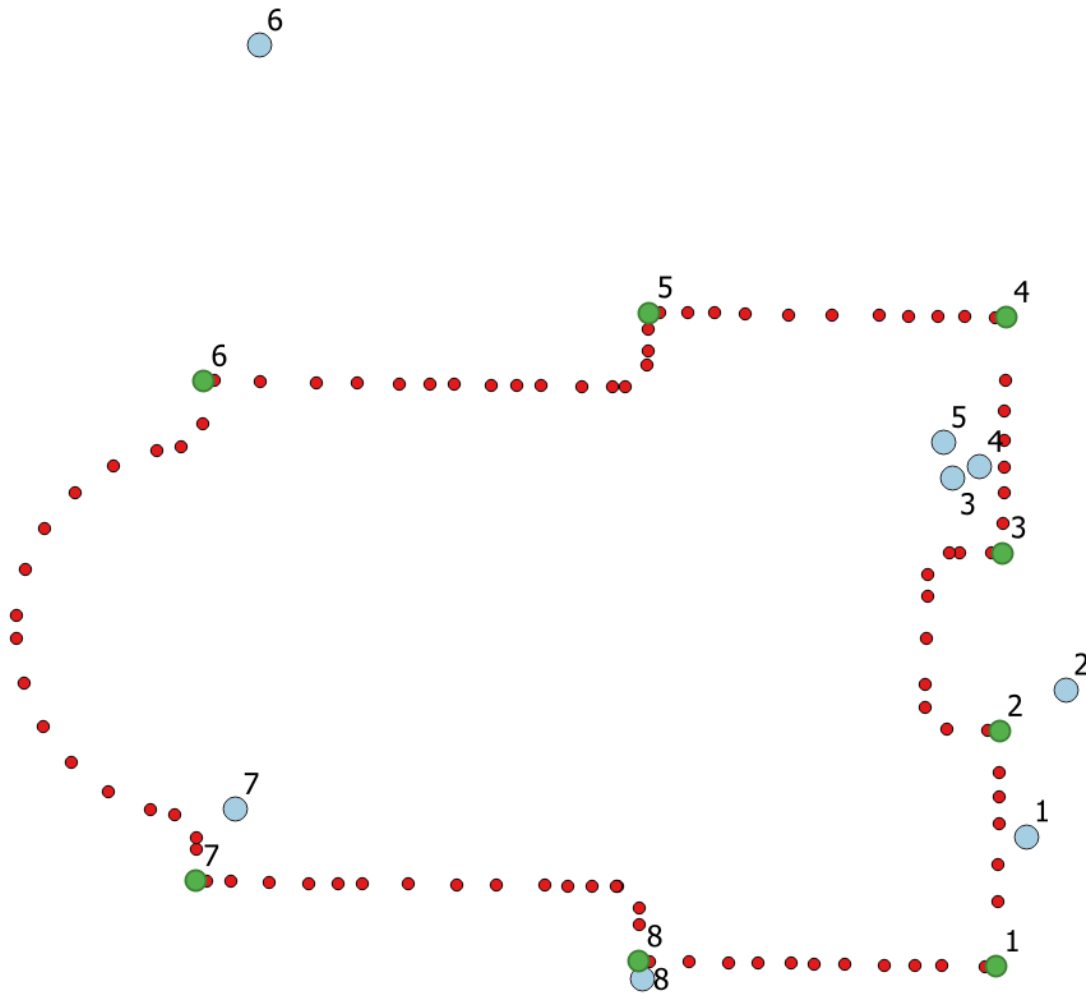


*Figure 5.95: Final results of the single point positioning in blue (RinexOn). Reference in green.*

The final results for single point positioning are presented on Table 5.28. The statistics are presented in Table 5.29.

*Table 5.29: Statistics of the results for single point positioning by RinexOn.*

| Statistics | East [m] | North [m] | Height [m] |
|---|---|---|---|
| Min [m] | -1.176 | -3.462 | -9.560 |
| Max [m] | 6.805 | 7.771 | 3.718 |
| Mean [m] | 1.194 | 1.031 | -1.727 |
| Median [m] | 0.808 | 1.311 | -1.229 |
| STD [m] | 2.451 | 3.561 | 3.701 |
| RMS [m] | 2.585 | 3.487 | 3.868 |

## *5.4.2.2 DGPS for RinexOn*

By using DGPS mode, 600 positions are computed for each 10 minutes session. Obtained files from RTKLIB represents the coordinates in units of geographic coordinate system (latitude, longitude and height). These coordinates are converted to ETRF UTM-32N coordinates (east, north and height) by using QGIS that was done in the previous experiment.

The results obtained for each point are shown epoch by epoch in Figure 5.96 and Figure 5.97. Statistics of DGPS results are calculated by MATLAB code and presented in Table 5.30. All related statistical error graphs are presented Figure 5.98 - Figure 5.113 respectively. Final results for each point are calculated by averaging all epochs and presented in Figure 5.114.
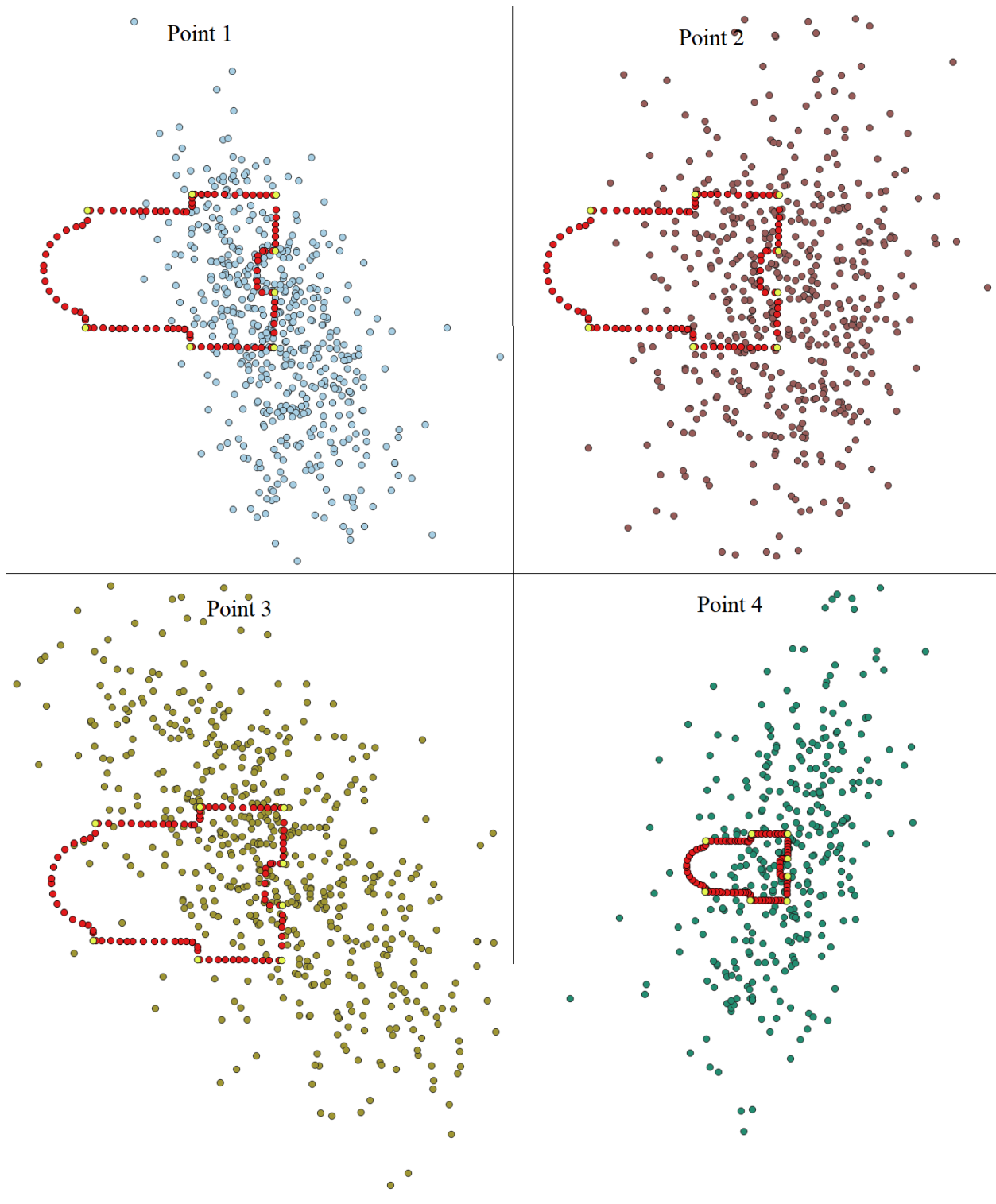
*Figure 5.96: Example of DGPS mode results (Point 1, Point 2, Point 3 and Point 4) (RinexOn data collected on June 11th, 2019).*
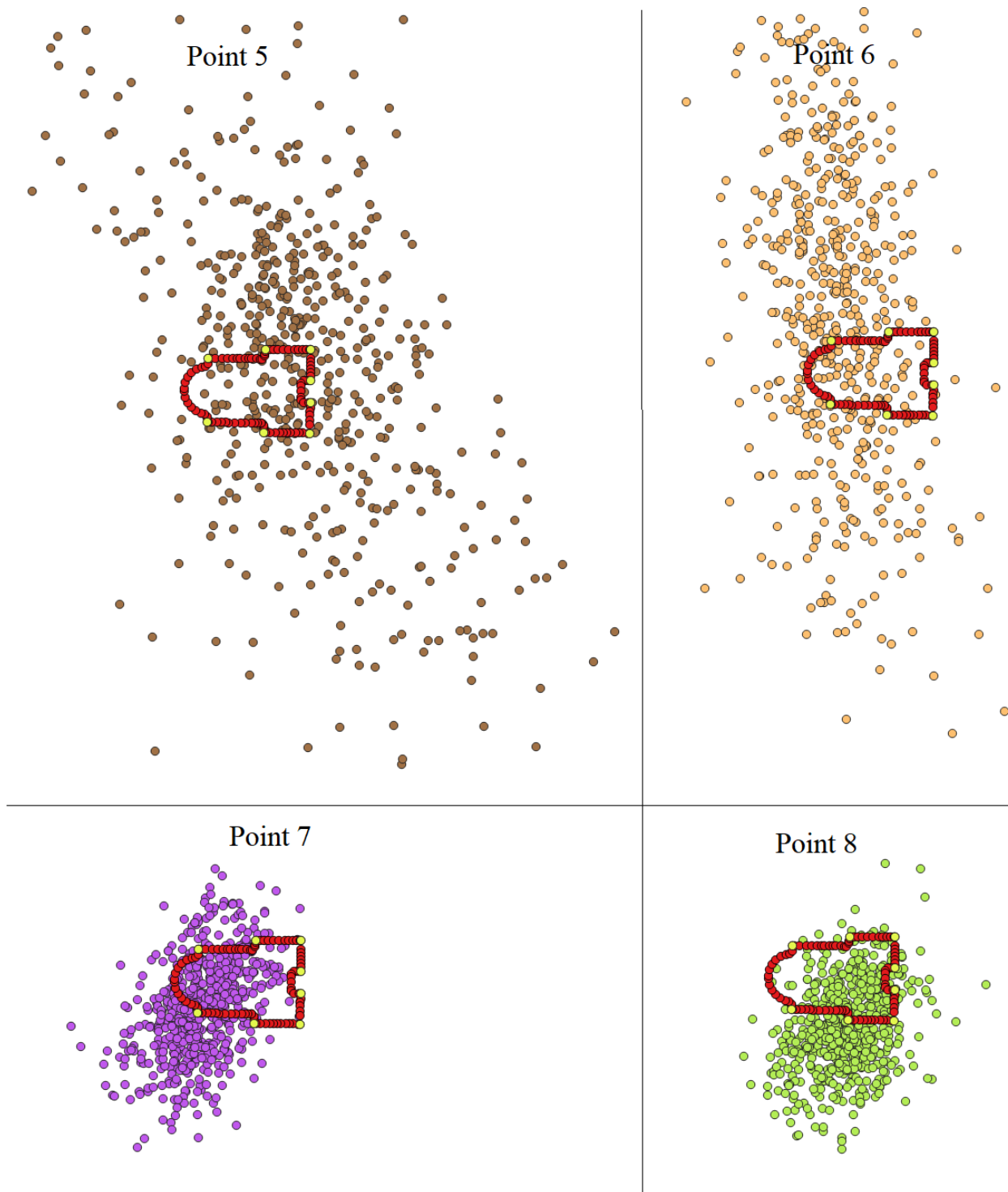
*Figure 5.97: Example of DGPS mode results (Point 5, Point 6, Point 7 and Point 8) (RinexOn data collected on June 11th, 2019).*

*Table 5.30: Statistics of DGPS (RinexOn data collected on June 11th, 2019).*

| Point ID | | East [m] | North [m] | Height [m] | ΔE [m] | ΔN [m] | ΔH [m] |
|---|---|---|---|---|---|---|---|
| Point 1 | MIN | 517537.520 | 5036063.133 | 111.552 | -13.755 | -21.002 | -48.615 |
| | MAX | 517573.557 | 5036116.229 | 216.323 | 22.283 | 32.093 | 56.155 |
| | Mean | 517551.662 | 5036085.783 | 160.217 | 0.388 | 1.647 | 0.050 |
| | Median | 517551.566 | 5036086.274 | 160.827 | 0.292 | 2.138 | 0.660 |
| | STD | 5.275 | 9.152 | 17.006 | 5.284 | 9.290 | 16.989 |
| Point 2 | MIN | 517532.692 | 5036050.183 | 105.911 | -18.648 | -39.397 | -54.293 |
| | MAX | 517572.077 | 5036121.715 | 224.705 | 20.737 | 32.134 | 64.501 |
| | Mean | 517551.929 | 5036089.028 | 162.470 | 0.590 | -0.552 | 2.266 |
| | Median | 517552.035 | 5036088.974 | 161.710 | 0.695 | -0.606 | 1.506 |
| | STD | 6.622 | 10.968 | 20.267 | 6.642 | 10.971 | 20.374 |
| Point 3 | MIN | 517515.549 | 5036061.989 | 53.389 | -35.874 | -31.719 | -106.825 |
| | MAX | 517581.026 | 5036131.201 | 278.656 | 29.602 | 37.493 | 118.442 |
| | Mean | 517550.295 | 5036094.719 | 155.076 | -1.128 | 1.012 | -5.138 |
| | Median | 517549.952 | 5036094.631 | 156.185 | -1.471 | 0.924 | -4.030 |
| | STD | 10.040 | 11.640 | 32.096 | 10.094 | 11.674 | 32.477 |
| Point 4 | MIN | 517502.253 | 5036032.043 | 79.393 | -49.240 | -67.119 | -80.793 |
| | MAX | 517582.617 | 5036192.792 | 218.158 | 31.123 | 93.630 | 57.972 |
| | Mean | 517551.014 | 5036095.744 | 160.721 | -0.480 | -3.418 | 0.535 |
| | Median | 517551.797 | 5036095.001 | 161.722 | 0.303 | -4.161 | 1.536 |
| | STD | 11.741 | 23.863 | 20.838 | 11.733 | 24.071 | 20.813 |
| Point 5 | MIN | 517500.245 | 5036002.876 | 68.007 | -42.986 | -96.393 | -92.194 |
| | MAX | 517606.336 | 5036170.946 | 276.525 | 63.104 | 71.676 | 116.324 |
| | Mean | 517549.462 | 5036096.279 | 164.397 | 6.231 | -2.991 | 4.196 |
| | Median | 517548.473 | 5036098.176 | 163.122 | 5.241 | -1.093 | 2.921 |
| | STD | 16.698 | 26.759 | 32.369 | 17.808 | 26.901 | 32.610 |
| Point 6 | MIN | 517506.797 | 5035976.366 | 33.059 | -26.102 | -121.319 | -127.135 |
| | MAX | 517564.108 | 5036186.360 | 332.797 | 31.209 | 88.675 | 172.602 |
| | Mean | 517534.079 | 5036103.823 | 160.395 | 1.180 | 6.138 | 0.201 |
| | Median | 517533.787 | 5036103.793 | 159.644 | 0.889 | 6.108 | -0.550 |
| | STD | 8.696 | 29.740 | 38.971 | 8.768 | 30.339 | 38.935 |
| Point 7 | MIN | 517509.910 | 5036061.891 | 72.413 | -22.804 | -24.221 | -87.786 |
| | MAX | 517551.308 | 5036112.167 | 235.130 | 18.594 | 26.055 | 74.931 |
| | Mean | 517533.578 | 5036087.209 | 158.335 | 0.864 | 1.097 | -1.864 |
| | Median | 517533.247 | 5036087.368 | 157.041 | 0.532 | 1.256 | -3.159 |
| | STD | 6.399 | 8.910 | 24.821 | 6.451 | 8.970 | 24.871 |
| Point 8 | MIN | 517524.135 | 5036060.881 | 83.922 | -18.855 | -23.367 | -76.259 |
| | MAX | 517567.896 | 5036112.515 | 241.073 | 24.907 | 28.268 | 80.892 |
| | Mean | 517542.731 | 5036082.948 | 159.055 | -0.259 | -1.300 | -1.126 |
| | Median | 517543.002 | 5036082.531 | 159.429 | 0.012 | -1.716 | -0.752 |
| | STD | 6.156 | 8.047 | 27.190 | 6.156 | 8.145 | 27.191 |
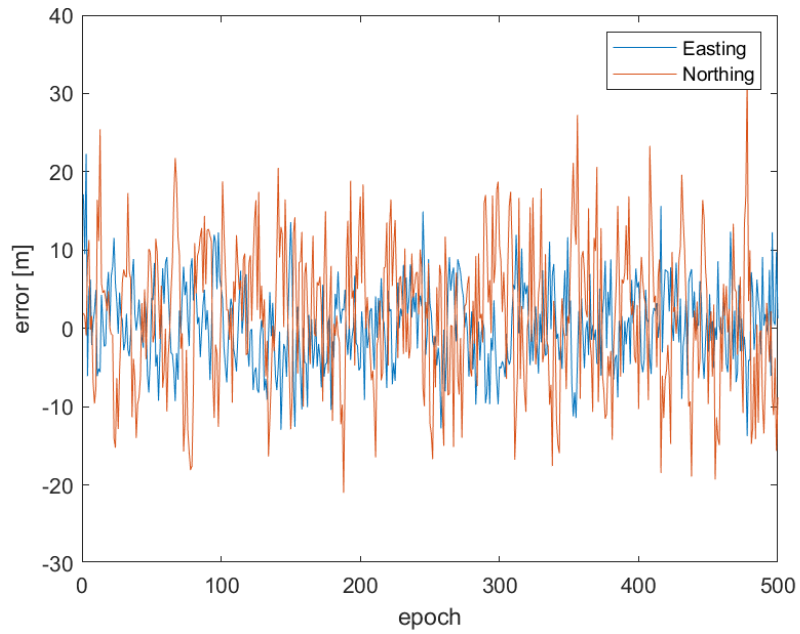
*Figure 5.98: Horizontal errors of DGPS for each epoch on Point 1 with respect to reference. (RinexOn obtained on June 11th, 2019).*
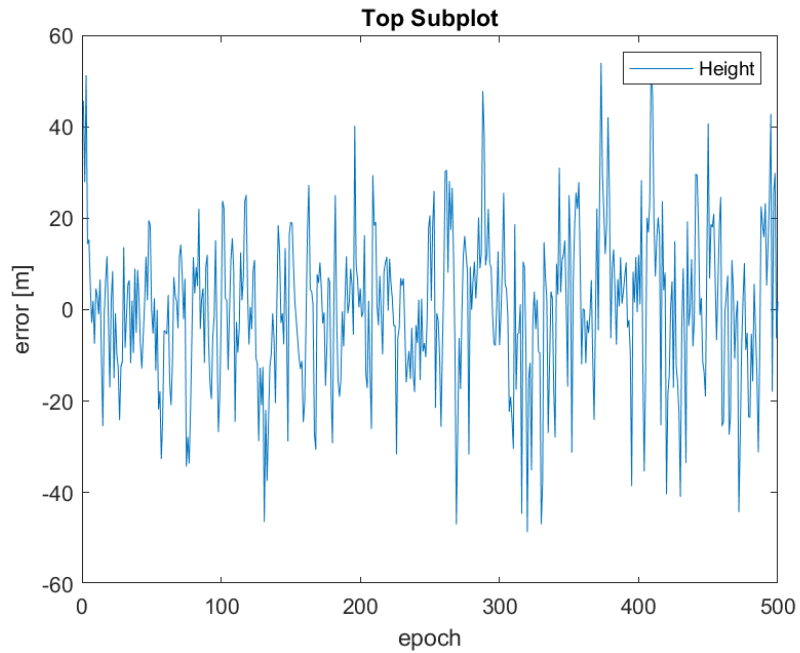


*Figure 5.99: Vertical errors of DGPS for each epoch on Point 1 with respect to reference. (RinexOn obtained on June 11th, 2019).*
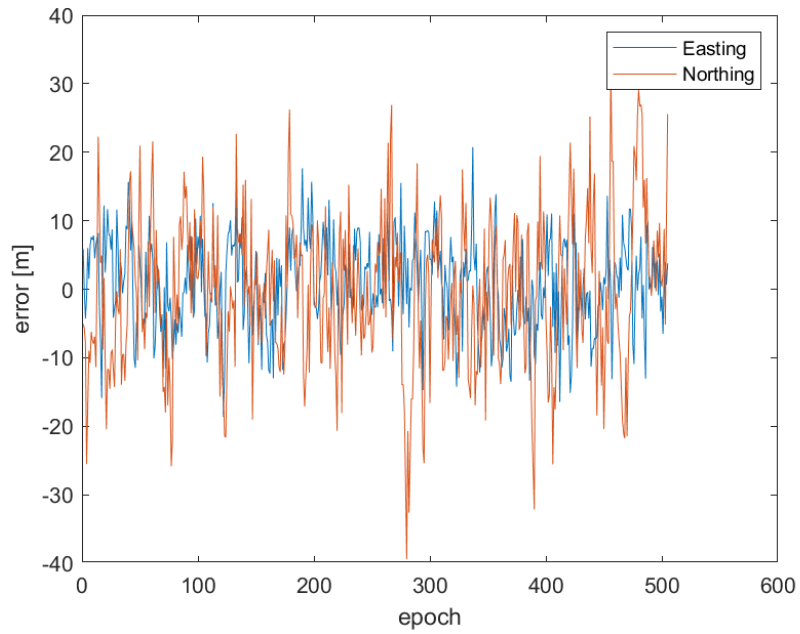
*Figure 5.100: Horizontal errors of DGPS for each epoch on Point 2 with respect to reference. (RinexOn obtained on June 11th, 2019).*
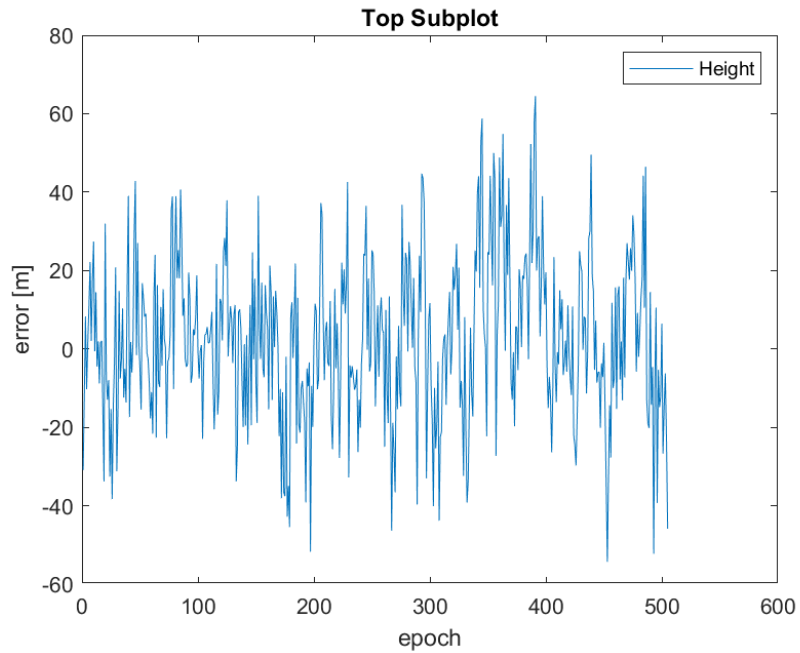


*Figure 5.101: Vertical errors of DGPS for each epoch on Point 2 with respect to reference. (RinexOn obtained on June 11th, 2019).*

*Figure 5.102: Horizontal errors of DGPS for each epoch on Point 3 with respect to reference. (RinexOn obtained on June 11th, 2019).*



*Figure 5.103: Vertical errors of DGPS for each epoch on Point 3 with respect to reference. (RinexOn obtained on June 11th, 2019).*
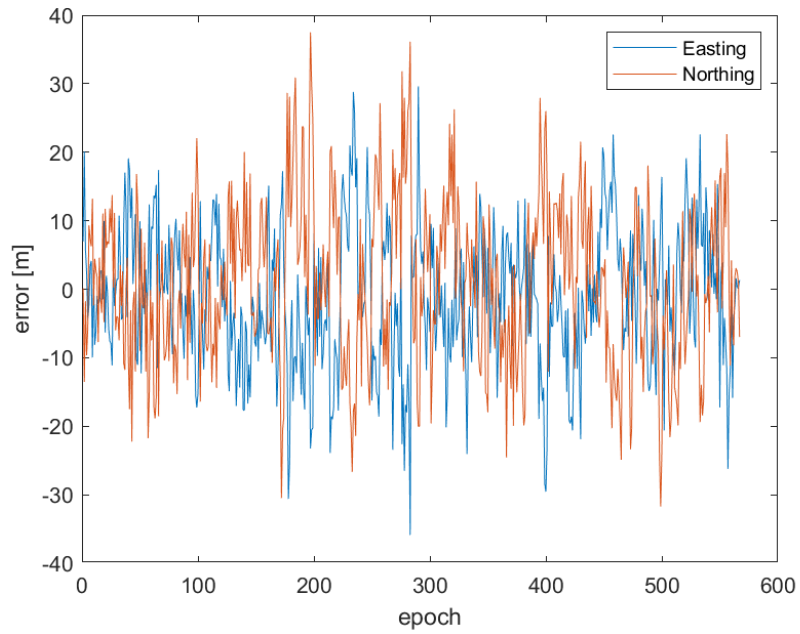
*Figure 5.104: Horizontal errors of DGPS for each epoch on Point 4 with respect to reference. (RinexOn obtained on June 11th, 2019).*



*Figure 5.105: Vertical errors of DGPS for each epoch on Point 4 with respect to reference. (RinexOn obtained on June 11th, 2019).*

*Figure 5.106: Horizontal errors of DGPS for each epoch on Point 5 with respect to reference. (RinexOn obtained on June 11th, 2019).*
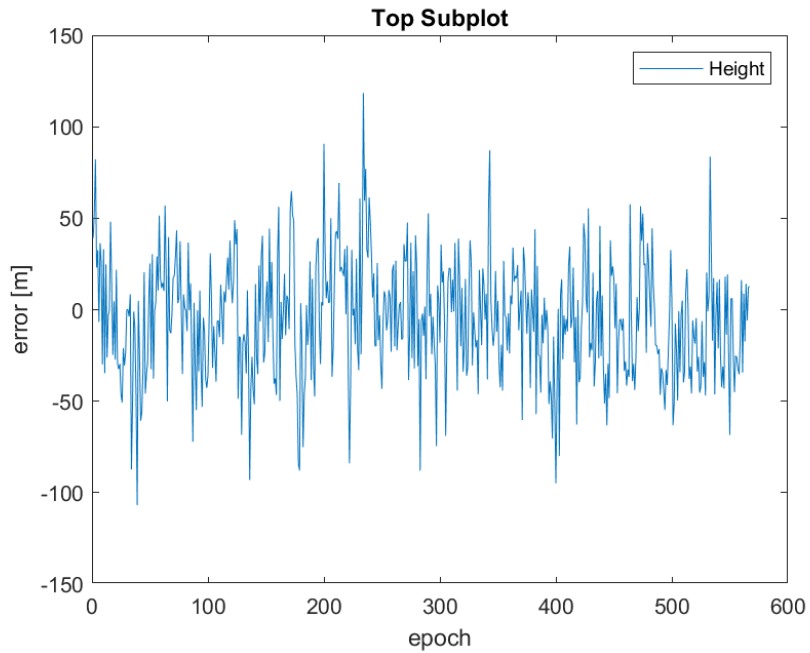


*Figure 5.107: Vertical errors of DGPS for each epoch on Point 5 with respect to reference. (RinexOn obtained on June 11th, 2019).*
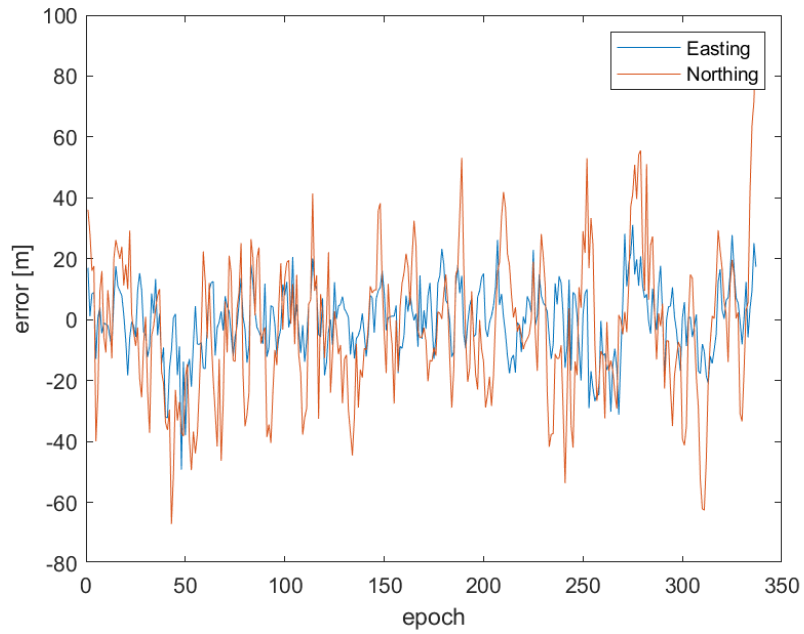
181
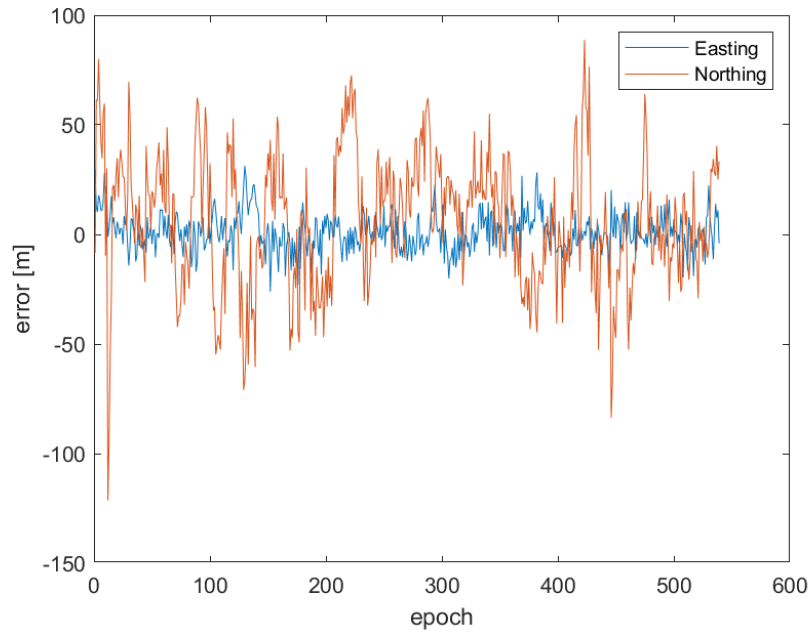
*Figure 5.108: Horizontal errors of DGPS for each epoch on Point 6 with respect to reference. (RinexOn obtained on June 11th, 2019).*
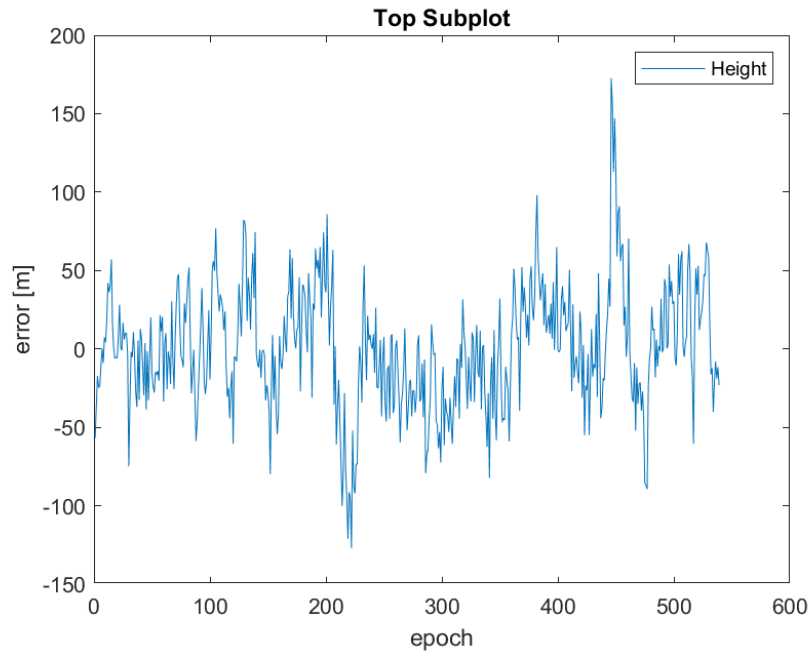


*Figure 5.109: Vertical errors of DGPS for each epoch on Point 6 with respect to reference. (RinexOn obtained on June 11th, 2019).*

*Figure 5.110: Horizontal errors of DGPS for each epoch on Point 7 with respect to reference. (RinexOn obtained on June 11th, 2019).*
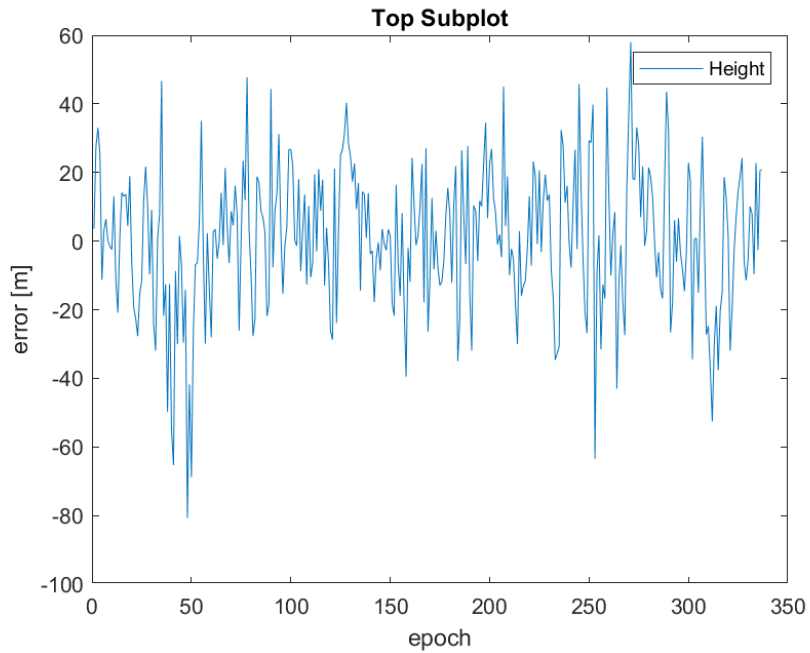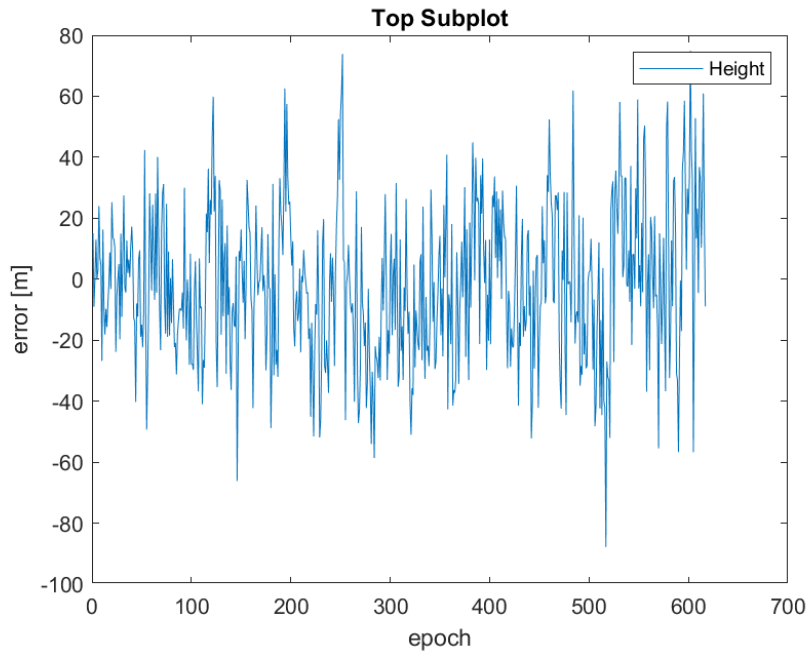


*Figure 5.111: Vertical errors of DGPS for each epoch on Point 7 with respect to reference. (RinexOn obtained on June 11th, 2019).*
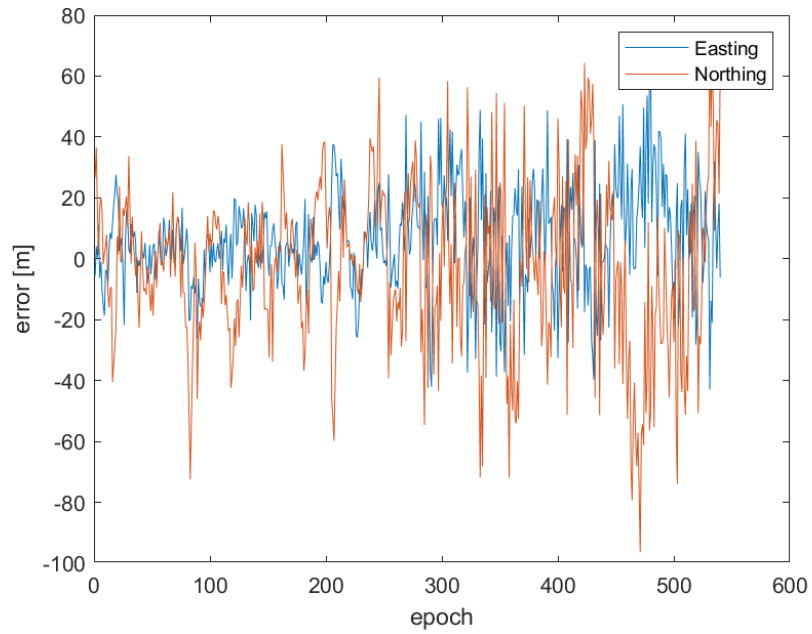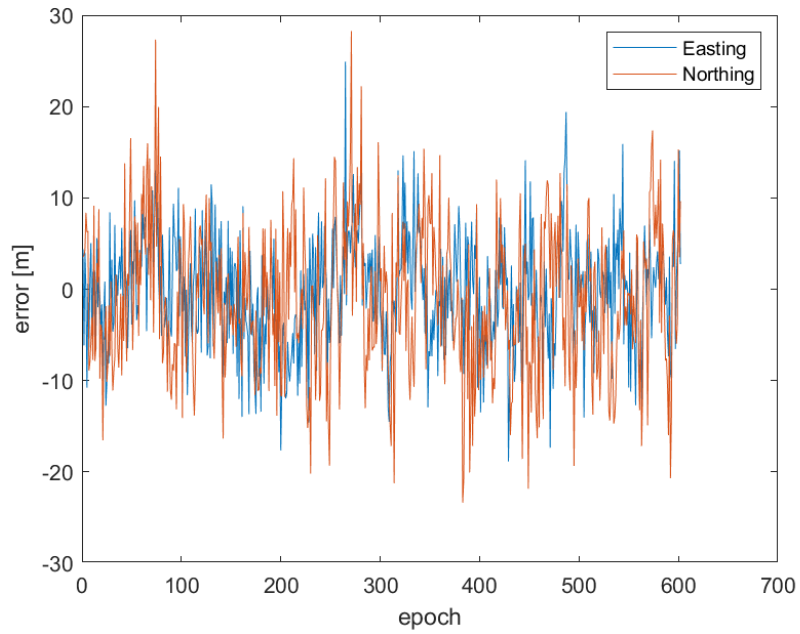
*Figure 5.112: Horizontal errors of DGPS for each epoch on Point 8 with respect to reference. (RinexOn obtained on June 11th, 2019).*
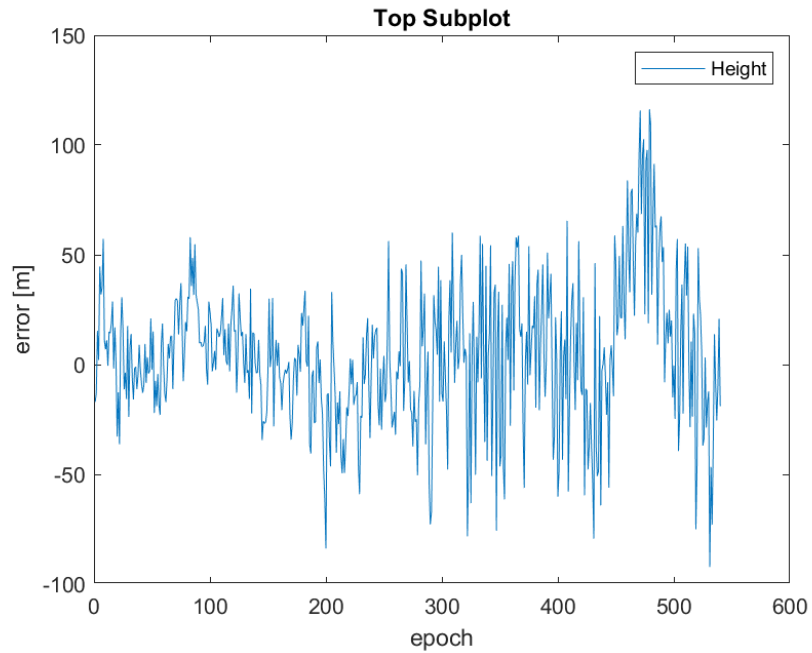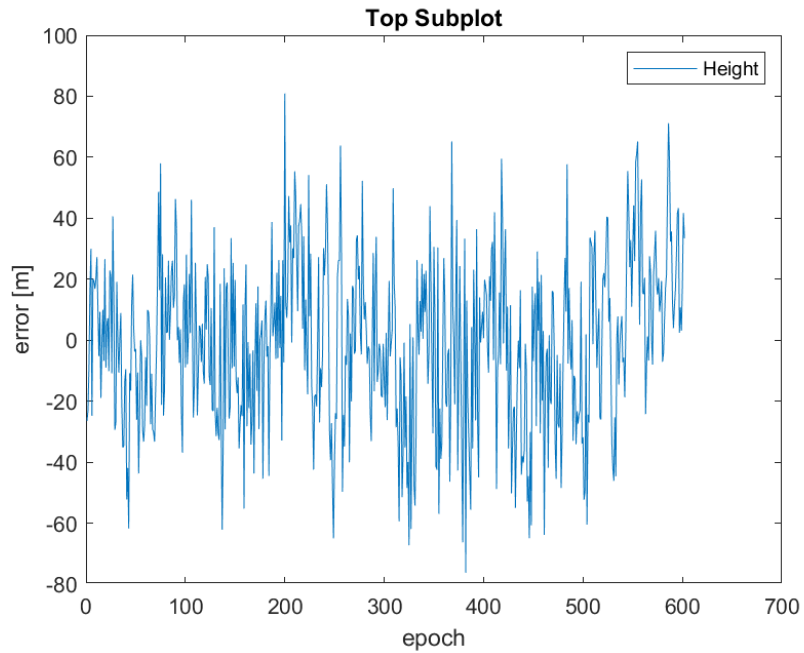


*Figure 5.113: Vertical errors of DGPS for each epoch on Point 8 with respect to reference. (RinexOn obtained on June 11th, 2019).*
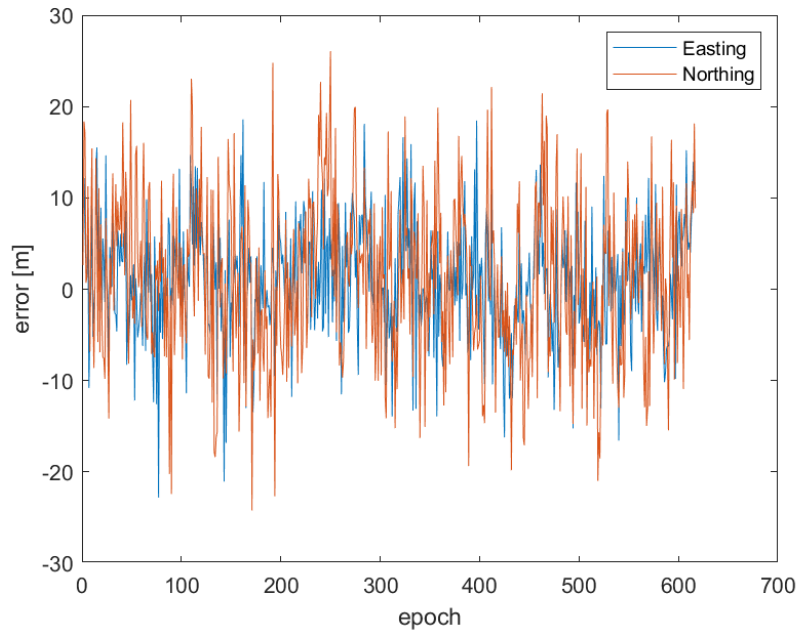
*Table 5.31: Averaged the DGPS results by RinexOn as a final results.*

| Point ID | RinexON | | | | | |
|---|---|---|---|---|---|---|
| | East [m] | North [m] | Height [m] | ΔE [m] | ΔN [m] | ΔH [m] |
| 1 | 517551.662 | 5036085.783 | 160.217 | 0.388 | 1.647 | 0.050 |
| 2 | 517551.929 | 5036089.028 | 162.470 | 0.590 | -0.552 | 2.266 |
| 3 | 517550.295 | 5036094.719 | 155.076 | -1.128 | 1.012 | -5.138 |
| 4 | 517551.014 | 5036095.744 | 160.721 | -0.480 | -3.418 | 0.535 |
| 5 | 517549.462 | 5036096.279 | 164.397 | 6.231 | -2.991 | 4.196 |
| 6 | 517534.079 | 5036103.823 | 160.395 | 1.180 | 6.138 | 0.201 |
| 7 | 517533.578 | 5036087.209 | 158.335 | 0.864 | 1.097 | -1.864 |
| 8 | 517542.731 | 5036082.948 | 159.055 | -0.259 | -1.300 | -1.126 |



*Figure 5.114: Final results of DGPS by RinexOn data collected on June 11th, 2019 are in blue, reference in red are presented.*

The final results for DGPS are presented above. The statistics are presented in Table 5.32. There is slightly improvement on East 0.2 meters, on North 0.6 meters, on Height 1.2 meters.

*Table 5.32: Statistics of the results for single point positioning by RinexOn*

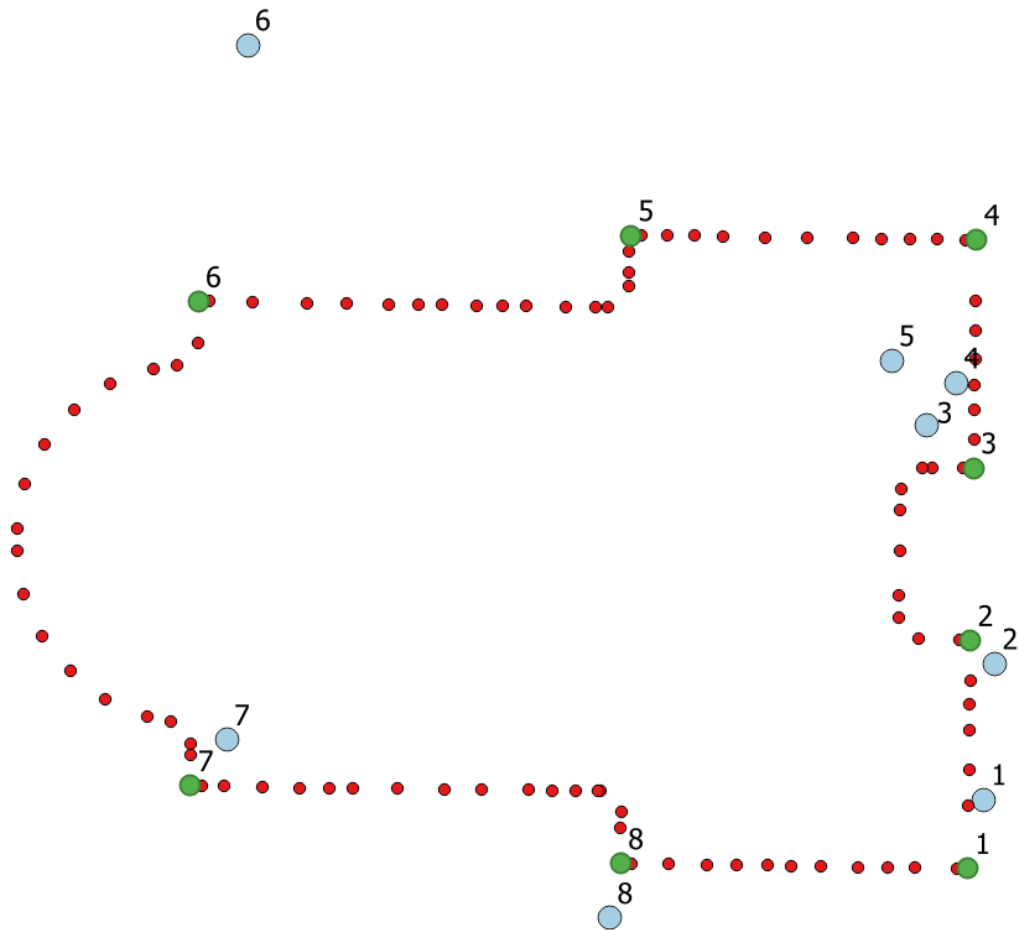| Statistics | East [m] | North [m] | Height [m] |
|---|---|---|---|
| Min [m] | -1.128 | -3.418 | -5.138 |
| Max [m] | 6.231 | 6.138 | 4.196 |
| Mean [m] | 0.923 | 0.204 | -0.110 |
| Median [m] | 0.489 | 0.230 | 0.125 |
| STD [m] | 2.274 | 3.045 | 2.780 |
| RMS [m] | 2.319 | 2.856 | 2.603 |

## 5.4.2.3 Static for RinexOn

By using static mode, 600 iterations on epochs are done for each 10 minutes session. Because RinexOn data does not have discontinuity problem in the L1 phase observations. All epoch results could been computed by RTKLIB as done for DGPS results for RinexOn.

Obtained files from RTKLIB represents the coordinates in units of geographic coordinate system (latitude, longitude and height). These coordinates are converted to ETRF UTM-32N coordinates (east, north and height) by using QGIS that was done in the previous experiment.

The results obtained for each iteration are shown epoch by epoch in Figure 5.115 and Figure 5.116. It can be easily noticed on the Figures that iterations are tightly spread for most of the points. However, Point 4 and Point 5 iteration results are going further from reference positions. Statistics of static results are calculated by MATLAB code and presented in Table 5.33 and Table 5.34. All related statistical error graphs are presented Figure 5.117 - Figure 5.124 respectively. Final results for each point are presented in Figure 5.125.
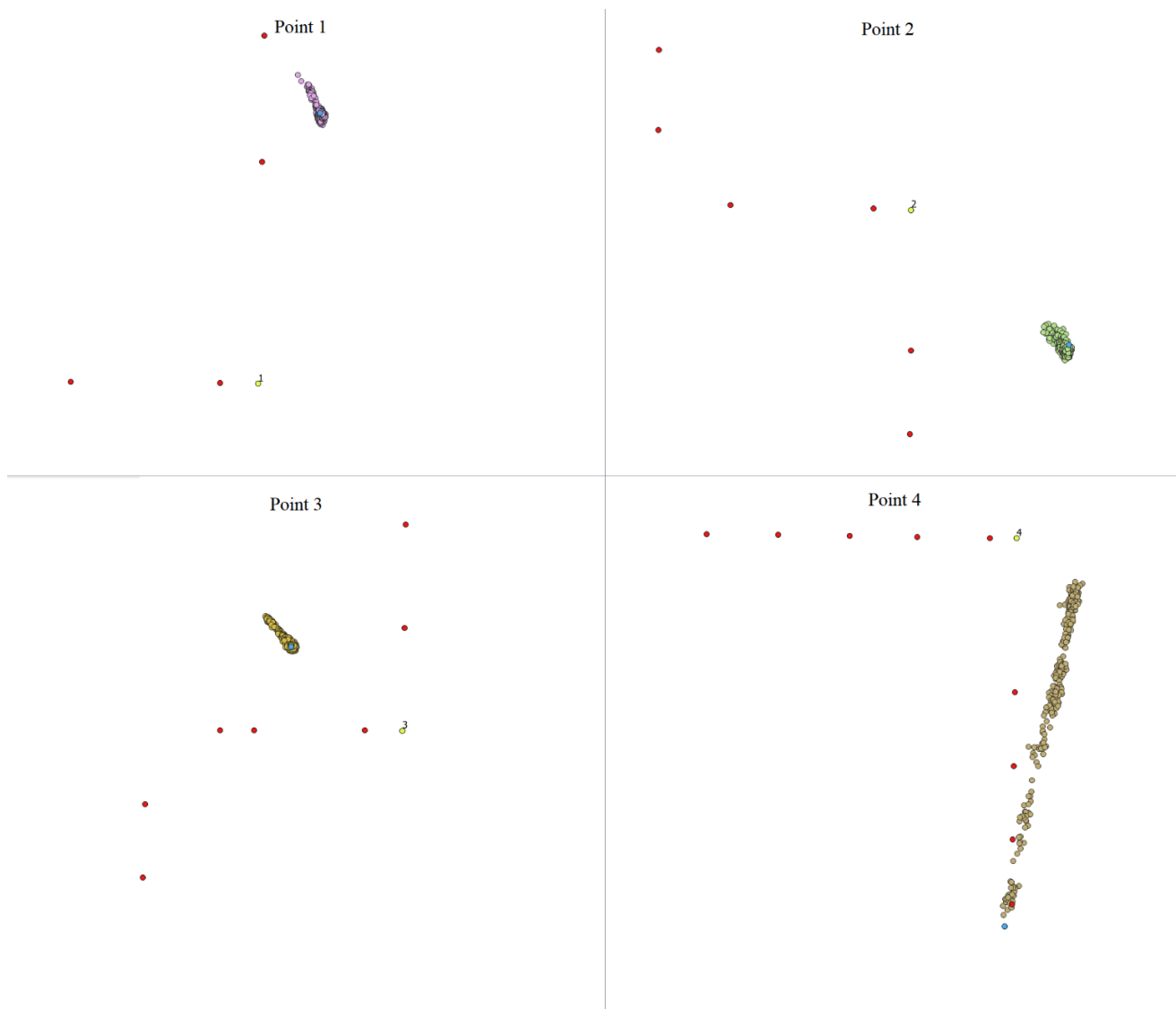
*Figure 5.115: The all results from RTKLIB for static mode (Point 1, Point 2, Point 3 and Point 4) (RinexOn data collected on June 11th, 2019).*
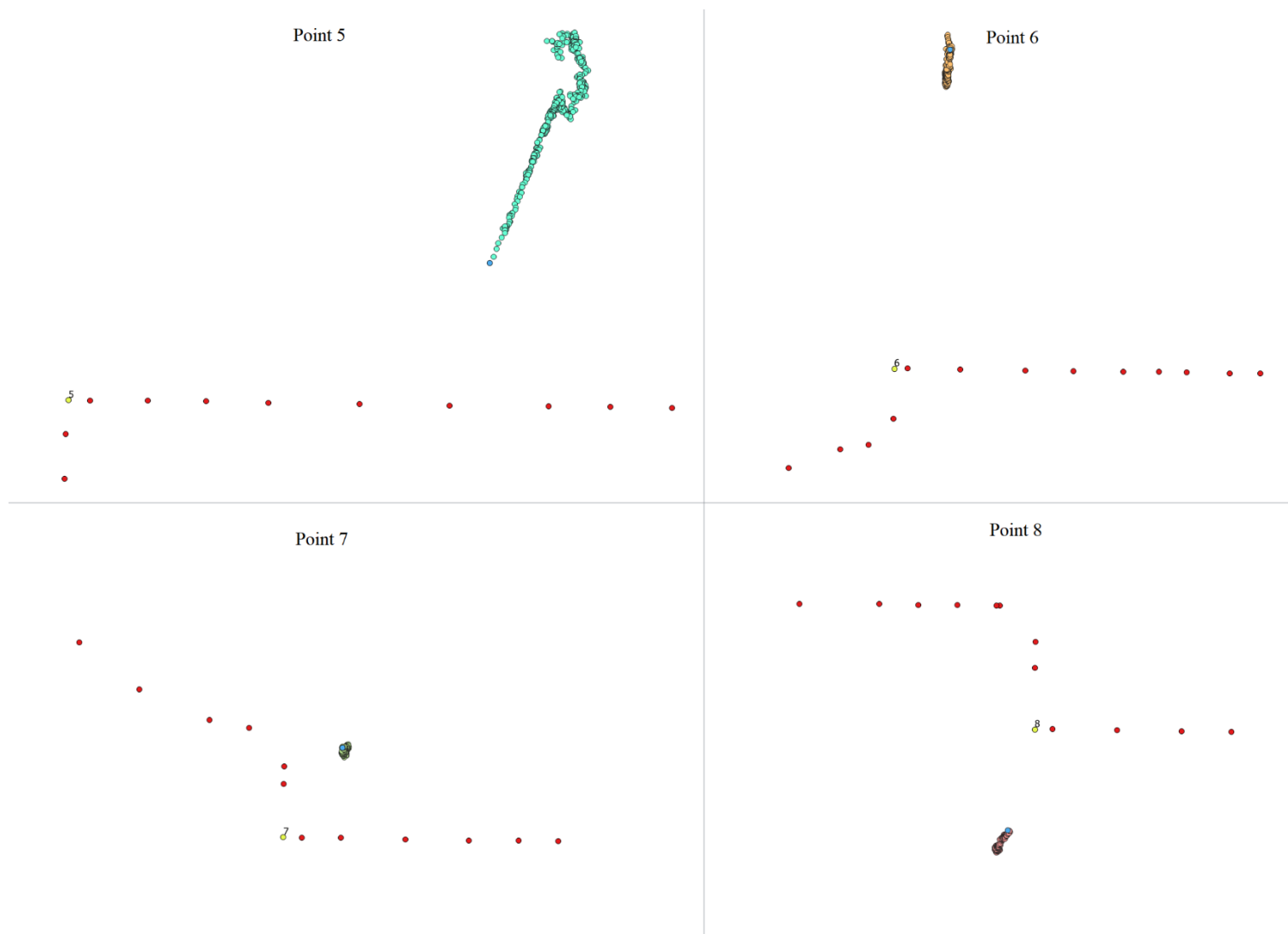
*Figure 5.116: The all results from RTKLIB for static mode (Point 5, Point 6, Point 7 and Point 8) (RinexOn data collected on June 11th, 2019).*

188

*Table 5.33: The final results of static mod for RinexOn observations.*

| Point ID | Reference | | | RinexOn | | | ΔE [m] | ΔN [m] | ΔH [m] |
|---|---|---|---|---|---|---|---|---|---|
| | East [m] | North [m] | Height [m] | East [m] | North [m] | Height [m] | | | |
| 1 | 517551.274 | 5036084.135 | 160.167 | 517551.693 | 5036085.965 | 160.194 | 0.419 | 1.830 | 0.027 |
| 2 | 517551.340 | 5036089.580 | 160.204 | 517552.405 | 5036088.666 | 161.501 | 1.065 | -0.914 | 1.297 |
| 3 | 517551.423 | 5036093.707 | 160.214 | 517550.671 | 5036094.274 | 155.559 | -0.753 | 0.567 | -4.655 |
| 4 | 517551.493 | 5036099.161 | 160.186 | 517551.379 | 5036095.468 | 161.875 | -0.114 | -3.693 | 1.689 |
| 5 | 517543.232 | 5036099.269 | 160.201 | 517547.886 | 5036100.787 | 160.275 | 4.654 | 1.518 | 0.074 |
| 6 | 517532.899 | 5036097.684 | 160.194 | 517534.001 | 5036104.020 | 158.610 | 1.102 | 6.336 | -1.584 |
| 7 | 517532.715 | 5036086.111 | 160.199 | 517533.544 | 5036087.370 | 158.070 | 0.829 | 1.259 | -2.130 |
| 8 | 517542.990 | 5036084.247 | 160.181 | 517542.611 | 5036082.824 | 159.315 | -0.379 | -1.423 | -0.866 |

*Table 5.34: Statistics of static mod solutions for RinexOn.*

| Statistics | East [m] | North [m] | Height [m] |
|---|---|---|---|
| Min [m] | -0.753 | -3.693 | -4.655 |
| Max [m] | 4.654 | 6.336 | 1.689 |
| Mean [m] | 0.853 | 0.685 | -0.769 |
| Median [m] | 0.624 | 0.913 | -0.420 |
| STD [m] | 1.681 | 2.939 | 2.045 |
| RMS [m] | 1.789 | 2.833 | 2.062 |

*Figure 5.117: Errors of static for each epoch on Point 1 with respect to reference. (RinexOn data obtained on June 11th, 2019)*



*Figure 5.118: Errors of static for each epoch on Point 2 with respect to reference. (RinexOn data obtained on June 11th, 2019)*

*Figure 5.119: Errors of static for each epoch on Point 3 with respect to reference. (RinexOn data obtained on June 11th, 2019)*
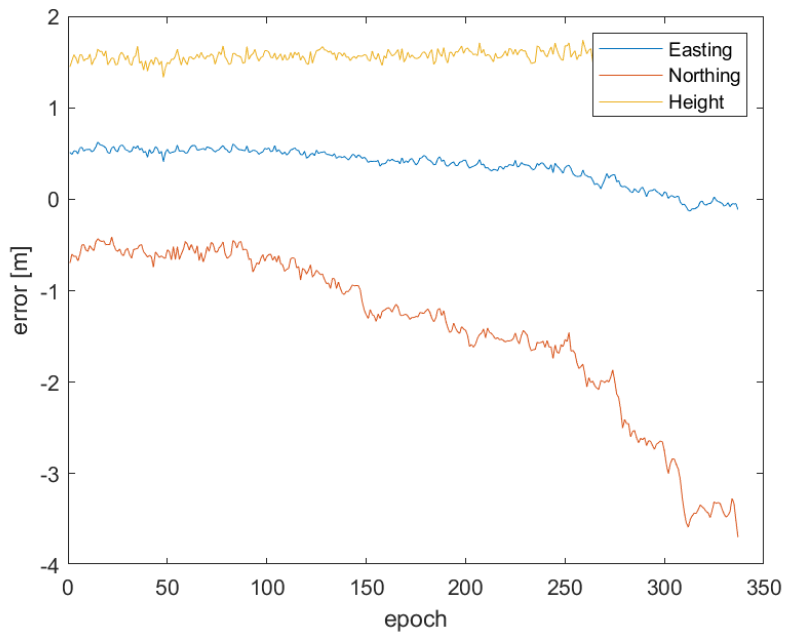


*Figure 5.120: Errors of static for each epoch on Point 4 with respect to reference. (RinexOn data obtained on June 11th, 2019)*

191
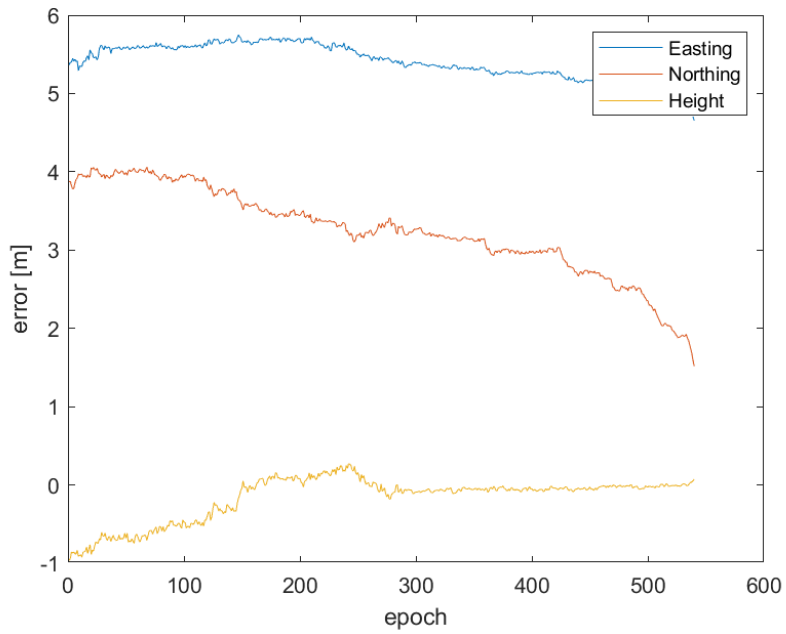
*Figure 5.121: Errors of static for each epoch on Point 5 with respect to reference. (RinexOn data obtained on June 11th, 2019)*
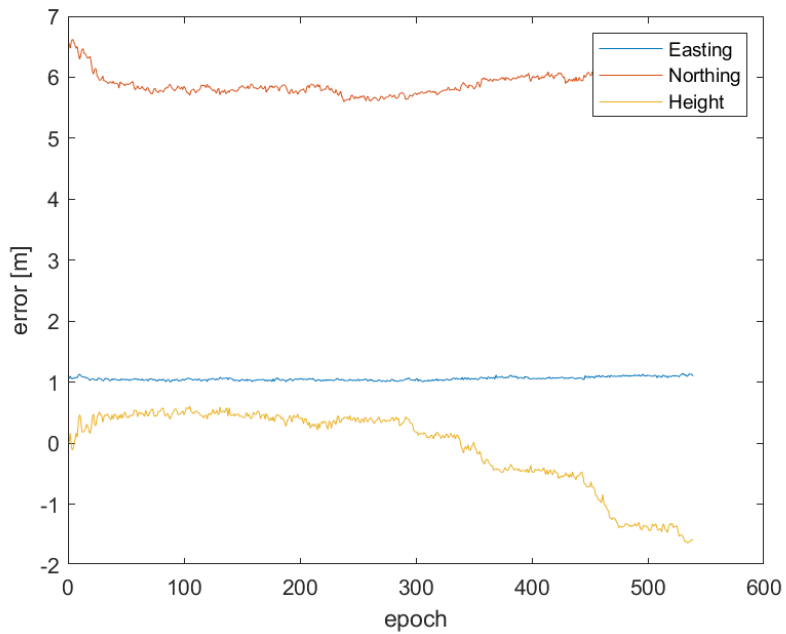


*Figure 5.122: Errors of static for each epoch on Point 6 with respect to reference. (RinexOn data obtained on June 11th, 2019)*
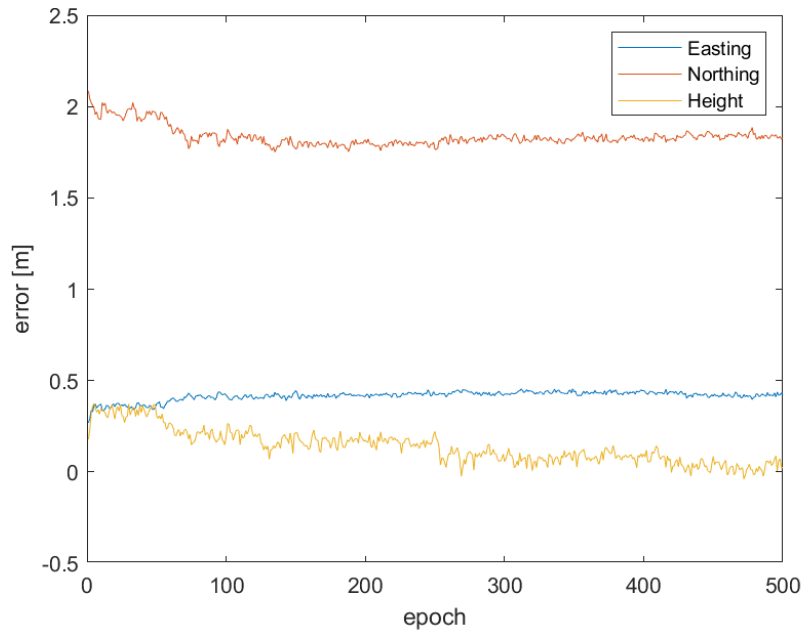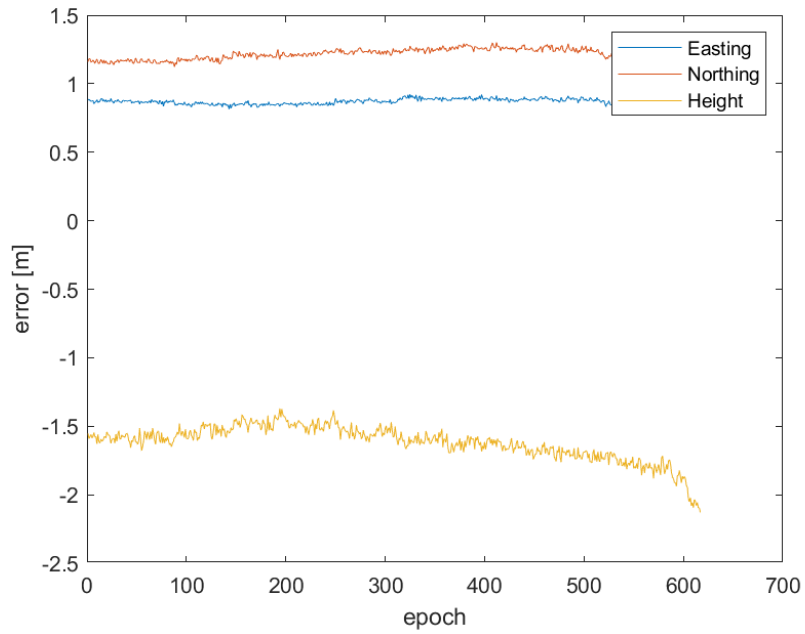
*Figure 5.123: Errors of static for each epoch on Point 7 with respect to reference. (RinexOn data obtained on June 11th, 2019)*



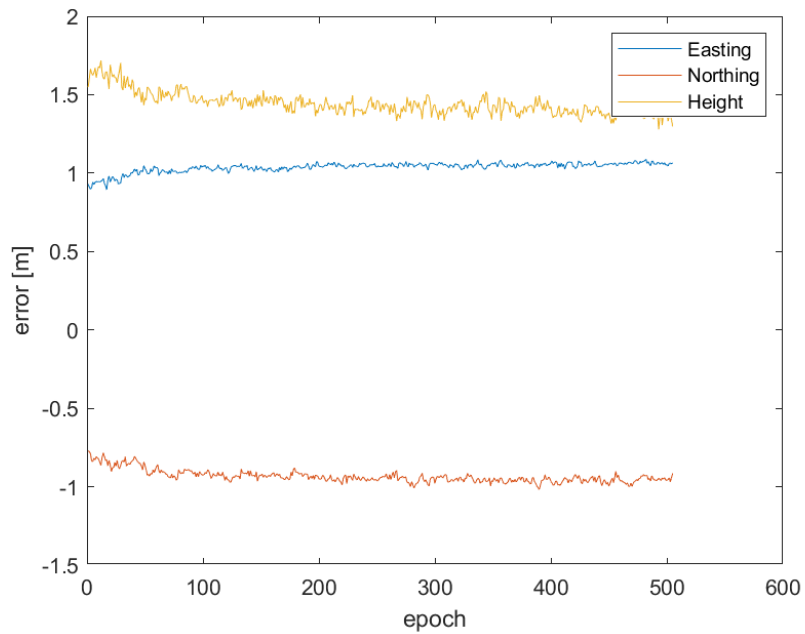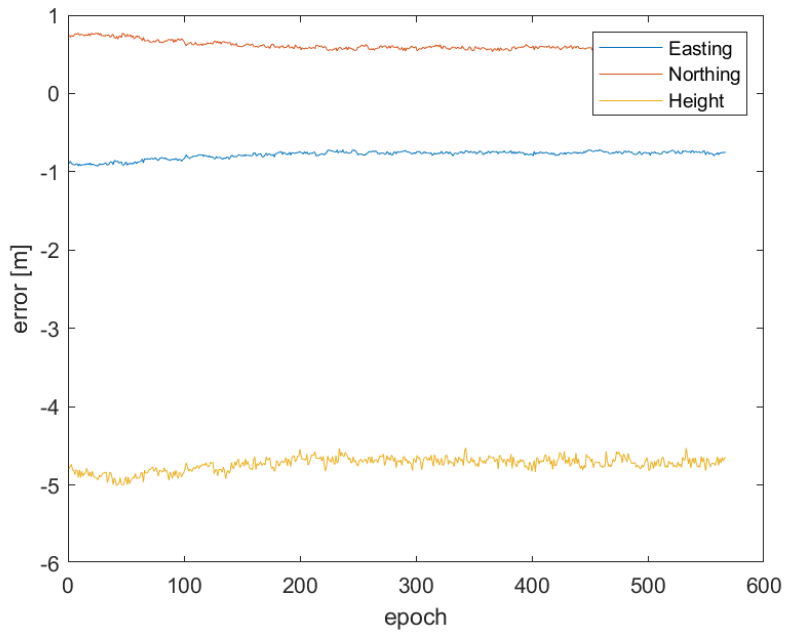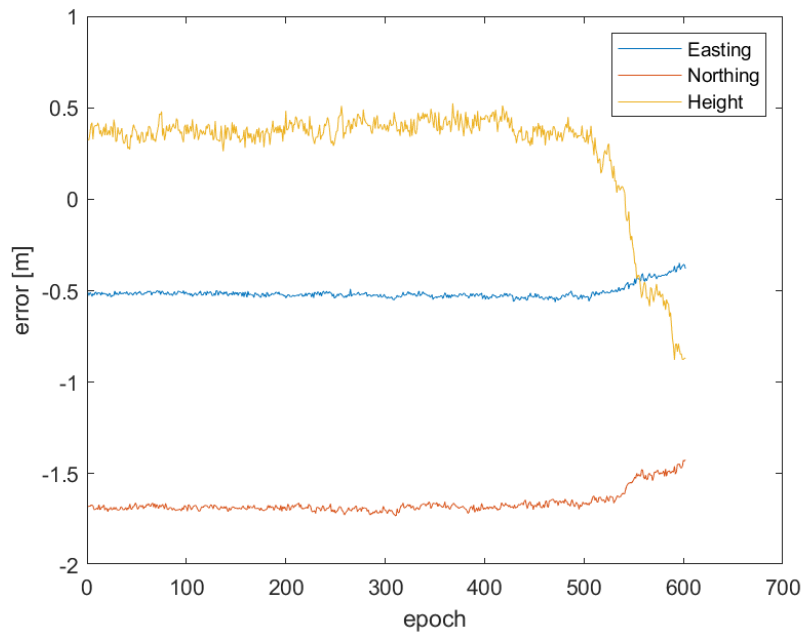*Figure 5.124: Errors of static for each epoch on Point 8 with respect to reference. (RinexOn data obtained on June 11th, 2019)*
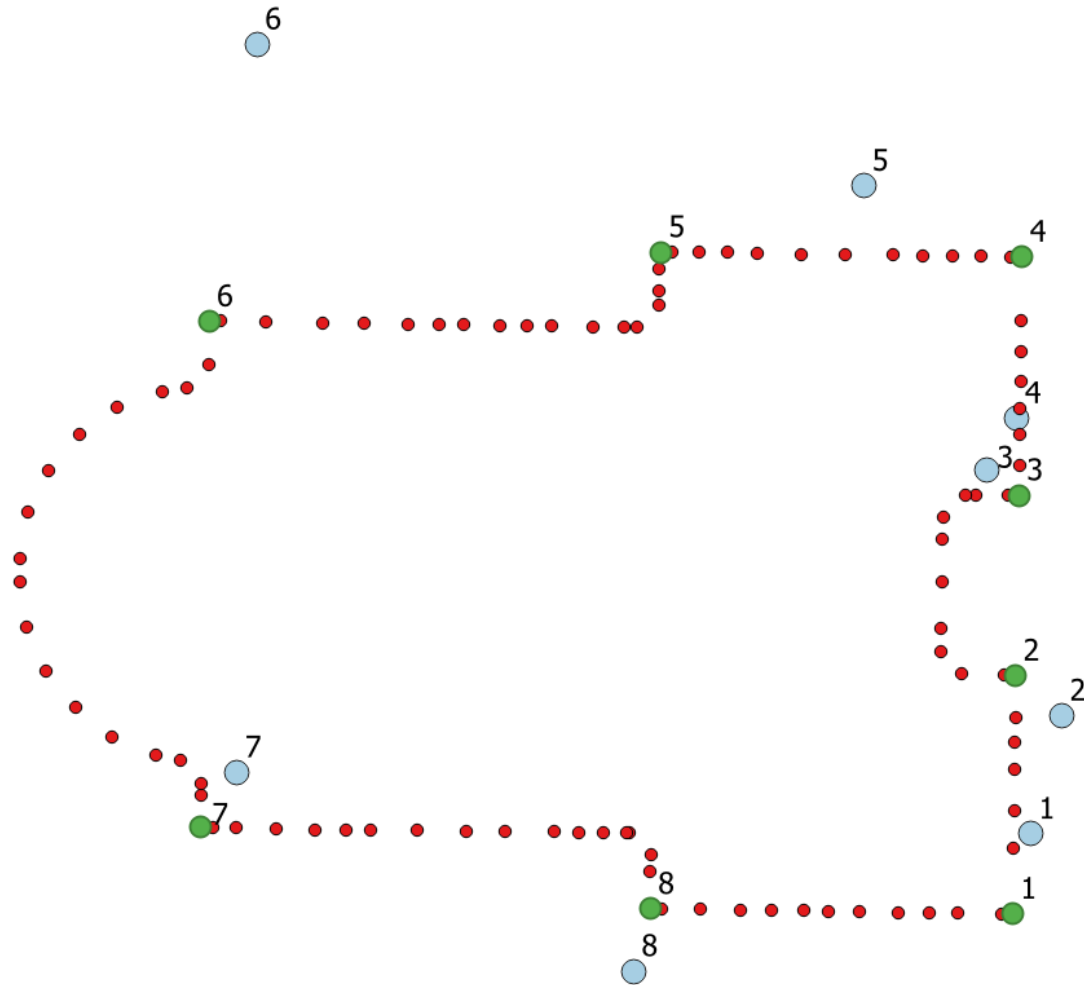
*Figure 5.125: Final results of static (RinexOn data collected on June 11<sup>th</sup>, 2019).*

The comparison between single point positioning (see Table 5.29) and static (see Table 5.34) shows that the similar improvement exist for static on East 0.8 meters, on North 0.6 meters, on Height 1.8 meters.

The simple comparison between results obtained from Geo++ RINEX Logger and RinexOn show that Geo++ RINEX Logger has slightly better accuracies. However, observations with Geo++ RINEX Logger and RinexOn are made in different days. Probably, this could be the reason of the difference between accuracies reached with different applications.

194

# 6 CONCLUSION AND RECOMMEDATION

In the research, single frequency GNSS receivers are tested in order to assess their accuracy to use for navigation and scientific purposes. With this aspect, accuracy assessment of relative static point positioning that is practiced for U-blox LEA-4T. RTKLIB has been tested for processing the single frequency U-blox data. Then, Samsung Galaxy S8 is studied as low-cost single frequency receiver with single point positioning, DGPS and static point positioning approach. In order to log desired data in android smartphone, OruxMap, GNSS Logger, Geo++ RINEX Logger and RinexOn applications are tested. Study on Samsung device is covered data obtained from API Level 23 and API Level 24 features. The raw GNSS measurement data has been processed with RTKLIB.

For accuracy assessments, one reference network with stop-and-go surveying technique, one reference trajectory with kinematic surveying technique are established surveying them with geodetic receiver Leica GRX1200. The reference network has 100 points and covers approximately 75 meters round around fountain in front of the Politecnico di Milano, Leonardo Campus. The estimated points from several surveys are averaged to create reference network. On the other hand, the reference trajectory is approximately 275 meters long which is placed near reference network. The point cloud obtained by several kinematic surveys are filtered to obtain reference trajectory. With k-means and implemented clustering method by author, 4 alternatives are created for reference trajectory.

Then, Experiment 1 is performed with U-blox LEA-4T which is a single-frequency GNSS receiver that accesses only L1 frequency. The main purpose of the experiment is the assessment of accuracy of relative static data processing for L1 receivers. For this, before the smartphone raw GNSS measurement processing, as a single frequency receiver, U-blox LEA-4T data accuracy is wanted to be studied for short sessions (5 – 10 minutes) which was not studied with current data before. Results can be mentioned as satisfactory with cm level accuracy for fixed results. However, only the 52% of the total sessions gave the fixed solution for 10 minutes sessions. Only the 23% of the total for 5 minutes sessions are fixed. On the other hand, float solutions are obtained for all session with RTKLIB. Float solutions for 10 minutes sessions have decimeters level accuracy with 45cm maximum error on Height. Meter level accuracy is obtained for 5 minutes sessions with 105cm maximum error on Height.

In the end, the performance of RTKLIB was quite promising to process single frequency data even for 5 – 10 minutes sessions. This was important at the point, because this means RTKLIB could be eligible for processing Samsung Galaxy S8's raw GNSS measurements on the continuation of the research.

All other experiments are performed with Samsung Galaxy S8 which has a single-frequency GNSS receiver with internal antenna. The main purpose of the Experiment 2 is the assessment of accuracy of position information obtained from Samsung chipset in real-time. On the reference network, position information is logged by OruxMaps application with a sampling rate of 1 HZ. Application is used in motion for kinematic approach. Error calculated as a distance between estimated point and the closest reference point. At the final, accuracies are obtained on meters level as expected. The maximum error is 8 meters for the experiment.

In Experiment 3, the performance of the Samsung Galaxy S8 receiver is tested on reference trajectory. The experiments focus the kinematic approach as Experiment 2; therefore, data is collected in motion. This time, raw GNSS measurement are collected additionally to the provided position information in real-time by Samsung chipset. In this purpose, by using OruxMaps, estimated point positions in real-time by Samsung chipset and the raw GNSS measurements are collected simultaneously by GNSS Logger. The raw GNSS measurements are post-processed with GNSS Analysis Tool on the desktop by Weighted Least Square Estimation. Errors are calculated as a distance between estimated point and the closest reference point as done in Experiment 2. In the experiment, OruxMaps observations in real-time reach ten meters accuracy. Error goes up to maximum 15 meters. On the other hand, post-processing accuracies obtained by GNSS Analysis Tool are worse than accuracies in real-time. Error goes up until 50 meters. Absolutely, the reason behind the post-processed raw measurements by GNSS Analysis Tool provide less accuracy and noisier results than position generated by Samsung Galaxy S8 chipset in real time, could been caused by smartphone chipset is using the additional instruments such as echo sounder, sonars, anemometer, gyrocompass. Besides, smartphone chipset could be using a stronger filtering than Weighted Least Square Estimation which GNSS Analysis Tool uses in processing.

Additionally, the end of Experiment 3, four alternative reference trajectories (k-means k=270 and k=540; and, implemented clustering method T=25cm and T=50cm) are compared with each other. Because the alternatives are very similar, no significate difference is noticed.

In the final, in Experiment 4, the aim is the assessment of accuracy of the single frequency smartphone receiver for static approach. In this aspect, Geo++ RINEX Logger and RinexOn android applications are tested to store raw GNSS measurements with Samsun Galaxy S8. Both applications provide the output in RINEX 3.03 format. Some analysis on the printed RINEX files shows that Geo++ RINEX Logger has an incorrect reconstruction and decoding of RINEX format for different periods of Galileo and BeiDou observations. However, when processing of only GPS observations, these errors have no impact. Additionally, another analysis on RINEX files shows the significant discontinuity of the phase observations acquired by Geo++ RINEX Logger. No problem about RINEX format and discontinuity of the phase observations is observed with RinexOn.

Then, in Experiment 4, RTKLIB is used for processing as it was tested with U-blox data in Experiment 1. Collected 10 minutes session raw measurements are processed in Single Point Positioning, DGPS and Static mode by RTKLIB. As it is experienced before in Experiment 1, RTKLIB have some issues for processing single frequency raw GNSS measurements for short sessions. Because Samsung Galaxy S8 raw data is noisier then U-blox's and it was not possible to obtained fixed results by RTKLIB, float solutions are calculated. With Single Point Positioning for Day 1 observations (by Geo++ RINEX Logger), 1 meter accuracy on East, 2.4 meters accuracy on North, 3.3 meters accuracy on Height is obtained. The statistics of the results for DGPS and static post-processing shows some improvements on the accuracies. 0.8 meter accuracy improvement on North and 0.6 meter accuracy improvement on Height are observed. No improvements are noticed on East which already has 1 meter accuracy for Single Point Positioning. The results obtained by DGPS and static post-processing has no significant difference.

On the other hand, with Single Point Positioning for Day 2 observations (by RinexOn), 2.5 meter accuracy on East, 3.4 meters accuracy on North, 3.8 meters accuracy on Height is obtained. DGPS and static post-processing improved the accuracies on East 0.8 meter, on North 0.6 meter, on Height 1.8 meters. Also, for Day 2 observations (by RinexOn), no significant difference is noticed between by DGPS and static post-processing results.

Additionally, a simple comparison between results obtained on Day 1 (by Geo++ RINEX Logger) and Day 2 (by RinexOn) shows that Geo++ RINEX Logger has slightly better accuracies. However, RinexOn is providing better structured RINEX format. It has to be considered, observations with Geo++ RINEX Logger and RinexOn are made different days. Probably, this could be the reason of the difference between accuracies reached with different applications.

Nowadays, in the mass market, there are some smartphones with double frequency receivers. On the future, continue to the research with these devices can be very interesting in order to verify the improvement of the smartphone receivers. Double frequency receivers provide the possibility to remove ionospheric effects. Therefore, this could provide better accuracies for the smartphones.

# 7 APPENDIX A. The Code of K-Means

Appendix B. contains the "MATLAB" code which is used for k-means clustering algorithm with the aim of creating the reference on point cloud. In the code, defined *"k-means function"* is used. For detailed information about the function, researchers can visit:

https://www.mathworks.com/help/stats/kmeans.html#buefthh-3

```matlab
clear all
% to import data
G1_S1 = importdata('G1-S1_organized.csv',',');
G1_S2 = importdata('G1-S2_organized.csv',',');
G2_S1 = importdata('G2-S1_organized.csv',',');
G2_S2 = importdata('G2-S2_organized.csv',',');
G3_S1 = importdata('G3-S1_organized.csv',',');
G3_S2 = importdata('G3-S2_organized.csv',',');
G4_S1 = importdata('G4-S1_organized.csv',',');
G4_S2 = importdata('G4-S2_organized.csv',',');

% to create 2D point coordinates matrix
kinematic = [G1_S1; G1_S2; G2_S1; G2_S2; G3_S1; G3_S2; G4_S1; G4_S2];
% to enter the k-means algorithm function
[g,c] = kmeans(kinematic, 270,'Replicates',25);
% to plot
gscatter(kinematic(:,1),kinematic(:,2),g,'kgbr','++')
hold on
plot(c(:,1),c(:,2), 'o')
% to export the data
dlmwrite('kmean_270.txt',c,'delimiter','\t','precision',12);
```

# 8 APPENDIX B. The Code of Implemented Clustering Method by the Author

Appendix B. contains the "MATLAB" code which is used for implemented clustering method by the author with the aim of creating the reference on point cloud. "TRUE_POINTS" matrix is the result of the code.

```matlab
clear all
% to import data
G1_S1 = importdata('G1-S1_organized.csv',',');
G1_S2 = importdata('G1-S2_organized.csv',',');
G2_S1 = importdata('G2-S1_organized.csv',',');
G2_S2 = importdata('G2-S2_organized.csv',',');
G3_S1 = importdata('G3-S1_organized.csv',',');
G3_S2 = importdata('G3-S2_organized.csv',',');
G4_S1 = importdata('G4-S1_organized.csv',',');
G4_S2 = importdata('G4-S2_organized.csv',',');

% to create 2D point coordinates matrix
% the first point will be the starting point of clustering
kinematic =[G1_S1; G1_S2; G2_S1; G2_S2; G3_S1; G3_S2; G4_S1; G4_S2];
dlmwrite('all_kinemtics.txt',kinematic,'delimiter','\t','precision',12);
% to enter threshold distance for clustering
THRESHOLD = 0.50;

% LOOP
TRUE_POINTS=[];
group = [];
i_end = length(kinematic);
j = 0;

for i = 1:i_end

    if size(kinematic,1) > 1

        % to create distance matrix
        d = pdist(kinematic,'euclidean');
        d = d(1:(size(kinematic,1)-1));

        % to find and locate minimum value
        [Min,I] = min(d);

        if j==0
            temp_group = [kinematic(1,:); kinematic(I+1,:)];
```

```matlab
        else
            temp_group = [temp_group; kinematic(I+1,:)];
        end

        temp_mean = mean(temp_group);
        temp_d = pdist([temp_mean; temp_group],'euclidean');
        temp_d = temp_d(1:(size(temp_group,1)));
        [temp_max,J] = max(temp_d);

        if temp_max < THRESHOLD
            group = [group; kinematic(I+1,:)];
            kinematic(I+1,:) = [];
            kinematic(1,:) = temp_mean;
            j=1;
        else
            group=[temp_group(1,:);group];
                    if size(group,1)>1
            TRUE_POINTS=[TRUE_POINTS; mean(group,1)];

            fprintf("%d\n", size(TRUE_POINTS,1))
                    end
            kinematic(1,:)=[];
            group = [];
            j = 0;
        end

        clear d

        clear temp_mean
        clear temp_d

    else
        TRUE_POINTS=[TRUE_POINTS; kinematic(1,:)];
    end

end




plot(TRUE_POINTS(:,1),TRUE_POINTS(:,2), 'o')

dlmwrite('max50cm_radius.txt',TRUE_POINTS,'delimiter','\t','precision',12);
fprintf("Fine\n")
```

# 9 APPENDIX C. GNSS Analysis Tool Reports

This appendix contains examples of GNSS Analysis Tool final reports. For each survey, a report was added below. Survey 1 and Survey 2 final reports can be found in order.

**Survey 1 of Analysis Tool Report**

## 9.1 Android GNSS Analysis For Survey 1

**Table of Contents**

## 9.1.1 Test Summary

```
This analysis is for a stationary receiver, with open sky.
Data directory:
~\Desktop\GnssAnalysisFiles\yourSubdirectory\20180531_1547\
Log file: GNSSRESULTS.paramUsed.prFileName
GnssLogger: v2.0.0.1
GNSS Analysis App: v2.6.1.0
Phone: samsung Model: SM-G950F
Android version: 7.0
```
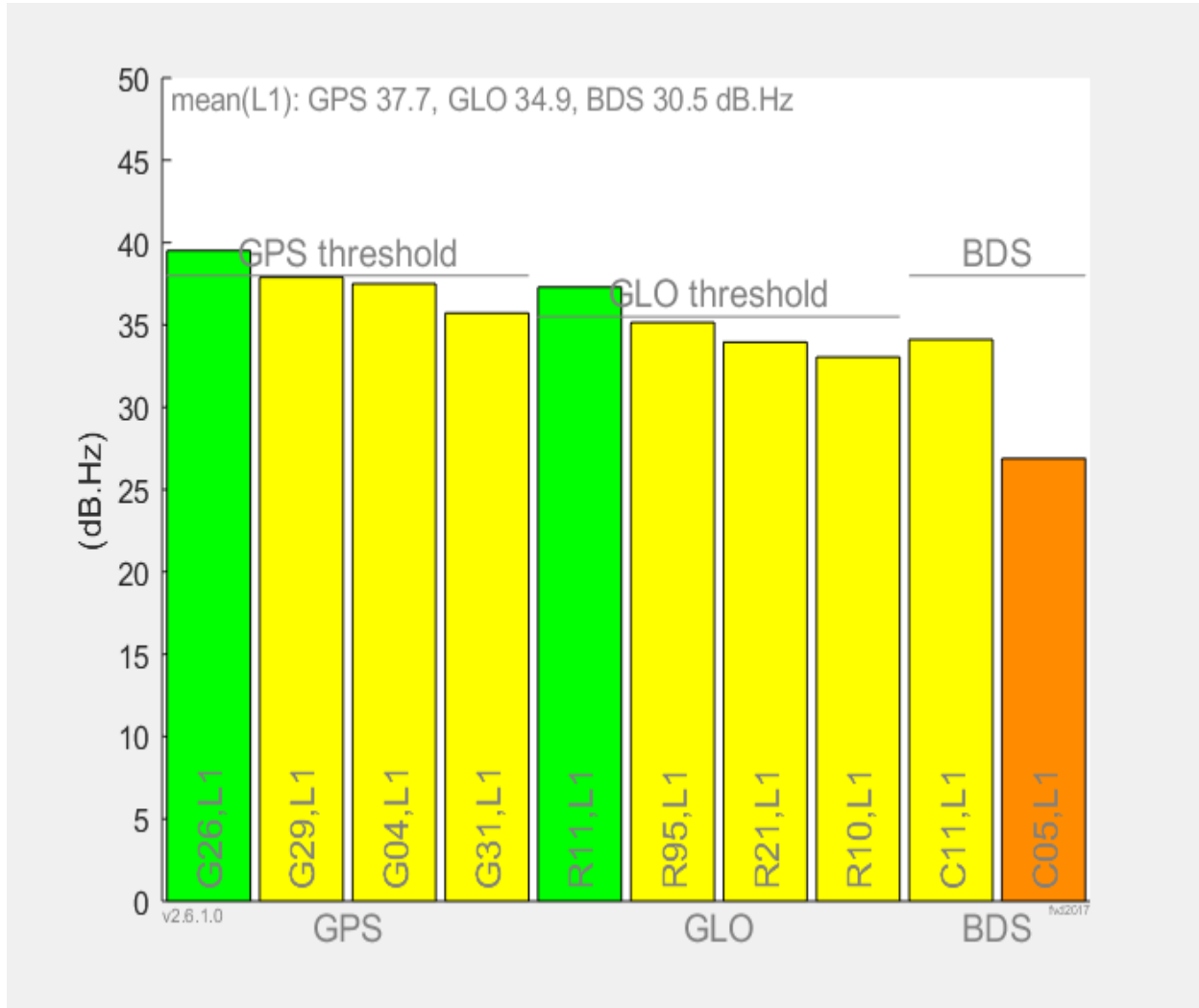
Note: Later Android version is available - check this website https://source.android.com/setup/start/build-numbers

**API.**

```
GnssClock Errors. Missing Fields: DriftNanosPerSecond,
DriftUncertaintyNanosPerSecond.
GnssMeasurement Errors. None.
WARNING, Recommended Fields Missing: CarrierFrequencyHz, AgcDb,
CarrierFrequencyHz.
```
API FAIL BECAUSE OF MISSING FIELDS
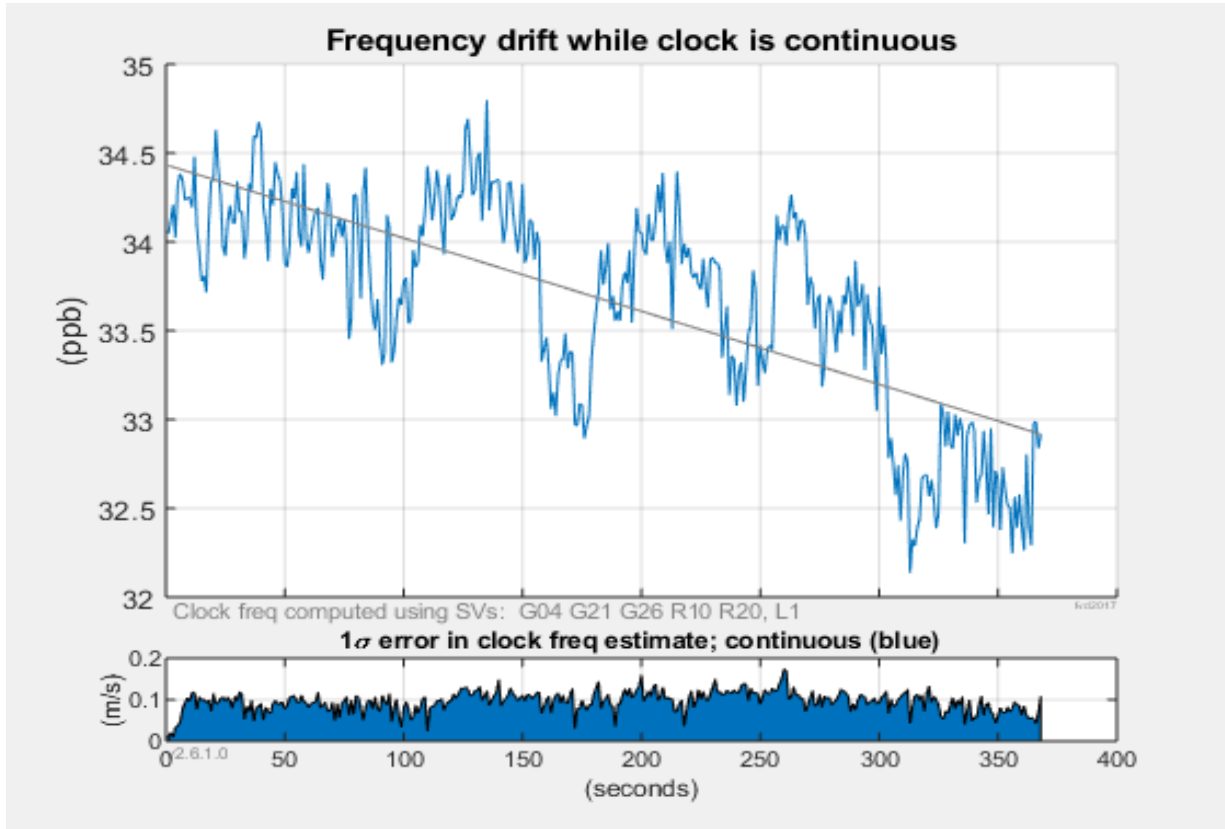
**Received Signal Analysis.**



```
GPS(L1), mean of strongest 4 median C/No = 37.7 dBHz
Pass/fail reference threshold = 38.0 dBHz
Errors. Signals -0.3 dB compared to reference
FAIL BECAUSE OF WEAK SIGNALS

GLO(L1), mean of strongest 4 median C/No = 34.9 dBHz
Pass/fail reference threshold = 35.5 dBHz
Errors. Signals -0.6 dB compared to reference
FAIL BECAUSE OF WEAK SIGNALS


BDS(L1), mean of strongest 2 median C/No = 30.5 dBHz
Pass/fail reference threshold = 38.0 dBHz
Errors. Signals -7.5 dB compared to reference
FAIL BECAUSE OF WEAK SIGNALS
```
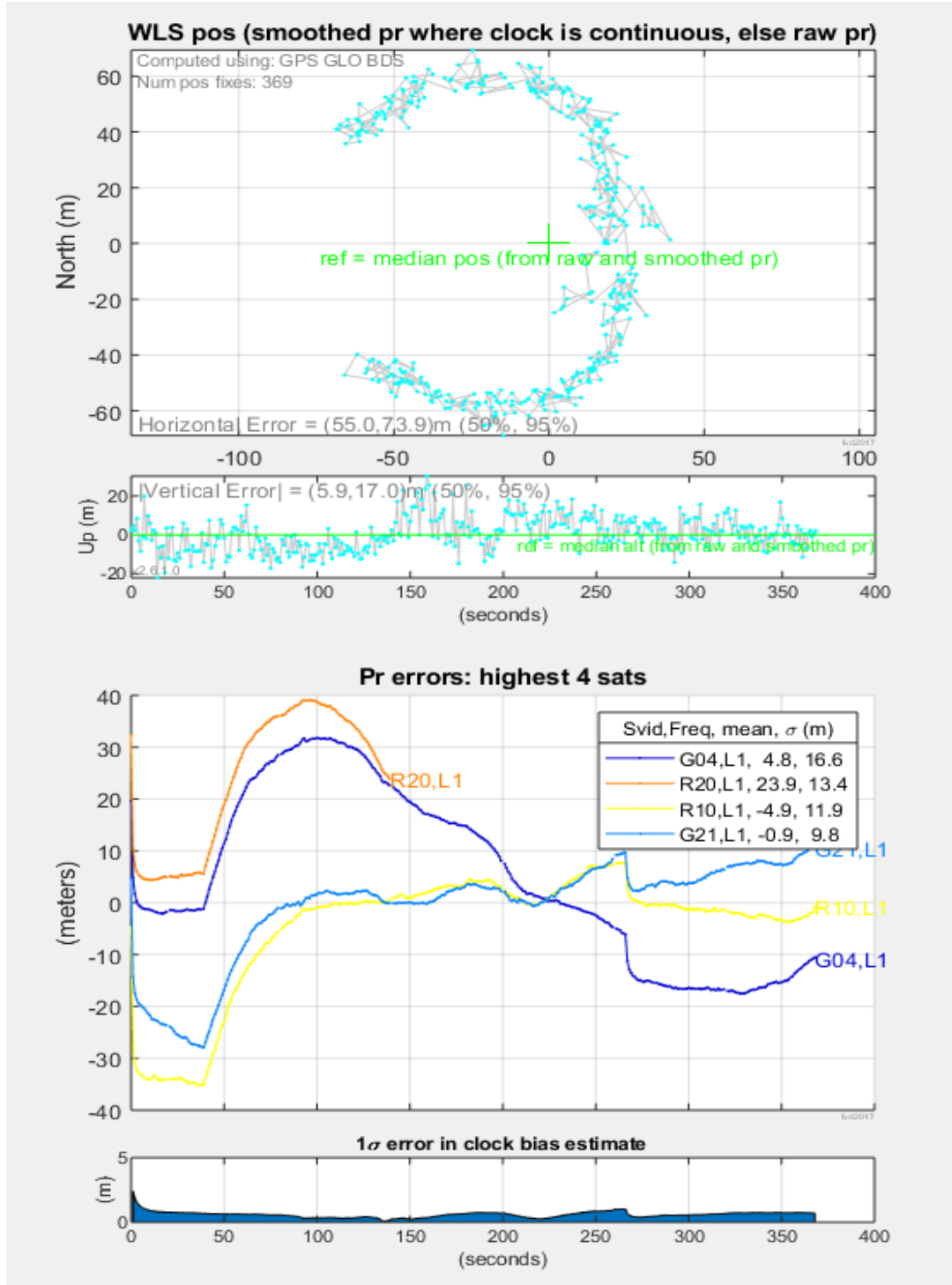
**FAIL**

**Receiver Clock Analysis.**



**Frequency drift while clock is continuous**

Clock freq computed using SVs: G04 G21 G26 R10 R20, L1

**1σ error in clock freq estimate; continuous (blue)**

(seconds)

```
|GNSS receiver clock rate|,  max, 34.80 ppb
|GNSS receiver clock drift rate|, 0.00 ppb/s
```

**Pseudorange Analysis.**



```
|error| of mean WLS position from ref = median pos (from raw and smoothed
pr), 10.2 meters
|PR errors| 95% < 34.1 meters
```
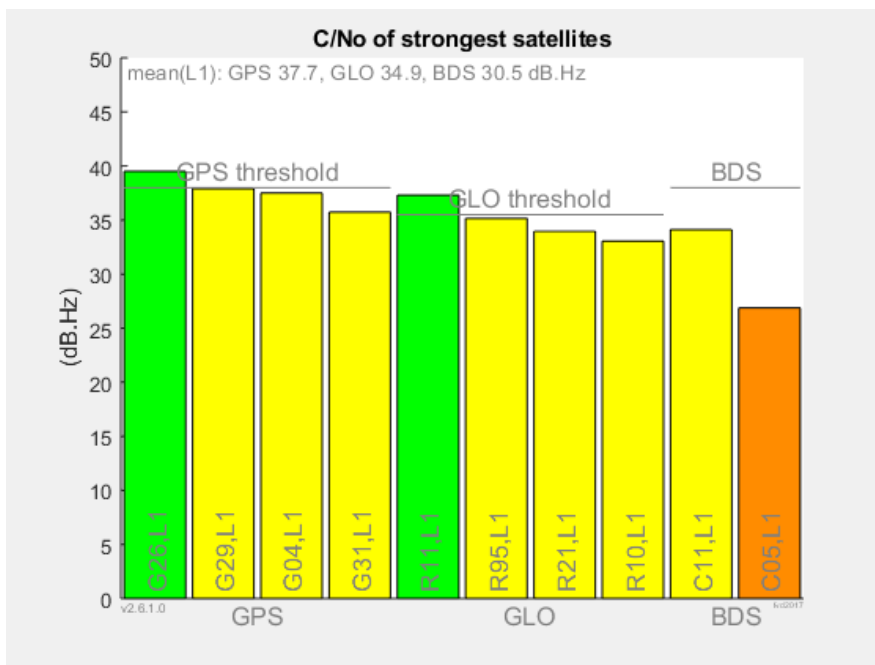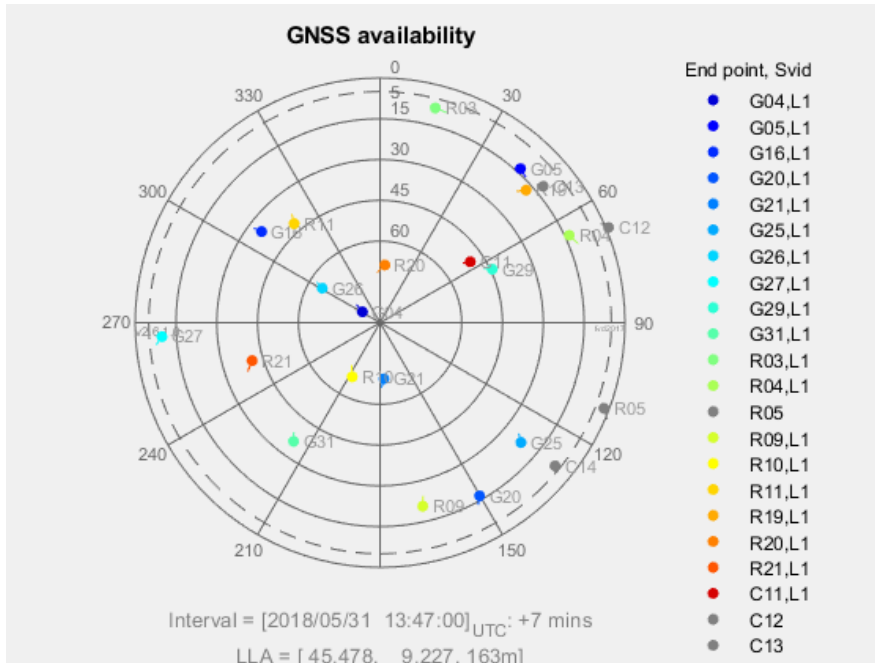**PASS**
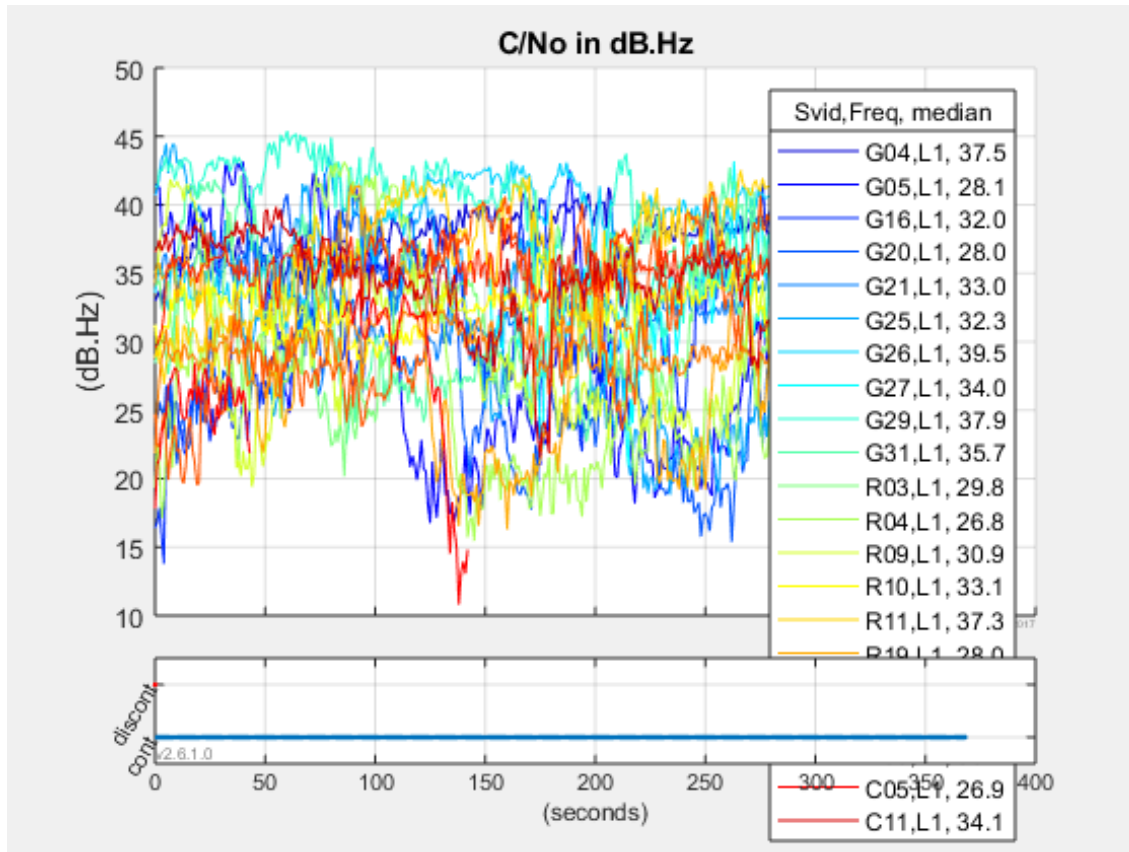
## 9.1.2 C/No Explanation

These plots show
1) Satellites available above the horizon
   Gray dot means the satellite was above the horizon, but not tracked.
2) Carrier to Noise Density ratio (C/No) of the strongest satellites
   above 5 degrees elevation (bar graph)
   Each bar shows the median C/No for that satellite signal.
3) C/No of all satellites above 5 degrees elevation (line graph)

C/No in dB.Hz

Svid,Freq, median
- G04,L1, 37.5
- G05,L1, 28.1
- G16,L1, 32.0
- G20,L1, 28.0
- G21,L1, 33.0
- G25,L1, 32.3
- G26,L1, 39.5
- G27,L1, 34.0
- G29,L1, 37.9
- G31,L1, 35.7
- R03,L1, 29.8
- R04,L1, 26.8
- R09,L1, 30.9
- R10,L1, 33.1
- R11,L1, 37.3
- R19,L1, 28.0
- C05,L1, 26.9
- C11,L1, 34.1

The GPS reference threshold is set to 38 dBHz. Well built phones,
in open sky, have GPS satellites stronger than this threshold.
GLONASS threshold is 2.5dB lower, since GLO signal is 2.5dB weaker,
(see GPS and GLONASS ICDs).

For your log file the C/No results are:

GPS(L1), mean of strongest 4 median C/No = 37.7 dBHz
Pass/fail reference threshold = 38.0 dBHz
Errors. Signals -0.3 dB compared to reference
FAIL BECAUSE OF WEAK SIGNALS

GLO(L1), mean of strongest 4 median C/No = 34.9 dBHz
Pass/fail reference threshold = 35.5 dBHz
Errors. Signals -0.6 dB compared to reference
FAIL BECAUSE OF WEAK SIGNALS

BDS(L1), mean of strongest 2 median C/No = 30.5 dBHz
Pass/fail reference threshold = 38.0 dBHz
Errors. Signals -7.5 dB compared to reference
FAIL BECAUSE OF WEAK SIGNALS

## 9.1.3 Receiver Clock Explanation

This plot shows the clock frequency offset while the receiver is
continuously tracking satellites.
Clock drift rate is computed for continuous intervals > 20 samples.
Frequency offset within +- 500 ppb, and drift rate within +- 2 ppb/s is
consistent with good TCXO behavior.
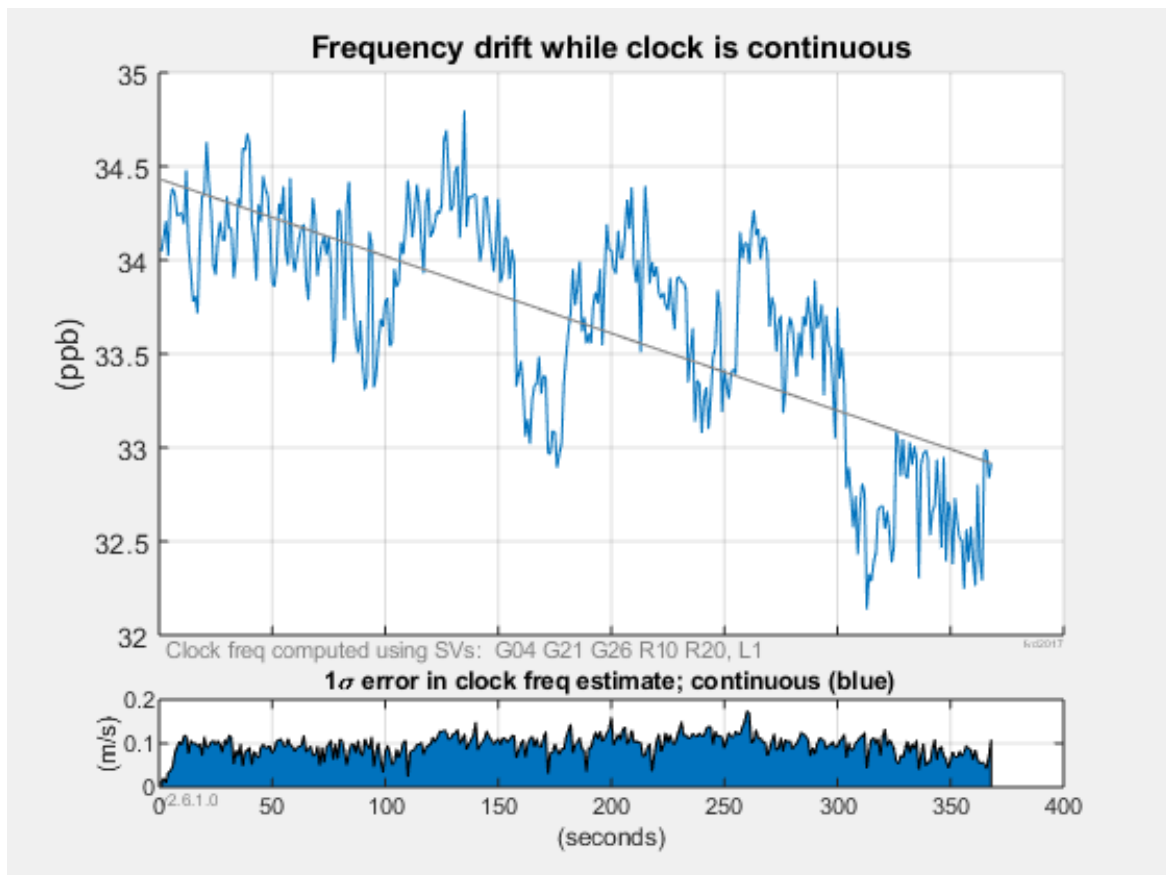


For your log file the continuous clock behavior is:
  |GNSS receiver clock rate|,  max, 34.80 ppb
  |GNSS receiver clock drift rate|, 0.00 ppb/s
  PASS
There are no clock discontinuities in your log file.

### 9.1.4  Pseudorange Explanation

This plot shows the WLS (Weighted Least Squares) position solution,
using the GNSS pseudoranges for satellites above 5 degrees elevation,
pseudoranges are smoothed when the clock is continuous.
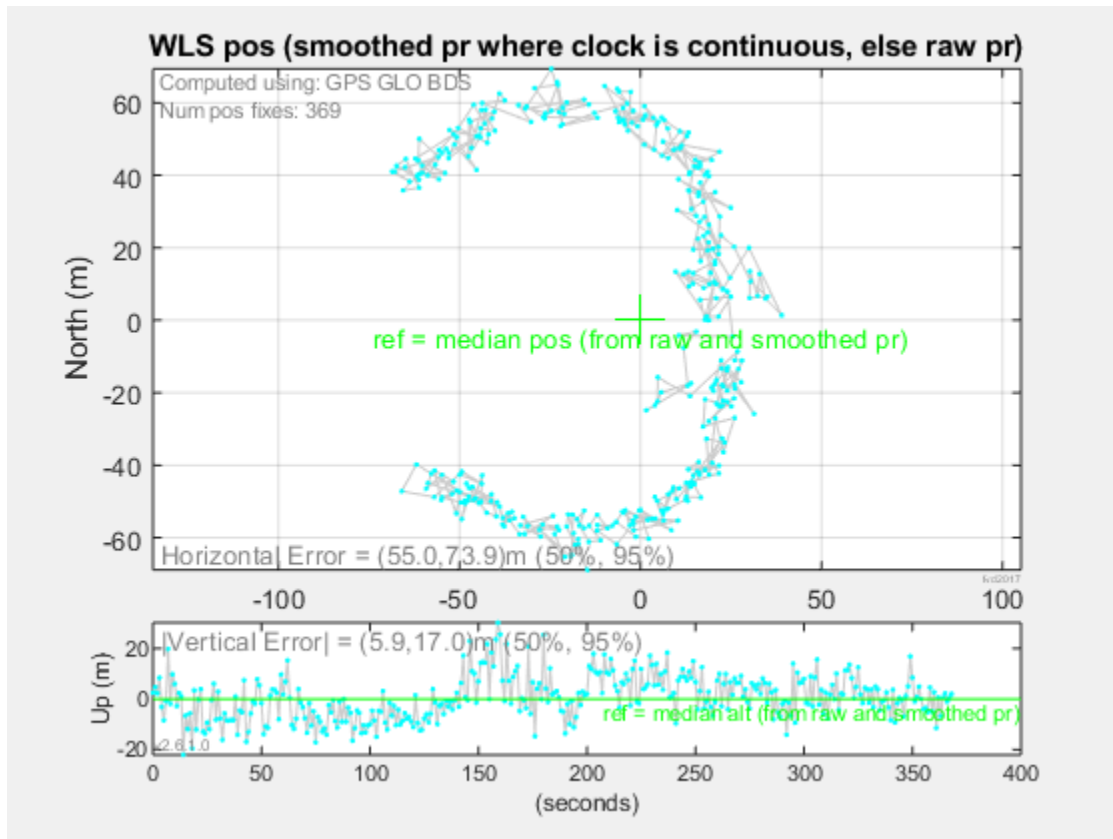


In open sky the expected WLS horizontal scatter is about 10 to 20 meters.
Smaller when clock is continuous and pr is smoothed. Larger when near
buildings.

The next plots shows the pseudorange errors, that is:
the measured pseudorange minus the expected pseudorange,
computed using the reference position

Pr errors: highest 4 sats
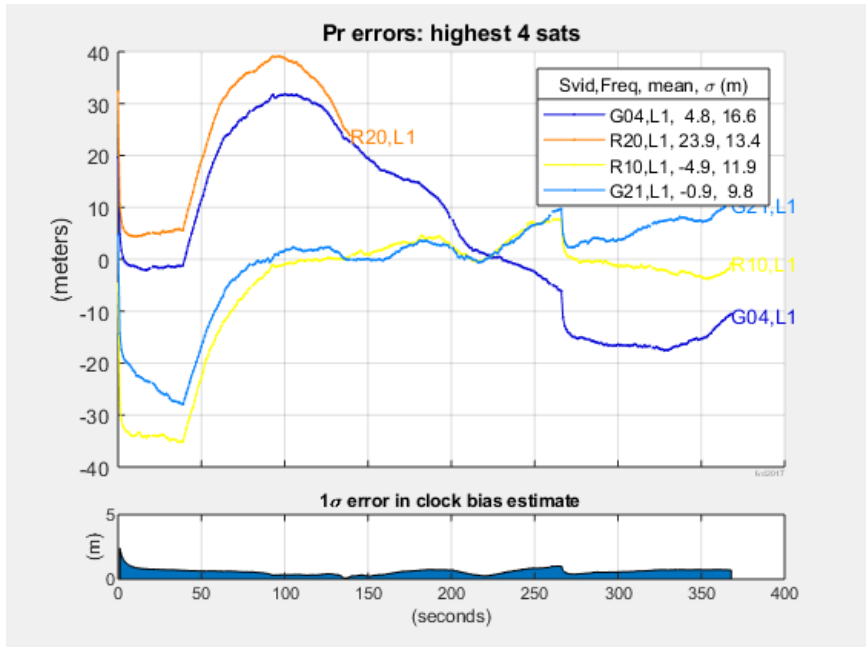
Errors are computed from pseudoranges, smoothed where clock is continuous.
Only satellites above 5 degrees elevation are shown.

Under open sky, errors for high satellites should be < 50 meters (95%).
For your log file the error analysis results are:
  |PR errors| 95% < 34.1 meters
  PASS

The next plot shows the errors for all GNSS satellites.
The low satellites often have larger errors from multipath and
unmodeled atmospheric delays.



Pr errors (smoothed pr where clock is continuous, else raw pr)

211
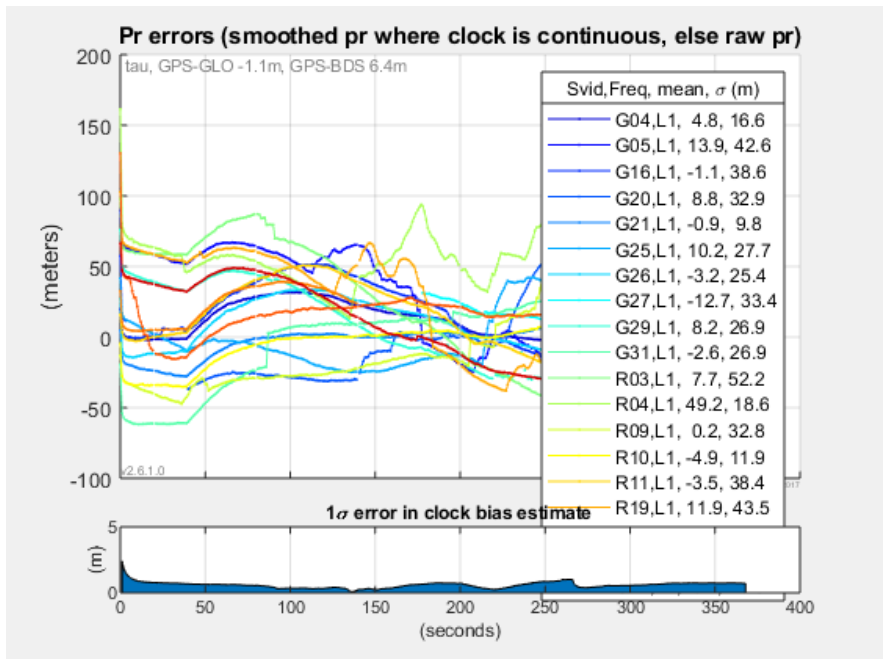
**Survey 2 of Analysis Tool Report**

## 9.2 Android GNSS Analysis For Survey 2

**Table of Contents**

## 9.2.1 Test Summary

```
This analysis is for a stationary receiver, with open sky.
Data directory:
~\Desktop\GnssAnalysisFiles\yourSubdirectory\
Log file: GNSSRESULTS.paramUsed.prFileName
GnssLogger: v2.0.0.1
GNSS Analysis App: v2.6.1.0
Phone: samsung Model: SM-G950F
Android version: 7.0
```

Note: Later Android version is available - check this website https://source.android.com/setup/start/build-numbers

**API.**
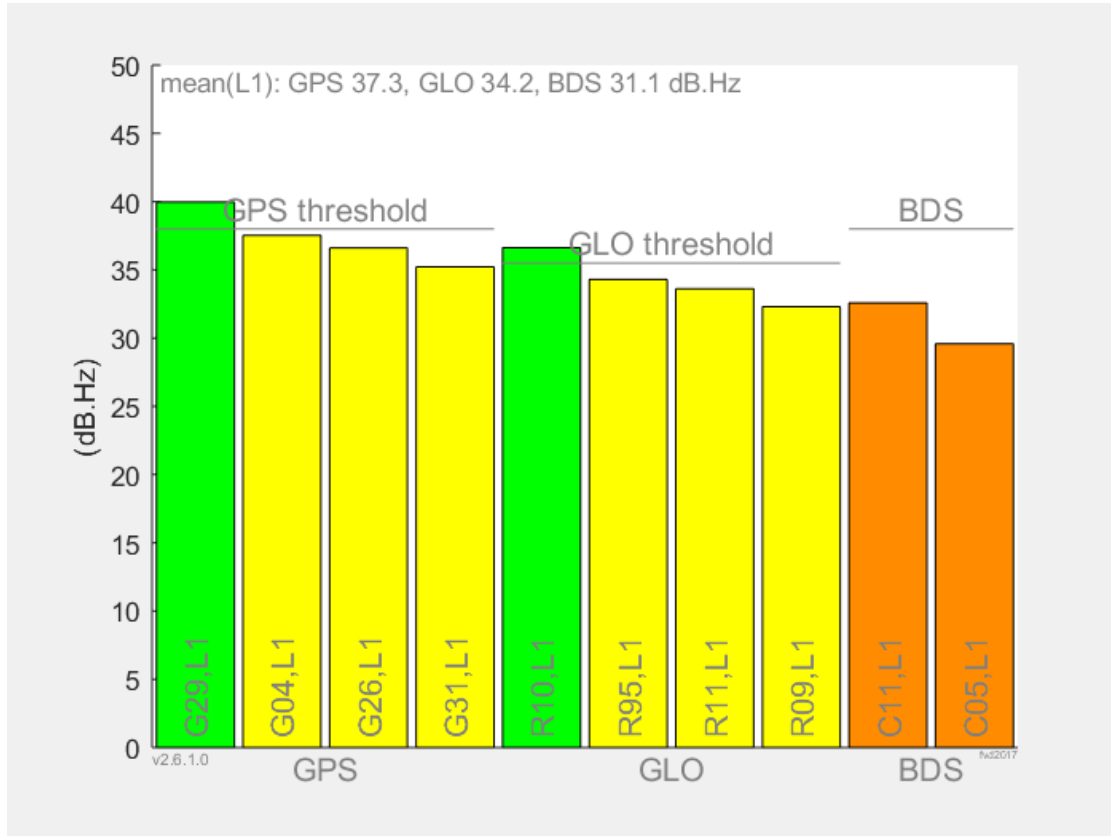
```
GnssClock Errors. Missing Fields: DriftNanosPerSecond,
DriftUncertaintyNanosPerSecond.
GnssMeasurement Errors. None.
WARNING, Recommended Fields Missing: CarrierFrequencyHz, AgcDb,
CarrierFrequencyHz.
API FAIL BECAUSE OF MISSING FIELDS
```

**Received Signal Analysis.**



```
GPS(L1), mean of strongest 4 median C/No = 37.3 dBHz
Pass/fail reference threshold = 38.0 dBHz
Errors. Signals -0.7 dB compared to reference
FAIL BECAUSE OF WEAK SIGNALS

GLO(L1), mean of strongest 4 median C/No = 34.2 dBHz
Pass/fail reference threshold = 35.5 dBHz
Errors. Signals -1.3 dB compared to reference
FAIL BECAUSE OF WEAK SIGNALS


BDS(L1), mean of strongest 2 median C/No = 31.1 dBHz
Pass/fail reference threshold = 38.0 dBHz
Errors. Signals -6.9 dB compared to reference
FAIL BECAUSE OF WEAK SIGNALS
```
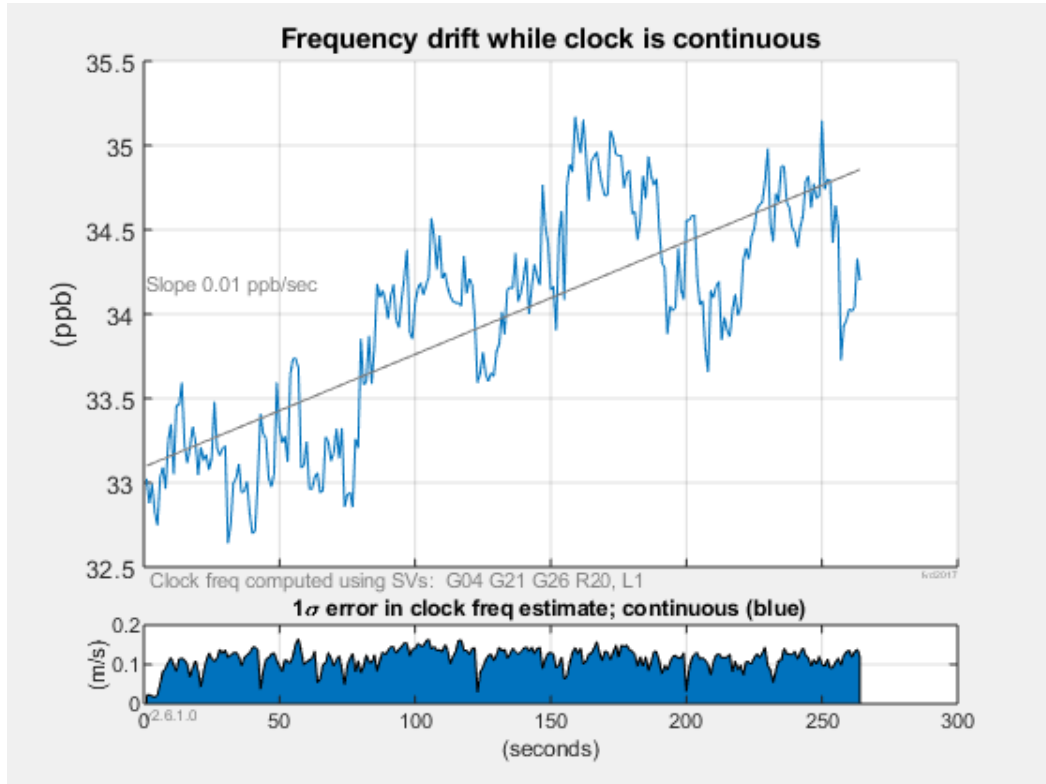
**FAIL**

**Receiver Clock Analysis.**



Frequency drift while clock is continuous

```
|GNSS receiver clock rate|,  max, 35.17 ppb
|GNSS receiver clock drift rate|, 0.01 ppb/s
```

**Pseudorange Analysis.**
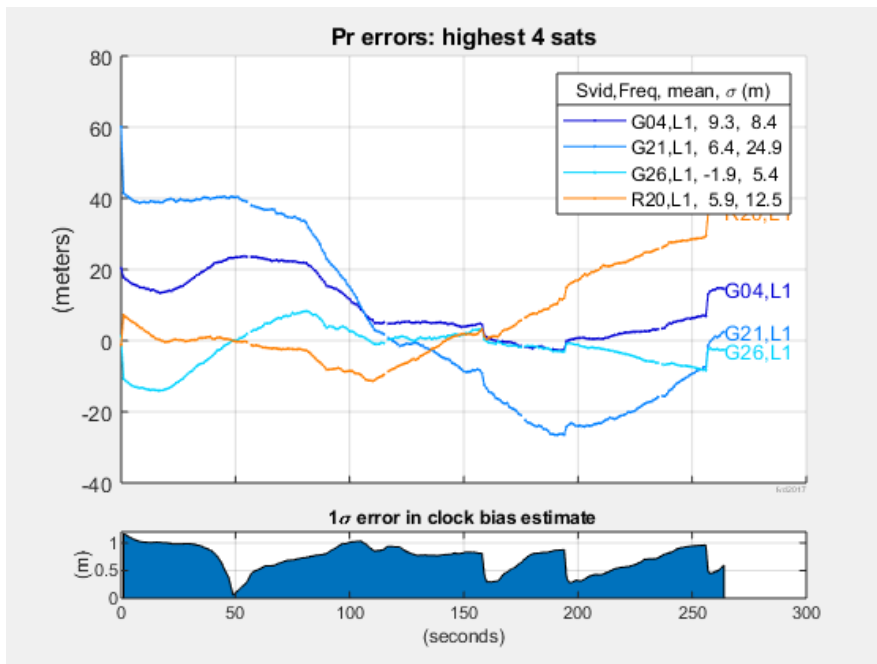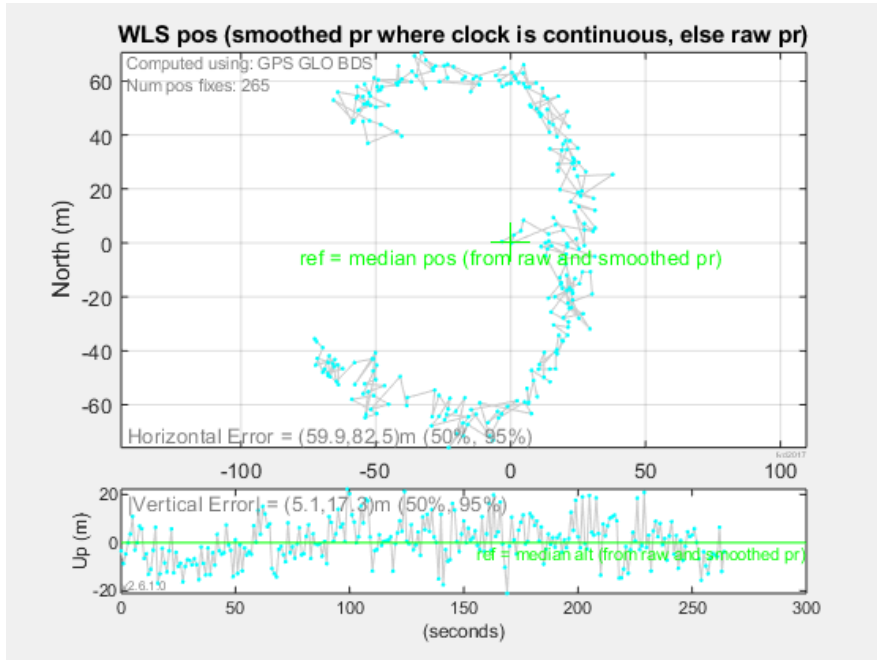




```
|error| of mean WLS position from ref = median pos (from raw and smoothed
pr), 14.9 meters
|PR errors| 95% < 38.9 meters
```
**PASS**

## 9.2.2  C/No Explanation

```
These plots show
1) Satellites available above the horizon
    Gray dot means the satellite was above the horizon, but not tracked.
2) Carrier to Noise Density ratio (C/No) of the strongest satellites
    above 5 degrees elevation (bar graph)
    Each bar shows the median C/No for that satellite signal.
3) C/No of all satellites above 5 degrees elevation (line graph)
```

C/No in dB.Hz

The GPS reference threshold is set to 38 dBHz. Well built phones,
in open sky, have GPS satellites stronger than this threshold.
GLONASS threshold is 2.5dB lower, since GLO signal is 2.5dB weaker,
(see GPS and GLONASS ICDs).

For your log file the C/No results are:

GPS(L1), mean of strongest 4 median C/No = 37.3 dBHz
Pass/fail reference threshold = 38.0 dBHz
Errors. Signals -0.7 dB compared to reference
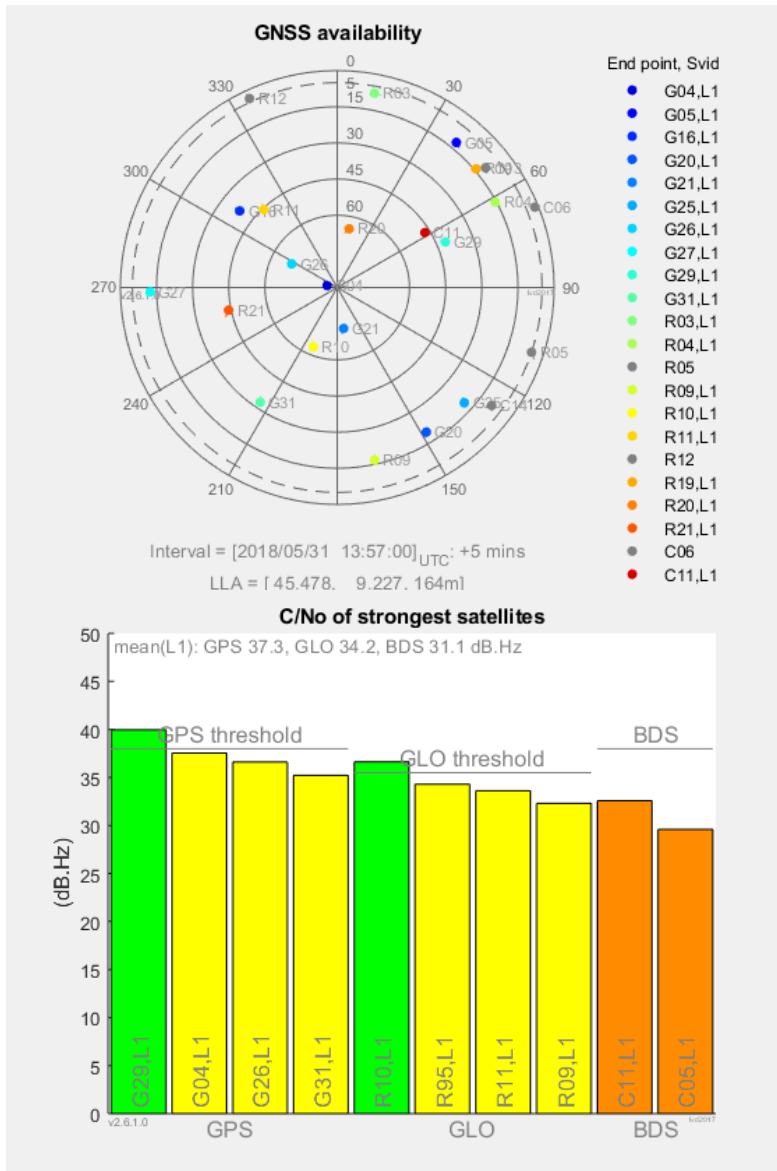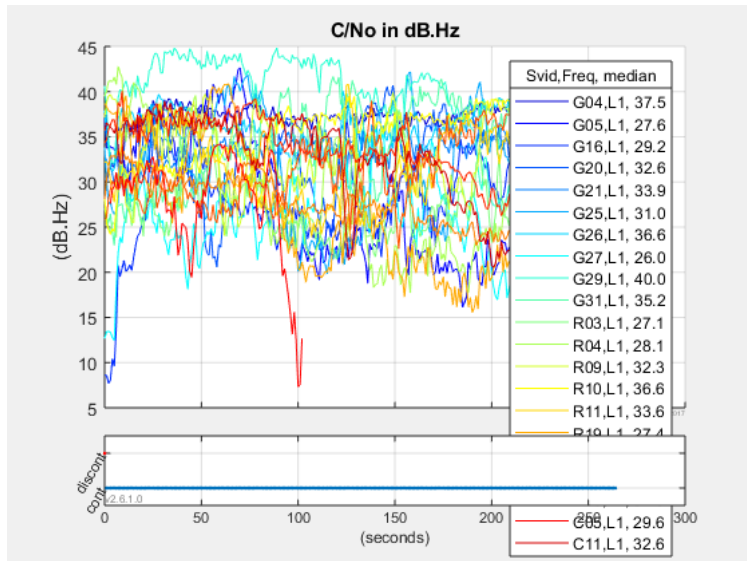FAIL BECAUSE OF WEAK SIGNALS

GLO(L1), mean of strongest 4 median C/No = 34.2 dBHz
Pass/fail reference threshold = 35.5 dBHz
Errors. Signals -1.3 dB compared to reference
FAIL BECAUSE OF WEAK SIGNALS


BDS(L1), mean of strongest 2 median C/No = 31.1 dBHz
Pass/fail reference threshold = 38.0 dBHz
Errors. Signals -6.9 dB compared to reference
FAIL BECAUSE OF WEAK SIGNALS


## 9.2.3 Receiver Clock Explanation

This plot shows the clock frequency offset while the receiver is

continuously tracking satellites.

Clock drift rate is computed for continuous intervals > 20 samples.

Frequency offset within +- 500 ppb, and drift rate within +- 2 ppb/s is

consistent with good TCXO behavior.

**Frequency drift while clock is continuous**

Slope 0.01 ppb/sec

Clock freq computed using SVs:  G04 G21 G26 R20, L1

**1σ error in clock freq estimate; continuous (blue)**
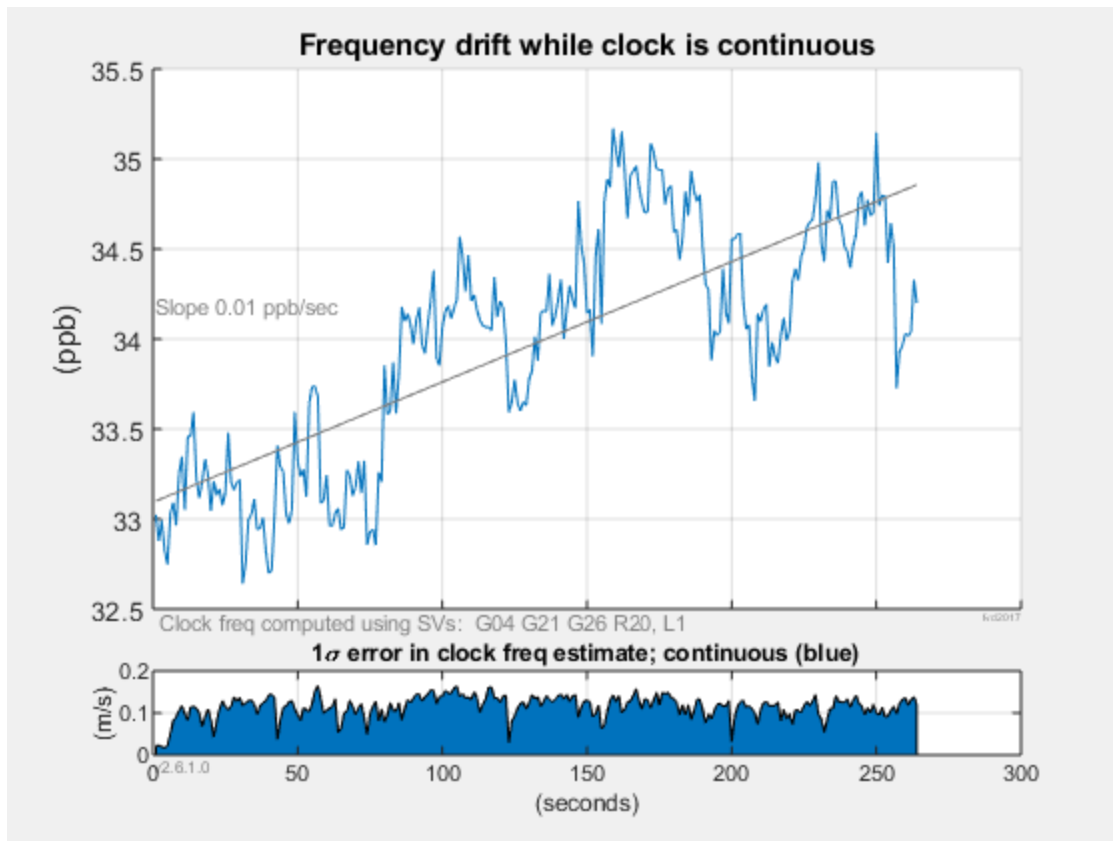
For your log file the continuous clock behavior is:

  |GNSS receiver clock rate|, max, 35.17 ppb

  |GNSS receiver clock drift rate|, 0.01 ppb/s

  PASS

There are no clock discontinuities in your log file.

## 9.2.4  Pseudorange Explanation

This plot shows the WLS (Weighted Least Squares) position solution, using the GNSS pseudoranges for satellites above 5 degrees elevation, pseudoranges are smoothed when the clock is continuous.

**WLS pos (smoothed pr where clock is continuous, else raw pr)**
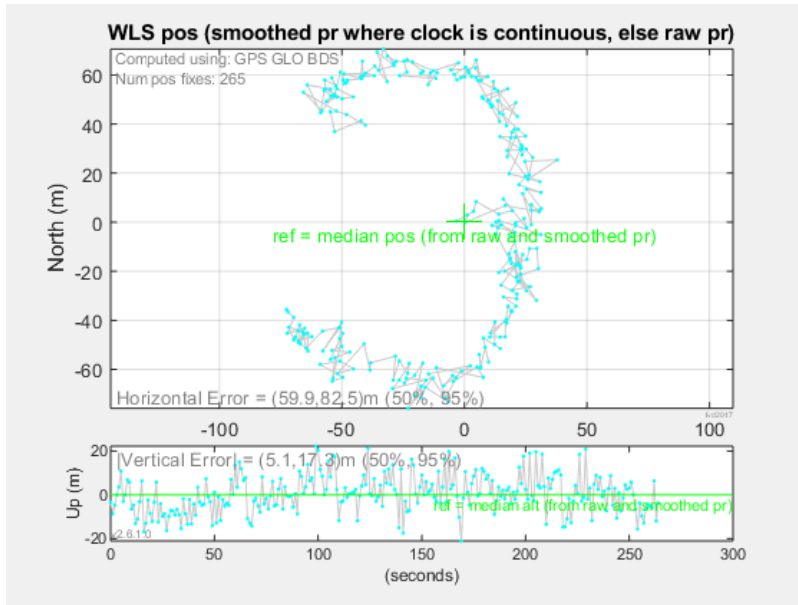
In open sky the expected WLS horizontal scatter is about 10 to 20 meters.
Smaller when clock is continuous and pr is smoothed. Larger when near
buildings.

The next plots show the pseudorange errors, that is:
the measured pseudorange minus the expected pseudorange,
computed using the reference position



**Pr errors: highest 4 sats**

219
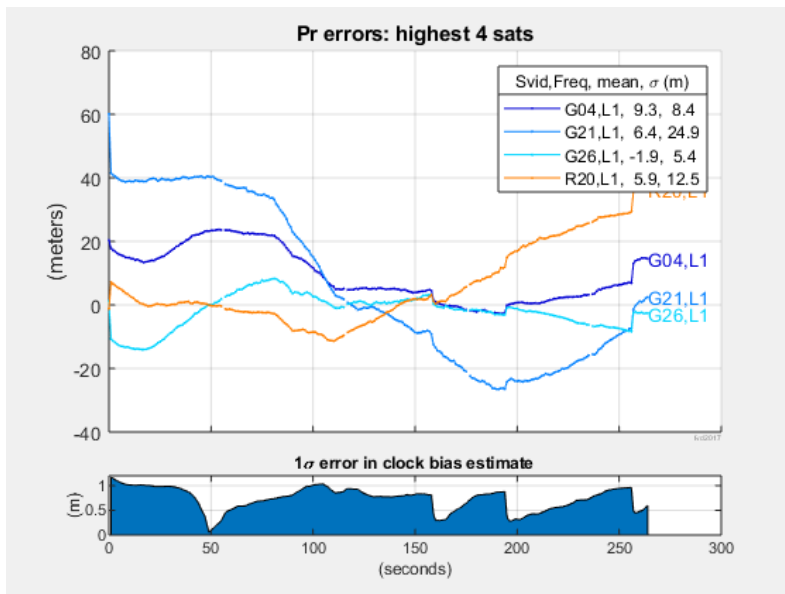
Errors are computed from pseudoranges, smoothed where clock is continuous.
Only satellites above 5 degrees elevation are shown.

Under open sky, errors for high satellites should be < 50 meters (95%).
For your log file the error analysis results are:
  |PR errors| 95% < 38.9 meters
  PASS

The next plot shows the errors for all GNSS satellites.
The low satellites often have larger errors from multipath and
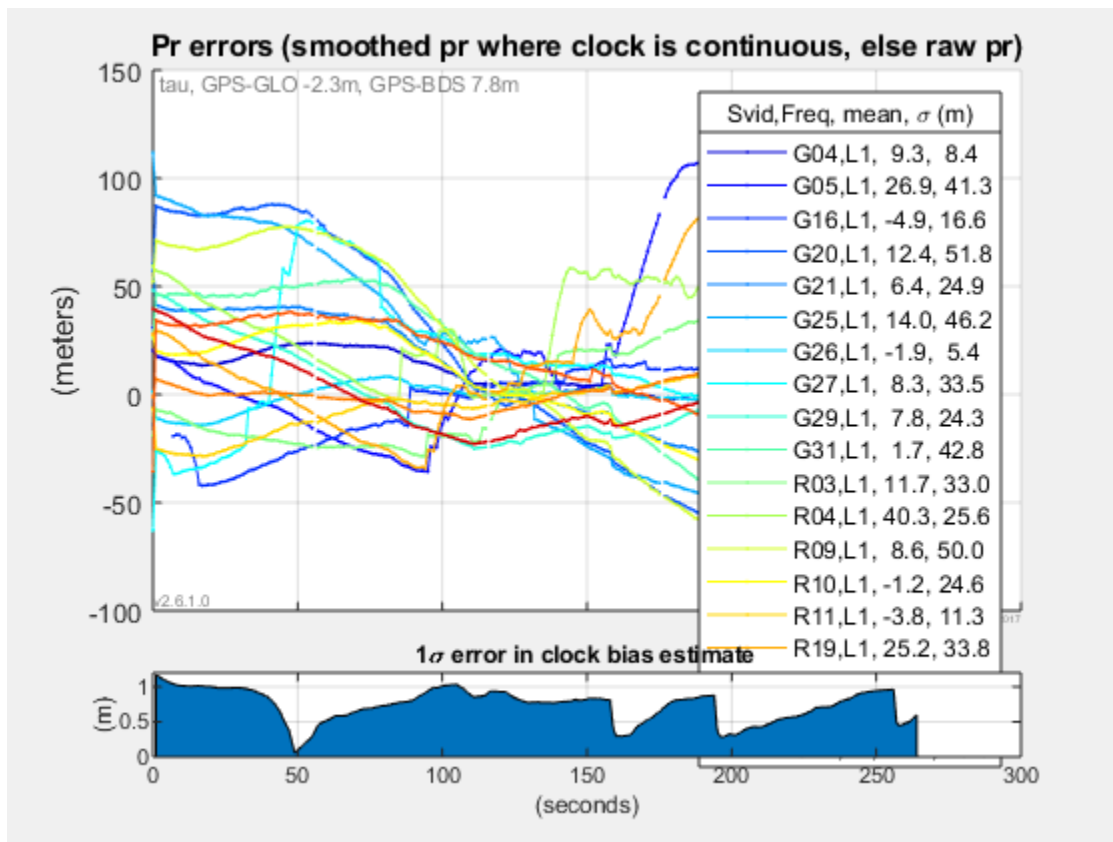unmodeled atmospheric delays.

# 10 Bibliography

Blewitt, G. (1997). *Basics of the GPS Techniques: Observation Equations.* Department of Geomatics, University of Newcastle, Newcastle, United Kingdom.

China Satellite Navigation Office. (2017, December). BeiDou Navigation Satellite System. *Open Service Signal B1C (Version 1.0).*

Coordination Scientific Information Center. (2016). *GLONASS Interface Control Document - Navigational radiosignal in bands L1, L2.* Moscow: Russian Institute of Space Device Engineering. Retrieved from https://www.unavco.org

Department of Defense. (2001). *Global Positioning System standard positioning service performance standard.* Washington DC: the US Assistant for GPS, Positioning and Navigation, Defense Pentagon.

Edurev. (2019). *Edurev*. Retrieved from Matlab Overview: Advantages and Disadvantages of Engineering Software: https://edurev.in

*European Global Navigation Satellite System Agency*. (2017, Aug 29). Retrieved from European GNSS Agency: https://www.gsa.europa.eu/

European GNSS Agency. (2016). *GNSS User Technology Report.* Luxembourg: Publications Office of the European Union. doi:10.2878/760803

European Union. (2018, Nov 14). *European GNSS (Galileo) Open service - Signal in space interface control document.* Retrieved from GalileoGNSS: galileognss.eu

Feairheller, S., & Clark, R. (2006). Other satellite navigation systems. In E. Kaplan, & C. Hegarty, *Understanding GPS – principles and applications* (2nd edition ed., pp. 595-634). Norwood: Artech House.

G S, R. (2010). *Global Navigation Satallite Systems With Essential of Satellite Communications.* New Delhi: Tata McGraw Hill Education Private Limited.

*Geographic Information Source*. (2013, May 3). Retrieved from https://www.nedir.com/gnss

*Global Positioning System*. (2017, Dec 18). Retrieved from Official U.S goverment information about the Global Positioning System (GPS) and related topics: https://www.gps.gov/

GNSS science support centre - eESA. (2014, September 18). *GLONASS Services*. Retrieved from Standard Precision Service: https://gssc.esa.int/

GNSS science support centre - eESA. (2018, July 26). *Galileo General Introduction - navipedia*. Retrieved from GNSS science support cetre - eESA: https://gssc.esa.int

Goad, C. (1974). A modified Hopfield tropospheric refraction correction model. *American Geophysical Union Annual Fall Meeting (abstract)*, (p. 28). San Francisco, CA.

Grec, F. (2014/15). Low-Cost GNSS Receivers for Geodetic Local Monitoring. Milano, MI, Italy: Politecnico di Milano, Scuola di Ingegneria Civile, Ambientale e Territoriale, Corso di Laurea in Environmental and Geomatic Engineering .

Habrich, H. (1999). Geodetic applications of the global navigation satellite system (GLONASS). *PhD dissertation*. Switzerland: University of Berne.

Hegarty, C. J. (2014, May). The Modernized GPS Civil Signals. *Official U.S. government information about the Global Positioning System (GPS) and related topics.* The MITRE corporation. Retrieved from https://www.gps.gov/multimedia/presentations

Hein, G., & Pany, T. (2002). Architecture and Signal Design of the European Satellite Navigation. *Journal of Global Positioning Systems, Vol. 1*, No. 2:73-84.

Hofman-Wellenhof, B., Lichtenegger, H., & Wasle, E. (2008). *GNSS.* Wien: SpringerWienNewYork.

Hopfield , H. (1969). Two-quartic tropospheric refractivity profile for correcting satellite. *Journal of Geophysical Research, 74(18)*, 4487–4499.

Hudnut, K., & Titus, B. (2004). *GPS L1 civil signal modernization (L1C).* The Interagency GPS Executive Board. Retrieved from www.navcen.uscg.gov/gps

Jeffrey, C. (2010). *An Introduction to GNSS: GPS, GLONASS, Galileo and other Global Navigation Satellite Systems.* Calgary, Alberta, Canada: NovAtel Inc.

Leica Geosystems AG. (2009). *Leica GRX1200+ Series - High Performance GNSS Reference Receivers.* Retrieved from Hexagon Geosystems - Leica Geosystems: www.leica-geosystems.com

MacQueen, J. B. (1967). Some Methods for classification and Analysis of Multivariate Observations. *Proceedings of 5-th Berkeley Symposium on Mathematical Statistics and Probability* (pp. 1:281-297). Berkeley: University of California Press.

*NASA.* (2017, Apr 7). Retrieved from The National Aeronautics and Space Administration (NASA): https://www.nasa.gov

National Imagery and Mapping Agency. (2000). *Department of Defense World Geodetic System 1984.* NIMA.

Nayak, R., Cannon, M., Wilson, C., & Zhang, G. (2005). Slant TEC data ingestion in the modified NeQuick ionosphere electron density model. New Delhi, India: The XXVIII General Assembly of the International Union of Radio Science.

Negretti, M. (2013/2016). *Low cost GNSS receivers: Navigation and monitoring activities.* Milano: Politecnico di Milano, Department of Civil and Environmental Engineering, Doctoral Programme in Environmental and Infrastructure Engineering.

*NovAtel.* (2010). Retrieved from NovAtel Inc. Heaxagon Calgary: https://www.novatel.com/

O'D Riscoll, C. (2010, July). *GNSS Solutions: Carrier phase and its measurement for GNSS.* Retrieved from Inside GNSS: http://insidegnss.com/

OSGeo. (2019, March 27). *The Open Source Geospatial Foundation*. Retrieved from QGIS Desktop: https://www.osgeo.org/projects/qgis/

Philippov, V., Sutiagin, I., & Ashjaee, J. (1999). Measured characteristics of dual depth dual frequency choke ring for multipath rejection in GPS receivers. *Proceedings of ION GPS-99* (pp. 793–796). Nashville, Tennessee: 12th International Technical Meeting of the Satellite Division of the Institute of Navigation.

QGIS. (2019, March 27). *QGIS*. Retrieved from A Free and Open Source Geographic Information System: https://www.qgis.org/en/site/

Rizos, C. (n.d.). Making Sense of GNSS Techniques. In J. D. Bossler, *Manual of Geospatial Science and Technology* (2nd ed., pp. 177-187). Bova Raton London New York: CRC Press.

Saastamoinen, J. (1973). Contribution to the theory of atmospheric refraction. *Bulletin Géodésique, 107*, 13-34.

Seeber, G. (2003). *Satellite geodesy: foundations, methods, and applications* (2nd ed.). Berlin New York: Walter de Gruyter.

Skournetou, D., & Lohan, E.-S. (2011). Comparison of Single and Dual Frequency GNSS Receivers in the Presence of Ionospheric and Multipath errors. *Personal Satellite Services: Third International ICST Conference* (pp. pp.402-410). Malaga, Spain: Tampere University of Technology, P.O. Box 553 Tampere, Finland. Retrieved from http://www.cs.tut.fi/tlt/pos/

Swann, J. (2006). Will GPS and Galileo have the same or interoperable reference systems? In G. Lachapelle, & M. Petovello, *GNSS Solutions: Reference systems, UTC leapsecond, and L2C receivers?* (pp. 57-66). Inside GNSS.

Tawk, Y. (2013). *Advanced Algorithmic and Architecture Designs for Future Satellite Navigation Receivers.*

The State Council Information Office of the People's Republic of China. (2016). *China's BeiDou Navigation* (First Edition ed.). Beijing, 24 Baiwanzhuang Road, Beijing 100037, China: Foreign Languages Press Co. Ltd. Retrieved from http://en.beidou.gov.cn

Tranquilla, J., & Carr, J. (1990/91). GPS multipath field observations at land and water sites. *Navigation, 37(4)*, 393-414.

ublox. (2007, 12 4). *LEA-4T ANTARIS 4 Programmable GPS Module with Precision Timing.* Retrieved from ublox: https://www.u-blox.com/

United Nations. (2004). *Report of the action team on global navigation satellite systems (GNSS).* Vienna, Austria, July 19-30, 1999: Follow up to the Third United Nations Conference on the Exploration and Peaceful Uses of Outer Space (UNISPACE III).

UNOOSA. (n.d.). *United Nations.* Retrieved from United Nations Office for Outer Space Affairs: http://www.unoosa.org/

*USNO.* (n.d.). Retrieved from The United States Naval Meteorology and Oceanography Command (NMOC): https://www.usno.navy.mil/

Vdovin, V., & Dorofeeva, A. (2012). *Global Navigation Satellite System - Global Geocentric Coordinate System of the Russian Federation.* Ministry of Defence of the Russian Federation. Moscow: WG D – Reference Frames, Timing and Applications.

York University. (2019). *York University*. Retrieved from Matlab: Lesson 1: https://www.yorku.ca/jdc/Matlab/Lesson1.htm